Supersymmetric small-field inflation with tribrid superpotentials

Inauguraldissertation
zur
Erlangung der Würde eines Doktors der Philosophie
vorgelegt der
Philosophisch-Naturwissenschaftlichen Fakultät
der Universität Basel

von

David Maik Nolde
aus Deutschland

Basel, 2016

Genehmigt von der Philosophisch-Naturwissenschaftlichen Fakultät

auf Antrag von

Prof. Dr. Stefan Antusch, Prof. Dr. Wilfried Buchmüller

Basel, den 22.03.2016

Prof. Dr. Jörg Schibler

Dekan

Abstract

In this thesis, we study supersymmetric models of tribrid inflation and new inflation, both of which can be realized with a tribrid superpotential.

In the first part, we focus on tribrid inflation, deriving relations between cosmological observables and model parameters as well as providing guidelines for embedding tribrid inflation in realistic particle physics models. As an example application, we show how tribrid inflation can be realized in an explicit model of the leptonic flavour structure based on a discrete family symmetry, and how the production of topological defects after inflation can be avoided in such a model. Finally, we consider the possibility of generating the non-renormalizable operators of the tribrid superpotential at a sub-Planckian mass scale, which extends the applicability of tribrid inflation to some models with intermediate energy scales.

In the second part, we study new inflation with tribrid superpotentials. We first calculate the effects of the imaginary inflaton component on the primordial perturbations, which are generic for supersymmetric realizations of new inflation and not specific to the tribrid superpotential. Afterwards, we show how the tribrid superpotential coupling provides not only a mechanism for dynamically generating the initial conditions for new inflation, but also an effective inflaton decay channel for reheating after inflation. We also study the different preheating mechanisms in this setup and discuss under which conditions preheating can affect the final reheating phase.

In the last part, we consider whether small-field models of slow-roll inflation would remain viable if large primordial tensor perturbations were observed. In particular, we explain why such an observation would imply a scale-dependent running of the spectral index, and we derive a general slow-roll bound to prove that an observation of tensor modes close to the current upper bound has the potential to rule out the entire framework of small-field slow-roll inflation employed throughout this thesis.

This thesis is based on the author's work conducted from July 2012 until January 2016 at the University of Basel. This work has been partly published in [1–7]:

- S. Antusch and D. Nolde,
  Matter inflation with A_4 flavour symmetry breaking,
  JCAP **1310** (2013) 028, arXiv:1306.3501 [hep-ph].

- D. Nolde,
  Effects of the imaginary inflaton component in supergravity new inflation,
  JCAP **1311** (2013) 028, arXiv:1310.0820 [hep-ph].

- S. Antusch, D. Nolde and S. Orani,
  Hilltop inflation with preinflation from coupling to matter fields,
  JCAP **1405** (2014) 034, arXiv:1402.5328 [hep-ph].

- S. Antusch and D. Nolde,
  BICEP2 implications for single-field slow-roll inflation revisited,
  JCAP **1405** (2014) 035, arXiv:1404.1821 [hep-ph].

- S. Antusch, F. Cefalà, D. Nolde and S. Orani,
  False vacuum energy dominated inflation with large r and the importance of κ_s,
  JCAP **1410** (2014) 015, arXiv:1406.1424 [hep-ph].

- S. Antusch, D. Nolde and S. Orani,
  Hill crossing during preheating after hilltop inflation,
  JCAP **1506** (2015) 009, arXiv:1503.06075 [hep-ph].

- S. Antusch and D. Nolde,
  Realising effective theories of tribrid inflation: Are there effects from messenger fields?,
  JCAP **1509** (2015) 055, arXiv:1505.06910 [hep-ph].

Contents

Acknowledgements

First of all, I would like to thank my thesis supervisor Prof. Dr. Stefan Antusch for offering me the opportunity to conduct research on such a fascinating topic and in such a positive, stimulating work environment, and for his invaluable guidance throughout these past four years. Secondly, I thank my thesis referee Prof. Dr. Wilfried Buchmüller for kindly accepting to read this thesis.

Furthermore, I want to thank Stefano Orani, Francesco Cefalà, Constantin Sluka, Oliver Fischer and Vinzenz Maurer for many useful physics discussions and for creating an enjoyable working atmosphere. I would also like to express my gratitude to Francesco Cefalà, Jonas Sattel and Giti Khavari for proofreading parts of this thesis, and to Barbara Kammermann for gracefully resolving all bureaucratic challenges during my stay in Basel.

Moreover, I thank my wonderful friends and relatives for their support and encouragement during these years. Finally, I would like to express my deep gratitude to Giti Khavari for her love and patience and for enriching every single day of my life.

Part I

Introduction

Chapter 1

Introduction

Our current understanding of the universe is based on two complementary theories: the Standard Model (SM) of particle physics which describes visible matter and all forces excluding gravity, and the ΛCDM model of cosmology which describes the large-scale evolution of the universe in terms of just six free parameters.

While the late-time cosmological evolution is rather well understood, there is greater theoretical uncertainty about the earlier stages. The recent data from the Planck satellite confirms the generic predictions of an initial phase of slow-roll inflation [8, 9]: the primordial perturbations seem to be Gaussian, adiabatic and nearly scale invariant. However, these predictions are shared by many models of inflation, and thus it is still unknown which model of inflation is the correct one.

We also know that the SM is incomplete. At the very least, it must be extended by a dark matter candidate and a mechanism for generating neutrino masses [10]. In addition, the SM does not explain some of the apparent patterns within the theory, e.g. the fact that all fermions come in three copies with hierarchically different masses. Though it is possible to take these apparent patterns as given, they could be explained naturally by extensions of the Standard Model like Grand Unified Theories (GUTs), which unify the forces in a single gauge group and each family of fermions in representations of that group [11–13], or family symmetries, which could explain the flavour structure including the patterns of quark and lepton mixing [14–17]. Another noteworthy extension of the SM is supersymmetry (SUSY), which can provide a dark matter candidate [18–20] and the gauge coupling unification required for GUTs [21, 22].

Many of these extensions of particle physics beyond the Standard Model (BSM) predict new particles or processes at some high energy scales beyond the reach of collider experiments, which makes these theories very difficult to test. However, the early universe had extremely high energy densities, particularly during inflation. Realizing inflation within realistic particle physics models could therefore improve the predictivity both of BSM particle physics and of inflation: the high energies during inflation mean that BSM processes can affect the inflationary dynamics, and the particle physics embedding can fix some of the inflaton couplings, leading to predictions for the primordial perturbations and for reheating.

Supersymmetric tribrid inflation is a particularly promising candidate for connecting inflation with particle physics [23–28]. The inflaton of tribrid inflation can be charged under symmetries, including gauge symmetries [25]; it is therefore possible to identify the inflaton

with some matter field, like a sneutrino or a slepton-Higgs direction, such that constraints on the inflaton potential can be related to constraints on visible sector particle physics. In addition, tribrid inflation ends with a rapid phase transition in which another scalar field acquires a large vacuum expectation value. This phase transition can be naturally related to the spontaneous breaking of a high energy particle physics symmetry like a GUT or family symmetry.

Another interesting possibility is new inflation, in which the symmetry breaking field itself is the inflaton candidate [29–36]. The phase transition is not rapid in this case, and the universe expands as the inflaton field slowly rolls towards the symmetry breaking minimum of its potential.

Tribrid inflation and new inflation can be interpreted as different regimes of the same theory. Given a supersymmetric theory with a tribrid superpotential, the mass of the symmetry breaking field determines whether the phase transition happens rapidly or slowly, leading to tribrid inflation or new inflation, respectively.

The goal of this thesis is to explore both cases. Beyond calculating their predictions for the primordial perturbations, we also study how they can be embedded in realistic particle physics models, and how such an embedding relates cosmological and particle physics observables.

We start with an introduction to inflation, reheating and supersymmetry in chapters 2–5, with particular focus on those aspects which are relevant for this thesis.

After these preliminaries, we introduce the tribrid superpotential and tribrid inflation in chapter 6. We derive relations between the cosmological observable α_{s} and various model parameters, and we provide simple guidelines for embedding tribrid inflation in realistic models. As an explicit example, we apply these results to a lepton flavour model based on an A_4 family symmetry in chapter 7, in which tribrid inflation can be realized using either a slepton-Higgs combination or a right-handed sneutrino as the inflaton field. We also show how the production of topological defects can be avoided for one specific inflaton direction. Finally, in chapter 8, we consider the possibility of generating the non-renormalizable operators in the tribrid superpotential from renormalizable couplings to messenger fields at a sub-Planckian mass scale, which extends the applicability of our results on tribrid inflation to some models with intermediate mass scales.

Afterwards, we turn to supersymmetric new inflation. We start in chapter 9 with calculating the effect of the inflaton field's imaginary component on the primordial spectrum of perturbations. In chapter 10, we consider the consequences of realizing new inflation with a tribrid superpotential, which implies a coupling of the inflaton to another scalar field. We show that such a coupling offers a mechanism for generating the initial conditions of new inflation dynamically, and that it also provides an effective decay channel for reheating after inflation. Finally, in chapter 11, we study the different stages of preheating in this model, and we discuss under which conditions preheating can have significant effects on the final reheating phase.

We close with chapter 12, where we consider the implications of a possible future

observation of primordial gravity waves for small-field model building. We explain why in small-field inflation, $r \gtrsim 10^{-2}$ requires a scale-dependent running of the spectral index, and we derive a general slow-roll bound to prove that a measurement of r close to its current upper bound has the potential to rule out the entire framework of small-field slow-roll inflation employed throughout this thesis.

Part II

Theoretical foundations

Chapter 2

Slow-roll inflation

In these first chapters, we introduce the theoretical background for our later work on inflation in supergravity.

We first discuss inflation, starting with the homogeneous background equations in chapter 2. In chapter 3 we explain how to calculate the quantum fluctuations during inflation for any given model of slow-roll inflation, from which we can derive testable predictions for the primordial scalar and tensor perturbations. This is complemented by the introduction to reheating in chapter 4, where we discuss how the inflaton field's energy gets converted into a hot bath of elementary particles, leading to additional predictions for e.g. the non-thermally produced baryon asymmetry or dark matter abundance. Chapter 5 then provides the final ingredients for our later analysis by introducing supersymmetry with special focus on those aspects relevant to building supersymmetric models of inflation.

These chapters focus on the particular concepts and equations used in the main part of this thesis. For a broader and more detailed introduction, we refer to textbook reviews of cosmology [37–39], inflation [40–42], reheating [43, 44] and supersymmetry [45–48].

In this chapter, we will discuss slow-roll inflation at the level of the homogeneous field equations. We briefly explain the basic idea of and observational evidence for cosmic inflation, and then go on to introduce slow-roll inflation driven by a real scalar field, the slow-roll approximation, and a selection of the most popular basic models of slow-roll inflation on which most other models are based.

2.1 Motivation

2.1.1 The ΛCDM model

Over the last decades, a series of complementary observations has confirmed the ΛCDM model as the current standard model of cosmology [49]. With only six free parameters, it can fit all cosmological observations, including the cosmic microwave background (CMB) with its temperature and polarization fluctuations [8, 9, 50, 51], the baryon acoustic oscillation (BAO) peak in the matter power spectrum [52–54], the abundance of primordial elements from Big Bang nucleosynthesis (BBN) [55], and measurements of supernova redshifts [56, 57].

The ΛCDM model is very simple by construction. The ΛCDM universe is filled with baryonic matter, dark matter, radiation, and a constant vacuum energy (or equivalently a

cosmological constant). It is almost homogeneous and isotropic; the only initial inhomogeneities are Gaussian fluctuations of the total energy density with a power spectrum that is determined by an amplitude A_s and a spectral index n_s. The base ΛCDM universe is also flat, i.e. the total energy density is equal to the critical density.

The assumption of approximate isotropy is motivated by observations of the CMB and large scale structure. If we also assume that, in line with the cosmological principle, our planet does not have a special position in the universe, this implies homogeneity. The other assumptions are justified mostly by a desire for minimality: the resulting model has only six free parameters which are fitted to the observations.

In the ΛCDM model without inflation, the universe has a finite age of 13.7 billion years, and it starts with extremely high energy densities, i.e. a thermal bath of extremely high temperature which behaves like radiation.[1]

2.1.2 Initial conditions of the ΛCDM model

Horizon problem

The initial conditions of the ΛCDM model are very peculiar: the universe at very early times is almost homogeneous, and the tiny density perturbations have the same statistical properties everywhere. We know that this must have been the case at the time when the CMB decoupled at about $t \sim 300{,}000$ years, because we observe that the CMB is statistically isotropic. However, there is no causal mechanism by which all of the different points in the sky from which we observe CMB photons could have interacted before decoupling, because even at decoupling (when the universe was still smaller) most of them were separated by a far greater distance than a photon emitted at any time $t > 0$ could have travelled within 300,000 years in a radiation-dominated universe [37, 39].

The initial conditions must therefore be tuned by hand to be simultaneously identical in many causally disconnected patches to explain the isotropy of the CMB. This is known as the horizon problem.

Flatness problem

The base ΛCDM model arbitrarily assumes that the universe is flat, because all observations are perfectly consistent with $\Omega_\mathrm{k} = 0$, and if one allows for any deviation from the critical energy density, parametrized by $\Omega_\mathrm{k} \neq 0$, the observations constrain $|\Omega_\mathrm{k}| \lesssim 10^{-2}$ at a 95% confidence level (CL).

However, in the Big Bang cosmology without inflation, $\Omega_\mathrm{k} \simeq 0$ might be considered fine-tuning, because $\Omega_\mathrm{k} = 0$ is an unstable fixed point for radiation or matter dominated universes. If one assumes some initial non-zero $|\Omega_\mathrm{k}|$ at early times, it quickly grows to

[1] Naively extrapolating back the Friedmann equations, one finds a singularity with infinite energy density at an early time 13.7 billion years ago. This singularity is usually called the Big Bang and defines the cosmic time $t = 0$. However, General Relativity is not expected to be valid at energies above the Planck scale, and the extrapolation can only be trusted for times for which the energy density is sub-Planckian.

much larger values. To be consistent with $|\Omega_\mathrm{k}| < 10^{-2}$ today, the initial Ω_k must be really tiny, e.g. $|\Omega_\mathrm{k}(t_\mathrm{Pl})| \lesssim 10^{-60}$ at the time when energy densities were close to the Planck scale [37, 42]. This apparent fine-tuning is historically known as the flatness problem.[2]

Monopole problem

Many popular Grand Unified Theories (GUTs), which provide a unified description of the fundamental forces and elementary particles in terms of some unified gauge symmetry, predict that the spontaneous breaking of these GUT symmetries in the early universe would produce magnetic monopoles [59, 60]. However, there are strong observational upper bounds on the abundance of such monopoles in our universe, in conflict with those GUTs' predictions. Similar problems appear in other high-energy extensions of particle physics beyond the Standard Model, since any stable particle species with very high mass tends to be overproduced in the early universe [37].

2.1.3 Generating the initial conditions by cosmic inflation

All of the above issues can be naturally solved by cosmic inflation, which is a period of rapid accelerated expansion of the universe at very early times [60].

As all distances are stretched enormously, any pre-existing matter and radiation gets diluted. After a sufficiently long period of inflation, this dilution means that any given volume, including our observable universe, is filled with nothing but vacuum energy, making the universe everywhere homogeneous and isotropic up to vacuum quantum fluctuations. This solves both the horizon problem and the monopole problem. One can also show that inflation exponentially suppresses Ω_k, solving the flatness problem.

In addition to solving the above problems, the vacuum quantum fluctuations during inflation generate the small inhomogeneities we observe in the CMB and large scale structure, and their statistical properties can be predicted for any given model of inflation. This will be discussed in more detail in chapter 3.

To solve the horizon and flatness problems, the universe should expand at least by a factor of about $a \gtrsim e^{60}$. If the total expansion is close to this bound, the observable universe might retain some residual imprint from the pre-inflationary initial conditions which might be observable in cosmological experiments. However, in most models of inflation, the total amount of expansion is much greater. In that case, any pre-existing initial conditions are totally diluted away, and for all practical purposes we can assume that the universe starts out exactly in its vacuum state. In that sense, inflation "predicts" the initial conditions of the observable universe.

[2] Whether or not $\Omega_\mathrm{k} = 0$ constitutes fine-tuning depends on the probability measure that one applies. For example, using the canonical Liouville measure on the space of FRW universes, the probability to have $\Omega_\mathrm{k} = 0$ is equal to 100% [58]. Using this measure, there is no flatness problem – almost all Friedmann universes are perfectly flat.

2.2 Scalar field in FRW spacetime

The most popular mechanism for realizing an early period of cosmological inflation is "slow-roll inflation" where spacetime expands exponentially due to the potential energy of a scalar field, the so-called "inflaton". In this section, we briefly introduce the equations of motion of a Friedmann-Robertson-Walker (FRW) spacetime coupled to n homogeneous scalar fields, which describe the dynamics of slow-roll inflation at the homogeneous background level.

2.2.1 Friedmann equations for ideal fluid

According to general relativity, the evolution of the spacetime metric $g_{\mu\nu}$ can be calculated from the Einstein equations [40]:

$$R_{\mu\nu} - \frac{R}{2} g_{\mu\nu} - \Lambda g_{\mu\nu} \;=\; T_{\mu\nu}, \tag{2.1}$$

where $T_{\mu\nu}$ is the energy-momentum tensor describing the matter content of the universe, and

$$\begin{aligned} R_{\mu\nu} &= \partial_\alpha \Gamma^\alpha_{\mu\nu} - \partial_\nu \Gamma^\alpha_{\mu\alpha} + \Gamma^\alpha_{\beta\alpha}\Gamma^\beta_{\mu\nu} - \Gamma^\alpha_{\beta\nu}\Gamma^\beta_{\alpha\mu}, \\ R &= g^{\mu\nu} R_{\mu\nu}, \\ \Gamma^\mu_{\alpha\beta} &= \frac{g^{\mu\nu}}{2}\left[\partial_\alpha g_{\beta\nu} + \partial_\beta g_{\alpha\nu} - \partial_\nu g_{\alpha\beta}\right]. \end{aligned}$$

The Einstein equations (2.1) are a set of 10 partial differential equations which usually cannot be solved exactly. However, in cosmology we can solve them approximately using perturbation theory. Observations indicate that the universe is homogeneous and isotropic on large scales, so we solve the Einstein equations for a perfectly homogeneous and isotropic universe and later add any inhomogeneities as perturbations.

For a universe which is homogeneous and isotropic, $g^{\mu\nu}$ takes the form of the Friedmann-Robertson-Walker (FRW) metric [37]:

$$ds^2 \;=\; dt^2 - a^2(t)\left(\frac{dr^2}{1-k_c r^2} + r^2\left(d\theta^2 + \sin^2(\theta) d\phi^2\right)\right). \tag{2.2}$$

Eq. (2.2) uses comoving coordinates, which means that free-falling observers keep fixed coordinates r, θ and ϕ, while the physical distance between them scales with $a(t)$. Due to our strong symmetry assumptions, the metric is completely characterized by a single dynamical variable $a(t)$, the so-called "scale factor".

The constant k_c parametrizes the curvature. Throughout this thesis, we will use $k_c = 0$ which corresponds to a perfectly flat universe: even if $k_c \neq 0$ at some initial time, the effect of k_c will quickly become negligible due to inflation [42], so we can set $k_c = 0$ for simplicity if inflation lasts long enough. The Friedmann metric is then identical to the Minkowski metric except for the scale factor $a(t)$ describing the uniform expansion of the universe:

$$ds^2 \;=\; dt^2 - a^2(t)\left(dx^2 + dy^2 + dz^2\right). \tag{2.3}$$

To derive the equations of motion for $a(t)$ from eq. (2.1), we have to make some assumptions about $T_{\mu\nu}$. In cosmology, $T_{\mu\nu}$ often takes the form of a perfect fluid described by an energy density $\rho(t)$ and a pressure $p(t)$ [40]:

$$T_{\mu\nu} = (\rho + p)u_\mu u_\nu - p\, g_{\mu\nu}, \tag{2.4}$$

where u is the fluid velocity vector. In the fluid's local rest frame, we have:

$$T^\mu_{\ \nu} = \begin{pmatrix} \rho & 0 & 0 & 0 \\ 0 & -p & 0 & 0 \\ 0 & 0 & -p & 0 \\ 0 & 0 & 0 & -p \end{pmatrix}. \tag{2.5}$$

To derive the equations of motion for $a(t)$ for a flat universe ($k_\mathrm{c} = 0$), we can insert the FRW metric from eq. (2.3) and $T_{\mu\nu}$ from eq. (2.5) into the Einstein equations (2.1). This yields the famous Friedmann equations [40]:

$$\mathcal{H}^2 \equiv \left(\frac{\dot{a}}{a}\right)^2 = \frac{\rho}{3}, \tag{2.6}$$

$$\dot{\mathcal{H}} + \mathcal{H}^2 = \frac{\ddot{a}}{a} = -\frac{\rho + 3p}{6}, \tag{2.7}$$

where we introduced $\mathcal{H}(t) \equiv \dot{a}/a$ which is often called the "Hubble constant" even though it is generally time-dependent.

The Friedmann eqs. (2.6)–(2.7) are two equations for three dynamical variables $a(t)$, $\rho(t)$ and $p(t)$. To complete the system of equations, we also need the equation of state for the fluid:

$$w(t) \equiv \frac{p(t)}{\rho(t)}. \tag{2.8}$$

Some important cases for cosmology have a constant equation of state parameter $w(t)$: ultra-relativistic matter (also called "radiation") has $w = 1/3$, non-relativistic matter (also called "dust") has $w = 0$, and a cosmological constant or vacuum energy has $w = -1$. For such a constant w, the Friedmann equations can be solved analytically [40]:

$$\rho(t) \propto a(t)^{-3(w+1)}, \tag{2.9}$$

$$a(t) \propto \begin{cases} t^{\frac{2}{3(w+1)}} & w \neq -1, \\ \exp(\mathcal{H}_0 t) & w = -1. \end{cases} \tag{2.10}$$

Note that inflation, which is defined as a period of accelerated expansion ($\ddot{a} > 0$), requires $w < -1/3$. This cannot be realized with ordinary matter or radiation, as these have $0 \leq w \leq 1/3$, but it can be realized with vacuum energy, e.g. the potential energy of a homogeneous scalar field.

It is also useful to note that in an expanding universe with $w > -1$, $a(t)$ and $\rho(t)$ are both monotonous functions of cosmic time t. We can therefore use a, ρ and t interchangeably, using whichever is most convenient as a time variable and treating the others as functions of that variable. For example, we will often specify times in terms of a, with $\rho(a)$ and $t(a)$ as dependent variables.

Another important convention is that a is often rewritten in terms of "e-folds" which are defined as

$$N := \ln\left(\frac{a}{a_0}\right), \tag{2.11}$$

where a_0 is the scale factor at some given time t_0. This is used particularly in the context of (quasi-)exponential expansion, where each e-fold corresponds to a time interval of one Hubble time $t_{\mathcal{H}} = 1/\mathcal{H}$.

2.2.2 Homogeneous scalar fields in FRW spacetime

The action of n scalar fields ϕ_i minimally coupled to gravity is given by [41]

$$S = \int \mathrm{d}^4\mathrm{x}\sqrt{-g}\left(-\frac{R}{2} - V(\phi_1,\ldots,\phi_n) + \frac{1}{2}\sum_{i=1}^{n}(\partial_\mu\phi_i)(\partial^\mu\phi_i)\right), \tag{2.12}$$

where $\sqrt{-g} = \sqrt{-\det g^{\mu\nu}}$.

The equations of motion can be derived from $\delta S = 0$, varying this action with respect to the metric $g^{\mu\nu}$ and the scalar fields ϕ_i. To find the equations of motion at the homogeneous background level, we restrict $g^{\mu\nu}$ to the flat FRW metric of eq. (2.3) and $\phi_i(x^\mu) = \phi_i(t)$ to spatially homogeneous fields. This results in the Friedmann equations for $a(t)$ and for the scalar fields $\phi_i(t)$ [41]:

$$\mathcal{H}^2 = \frac{1}{3}\left(V + \frac{1}{2}\sum_{i=1}^{n}\dot{\phi}_i^2\right), \tag{2.13}$$

$$\ddot{\phi}_i + 3\mathcal{H}\dot{\phi}_i + \frac{\partial V}{\partial\phi_i} = 0. \tag{2.14}$$

Note that for a constant scalar field ϕ with potential energy $V(\phi) = V_0$, eq. (2.13) implies a constant $(\dot{a}/a) \equiv \mathcal{H} = \sqrt{V_0/3}$. Solving this for $a(t)$, one finds that the universe expands exponentially with $a(t) = a_0\exp(\mathcal{H}t)$.

For realizing inflation, we cannot use a truly constant scalar field, because inflation must eventually end and the inflaton field's energy must be converted to the matter particles we see today. To realize inflation from a scalar field, we instead use a *nearly* constant scalar field which has a very flat scalar potential and therefore moves very slowly, leading to quasi-exponential expansion $a(t) \simeq a_0\exp(\mathcal{H}t)$. This mechanism is called "slow-roll inflation".

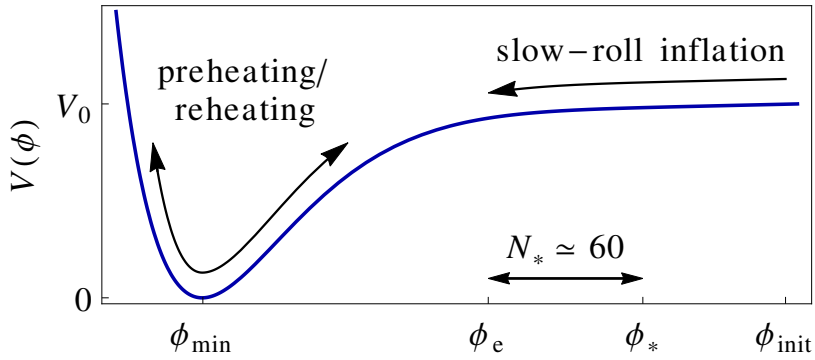

Figure 2.1: Schematic dynamics of slow-roll inflation: inflation starts for some homogeneous inflaton field value $\phi_{\rm init}$ in a nearly flat region of its scalar potential $V(\phi)$. The universe expands exponentially due to the nearly constant vacuum energy $V \simeq V_0$ while ϕ very slowly rolls down the small gradient of its potential. Inflation ends when the inflaton field reaches the end of the flat plateau at $\phi_{\rm e}$, and the inflaton quickly rolls down the steep part of its potential towards its true minimum.

2.2.3 Slow-roll inflation with a single scalar field

The dynamics of slow-roll inflation is depicted in fig. 2.1. Inflation starts for some homogeneous inflaton field value $\phi_{\rm init}$ in a nearly flat region of its scalar potential $V(\phi)$. Because the potential is close to flat, the inflaton field moves very slowly: it has very little kinetic energy, and its potential energy is nearly constant because the field changes so slowly. The energy density is therefore dominated by a nearly constant potential energy $V(\phi) \simeq V_0$, which leads to quasi-exponential expansion.

Inflation eventually ends when the inflaton leaves the nearly flat plateau at $\phi_{\rm e}$ after which it quickly rolls down the steep gradient towards the minimum of the potential.[3] The inflaton field then performs damped oscillations around the minimum and its energy gets converted into a hot plasma of elementary particles in a process called reheating (see chapter 4 for details). After reheating, the universe is dominated by radiation, and the cosmological evolution continues as in conventional ΛCDM Big Bang cosmology.

The solution to the horizon problem requires that the universe expands by at least $N_* \sim 60$ e-folds. The dynamics during the last N_* e-folds leave some imprint on cosmological scales due to the inflaton field's quantum fluctuations during that time, which will be discussed in chapter 3.

The earlier phases of inflation, more than N_* e-folds before the end of inflation, only affect scales much larger than the observable universe. For this reason, we do not need to

[3]For the purpose of inflation, that minimum is usually assumed to have $V(\phi_{\rm min}) = 0$. In principle, it could have a tiny non-zero value corresponding to the cosmological constant of the ΛCDM model, thus explaining the cosmological constant in terms of the vacuum energy of a scalar field. However, the cosmological constant is many orders of magnitude smaller than all energy scales relevant for the inflation models considered in this thesis, so we can neglect it and set $V(\phi_{\rm min}) = 0$.

know anything about the initial conditions near $\phi_{\rm init}$ to calculate predictions.[4]

2.3 Slow-roll approximation

So far, our assumption of homogeneity and isotropy has allowed us to simplify the Einstein eqs. (2.1) to the much simpler eqs. (2.13)–(2.14). However, even the simpler eq. (2.14) is a second-order non-linear differential equation which makes analytic calculations very difficult. The slow-roll approximation makes use of the fact that the inflaton is rolling very slowly, and therefore the highest time derivatives of the inflaton field are generally subdominant. Neglecting them, we can derive approximate first-order differential equations of motion which turn out to be supremely useful for analytic studies of the inflationary background dynamics.

2.3.1 Slow-roll equations of motion to leading order

To leading order, the slow-roll approximation [62] corresponds to neglecting the highest-order time derivative of ϕ in eqs. (2.13)–(2.14):

$$\mathcal{H} \simeq \sqrt{V/3}, \tag{2.15}$$

$$\dot{\phi}_i \simeq -\frac{1}{3\mathcal{H}}\frac{\partial V}{\partial \phi_i}. \tag{2.16}$$

Note that eq. (2.16) is a first-order ordinary differential equation (ODE), in contrast to the original eq. (2.13) which was a second-order ODE. This may seem puzzling at first, because the solution of a first-order ODE is uniquely specified from the initial field values $\phi_i(t_{\rm init})$ whereas a second-order ODE's solution also depends on the initial velocities $\dot{\phi}_i(t_{\rm init})$. What happens to the dependence on the initial velocities?

The answer is inflation: the initial velocity is damped away by the "Hubble damping" term $3\mathcal{H}\dot{\phi}$ in eq. (2.14). This is known as the "slow-roll attractor" [62]: during inflation, the inflaton field's velocity asymptotically approaches that of the slow-roll attractor eq. (2.16).

If inflation lasts long enough, we can therefore just use eqs. (2.15)–(2.16) during inflation, because during the final N_* e-folds (and only those have observable consequences) all inflationary solutions of the exact eqs. (2.13)–(2.14) will approximately match the result of the much simpler eqs. (2.15)–(2.16), independently of the initial $\dot{\phi}$ at the beginning of inflation.

Eqs. (2.15)–(2.16) can be combined to derive a formula for the number of e-folds of

[4] If inflation lasts only the minimum required number of e-folds, there may be some effect of pre-inflationary initial conditions on the largest observable scales [61]. In this thesis, we always assume that inflation lasts long enough for such effects to be negligible.

expansion realized while the inflaton field rolls from ϕ_1 to ϕ_2:

$$\Delta N \simeq \int_{\phi_2}^{\phi_1} \mathrm{d}\phi \, \frac{V(\phi)}{V'(\phi)}. \tag{2.17}$$

This expression is also valid in multi-field models if the integration is performed along the inflaton trajectory and $V'(\phi)$ is replaced by $|(\partial V/\partial\phi_1, \partial V/\partial\phi_2, ..., \partial V/\partial\phi_n)|$.

2.3.2 Slow-roll parameters

The slow-roll approximation can be formally derived as a series expansion in small "slow-roll parameters" [62], in which case eqs. (2.15)–(2.17) are the leading-order expressions. One can either expand in derivatives of the scalar potential with respect to the inflaton field(s) or in terms of time derivatives of the Hubble parameter. In this thesis, we choose the first approach.

Assuming a single inflaton field ϕ with potential $V(\phi)$, the first four slow-roll parameters are then defined as [62]

$$\varepsilon(\phi) = \frac{1}{2}\left(\frac{V'}{V}\right)^2, \tag{2.18a}$$

$$\eta(\phi) = \frac{V''}{V}, \tag{2.18b}$$

$$\xi^2(\phi) = \frac{V'V'''}{V^2}, \tag{2.18c}$$

$$\sigma^3(\phi) = \frac{(V')^2V''''}{V^3}, \tag{2.18d}$$

where primes denote derivatives with respect to ϕ. One can also define slow-roll parameters involving even higher derivatives, but those will not be used explicitly in this thesis.

ξ^2 is often treated as second-order and σ^3 as third-order in the slow-roll expansion, assuming that they are suppressed like η^2 and η^3 respectively. Though this is true in many popular models, it is not actually required for slow-roll inflation, and one can easily construct models in which ξ^2 and σ^3 can be as large as the first two slow-roll parameters. For this reason, we will generally include ξ^2 and σ^3 in our first-order slow-roll calculations.

Note that $\varepsilon < 1$ and $|\eta| < 1$ are necessary but not sufficient conditions for slow-roll inflation. In addition to the smallness of these two parameters, we must also assume that $\dot{\phi}$ is close to the slow-roll attractor solution from eq. (2.16). This extra condition is usually easy to fulfil because the attractor solution is quickly reached during inflation. However, we still have to assume that the initial conditions allow for inflation to start.[5]

[5]This is less restrictive than it may seem. The initial conditions for inflation just have to be satisfied in a single patch of the pre-inflationary universe. This small patch then inflates to a volume larger than the observable universe, and we can never observe the many patches where the initial conditions were not

For models with multiple inflaton fields, the first two slow-roll parameters can be generalized as

$$\varepsilon(\vec{\phi}) = \frac{1}{2V^2}\sum_i \left(\frac{\partial V}{\partial \phi_i}\right)^2, \tag{2.19a}$$

$$\eta_{ij}(\vec{\phi}) = \frac{1}{V}\frac{\partial^2 V}{\partial\phi_i \partial\phi_j}, \tag{2.19b}$$

with a square matrix η_{ij} instead of a single slow-roll parameter η.

The condition that η must be small is more tricky in multi-field models. Slow-roll inflation is still possible if η_{ij} has a large positive eigenvalue orthogonal to the inflaton trajectory. A simple example is inflation with an inflaton field ϕ in the presence of a decoupled second field χ which is very heavy during inflation. In that case, inflation would just happen due to the slow-roll of ϕ, and χ would be stabilized due to its large mass. In such a case, $\eta_{\chi\chi} \gg 1$ only indicates that χ does not participate in the dynamics during inflation, and the model can be treated as a single-field model with ϕ as the only dynamical degree of freedom.

A large negative eigenvalue of η_{ij} generally spoils slow-roll inflation: such a negative eigenvalue indicates a tachyonic mass, which makes any small fluctuations grow exponentially (see section 4.2.2). With an eigenvalue $\eta \lesssim -1$, even tiny quantum fluctuations quickly grow to values large enough to disrupt the classical slow-roll dynamics and terminate inflation.

2.3.3 Calculating ϕ_e and ϕ_* from slow-roll parameters

Since ε and η must be small for slow-roll inflation, we can estimate the end-of-inflation inflaton field value ϕ_e from either $\varepsilon(\phi_\mathrm{e}) = 1$ or $|\eta(\phi_\mathrm{e})| = 1$, whichever happens earlier.[6] Models of hybrid inflation are an exception to this rule, see section 2.4.3.

We will often need to determine the inflaton field value ϕ_* at the time when the primordial perturbations on CMB scales are generated, $N_* \simeq 50$–60 e-folds before the end of inflation. This can be done using eq. (2.17):

$$N_* \simeq \int_{\phi_\mathrm{e}}^{\phi_*} \mathrm{d}\phi \, \frac{V(\phi)}{V'(\phi)} \tag{2.20}$$

and then solving for ϕ_*, plugging in the ϕ_e that one calculates as discussed above.

suitable for inflation. This is very different from the ΛCDM model without inflation, where the initial conditions have to be finely tuned everywhere in the universe at once, over many causally disconnected regions.

[6] Close to the end of inflation, the slow-roll approximation is already getting inaccurate; however, this is normally not an issue because the cosmological predictions mostly depend on the behaviour around ϕ_*, not around ϕ_e.

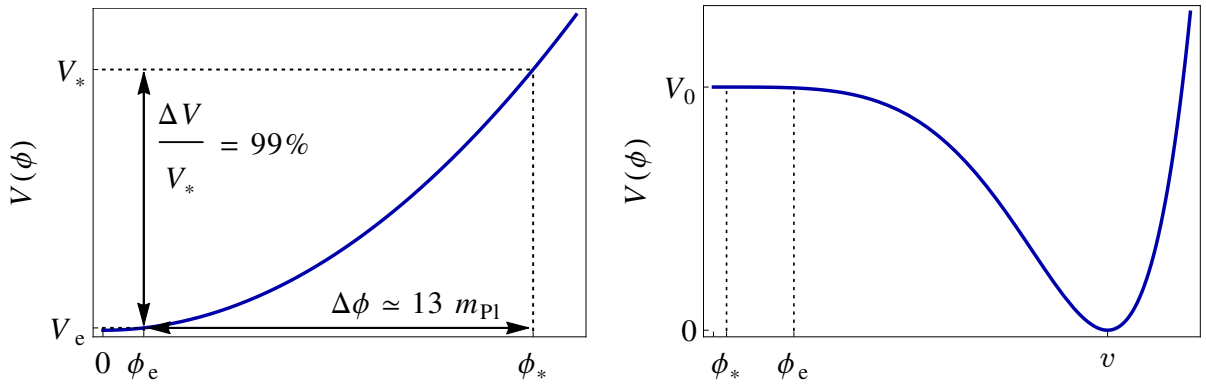

Figure 2.2: Potentials for chaotic inflation with $\ell = 2$ (left) and for new inflation with $\ell = 4$ (right). Inflation happens as the inflaton rolls down the potential gradient through ϕ_* to ϕ_e. For chaotic inflation, the inflaton rolls from large $\phi \gg 1$ towards $\phi = 0$, and for new inflation, the field rolls from $\phi \simeq 0$ towards $\phi = v$.
We see that chaotic inflation is a large-field model: the inflaton field moves over super-Planckian distances $\Delta\phi > 1$ during inflation. The vacuum energy also changes dramatically during chaotic inflation, with $V(\phi_e) \simeq 10^{-2} V(\phi_*)$.
In new inflation, the inflaton field moves only by $\Delta\phi \ll v$ during inflation and settles at $\phi \simeq v$ after inflation. For $v \ll 1$, the model is therefore clearly a small-field model in which the field travels sub-Planckian distances. As usual in small-field models, the vacuum energy is nearly constant during inflation: $V_* \simeq V_e \simeq V_0$. In this plot, ϕ_e and ϕ_* are marked for $v = 1$ so that they can be distinguished from $\phi = 0$ on the scale of the plot; for $v < 1$, ϕ_* and ϕ_e are a factor of v^2 closer to $\phi = 0$.

2.4 Popular models of slow-roll inflation

In this section, we want to introduce three of the most popular benchmark models of slow-roll inflation: chaotic inflation, new inflation and hybrid inflation. Many of the more complicated models in the literature are variations of these three basic templates, and they can be used as simple examples to illustrate the qualitative features of slow-roll inflation.

2.4.1 Chaotic inflation

Consider the inflaton potential of chaotic inflation [63]

$$V_{\text{chaotic}} = \lambda\phi^\ell, \tag{2.21}$$

with $\ell \geq 2$, depicted in the left plot of fig. 2.2. The slow-roll parameters can be calculated from eqs. (2.18a)–(2.18b):

$$\varepsilon = \frac{\ell^2}{2\phi^2}, \qquad \eta = \frac{\ell(\ell-1)}{\phi^2}. \tag{2.22}$$

Inflation is possible for small slow-roll parameters, which corresponds to large ϕ. The end of inflation can be estimated from $\varepsilon(\phi_\mathrm{e}) = 1$ or $|\eta(\phi_\mathrm{e})| = 1$, whichever happens earlier. For $\ell \geq 2$, this leads to

$$\phi_\mathrm{e} \,=\, \sqrt{\ell(\ell-1)}. \tag{2.23}$$

The inflaton field value ϕ_* at $N_* \simeq 50$–60 e-folds before the end of inflation can be calculated from eq. (2.20):

$$N_* \,=\, \int_{\phi_\mathrm{e}}^{\phi_*} \mathrm{d}\phi\, \frac{\phi}{\ell} \,=\, \frac{1}{2\ell}(\phi_*^2 - \phi_\mathrm{e}^2), \tag{2.24}$$

which leads to

$$\phi_* \,=\, \sqrt{2\ell N_* + \ell(\ell-1)} \,\gtrsim\, 10\sqrt{\ell}. \tag{2.25}$$

Note that chaotic inflation requires field values way above the Planck scale: $\phi_* \gg 1$. In addition, the inflaton field also moves by more than a Planck scale during inflation: $\Delta\phi = \phi_* - \phi_\mathrm{e} \gg 1$, so one cannot get sub-Planckian fields by a field redefinition $\phi(t) = \tilde{\phi}(t) + \text{const}$. For this reason, chaotic inflation is known as a "large-field" model of inflation.

Large-field models of inflation can predict observable gravity waves to a degree that is not possible in small-field models (see chapter 12 for an extended discussion). However, they are theoretically challenging because the inflaton potential $V(\phi)$ cannot be derived as a power series in an effective field theory (EFT) approach. Instead, one needs to know the precise form of $V(\phi)$ including all non-renormalizable terms, because even Planck-suppressed terms affect the dynamics if $\Delta\phi \gtrsim 1$. For this reason, chaotic inflation models generally require some assumption concerning the UV completion of the theory, e.g. by postulating some symmetries that forbid non-renormalizable contributions to $V(\phi)$.

2.4.2 New inflation

In new inflation [64], also called hilltop inflation, the inflaton field rolls down from a local maximum of the inflaton potential as depicted in the right plot of fig. 2.2. We will consider hilltop inflaton potentials of the form

$$V_\mathrm{hilltop} \,=\, V_0 \left(1 - \frac{\phi^\ell}{v^\ell}\right)^2, \tag{2.26}$$

with $\ell \geq 3$ and $v \ll 1$. Hilltop inflation occurs for $\phi \ll v$. The slow-roll parameters can be calculated from eqs. (2.18a)–(2.18b):

$$\varepsilon \,=\, \frac{2\ell^2}{v^{2\ell}}\phi^{2\ell-2} + ..., \qquad \eta \,=\, -\frac{2\ell(\ell-1)}{v^\ell}\phi^{\ell-2} + ..., \tag{2.27}$$

where the dots denote terms suppressed by higher powers of $(\phi/v)^\ell$. For $\phi \ll v^{\frac{\ell}{\ell-2}}$, the slow-roll parameters are small and slow-roll inflation is possible. The end of slow-roll inflation happens due to $|\eta(\phi_\mathrm{e})| = 1$ which happens much earlier than $\varepsilon = 1$. Taking only the leading term in eq. (2.27) for η, we get

$$\phi_\mathrm{e}^{\ell-2} \;=\; \frac{v^\ell}{2\ell(\ell-1)}. \tag{2.28}$$

To find ϕ_* to leading order in the slow-roll parameters, we use eq. (2.20):

$$N_* \;=\; \int_{\phi_\mathrm{e}}^{\phi_*} \mathrm{d}\phi\; \frac{-v^\ell}{2\ell}\phi^{1-\ell} \;=\; \frac{v^\ell}{2\ell(\ell-2)}\left(\phi_*^{2-\ell} - \phi_\mathrm{e}^{2-\ell}\right) \;\simeq\; \frac{v^\ell}{2\ell(\ell-2)}\phi_*^{2-\ell} - \frac{\ell-1}{\ell-2}, \tag{2.29}$$

which we can solve for ϕ_*:

$$\phi_*^{\ell-2} \;=\; \frac{v^\ell}{2\ell[(\ell-2)(N_*+1)+1]} \;\simeq\; \frac{v^\ell}{2\ell(\ell-2)N_*}. \tag{2.30}$$

For sub-Planckian $v \ll 1$, we find $|\phi_*| < |\phi_\mathrm{e}| \ll v$, so slow-roll inflation occurs very close to the hilltop. In fig. 2.2, ϕ_e and ϕ_* have been marked for $v = 1$ so that they can be distinguished from $\phi = 0$ on the scale of the plot. For $v < 1$, ϕ_* and ϕ_e are a factor of $v^{\frac{\ell}{\ell-2}}$ closer to $\phi = 0$.

With $\Delta\phi \ll v \ll 1$, models of new inflation are small-field models. As we will discuss in chapter 12, small-field models generally produce very low amplitudes of primordial gravity waves compared to large-field models. A distinct advantage of small-field models is that the inflaton potential can be derived in an EFT series expansion, because terms with sufficiently high powers of ϕ/m_Pl are naturally suppressed by small field values and can therefore be neglected. This makes small-field models relatively insensitive to the details of the UV completion compared to large-field models.

2.4.3 Hybrid inflation

Hybrid inflation is based on a scalar inflaton field ϕ and a scalar "waterfall field" χ with the potential [65]

$$V_\mathrm{hybrid}(\phi,\chi) \;=\; V_0\left(1 - \frac{\chi^2}{v^2}\right)^2 + \frac{\lambda}{2}\phi^n\chi^2 + \widetilde{V}(\phi). \tag{2.31}$$

Fig. 2.3 shows V_hybrid for $n = 2$. Inflation can happen in a flat valley with $\chi = 0$ where the effective mass of χ is positive, with

$$m_\chi^2(\phi) \;=\; \lambda\phi^n - \frac{4V_0}{v^2}. \tag{2.32}$$

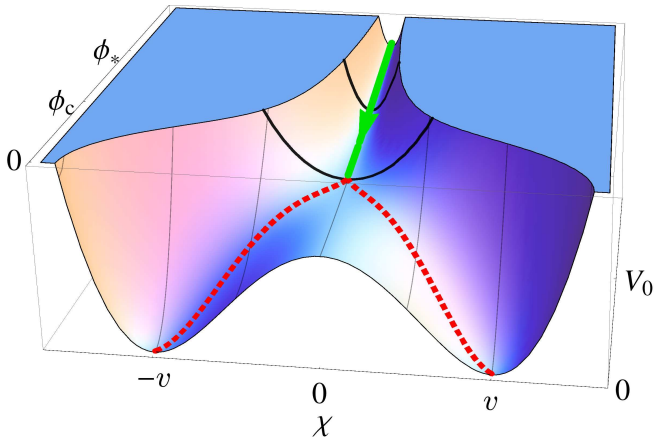

Figure 2.3: Potential for hybrid inflation with $n = 2$. Inflation happens while ϕ rolls along the nearly flat valley with $\chi = 0$ and $\phi > \phi_c$ marked by the thick green line. When ϕ drops below the critical value ϕ_c, the mass of χ becomes tachyonic: it becomes unstable and quickly goes along the red dashed line to $\chi = \pm v$, terminating inflation.

Along this valley, which is marked with a green line in fig. 2.3, χ is stabilized at zero and we effectively have single-field inflation in ϕ with the scalar potential $(V_0 + \tilde{V})$.

However, when ϕ becomes so small that $m_\chi^2(\phi) < 0$, then χ terminates inflation in a "waterfall transition": its quantum fluctuations grow exponentially and the fields quickly move towards the minima at $\chi = \pm v$, $\phi = 0$. If the tachyonic mass $|m_\chi|$ is large enough, this transition happens very quickly. In that case, the critical inflaton value ϕ_c where m_χ becomes tachyonic marks the end of inflation, with

$$m_\chi^2(\phi_c) = 0. \tag{2.33}$$

The inflaton value ϕ_* at N_* e-folds before the end of inflation can then be calculated as usual by plugging $\phi_e = \phi_c$ into eq. (2.20) and solving for ϕ_*. The result strongly depends on $\tilde{V}$, and models of hybrid inflation can be large-field or small-field models depending on the shape of $\tilde{V}$.

After the waterfall transition, χ ends up either at $+v$ or at $-v$. Which of the degenerate vacua is reached depends on the random quantum fluctuations in χ around the critical point, and different patches of the observable universe can end up in different vacua, potentially producing topological defects like domain walls if the transition breaks e.g. a $\mathbb{Z}_n$ symmetry as for the potential of eq. (2.31), or cosmic strings if it breaks e.g. a $U(1)$ symmetry. Since these defects are produced at the end of inflation, they are not diluted away, and their non-detection can strongly constrain models of hybrid inflation which predict the production of such defects.

Chapter 3

Quantum fluctuations during inflation

In the last chapter, we have discussed how a homogeneous scalar field can drive a period of rapid exponential expansion. This process dilutes away all pre-existing inhomogeneities, so that the only remaining source of inhomogeneities are vacuum quantum fluctuations. In models of inflation, these quantum fluctuations are the seeds of all inhomogeneities we observe in our universe, like the CMB anisotropies and matter overdensities (planets, galaxies and superclusters).

Their statistical properties can be predicted for any given model of inflation, and comparing these predictions with cosmological observations can rule out many models of slow-roll inflation or constrain the model parameters.

In this chapter, we discuss several methods for calculating the spectrum of primordial inhomogeneities in slow-roll inflation. We start with a brief discussion of how the inflaton perturbations can be quantized and how their quantum fluctuations can be calculated. In order to calculate observable quantities, we also introduce gauge-invariant measures of scalar and tensor perturbations. We then continue with approximate solutions: for single-field inflation, we provide simple formulas based on the slow-roll parameters, and for multi-field inflation, we introduce the δN formalism.

This entire chapter will be based on leading order perturbation theory. We know from observations that the early universe is nearly homogeneous and isotropic, e.g. from the smallness of the CMB temperature anisotropies which have $\Delta T/T \sim 10^{-5}$. For this reason, we can generally assume that during inflation, the inflaton fluctuations $\delta\phi$ can be treated as small perturbations around the homogeneous background characterized by $\overline{\phi}(t)$ and $\mathcal{H}(t)$.

3.1 Quantum fluctuations of scalar fields in de Sitter space

In this section, we introduce the formalism for calculating quantum fluctuations of the inflaton field and of the metric. We start with the quantum fluctuations $\delta\phi$ of a single inflaton field in FRW spacetime and then explain how to convert them into the gauge-invariant curvature perturbation ζ. We also briefly discuss tensor perturbations, and we introduce the notion of power spectra which allow for easy comparison of the calculated scalar and tensor perturbations with experimental bounds. This section is based mostly on [40, 41].

3.1.1 Inflaton perturbations

Classical equation of motion

Consider the equation of motion of a scalar field $\phi(t, \vec{x})$ with comoving coordinates $\vec{x}$ and scalar potential $V(\phi)$ in unperturbed FRW spacetime [41]:

$$\ddot{\phi} - \frac{1}{a^2}\vec{\nabla}^2\phi + 3\mathcal{H}\dot{\phi} + \frac{\partial V}{\partial \phi} = 0. \tag{3.1}$$

We are interested in small quantum fluctuations $\delta\phi$ around a homogeneous background solution $\overline{\phi}$, so we define

$$\phi(\vec{x}, t) = \overline{\phi}(t) + \delta\phi(\vec{x}, t). \tag{3.2}$$

The homogeneous background solution $\overline{\phi}(t)$ can be calculated from eqs. (2.13)–(2.14) or eqs. (2.15)–(2.16) as discussed in chapter 2. For small perturbations $\delta\phi$, we can expand eq. (3.1) to linear order in $\delta\phi$:

$$\delta\ddot{\phi} + 3\mathcal{H}\delta\dot{\phi} + \left(V''(\overline{\phi}) - \frac{1}{a^2}\vec{\nabla}^2\right)\delta\phi = 0. \tag{3.3}$$

The advantage of this linearisation in $\delta\phi$ is that eq. (3.3) can be converted to ordinary differential equations by a Fourier transformation:

$$\delta\ddot{\phi}_{\vec{k}} + 3\mathcal{H}\delta\dot{\phi}_{\vec{k}} + \left(V''(\overline{\phi}) + \frac{k^2}{a^2}\right)\delta\phi_{\vec{k}} = 0, \tag{3.4}$$

where $\delta\phi_{\vec{k}}(t)$ is the Fourier component of $\delta\phi(t, \vec{x})$ to the comoving wavevector $\vec{k}$.

Quantization of $\delta\phi$

When $\delta\phi$ is quantized, the equation of motion applies to the field operator $\delta\hat{\phi}$. Its Fourier transform can be expressed in terms of complex mode functions $\phi_{\vec{k}}(t)$ and annihilation operators $\hat{a}_{\vec{k}}$ [41]:

$$\delta\hat{\phi}_{\vec{k}}(t) = \phi_{\vec{k}}(t)\hat{a}_{\vec{k}} + \phi^*_{\vec{k}}(t)\hat{a}^\dagger_{-\vec{k}}, \tag{3.5}$$

where the mode functions $\phi_{\vec{k}}$ satisfy eq. (3.4).

The initial conditions for the mode functions can be determined if we assume that at early times, $\delta\hat{\phi}$ is in its vacuum state, because any particles (i.e. excitations of the lowest-energy state) are diluted away by the earlier period of inflation.[1] Then the initial

[1] In this thesis, we assume that inflation lasts long enough to erase the traces of anything that happens much more than N_* e-folds before the end of inflation. In principle, it is also possible that inflation only lasts the minimum of $N_* \sim 50$–60 e-folds required to solve the horizon problem. In that case, the predictions on the largest observable scales retain some imprint of the pre-inflationary dynamics [61].

conditions for the mode functions are given by the Minkowski vacuum [41]:

$$\phi_{\vec{k}}^{(\mathrm{vac})}(t) \;=\; \frac{\mathcal{H}}{\sqrt{2k^3}}\left(i+\frac{k}{a\mathcal{H}}\right)e^{ik/(a\mathcal{H})}. \tag{3.6}$$

The derivation of eq. (3.6) assumes a constant $\mathcal{H}$ which is a good approximation during slow-roll inflation. Eq. (3.6) is independent of the potential because at early times the term $k^2/a^2 \propto e^{-2\mathcal{H}t}$ always dominates over $V''(\overline{\phi})$.

With the mode eqs. (3.4) and the initial conditions from eq. (3.6), the quantum fluctuations $\delta\hat{\phi}$ are in principle fully determined up to non-linear corrections of $\mathcal{O}(\delta\phi^2)$.

Including backreaction from metric perturbations

So far, we have assumed that the background metric is that of an unperturbed FRW universe. However, since the metric is coupled to ϕ via the Einstein eqs. (2.1), any inhomogeneities $\delta\phi$ can source inhomogeneous perturbations of the FRW metric which then backreact on the evolution of $\delta\phi$. Using spatially-flat gauge, backreaction can be accounted for by using the Mukhanov-Sasaki equation [41]

$$\frac{\partial^2 v_{\vec{k}}}{\partial\tau^2}+\left(k^2-\frac{1}{z}\frac{\partial^2 z}{\partial\tau^2}\right)v_{\vec{k}} \;=\; 0, \tag{3.7}$$

with conformal time τ defined by $dt = a(t)d\tau$ and

$$v_{\vec{k}} \;\equiv\; a\,\phi_{\vec{k}}, \qquad z \;\equiv\; \frac{a\dot{\overline{\phi}}}{\mathcal{H}}, \tag{3.8}$$

where $\overline{\phi}(t)$ and $\mathcal{H}(t)$ are the homogeneous background quantities calculated from eqs. (2.13)–(2.14).

However, during slow-roll inflation backreaction is usually small until well after horizon exit (the time at which $k/a \sim \mathcal{H}$) [41], so it is often sufficient to use eq. (3.4).

3.1.2 Curvature perturbation

In general relativity, general coordinate transformations can transform inflaton perturbations into metric perturbations and vice versa. Since observables cannot depend on the choice of a coordinate system, it is generally useful to use gauge-invariant quantities to compare the theoretical predictions with experimental data.

For inflation, a gauge-invariant measure of the linear scalar perturbations is the curvature perturbation ζ [40, 41]:

$$\zeta \;=\; \Psi - \mathcal{H}\frac{\delta\rho}{\dot{\overline{\rho}}}, \tag{3.9}$$

where Ψ is the spatial scalar metric perturbation. To leading order in the slow-roll approximation and using the spatially-flat gauge $\Psi = 0$, this can be expressed in terms of the inflaton field as [41]

$$\zeta = -\mathcal{H}\frac{\delta\phi}{\dot{\phi}}. \tag{3.10}$$

An important property of ζ is that it is constant on super-horizon scales ($k/a \ll \mathcal{H}$) if the perturbations are adiabatic, which is guaranteed in single-field models of inflation [40, 66]. To calculate the perturbations generated during single-field inflation, it is therefore sufficient to calculate the perturbations for each mode k briefly after (k/a) becomes small compared to $\mathcal{H}$, since it remains constant afterwards.[2]

Another common gauge invariant measure of the scalar perturbations is the comoving curvature perturbation $\mathcal{R}$ [40]. However, since $\mathcal{R} = \zeta$ during slow-roll inflation and on superhorizon scales, we will not need to distinguish between $\mathcal{R}$ and ζ in this thesis.

3.1.3 Tensor perturbations

Since the metric $g^{\mu\nu}$ is a tensor, it can also have tensor perturbations. Expanding the Einstein-Hilbert action to second order in the tensor perturbations, one finds that the two polarization modes h_+ and $h_\times$ each have the action of a scalar field up to a normalization factor [41]. The tensor perturbations can therefore be calculated just like the perturbations of scalar fields, using eq. (3.7) with [40]

$$v = \frac{a h_{+,\times}}{2}. \tag{3.11}$$

Since they obey the same equations up to a rescaling, tensor and scalar perturbations are tightly related to each other. Their only difference arises from their different normalization proportional to $z/a = \dot{\phi}/\mathcal{H}$ which is determined by the background dynamics of the inflaton field.

Note that the tensor fluctuations are already gauge-invariant [40], so we can directly compare the perturbations calculated for $h_{+,\times}$ with observations.

3.1.4 Power spectra

To compare the statistical properties of scalar and tensor perturbations with observations, we introduce the power spectrum $\mathcal{P}_\varphi(k,t)$ for the quantum field $\hat{\varphi}(t,\vec{x})$ with mode functions $\varphi_k(t)$:

$$\mathcal{P}_\varphi(k,t) \equiv \frac{k^3}{2\pi^2}|\varphi_k(t)|^2. \tag{3.12}$$

[2] In fast-roll inflation, the freeze-out of curvature perturbations can be delayed [67], and special care must be taken to evaluate ζ at a later time after it has become constant.

In inflationary cosmology, the power spectrum only depends on $k = |\vec{k}|$ because the universe is statistically isotropic.

The power spectrum is related to the variance by [41]

$$\langle \varphi^2(t, \vec{x}) \rangle \;=\; \int (\log k) \mathcal{P}_\varphi(k, t). \tag{3.13}$$

In cosmology, this integral is usually divergent both in the infrared (IR) and ultraviolet (UV), so it must be regularized using cutoffs k_{IR} and k_{UV}. The IR divergence is physically harmless since we are not really interested in the entire coordinate space, which may extend over many event horizons, so we can regularize the IR divergence by considering a finite box e.g. of the size of the observable universe or of a single Hubble patch during inflation. The UV divergence is more similar to the usual quantum field theory (QFT) UV divergences, since it arises from summing over contributions with arbitrarily high momenta beyond the validity of our QFT, particularly above the energy scale of quantum gravity. We therefore apply a UV cutoff by hand in order to integrate only over k for which our QFT can be trusted.

Inflaton power spectrum

The power spectrum for the inflaton perturbations can be calculated from the mode functions:

$$\mathcal{P}_{\delta\phi}(k, t) \;=\; \frac{k^3}{2\pi^2} |\phi_k(t)|^2. \tag{3.14}$$

An important special case is the vacuum spectrum from eq. (3.6) which applies during inflation as long as $V''(\phi) \ll k^2/a^2$ and assuming that $\mathcal{H}$ remains approximately constant:

$$\mathcal{P}^{(\mathrm{vac})}_{\delta\phi}(k, t) \;=\; \frac{\mathcal{H}^2 + (k/a)^2}{4\pi^2}. \tag{3.15}$$

Power spectra of curvature and tensor perturbations

During single-field slow-roll inflation and using spatially-flat gauge, we can easily calculate the spectrum of curvature perturbations from $\mathcal{P}_{\delta\phi}$ using eq. (3.10):

$$\mathcal{P}_\zeta(k, t) \;=\; \left(\frac{\mathcal{H}}{\dot{\phi}} \right)^2 \mathcal{P}_{\delta\phi}(k, t). \tag{3.16}$$

Since the curvature perturbation freezes out after the horizon crossing time t_k given by

$$k = a(t_k) \mathcal{H}(t_k), \tag{3.17}$$

we can calculate the spectrum of curvature perturbations after inflation by evaluating eq. (3.16) at the time $\tilde{t}_k$ briefly after horizon exit [41]:

$$\mathcal{P}_\zeta(k, t \gg t_k) \simeq \frac{\mathcal{H}^4(\tilde{t}_k)}{4\pi^2 \dot{\bar{\phi}}^2(\tilde{t}_k)}. \tag{3.18}$$

In practice, since $\mathcal{H}$ and $\dot{\phi}$ vary slowly during slow-roll inflation, one usually sets $\tilde{t}_k = t_k$.

Since the tensor modes have the same equations of motion as the inflaton perturbations, the tensor spectrum is given by the inflaton spectrum except for a numerical factor accounting for canonical normalization and for the two polarization modes [41]:

$$\mathcal{P}_\mathrm{t}(k, t \gg t_k) \simeq \frac{2\mathcal{H}^2(\tilde{t}_k)}{\pi^2}. \tag{3.19}$$

Expansion of $\mathcal{P}_\zeta$ and $\mathcal{P}_\mathrm{t}$ for nearly scale-invariant spectrum

During inflation, the background inflaton field and the Hubble parameter change very slowly. For this reason, the power spectra in eqs. (3.18)–(3.19) depend very weakly on k. This motivates the parametrization of the primordial power spectra in the following way:

$$\mathcal{P}_\zeta(k) = A_\mathrm{s} \left(\frac{k}{k_*}\right)^{n_\mathrm{s}-1+\frac{\alpha_\mathrm{s}}{2}\ln\left(k/k_*\right)+\frac{\kappa_\mathrm{s}}{6}\ln^2\left(k/k_*\right)+\ldots}, \tag{3.20a}$$

$$\mathcal{P}_\mathrm{t}(k) = r \cdot A_\mathrm{s} \left(\frac{k}{k_*}\right)^{n_\mathrm{t}+\frac{\alpha_\mathrm{t}}{2}\ln\left(k/k_*\right)+\frac{\kappa_\mathrm{t}}{6}\ln^2\left(k/k_*\right)+\ldots}, \tag{3.20b}$$

with the amplitude of scalar perturbations A_s, the spectral index n_s, the running α_s, the running of the running κ_s, and the analogous quantities for the tensor spectrum. Note that for historical reasons, a scale-invariant spectrum corresponds to $n_\mathrm{s} = 1$ and $n_\mathrm{t} = 0$ due to their different definitions. Also, the tensor amplitude A_t is usually substituted by the tensor-to-scalar ratio $r = \mathcal{P}_\mathrm{t}(k_*)/\mathcal{P}_\zeta(k_*)$.

k_* is an arbitrary pivot scale. For easy comparison with CMB experiments, k_* should be chosen around $k_* \sim 0.05\ \mathrm{Mpc}^{-1}$ if today's scale factor is set to $a_0 = 1$.

The constraints on the primordial power spectra depend on the assumed cosmological model, see appendix B. In the base ΛCDM model, the recent constraints at 68% CL are [8]

$$A_\mathrm{s} = (2.21 \pm 0.08) \times 10^{-9}, \tag{3.21a}$$

$$n_\mathrm{s} = 0.965 \pm 0.005, \tag{3.21b}$$

with the tensor spectrum and all runnings set to zero by assumption. Allowing for non-zero α_s and κ_s, the bounds at 68% CL are [9]:

$$\alpha_\mathrm{s} = 0.009 \pm 0.010, \tag{3.22a}$$

$$\kappa_\mathrm{s} = 0.025 \pm 0.013. \tag{3.22b}$$

If we extend ΛCDM by $r > 0$, the bound on r at 95% CL is [51]

$$r < 0.09. \tag{3.23}$$

Comment on non-Gaussianity

To leading order in perturbation theory, the perturbations generated from inflation obey a Gaussian distribution. For such Gaussian distributions, the power spectrum contains all information.

However, the corrections from higher orders in perturbation theory can have a non-Gaussian distribution. Since $\delta\phi$ is small, such non-Gaussianity is strongly suppressed. In single-field slow-roll inflation, non-Gaussianity is generally predicted to be too small to be observed with the current experimental precision. However, in multi-field models, some observable degree of non-Gaussianity can be generated.

Since the models discussed in this thesis do not predict observable non-Gaussianity, we do not discuss it here in further detail and instead refer to e.g. [40, 68] for an introduction and further references.

3.2 Primordial perturbations in single-field slow-roll inflation

In single-field inflation, the curvature perturbation ζ is conserved on superhorizon scales $(k/a) \ll \mathcal{H}$, so it is sufficient to calculate the power spectrum around the time of horizon crossing at which $k/a \sim \mathcal{H}$. In principle, this can be achieved in three steps:

- Calculate the background evolution $\overline{\phi}(t)$ and $\mathcal{H}(t)$ from eqs. (2.13)–(2.14) or in the slow-roll approximation from eqs. (2.15)–(2.16).

- Calculate the evolution of the Mukhanov variable v_k from eq. (3.7), using the previously calculated background values for $\overline{\phi}(t)$ and $\mathcal{H}(t)$ to determine $z(\tau)$.

- Convert the results for v_k into $\mathcal{P}_\zeta(k)$ using eqs. (3.9) and (3.12), or using the simpler eq. (3.10) for a result valid to leading order in slow-roll.

This procedure has the advantage that it does not require the slow-roll approximation, so it is applicable very generally and it leads to precise results. However, except for a few special cases, the Mukhanov-Sasaki equation cannot be solved analytically. To get an analytical understanding of a model and its predictions, it is therefore often helpful to use simple analytical approximations.

3.2.1 Power spectra from slow-roll parameters

A particularly useful and widespread method is the calculation of the power spectra directly from the slow-roll parameters around the time of horizon exit. To leading order in the slow-

roll parameters as defined in eqs. (2.18a)–(2.18d), this leads to the result [40, 69, 70]

$$A_\mathrm{s} = \frac{V_*}{24\pi^2\varepsilon_*}, \tag{3.24a}$$
$$r = 16\varepsilon_*, \tag{3.24b}$$
$$n_\mathrm{s} = 1 - 6\varepsilon_* + 2\eta_* + 2q_1\xi_*^2 + 2q_2\sigma_*^3 + ..., \tag{3.24c}$$
$$\alpha_\mathrm{s} = -2\xi_*^2 - 2q_1\sigma_*^3 + ..., \tag{3.24d}$$
$$\kappa_\mathrm{s} = 2\sigma_*^3 + ..., \tag{3.24e}$$

where the stars indicate that a quantity should be evaluated at $\phi = \phi_*$, the dots denote slow-roll parameters involving higher derivatives of $V(\phi)$ which we usually neglect, and $q_1 \simeq 1.063$ and $q_2 \simeq 0.209$ are numerical constants.

ϕ_* can be calculated from eq. (2.20) for a given value of N_*. N_* should be chosen such that modes at the pivot scale k_* freeze out at the time t_* at which $\phi = \phi_*$: $k_* = a(t_*)\mathcal{H}(t_*)$. The precise value of N_* depends on the reheating period at the end of inflation, see chapter 4, but it is usually in the range $N_* \sim 50$–60.

Eqs. (3.24a)–(3.24e) can constrain the derivatives of $V(\phi)$ around ϕ_* from a measurement of the observables A_s, r, n_s, α_s and κ_s. In principle, this allows a reconstruction of the inflaton potential as a Taylor series if the observational constraints are tight enough. This is discussed in more detail in section 12.2.

3.2.2 Energy scale of inflation

Using A_s to rescale the potential

It is important to note that the overall energy scale of inflation only affects the amplitude of scalar perturbations A_s. In fact, it is more useful to write eq. (3.24a) in the form

$$V_* = 24\pi^2\varepsilon_* A_\mathrm{s}. \tag{3.25}$$

It is always possible to rescale the potential to achieve any value of A_s since the other observables in eqs. (3.24b)–(3.24e) depend only on the slow-roll parameters, and the slow-roll parameters consist of derivatives of V divided by powers of V such that any overall prefactor in the potential drops out. Also, the value ϕ_* at which the slow-roll parameters are evaluated does not depend on the overall prefactor of the potential, because such a prefactor also drops out in eq. (2.20).

Therefore, we can always to calculate the slow-roll predictions for a potential

$$V(\phi) = \gamma V_\mathrm{original}(\phi) \tag{3.26}$$

with an arbitrary $\gamma > 0$, then calculate all the predictions, and then choose a different γ using eq. (3.25) to achieve the correct value of A_s without changing any of the other predictions for the primordial spectra. In this sense, A_s is not a prediction of any model of inflation if the potential V contains an unspecified prefactor; instead the prefactor is

predicted using eq. (3.25) by fitting the correct A_s.[3] For example, in the models discussed in section 2.4, A_s is used to determine the coupling λ in chaotic inflation and the vacuum energy V_0 in small-field hilltop and hybrid inflation.

Using r to determine the absolute energy scale V_*

The energy scale of inflation depends not only on the well-measured A_s, but also on ε_*. We can eliminate ε_* in favour of r using eq. (3.24b) and plug in $A_\mathrm{s} = 2.2 \times 10^{-9}$ to find a formula for the energy density in terms of r:

$$V_* \simeq \left(10^{16}\,\mathrm{GeV}\right)^4 \left(\frac{r}{0.01}\right). \tag{3.27}$$

If we were to observe primordial gravity waves and thus some specific value of r, eq. (3.27) would fix the energy scale of inflation. However, so far observations can only put an upper bound $r < 0.09$ at 95% CL, which corresponds to an upper bound on the energy density of about $(2 \times 10^{16}\ \mathrm{GeV})^4$. The only lower bound comes from the requirement that reheating should finish at temperatures above those required for BBN, so inflation must happen at energies above the MeV scale [71].

3.3 δN formalism for multi-field inflation

In multi-field inflation, the calculation of the curvature perturbations is more involved: it is generally not sufficient to calculate $\mathcal{P}_\zeta$ at horizon crossing, and the simple eqs. (3.24a)–(3.24c) are replaced by formulas based on the δN formalism. We now discuss these two issues in turn.

3.3.1 Adiabatic condition for conservation of $\mathcal{P}_\zeta$

In the calculations above, we have assumed that ζ is conserved after horizon crossing so that we could compare its power spectrum $\mathcal{P}_\zeta(k, t_*)$ directly to the observational constraints on the primordial power spectrum without considering its evolution after t_*.[4] However, ζ is only conserved on superhorizon scales for *adiabatic* perturbations which satisfy [66]

$$p = p(\rho). \tag{3.28}$$

This condition is satisfied for single-field slow-roll inflation, because in that case both $p(\phi)$ and $\rho(\phi)$ are functions of the inflaton field ϕ, and $\rho(\phi)$ is monotonously decreasing along

[3] This procedure can only be applied when the one-loop corrections $\Delta V_\mathrm{loop}(\phi)$ to the inflaton potential are negligible, because they scale like $\gamma^2(c + \log\gamma)$, see eq. (5.25). The full inflaton potential can only be written in the required form (3.26) with a linear dependence on γ if $\Delta V_\mathrm{loop}(\phi)$ is negligible.

[4] The perturbations evolve again after horizon re-entry, but that later evolution is based on well-understood post-inflationary physics and is already accounted for in the observational constraints on $\mathcal{P}_\zeta(k)$.

the slow-roll trajectory. We can therefore invert $\rho(\phi)$ during inflation to get $\phi(\rho)$, which leads to $p(\phi(\rho))$ which satisfies eq. (3.28).

In multi-field inflation, the adiabaticity condition is generally not satisfied. Consider the simple example of two decoupled inflaton fields ϕ and χ with $V = \frac{1}{2}m_\phi^2\phi^2 + \frac{1}{2}m_\chi^2\chi^2$. In this case, the energy density $\rho(\phi, \chi)$ cannot be inverted to find functions $\phi(\rho)$ and $\chi(\rho)$, because for any given ρ, the energy might be either in the χ or in the ϕ field or some mixture of the two.

However, even in multi-field models, the adiabaticity condition is usually satisfied at some later time:

- Sometimes the evolution of the fields makes all but one of the fields become irrelevant, e.g. if χ moves towards its minimum $\chi = \chi_{\min}$ and does not contribute significantly to the energy density any more. After that has happened, the remaining field ϕ dominates the energy density so that $\rho(\phi, \chi) \simeq \rho(\phi)$ which can be inverted to give $\phi(\rho)$, and $\chi(\rho) \simeq \chi_{\min}$.

  How small χ must be to be negligible depends on the reheating process. $\chi(t_*) \ll \phi(t_*)$ is not a sufficient condition if χ is very long-lived compared to ϕ: χ can still come to dominate the universe after ϕ has decayed into radiation, since the radiation redshifts faster than the energy in the χ oscillations. In such cases, the adiabatic limit might not be reached before the end of reheating.

- The adiabatic condition is always satisfied after reheating if the entire energy density is converted into a thermal bath of particles with temperature T: in thermodynamic equilibrium, eq. (3.28) is satisfied with $p = p(T(\rho))$. The only non-adiabatic perturbations that can remain are non-thermal relics, e.g. dark matter that was produced non-thermally and never gets into thermal equilibrium, but such cases are constrained by the non-observation of cosmological isocurvature perturbations [9].

In multi-field models, we should calculate the spectrum $\mathcal{P}_\zeta$ at some late time at which the adiabatic condition is satisfied. Then we know that the important superhorizon modes are constant afterwards so that we can directly compare $\mathcal{P}_\zeta(k)$ to the experimental bounds.

3.3.2 δN formalism

A powerful tool for calculating the primordial perturbations in multi-field models of inflation is the δN formalism [72–75]. It is based on the fact that the curvature perturbation $\zeta(t, \vec{x})$ on a uniform-density hypersurface is given by the difference δN in the number of e-folds between a spatially-flat initial hypersurface and the uniform-density final hypersurface:

$$\zeta(t, \vec{x}) \;=\; \delta N(t, \vec{x}) \;=\; N(t, \vec{x}) - N_0(t). \tag{3.29}$$

We choose the initial flat hypersurface at the time t_* at which cosmological scales leave the horizon. The final hypersurface with constant energy density ρ_{final} should ideally be chosen

at some late time at which the perturbations are already adiabatic so that superhorizon modes remain constant afterwards.

As the inflaton fields' perturbations are very small, one can expand δN in powers of the field perturbations $\delta\phi_i$ on the initial flat hypersurface[5] (the index i denotes the i-th inflaton field):

$$\zeta \,=\, \delta N \,=\, \sum_i N_i\,\delta\phi_i \,+\, \sum_{i,j} N_{ij}\,\delta\phi_i\,\delta\phi_j \,+\, O(\delta\phi^3), \tag{3.30}$$

where we introduced the notation

$$N_i \,=\, \frac{\partial N}{\partial(\delta\phi_i)}, \quad N_{ij} \,=\, \frac{\partial^2 N}{\partial(\delta\phi_i)\partial(\delta\phi_j)}. \tag{3.31}$$

Inserting the de Sitter space field perturbations $\langle\delta\phi_i\rangle \,=\, 0$ and $\langle\delta\phi_i^2\rangle \,=\, \mathcal{H}^2/(2\pi)^2$ in eq. (3.30), one can derive the leading-order expression for the amplitude A_s of the primordial curvature perturbation power spectrum:

$$A_\mathrm{s} \,=\, \frac{\mathcal{H}_*^2}{4\pi^2}\sum_i N_i^2 \,=\, \frac{V_*}{12\pi^2}\sum_i N_i^2, \tag{3.32}$$

where a subscript star indicates that a quantity should be evaluated at the time of horizon crossing, and we have used the slow-roll eq. (2.15) to replace $\mathcal{H}_*$ with V_*.

With some extra work, one can also calculate the amplitude f_NL of the reduced bispectrum [73] as a measure of non-Gaussianity:

$$f_\mathrm{NL} \,=\, -\frac{5}{6}\frac{\sum_{ij} N_i N_j N_{ij}}{\left(\sum_i N_i^2\right)^2}, \tag{3.33}$$

and the spectral index n_s of the curvature perturbation [74]

$$n_\mathrm{s} \,=\, 1 - 2(\varepsilon_\mathcal{H})_* - \frac{2\sum_{ij}\left(\frac{\partial V}{\partial\phi_i}\right)_* N_j N_{ij}}{V_*\sum_i N_i^2}, \tag{3.34}$$

with $\varepsilon_\mathcal{H} \,\equiv\, -\dot{\mathcal{H}}/\mathcal{H}^2$ which is identical to ε to leading order in the slow-roll approximation [62]:

$$\varepsilon_\mathcal{H} \,=\, -\frac{\dot{\mathcal{H}}}{\mathcal{H}^2} \,\simeq\, \frac{1}{2V^2}\sum_i\left(\frac{\partial V}{\partial\phi_i}\right)^2 \,=\, \varepsilon. \tag{3.35}$$

For an example of how to use the δN formalism in practical applications, we refer to section 9.5 where we use it to calculate the primordial curvature perturbation in two-field models of new inflation.

[5]The requirement that the initial hypersurface is spatially flat means that the $\delta\phi_i$ must be calculated in spatially-flat gauge.

Chapter 4

Reheating

At the end of slow-roll inflation, the universe is filled with nothing but a nearly homogeneous scalar field and its quantum fluctuations. To successfully make the transition to the radiation-dominated early universe after inflation, the potential energy of the scalar field must be converted into a plasma of relativistic elementary particles. This process is called "reheating".

In this chapter, we will discuss the reheating phase and its implications for building and testing realistic particle physics models of inflation. We start with an overview of the different phases of reheating and the key observables which reheating can affect. We then go on to discuss the linear and non-linear stages of preheating during which particles coupled to the inflaton field can be produced non-perturbatively. Afterwards, we discuss the final stage of reheating by perturbative decays and thermalization.

4.1 Overview

4.1.1 Phases of preheating and reheating

The different phases of preheating and reheating are schematically depicted in fig. 4.1. Preheating starts at $\phi_{\rm e}$ where the inflaton field leaves the flat region of its potential (i.e. when $\varepsilon \gtrsim 1$ or $|\eta| \gtrsim 1$) and starts rolling towards its minimum. In the models relevant for this thesis, we can identify several qualitatively different stages of (p)reheating:

1. **Tachyonic preheating:** When the homogeneous inflaton field rolls down a region of the potential with large tachyonic mass $V''(\phi) \lesssim -\mathcal{H}^2$, its long-wavelength perturbations with $k^2 < -V''(\phi)$ grow exponentially.

   Tachyonic preheating can also happen for non-inflaton fields χ if their mass turns tachyonic. Most prominently, this happens at the end of hybrid inflation, where the waterfall field's vacuum fluctuations grow so rapidly that they quickly terminate inflation [76, 77].

2. **Parametric resonance:** If tachyonic preheating has not made ϕ completely inhomogeneous, the homogeneous inflaton field performs oscillations around the minimum which are damped by the Hubble friction term $3\mathcal{H}\dot{\phi}$ in eq. (2.14). These oscillations can drive resonant enhancement of the perturbations of ϕ and of any scalar field χ which has some suitable coupling to the inflaton field [44].

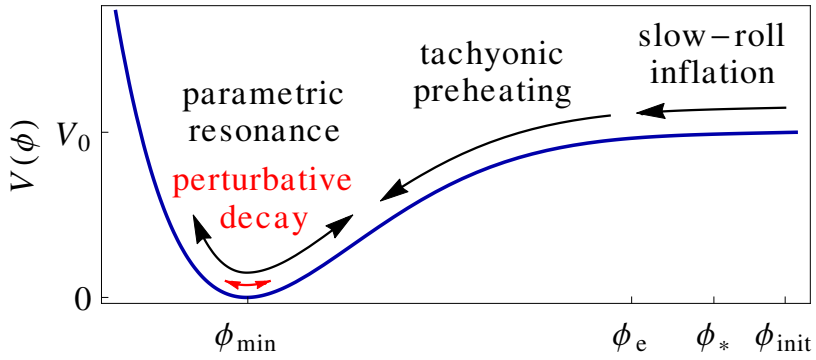

Figure 4.1: Phases of preheating and reheating. After slow-roll inflation ends at $\phi_{\rm e}$, the nearly homogeneous inflaton field quickly accelerates along the steep gradient of the potential towards $\phi_{\rm min}$, around which it performs damped oscillations due to Hubble damping. If it has a large tachyonic mass while rolling down, inflaton perturbations grow via "tachyonic preheating", and when the inflaton later oscillates with large amplitude, this often leads to production of particles coupled to the inflaton via "parametric resonance". Eventually, Hubble damping reduces the oscillation amplitude of the ϕ field so much that it can be interpreted as a collection of individual ϕ particles which decay by perturbative single-particle decays.

3. **Wave scattering and turbulence:** After resonant preheating, additional non-exponential particle production can occur due to driven turbulence [78], and features in the power spectra of perturbations are smeared out by rescattering.

4. **Perturbative decay:** Eventually, Hubble damping reduces the amplitude of all fields so much that they perform small oscillations around the quadratic minimum of the potential. These low-amplitude oscillations can be interpreted as a collection of individual particles of the corresponding fields.[1] If the oscillation amplitude (i.e. the particle density) is small enough, these inflaton particles will decay predominantly by perturbative single-particle decays.

5. **Thermalization:** The decay products are typically SM or MSSM particles which have very strong interactions (e.g. gauge interactions), so they are often assumed to thermalize very quickly [43]. However, thermalization can also be delayed, in which case the evolution of the non-thermal bath of decay products constitutes an extra stage of the reheating process [79, 80].

If preheating is very efficient, even tiny quantum fluctuations grow into perturbations with amplitudes as large as the homogeneous background field. In this case, the perturbative description as a homogeneous background and a small linear perturbation breaks down and the evolution of the universe must be calculated using non-perturbative methods as discussed in section 4.3.

[1] Recall that particles in quantum field theory are quantized excitations around the lowest energy state.

In this thesis, we only consider the preheating of scalar fields. Preheating of fermions is suppressed by Pauli blocking, so it might generically be expected to be subdominant. However, under certain circumstances it is also possible to have sizeable production of fermions during preheating [81, 82], particularly when preheating produces fermions with a broad range of momenta so that Pauli blocking is less effective.

4.1.2 Reheat temperature

A central result of any reheating calculation is the "reheat temperature" $T_{\rm R}$ at which the universe starts to be well-described by a thermal bath of particles.

The reheat temperature determines which particles can be produced as thermal relics: above some threshold temperatures, exotic particles can be produced thermally and later freeze out, leading to a thermal relic abundance determined by their masses and cross sections. For example, in supergravity models, high temperatures lead to an overproduction of gravitinos, which puts an upper bound on the reheat temperature of about $T_{\rm R} < 10^6$–10^{10} GeV, depending on the details of the SUSY model [83–85]. On the other hand, a sufficiently high reheat temperature might allow for thermal production of the correct dark matter abundance or of the baryon asymmetry, depending on the details of the particle physics model [37, 41, 48].

The reheat temperature also affects the expansion history of the early universe and thus N_*, which in turn affects the predictions for the primordial spectrum. The basic idea is that between inflation and reheating, the universe is dominated by a condensate of non-relativistic inflaton particles which redshift with $w \simeq 0$, whereas after reheating the universe is dominated by radiation which redshifts faster with $w \simeq 1/3$. Therefore, the reheat temperature determines the time (or equivalently the energy density) at which the energy density starts to redshift faster, which affects the matching of inflationary to CMB scales [44, 86]:

$$N_* \;=\; 63.3 + \frac{1}{4}\ln\left(\frac{V_*}{(10^{16}\,\mathrm{GeV})^4}\right) + \frac{1}{4}\ln\left(\frac{V_*}{\rho_{\rm end}}\right) - \frac{1}{12}\ln\left(\frac{\rho_{\rm end}}{\rho_{\rm R}}\right), \tag{4.1}$$

where $\rho_{\rm end}$ is the energy density at the end of inflation and $\rho_{\rm R}$ is the energy density at the onset of radiation domination. $\rho_{\rm R}$ is related to the reheat temperature $T_{\rm R}$ via [37]

$$\rho_{\rm R} \;=\; \frac{g_*\pi^2}{30}T_{\rm R}^4, \tag{4.2}$$

where g_* is the effective number of relativistic degrees of freedom with a weighting factor of 7/8 for fermions due to their Fermi statistics, e.g. $g_* = 106.75$ in the SM for $T \gtrsim 300$ GeV and $g_* = 228.75$ in the MSSM for temperatures above the mass of the heaviest visible sector sparticle [48].

4.2 Linear preheating

At the end of slow-roll inflation, the universe is nearly homogeneous, with small inhomogeneities given by vacuum fluctuations for the inflaton field ϕ and for any non-inflaton scalar field χ. We can therefore treat the inhomogeneities $\delta\phi(\vec{x},t)$ and $\delta\chi(\vec{x},t)$ as small perturbations around the classical background fields $\overline{\phi}(t)$ and $\overline{\chi}(t)$ analogously to chapter 3.

4.2.1 Mode equations

Repeating the steps leading to eq. (3.4) and quantizing the fields as in eq. (3.5), we again find the mode equations for $\delta\phi$ and $\delta\chi$:

$$\ddot{\phi}_{\vec{k}} + 3\mathcal{H}\dot{\phi}_{\vec{k}} + \left(\frac{\partial^2 V}{\partial\phi^2}(\overline{\phi},\overline{\chi}) + \frac{k^2}{a^2}\right)\phi_{\vec{k}} + \left(\frac{\partial^2 V}{\partial\phi\partial\chi}(\overline{\phi},\overline{\chi})\right)\chi_{\vec{k}} = 0, \tag{4.3}$$

$$\ddot{\chi}_{\vec{k}} + 3\mathcal{H}\dot{\chi}_{\vec{k}} + \left(\frac{\partial^2 V}{\partial\chi^2}(\overline{\phi},\overline{\chi}) + \frac{k^2}{a^2}\right)\chi_{\vec{k}} + \left(\frac{\partial^2 V}{\partial\phi\partial\chi}(\overline{\phi},\overline{\chi})\right)\phi_{\vec{k}} = 0, \tag{4.4}$$

with initial conditions given by eq. (3.6) at some early time during slow-roll inflation.

These first steps are identical to the calculation of the quantum fluctuations during inflation. During slow-roll inflation, the solution is dominated by the de Sitter space fluctuations due to the nearly constant $\mathcal{H}$, while the potential is so flat that the time-dependent mass term V'' is almost negligible in eqs. (4.3)–(4.4). During preheating, these same equations can have a very different behaviour because V'' is large and changes rapidly. In particular, they can exhibit instabilities which make some modes grow exponentially, which can be interpreted as rapid particle production.

Solving the mode equations for linear preheating

In principle, the effects of linear preheating can always be calculated by solving eqs. (4.3)–(4.4) with initial conditions matched to eq. (3.6) sufficiently early during inflation up to some very late time $t_{\text{final}} = t_{\text{R}}$ at which perturbative reheating is expected to occur.

In practice, it is usually neither possible nor necessary to solve the mode equations over such long time intervals:

- The matching to early times can be performed at different times for each mode k such that $\mathcal{H}$ is still roughly constant and $(k/a)^2 \gg V''$, in which case the de Sitter space solution is a good approximation.
- It is usually also sufficient to solve the mode equations over just a few e-folds up to $t_{\text{final}} \ll t_{\text{R}}$. If preheating is very efficient, the perturbations quickly grow to large values such that linear perturbation theory breaks down and the further evolution must be calculated non-perturbatively (see section 4.3). On the other hand, if preheating is inefficient early on, when oscillation amplitudes are large and V'' varies

most strongly, it is typically even more inefficient later when Hubble damping has reduced the oscillation amplitudes.

4.2.2 Tachyonic preheating

An important special case is "tachyonic preheating", which happens when $V'' < 0$ in eq. (4.3) or eq. (4.4). This occurs e.g. for the waterfall field χ at the end of hybrid inflation [76, 77].

Consider for example a constant tachyonic mass $\partial^2 V/\partial\chi^2 = -m_\chi^2 < 0$ in eq. (4.4):

$$\ddot{\chi}_{\vec{k}} + 3\mathcal{H}\dot{\chi}_{\vec{k}} + \left(m_\chi^2 + \frac{k^2}{a^2}\right)\chi_{\vec{k}} = 0. \tag{4.5}$$

If we consider a time interval much shorter than a Hubble time, we can neglect the expansion of the universe by setting $\mathcal{H} \simeq 0$ and $a \simeq 1$ to find the simple solution for $\chi_{\vec{k}}(t)$ over such a short time interval:

$$\chi_{\vec{k}}(t) \simeq c_{\vec{k}}\, e^{\omega_k t} + d_{\vec{k}}\, e^{-\omega_k t}, \qquad \text{with } \omega_k = \sqrt{m_\chi^2 - k^2}. \tag{4.6}$$

This is an oscillating solution for $k^2 > m_\chi^2$ and an exponentially growing (or decaying) solution for $k^2 < m_\chi^2$, with the fastest growth for infrared modes $k^2 \ll m_\chi^2$.[2]

For $m_\chi \gg \mathcal{H}$, the growing solution will grow extremely large in much less than a Hubble time, even starting from small vacuum fluctuations $\chi_{\vec{k}}(t_0) \sim \mathcal{H}/(2\pi)$. For this reason, in hybrid inflation with $m_\chi \gg \mathcal{H}$ the waterfall transition from $\chi = 0$ to $|\chi| = v$ is practically instantaneous.

Realistically, the mass m_χ is usually not constant throughout preheating. However, even if one includes a time-dependence for $m_\chi(t)$, one still finds that tachyonic mass terms $V'' \lesssim -\mathcal{H}^2$ lead to rapid growth of infrared modes [76].

4.2.3 Parametric resonance

Even for positive masses, large amplitude oscillations of the inflaton around its minimum can lead to rapid growth of perturbations via parametric resonance, both for the inflaton perturbations and for other fields coupled to the inflaton.

This is possible if the oscillation of the inflaton background field leads to strongly oscillating mass terms which violate the "adiabatic condition" [44]:

$$\text{adiabatic condition:} \quad \left|\frac{\dot{\omega}_k}{\omega_k^2}\right| \ll 1, \quad \text{with } \omega_k(t) = \sqrt{V'' + (k/a)^2}. \tag{4.7}$$

[2]The decaying solution is usually discarded because it quickly becomes negligible compared to the growing solution. However, care should be taken when the tachyonic region is crossed several times, e.g. if the inflaton field performs large-amplitude oscillations in a hilltop inflation potential and rolls back up the tachyonic region. In that case, the originally growing mode decays again, and the originally decaying mode grows, such that the growth and decay of the infrared modes over a full oscillation mostly cancels, see section 11.2.

When this condition is violated, the mode equations often have instabilities for certain wavenumbers k so that the spectrum of perturbations develops a peak around those unstable wavenumbers.

The instabilities can be calculated for quasi-periodic motion using a Floquet analysis as explained in [44]. Since Floquet theory only applies to periodic motion, this is possible only if Hubble damping is negligible over a single oscillation so that we can set $\mathcal{H} = 0$.

4.2.4 End of linear preheating

Linear preheating ends in one of two ways:

- If the perturbations $\delta\phi$ or $\delta\chi$ are amplified so strongly that non-linear terms like $\delta\phi^2$ or $\delta\chi^2$ can no longer be neglected, linear perturbation theory breaks down. This is particularly the case if the perturbation amplitude $\sqrt{\langle\delta\phi^2\rangle}$ becomes comparable to the background field's oscillation amplitude. In this case, the subsequent stages of preheating must be studied using non-linear methods like lattice simulations, see section 4.3.

- If all perturbations $\delta\phi$ and $\delta\chi$ remain sufficiently small throughout linear preheating, the universe remains dominated by the homogeneous inflaton field (plus small perturbations). The oscillation amplitudes continue to drop due to Hubble damping and preheating becomes increasingly ineffective. Eventually, the field amplitudes drop to such low values that the oscillating fields can be interpreted as collections of individual particles which decay via perturbative single-particle decays as explained in section 4.4.

4.3 Non-linear preheating

If preheating is efficient, perturbations quickly grow to large values so that linear perturbation theory becomes inapplicable. In this sense, linear perturbation theory is only useful to check whether or not preheating is efficient; to determine the outcome of efficient preheating, we must use other methods.

Semiclassical approach

In principle, the evolution of the universe featuring inhomogeneous scalar fields ϕ_i in FRW spacetime is given by the equation of motion for the field operators:

$$\ddot{\hat{\phi}}_i - \frac{1}{a^2}\vec{\nabla}^2\hat{\phi}_i + 3\mathcal{H}\dot{\hat{\phi}}_i + \frac{\partial V}{\partial\hat{\phi}_i} = 0. \tag{4.8}$$

A non-perturbative solution to the full quantum theory is generally not available. In the case of efficient preheating, we can instead work with a semiclassical approach:

- We work with classical fields ϕ_i which evolve according to the classical eq. (3.1). Since the large amplification of perturbations ensures large occupation numbers, we expect the classical limit to give a reasonably accurate description of the universe.
- The initial conditions are taken from the quantum theory: the fields ϕ_i are initialized as Gaussian random fields with correlators as computed from linear perturbation theory, at a sufficiently early time when the quantum fluctuations are still small and Gaussian.

In principle, the inhomogeneous ϕ_i can source perturbations of the metric which then backreact on the ϕ_i. This effect can be included by considering the metric perturbations as additional dynamical fields, though it is usually very small even for totally inhomogeneous and violent preheating [87]. For this reason, the metric backreaction is often neglected in calculations of preheating.

Lattice simulations

The problem is then reduced to solving the partial differential eq. (3.1) for some given initial conditions. In practice, this calculation is performed numerically using lattice simulations. Instead of d continuous spatial dimensions, we consider a discrete lattice with N^d comoving spatial grid points separated by a distance Δx:

$$\vec{x}_{i_1 \ldots i_d} = (i_1, ..., i_d)\Delta x, \qquad \text{with } i_1, ..., i_d \in \{1, N\}, \tag{4.9}$$

and we impose periodic boundary conditions at the edges of the lattice. Eq. (3.1) is thus converted from a partial differential equation into a set of N^d coupled ordinary differential equations (using a suitable discretization of the $\vec{\nabla}^2$ operator) which can be solved by standard numerical techniques.

The discretization introduces infrared and ultraviolet cutoffs k_{IR} and k_{UV} due to the maximum size $L = N\Delta x$ and the minimum distance Δx:

$$k_{\mathrm{IR}} = \frac{2\pi}{L} = \frac{2\pi}{N\Delta x}, \qquad k_{\mathrm{UV}} = \frac{2\pi}{\Delta x}. \tag{4.10}$$

Therefore, Δx and N must be chosen such that the most important perturbation modes (i.e. those which are amplified most) are within the range of scales spanned by the two cutoffs. In particular, if the largest and smallest relevant comoving scales are k_{max} and k_{min}, then the minimum required number of lattice points is

$$N^d = \left(\frac{k_{\mathrm{UV}}}{k_{\mathrm{IR}}}\right)^d \gg \left(\frac{k_{\mathrm{max}}}{k_{\mathrm{min}}}\right)^d, \tag{4.11}$$

which makes lattice simulations feasible only for models with a sufficiently small range of relevant comoving length scales.[3]

[3]The errors from discretization and imposing periodic boundary conditions are largest close to the cutoffs, so the cutoffs should be sufficiently far away from the most important scales to allow for good numerical precision in the relevant region.

Lattice simulations can be performed using publicly available codes, e.g. LATTICEEASY [88], DEFROST [87] or HLattice [89], of which HLattice also supports the inclusion of metric perturbations which are always neglected in LATTICEEASY and DEFROST.

4.4 Perturbative reheating

Over time, Hubble damping reduces all fields' oscillation amplitudes so that both the homogeneous background oscillations and the inhomogeneous perturbations eventually turn into small excitations around the minimum of the potential. These might be interpreted as a collection of individual particles which decay predominantly by single-particle decays [90].

If there is no efficient preheating, the energy is completely given by the homogeneous inflaton oscillations which have $k = 0$, so the inflaton particles are at rest with a particle number density

$$n_\phi \;=\; \rho_\phi / m_\phi, \tag{4.12}$$

where m_ϕ is the mass of ϕ at the minimum of the potential and $\rho_\phi = \frac{1}{2}\dot{\phi}^2 + \frac{1}{2}m_\phi^2\phi^2$.

In the case of efficient preheating, the energy density is usually transferred to the inhomogeneous modes with some larger k either of the inflaton ϕ or of some other particles χ_i or a combination of both. In this case, a detailed preheating calculation is required to find the correct initial conditions for the subsequent perturbative reheating phase.

4.4.1 Evolution of energy densities with single-particle decays

If the field amplitudes and momenta for all oscillating fields ϕ_i have been sufficiently redshifted at the start of perturbative reheating, we can work with evolution equations for the energy densities ρ_i for the non-relativistic matter species and $\rho_{\rm rad}$ for radiation [37]:

$$\dot{\rho}_i + 3\mathcal{H}\rho_i \;=\; -\Gamma_i \rho_i, \tag{4.13}$$

$$\dot{\rho}_{\rm rad} + 4\mathcal{H}\rho_{\rm rad} \;=\; \sum_i \Gamma_i \rho_i, \tag{4.14}$$

where the Γ_i are the decay rates for particle species i and we assume that all of the non-relativistic components decay into radiation.[4]

Eqs. (4.13)–(4.14) have very intuitive explanations. The terms $3\mathcal{H}\rho_i$ and $4\mathcal{H}\rho_{\rm rad}$ account for the dilution and redshifting of matter and radiation in an expanding universe, the decay

[4] If decays of one non-relativistic component ρ_i into another non-relativistic component ρ_j are possible and not negligible, the decay products of species j often have large momenta $k \gtrsim m_j$. In that case, j cannot be consistently modelled as a non-relativistic matter species. If the mass ratios are such that species i can decay into non-relativistic j, then these decays can be straightforwardly included in eq. (4.13) by adding the decay term to species i and adding a corresponding source term to species j.

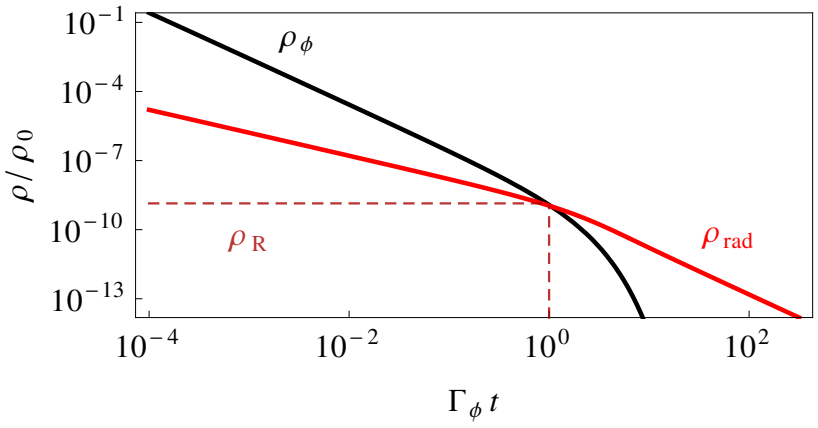

Figure 4.2: Evolution of energy densities during perturbative reheating from eqs. (4.13)–(4.14), assuming that a single inflaton field ϕ dominates the energy density after preheating. For $\Gamma_\phi < \mathcal{H}$ (which corresponds to $t < \Gamma_\phi^{-1}$), the effect of inflaton decays is negligible: the produced radiation energy density $\rho_{\rm rad}$ remains subdominant due to rapid redshifting, while $\rho_\phi \propto a^{-3}$ due to the expansion of the universe. Only for $\Gamma_\phi \gtrsim \mathcal{H}$ (which corresponds to $t \gtrsim \Gamma_\phi^{-1}$), the inflaton decay becomes effective and the energy is quickly converted to radiation. The dashed horizontal line denotes the reheating energy density $\rho_{\rm R}$ from the approximate eq. (4.15) which turns out to capture the numerical result very well.

rate term in eq. (4.13) describes the loss of particles due to single-particle decays, and the decay rate term in eq. (4.14) describes the creation of decay products from these decays.

$\rho_{\rm rad}$ includes all particles whose mass is negligible compared to the energy densities during reheating, e.g. SM or MSSM particles. We assume that they thermalize very quickly due to their gauge interactions so that $\rho_{\rm rad}$ describes a thermal bath of radiation, and reheating is complete when $\rho_{\rm rad}$ begins to dominate the universe.

With these simplifying assumptions, the late-time dynamics of reheating is determined by the coupled eqs. (2.6), (4.13) and (4.14). In particular, we can find the reheat temperature $T_{\rm R}$ from the energy density $\rho_{\rm R}$ at the time at which $\rho_{\rm rad}$ starts to dominate and we can track the abundance of non-thermal relics if we include them explicitly in eq. (4.13) (see e.g. eq. (4.16) for how to track the non-thermally produced lepton number).

4.4.2 Reheat temperature from inflaton decay rate

If reheating starts with only a single non-relativistic component ρ_ϕ (e.g. if preheating is not efficient and the energy density is dominated by the homogeneous oscillating inflaton field), the behaviour of eqs. (4.13)–(4.14) becomes particularly simple, see fig. 4.2. While $\mathcal{H} > \Gamma_\phi$, the effects of expansion dominate over the effects of the inflaton decay: redshifting dilutes away the radiation generated from the decays, and $\rho_\phi \gg \rho_{\rm rad}$. But eventually, the energy density is diluted to $\mathcal{H} < \Gamma_\phi$, after which point the conversion of ρ_ϕ into radiation is very rapid compared to the redshifting so that the universe quickly becomes dominated by radiation.

For a simple estimate, one can assume instantaneous decay of ρ_ϕ into radiation at the time when $\Gamma_\phi = \mathcal{H}$ so that $\rho_\mathrm{R} = 3\mathcal{H}_\mathrm{R}^2 \sim 3\Gamma_\phi^2$, which can be plugged into eq. (4.2) to find the reheat temperature [44]. A more precise result can be obtained from an approximate analytical solution to eqs. (4.13)–(4.14), which leads to the same functional form but a slightly different prefactor [37]:

$$T_\mathrm{R} \simeq \frac{1.2}{g_*^{1/4}}\sqrt{\Gamma_\phi}. \tag{4.15}$$

As shown in fig. 4.2, eq. (4.15) approximates the numerical solution of eqs. (4.13)–(4.14) very well.

4.4.3 Leptogenesis and dark matter abundance

Beyond the reheat temperature, which is important mostly for calculating N_* and for determining which particles can be produced as thermal relics (see section 4.1.2), perturbative reheating is also useful for calculating the non-thermal production of e.g. dark matter or net baryon number. For this purpose, the relevant out-of-equilibrium quantity should be added as an independent component to eq. (4.13) to keep track of its evolution during the reheating period.

An important example is non-thermal leptogenesis [91–95], the creation of net lepton number from inflaton decays, which happens naturally if the inflaton is identified with one of the right-handed sneutrinos [26] or if it decays through them [96]. To keep track of the lepton number density n_L, we can integrate [26]

$$\dot{n}_L + 3\mathcal{H}n_L = \sum_i \epsilon_i \Gamma_i \frac{\rho_i}{m_i}, \tag{4.16}$$

where ϵ_i is the net lepton number produced per single-particle decay of particle species i. Together with the entropy density s during radiation domination [37]

$$s = \frac{2\pi^2}{45} g_* T^3, \tag{4.17}$$

this allows us to calculate n_L/s at the time of reheating. For an adiabatically expanding universe, $s \propto a^{-3}$, thus n_L/s is not diluted by the expansion.

The lepton asymmetry is later converted to a baryon asymmetry by sphaleron processes, with

$$\frac{n_B}{n_\gamma} = 7.04\,\frac{n_B}{s} = 7.04\,\frac{C}{C-1}\frac{n_L}{s}, \tag{4.18}$$

where the conversion factor C depends on the particle content of the theory, with $C \simeq 1/3$ in the MSSM [91], and the relation of the entropy density s to today's photon density n_γ is given by $s = 7.04\,n_\gamma$ [37].

The prediction from reheating can then be compared to the empirical value $n_B/n_\gamma = (6.11 \pm 0.04) \times 10^{-10}$ which follows from the ΛCDM bound on $\Omega_B h^2 = (2.230 \pm 0.014) \times 10^{-2}$ [8] and $n_B/n_\gamma = (2.74 \times 10^{-8})\Omega_B h^2$ [91].

Chapter 5

Inflation in supergravity

In the past few chapters, we have discussed how to analyse inflation and preheating given the scalar potential $V(\vec{\phi})$ for all scalar fields $\vec{\phi} = (\phi_1, ..., \phi_n)$. We now explain how to construct the scalar potential V in supersymmetric models.

We start with a brief introduction to supersymmetry (SUSY), supergravity (SUGRA), the Minimal Supersymmetric Standard Model (MSSM), and their motivation from particle physics. We then discuss how to construct the scalar potential for chiral superfields from the superpotential W and the Kähler potential K. Finally, we introduce supersymmetric models of inflation, in particular SUSY realizations of new inflation and hybrid inflation.

This chapter will be focused on those aspects of supersymmetric model building which are relevant for inflation. For a more complete introduction to SUSY, we refer to e.g. [46, 47]. For an introduction to the MSSM, see e.g. [45, 48, 97].

5.1 Supersymmetry and supergravity

Supersymmetry is a postulated additional symmetry which relates bosons and fermions. In supersymmetry, fermions and bosons always come in pairs with equal masses and identical transformation properties under internal symmetries (e.g. gauge symmetries).

Since we do not observe these superpartners of equal mass in nature, supersymmetry must be spontaneously broken at low energies so that the superpartners to the Standard Model particles are out of reach of previous collider experiments. However, even spontaneously broken SUSY retains some properties which make it an attractive option for particle physics beyond the Standard Model.

5.1.1 Motivation

Beyond the theoretical beauty of SUSY as the unique non-trivial extension of the Poincaré group [98, 99], there are many phenomenologically attractive features of SUSY in general and the MSSM in particular: it solves the hierarchy problem, improves gauge coupling unification and provides a dark matter candidate.

Hierarchy problem

The mass of the scalar electroweak Higgs particle receives large radiative corrections Δm_h^2 from new physics above the electroweak scale, e.g. for a heavy scalar field X [45]

$$\Delta m_h^2 \sim \frac{\lambda}{8\pi^2} \cdot m_X^2 \ln(m_X^2) + ..., \tag{5.1}$$

where m_X is the mass of X and λ is its coupling to the Higgs particle.[1] Due to these large corrections, the Higgs mass will naturally be of the order of the highest mass scale of the theory unless the corrections and the tree-level contributions somehow cancel to the small observed value of $m_h \simeq 125$ GeV. If there is any new mass scale far above the electroweak scale, as e.g. in most models of inflation, this requires extreme fine-tuning.

In unbroken SUSY, the masses and couplings of fermions and bosons are related such that the corrections Δm_h^2 due to heavy fermions and heavy bosons automatically cancel each other, thus solving the hierarchy problem. For broken SUSY, some radiative corrections proportional to the SUSY breaking masses $m_{\rm SUSY}$ remain. To keep the fine-tuning small, $m_{\rm SUSY}$ should not be much greater than the electroweak scale, which is one of the primary reasons for expecting to find superpartners at TeV energies.

Grand Unification

In Grand Unified Theories (GUTs), the $SU(3) \times SU(2) \times U(1)$ product gauge group of the Standard Model is unified in a simple Lie group, e.g. $SU(5)$ or $SO(10)$, which is spontaneously broken to the SM gauge group below some energy $M_{\rm GUT}$. Such an approach also unifies the matter content of the SM. In $SO(10)$, for example, the fermions are contained in a single 16-plet per fermion family, with a right-handed neutrino automatically included [11].

However, unification of the SM gauge groups requires that the gauge couplings meet at some GUT symmetry breaking scale $M_{\rm GUT}$.[2] Unfortunately, the three gauge couplings do not meet in a single point in the SM. In the MSSM, the added superpartners change the running of the gauge couplings so that they approximately meet at the scale $M_{\rm GUT} \simeq 2 \times 10^{16}$ GeV [21, 22]. This makes the MSSM an attractive starting point for GUT model building.

Dark matter

Supersymmetric theories generally need an extra symmetry called R-parity to suppress exotic processes like proton decay [45]. One consequence of R-parity is that it makes the lightest supersymmetric particle (LSP) stable. If the LSP is not electrically charged, e.g. if

[1] Even indirect couplings e.g. via gauge interactions lead to similar corrections due to two-loop diagrams; the hierarchy problem is generic for heavy particles and does not depend on a particular type of coupling to the Higgs. It also applies to most other new physics at high energy scales like condensates or compactified extra dimensions. [45]

[2] This can be circumvented if the GUT symmetry is broken to the SM in multiple stages, see e.g. [12, 13].

the LSP is a neutralino or a gravitino, it is therefore an attractive dark matter candidate [18–20].

5.1.2 $N = 1$ supersymmetry

Since supersymmetry transforms bosons and fermions into each other, the supersymmetry generator Q is an anticommuting Weyl spinor — it carries half-integer spin and changes the commutation properties of the state it acts on. The $N = 1$ supersymmetry algebra[3] for this generator is given by [46]

$$\{Q_\alpha, \bar{Q}_{\dot{\beta}}\} = 2\sigma^\mu_{\alpha\dot{\beta}} P_\mu, \tag{5.2}$$

$$\{Q_\alpha, Q_\beta\} = \{\bar{Q}_{\dot{\alpha}}, \bar{Q}_{\dot{\beta}}\} = 0, \tag{5.3}$$

where α and β are spinor indices, $\bar{Q} = Q^\dagger$, $\sigma^\mu = (1, \vec{\sigma})$ and P_μ is the four-momentum operator.

Since fermions and bosons transform differently under Poincaré transformations, supersymmetry does not commute with Poincaré symmetry. Instead, the generators of SUSY and Poincaré transformations become part of a larger super-Poincaré algebra, with mixed commutators given e.g. in [46].

In this thesis, we assume that supersymmetry is a local symmetry. Since supersymmetry is a non-trivial extension of the Poincaré algebra, local supersymmetry implies general coordinate transformations, and as such it is a theory of gravity. For this reason, local supersymmetry is known as supergravity.

The representations of $N = 1$ supersymmetry are supermultiplets containing a boson and a fermion which differ by spin $\frac{1}{2}$ [46]. In this thesis, we only explicitly need chiral supermultiplets which contain one Weyl fermion field and one complex scalar field. In addition, a complete model also has vector supermultiplets which contain one gauge boson and one Weyl fermion, and a gravity supermultiplet which contains one spin-2 graviton and one spin-$\frac{3}{2}$ gravitino.

5.2 Supergravity Lagrangians for chiral superfields

In this section, we discuss how to construct the supergravity Lagrangian from a superpotential W and a Kähler potential K.

To analyse supersymmetric models of inflation, we are particularly interested in the scalar fields of the theory. We therefore focus on the case of chiral superfields $\hat{Y}_i$, each of which consists of a complex scalar field Y_i and a spin-$\frac{1}{2}$ Weyl fermion ψ_{Y_i}. For the

[3] It is possible to further extend the symmetry to $N \geq 2$ supersymmetry involving multiple supersymmetry generators. Such an extended symmetry implies a symmetry between left- and right-handed particles [46], so it must be broken to allow for the parity violating gauge group of the Standard Model. We only consider $N = 1$ supersymmetry in this thesis.

construction of Lagrangians involving spin-1 gauge bosons and spin-$\frac{1}{2}$ gauginos or the spin-2 graviton and spin-$\frac{3}{2}$ gravitino, see e.g. [45–47, 100].

We start with the scalar potential $V = V_F + V_D$, where V_F applies to all scalar fields and V_D is an extra contribution for fields which are charged under a gauge symmetry. We also provide formulas for the kinetic terms and for the fermion masses.

5.2.1 F-term scalar potential

The F-term scalar potential is determined by the superpotential W and the Kähler potential K [45–47]:

- The superpotential $W(Y_1, ..., Y_n)$ is a holomorphic function of the complex scalar fields Y_i. It has dimension [mass]^3, it must be invariant under gauge symmetry transformations, and it has two units of $U(1)_R$ charge.

- The Kähler potential $K(Y_1, ..., Y_n, Y_1^*, ..., Y_n^*)$ is a real function of the scalar fields Y_i and the complex conjugate fields Y_i^*. It has dimension [mass]^2 and it must be invariant under both gauge symmetry and $U(1)_R$ symmetry transformations.

Then the F-term scalar potential is [46, 47]

$$V_F = \mathrm{e}^K \left(\mathcal{D}_i K^{i\bar{j}} \mathcal{D}_j^* - 3|W|^2 \right), \tag{5.4}$$

where $K^{i\bar{j}}$ is the matrix inverse of the Kähler metric $K_{\bar{i}j} = \partial^2 K/(\partial Y_i^* \partial Y_j)$, and

$$\mathcal{D}_i \, = \, W_i + W K_i, \tag{5.5}$$

with lower indices i on W and K denoting a partial derivative with respect to Y_i.

The renormalizable part of V_F only depends on W:

$$V_F^{(\mathrm{ren})} \, = \, \sum_i |W_i|^2. \tag{5.6}$$

However, during slow-roll inflation, the Planck-suppressed corrections to the F-term inflaton potential are generically important (see section 5.4.3), so eq. (5.6) is mostly useful for post-inflationary physics and for estimates of the dynamics of heavy non-inflaton fields.

5.2.2 D-term scalar potential

For fields which are charged under a gauge symmetry, the scalar potential has an additional contribution, the so-called D-term potential V_D:

$$V \, = \, V_F + V_D. \tag{5.7}$$

V_D is related to the gauge transformation of the scalar fields [46]:

$$V_D \;=\; \sum_{a,b} \frac{g_a g_b}{2} \left(\mathrm{Re}\, f_{ab}^{-1}\right) G_i (T_a)^{ij} Y_j \, G_k (T_b)^{kl} Y_l, \tag{5.8}$$

where the indices a and b run over the generators T_a of the gauge group, g_a is the gauge coupling for the generator a, $f_{ab}(Y_i)$ is the gauge kinetic function which is δ_{ab} in the renormalizable case, and

$$G_i \;=\; K_i + \frac{W_i}{W}. \tag{5.9}$$

In the renormalizable SUSY case, the D-term potential has the simpler form [45]

$$V_D^{(\mathrm{ren})} \;=\; \frac{1}{2} \sum_a g_a^2 \left(Y_i^* (T_a)^{ij} Y_j \right)^2. \tag{5.10}$$

For MSSM gauge couplings g_i, the D-term potential for gauge non-singlets is generically extremely steep compared to the slow-roll inflaton potential. Throughout this thesis, we therefore assume that inflation happens along a "D-flat" trajectory so that V_D vanishes. For this reason, we will rarely include V_D explicitly, but interpret $V_D = 0$ as an a priori constraint on possible inflaton trajectories (see section C.1 for an example in Kähler-driven tribrid inflation).

5.2.3 Kinetic terms

The Kähler metric also rescales the kinetic terms for both scalars and fermions [46]:

$$\mathcal{L}_{\mathrm{kin}}^{(\mathrm{s})} = K_{\bar{i}j} (\partial_\mu Y_i)^* (\partial^\mu Y_j), \tag{5.11}$$

$$\mathcal{L}_{\mathrm{kin}}^{(\mathrm{f})} = K_{\bar{i}j} \, \Psi_i^\dagger \, i \bar{\sigma}^\mu \partial_\mu \, \Psi_j. \tag{5.12}$$

Canonical kinetic terms are generated from the canonical Kähler potential

$$K_{\mathrm{can}} \;=\; \sum_i Y_i^* Y_i. \tag{5.13}$$

A general Kähler potential can have further terms like $\kappa_i |Y_i|^4 / m_{\mathrm{Pl}}^2$ which can lead to more complicated kinetic terms. Since the formulas in chapters 2–4 for inflation assume canonical kinetic terms, the inflaton field must in principle be redefined as $\phi \to \tilde{\phi} = f(\phi)$ with a function $f(\phi)$ chosen such that the inflaton is canonically normalized throughout slow-roll inflation. However, if the additional terms in the Kähler potential are Planck-suppressed, the corrections due to canonical normalization are usually negligible in small-field models of single-field inflation (see appendix B of [28]).

5.2.4 Fermion mass matrix

To calculate the one-loop quantum corrections to the effective potential, we also need the mass matrix of the fermionic superpartners of the Y_i [46]:

$$(m_F)_{ij} = \mathrm{e}^{K/2}\left(W_{ij} + K_{ij}W + K_iW_j + K_jW_i + K_iK_jW - K^{k\bar{l}}K_{ij\bar{l}}\mathcal{D}_k\right), \tag{5.14}$$

with lower indices i on W and K denoting a partial derivative with respect to Y_i and lower indices $\bar{i}$ denoting a partial derivative with respect to Y_i^*. This fermion mass matrix consists of a simple renormalizable contribution W_{ij} plus Planck-suppressed supergravity corrections which are more complicated but often negligible.

5.3 The Minimal Supersymmetric Standard Model

The MSSM is the minimal supersymmetric extension of the Standard Model. Each of the SM fermions gets a scalar superpartner with which it forms a chiral superfield. In addition, the MSSM has chiral superfields for two separate Higgs doublets H_u and H_d, because the masses for up-type quarks and for down-type quarks cannot be generated by the same Higgs doublet in a supersymmetric theory [45, 46]. Finally, each of the SM vector fields gets a spin-$\frac{1}{2}$ superpartner with which it forms a vector supermultiplet.

The superpotential of the MSSM is [45]

$$W_{\mathrm{MSSM}} = y_{ij}^{(u)}Q_iH_uU_j + y_{ij}^{(d)}Q_iH_dD_j + y_{ij}^{(e)}L_iH_dE_j + \mu H_uH_d, \tag{5.15}$$

with implied summation over the family indices i and j. Q_i are the left-handed squark doublets, L_j are the left-handed slepton doublets, U_j and D_j are the right-handed up- and down-type squarks, E_j are the right-handed charged sleptons, the y_{ij} are the Yukawa matrices and μ is a mass parameter.

Motivated by the observed neutrino masses, the MSSM can also be extended by chiral multiplets made of right-handed neutrinos ψ_{N_j} and scalar sneutrinos N_j with the additional superpotential terms (again with implied summation over i and j):

$$\Delta W_{\mathrm{MSSM}}^{(\nu)} = y_{ij}^{(\nu)}L_iH_uN_j + \frac{1}{2}(m_N)_iN_i^2, \tag{5.16}$$

with $m_N = 0$ for Dirac neutrinos and $m_N \neq 0$ for Majorana neutrinos. Then the small neutrino masses can be generated either by choosing very small neutrino Yukawa couplings $y^{(\nu)}$ or by choosing large m_N to suppress the neutrino masses via the see-saw mechanism.

We know that SUSY must be broken spontaneously because we do not observe superpartners of equal mass. There are many possible mechanisms for SUSY breaking and it is not clear which of them might be realized in nature. However, in many cases SUSY breaking can be accounted for by adding dimensionful "soft SUSY breaking" parameters to the low-energy Lagrangian by hand, e.g. additional mass terms for the superpartners

of the SM fields [45, 100]. These soft SUSY breaking terms are often assumed to be TeV scale parameters: for smaller SUSY breaking masses, collider searches should have found some of the superpartners already, whereas for much larger SUSY breaking masses, SUSY can no longer solve the hierarchy problem.

For the purpose of this thesis, we assume that soft SUSY breaking is small enough to be negligible during inflation. This is a very weak assumption, as the energy scales during inflation in the models we consider are typically all above 10^{10} GeV, and the inflationary vacuum energy $V \simeq 3\mathcal{H}^2$ breaks SUSY very strongly during inflation.

5.4 Supersymmetric models of inflation

In this section, we discuss supersymmetric realizations of the new inflation and hybrid inflation models introduced in section 2.4. We will introduce the superpotentials that lead to these models, the conditions under which they become single-field models, and the non-renormalizable operators from the Kähler potential which generically generate Hubble-sized mass terms for all fields.

5.4.1 SUSY new inflation

New inflation can be realized in SUSY starting from the superpotential [29–31]

$$W_{\text{hilltop}} \;=\; \sqrt{V_0}\, S \left(1 - \frac{\Phi^\ell}{\mu^\ell}\right), \tag{5.17}$$

with complex scalar fields S and Φ, dimensionful constants $V_0 > 0$ and $\mu > 0$ and an integer $\ell \geq 3$.[4] Up to higher-order terms $\Delta W \propto S\Phi^{n\ell}$ with $n \geq 2$, this superpotential can be fixed by a $\mathbb{Z}_\ell$ and an $U(1)_R$ symmetry if the S field carries two units of $U(1)_R$ charge and the Φ field carries one unit of $\mathbb{Z}_\ell$ charge.

We also include the leading terms in a power series expansion of the Kähler potential

$$K \;=\; |S|^2 + |\Phi|^2 + (1+\beta)\,|\Phi S|^2 - \kappa_S\,|S|^4 + ... \tag{5.18}$$

Assuming that inflation happens along a D-flat direction, the scalar potential can be calculated from W and K using eq. (5.4):

$$V \;\simeq\; V_0 \left|1 - \frac{\Phi^\ell}{\mu^\ell}\right|^2 + \frac{\ell^2 V_0}{\mu^{2\ell}} \left|S\Phi^{\ell-1}\right|^2 + V_0(4\kappa_S\,|S|^2 - \beta\,|\Phi|^2). \tag{5.19}$$

We assume that $\kappa_S \gg \frac{1}{12}$ so that S has a mass above the Hubble scale $\mathcal{H}$ and is stabilized at 0 during inflation. We can then neglect this field from now on. We can also write the scalar component of Φ in terms of its modulus ϕ and phase θ:

$$\Phi \;=\; \frac{\phi}{\sqrt{2}} e^{i\theta}. \tag{5.20}$$

[4] $V_0 > 0$ and $\mu > 0$ can always be realized by field redefinitions $S \to e^{-i\arg(\sqrt{V_0})} S$ and $\Phi \to e^{i\arg(\mu)}\Phi$.

If $\theta = 2n\pi/\ell$ for some integer n, the model reduces to single-field hilltop inflation. In this case, the inflaton potential is

$$V \simeq V_0\left|1 - \frac{\phi^\ell}{v^\ell}\right|^2 - \frac{\beta V_0}{2}\phi^2, \tag{5.21}$$

with $v = \sqrt{2}\mu$, which is identical to eq. (2.26) up to the additional supergravity mass term $\Delta m_\phi^2 = -\beta V_0$.

In the more general case with $\arg(\Phi) \neq 2n\pi/\ell$, SUSY new inflation is actually a two-field model, and the extra degree of freedom can have an impact on the observables, particularly on n_s. This is discussed in more detail in chapter 9.

5.4.2 SUSY hybrid inflation

The simplest SUSY hybrid model is given by the superpotential [101–103]

$$W_\mathrm{hybrid} = \sqrt{V_0}\, S\left(1 - \frac{H^2}{\mu^2}\right), \tag{5.22}$$

where S and H are complex scalar fields and V_0 and μ are constants. Note that this superpotential is identical to the new inflation superpotential of eq. (5.17) with $\ell = 2$ and $H = \Phi$. Therefore, the scalar potential is given by eq. (5.19), provided that we again write K as in eq. (5.18) (with $\Phi \to H$).

For hybrid inflation, we assume that $\kappa_S \ll \frac{1}{12}$ so that S has a potential flat enough for slow-roll. With the definitions $S \equiv e^{i\theta}\phi/\sqrt{2}$, $H \equiv (\chi + i\psi)/\sqrt{2}$ and $\mu \equiv v/\sqrt{2}$, eq. (5.19) can be rewritten as

$$\begin{aligned} V = {} & V_0\left(1 - \frac{\chi^2}{v^2}\right)^2 + \frac{4V_0}{v^4}\phi^2\chi^2 + 2\kappa_S V_0\phi^2 - \frac{\beta V_0}{2}\chi^2 \\ & + \frac{V_0}{v^2}\left(2 + \frac{4\phi^2}{v^2} - \frac{\beta v^2}{2}\right)\psi^2 + \frac{V_0}{v^4}\left(2\chi^2\psi^2 + \psi^4\right). \end{aligned} \tag{5.23}$$

With sub-Planckian $v \ll 1$ and $\beta \lesssim \mathcal{O}(1)$, ψ has a positive super-Hubble mass and is stabilized at $\psi = 0$, so we can neglect it. Then the remaining scalar potential $V(\phi, \chi)$ is identical to the hybrid inflation potential of eq. (2.31) except for a Hubble-sized extra mass for χ:

$$V(\phi, \chi) = V_0\left(1 - \frac{\chi^2}{v^2}\right)^2 + \frac{\lambda}{2}\phi^2\chi^2 + \widetilde{V}_\mathrm{tree}(\phi) - \frac{1}{2}\beta V_0\chi^2, \tag{5.24}$$

with $n = 2$, $\lambda = 8V_0/v^4$ and $\widetilde{V}_\mathrm{tree}(\phi) = 2\kappa_S V_0\phi^2$.

An important property of hybrid inflation is that the quantum corrections to the effective inflaton potential are often important. At one loop, they are given by [104–107]

$$\Delta V_{\text{loop}} \;=\; \frac{1}{64\pi^2}\sum_i (-1)^{2s_i}\, m_i^4(\phi)\left[\ln\left(\frac{m_i^2(\phi)}{Q^2}\right) - \frac{3}{2}\right], \tag{5.25}$$

where $m_i(\phi)$ is the mass and s_i the spin of the i-th particle degree of freedom, and Q is the $\overline{MS}$ renormalization scale. In unbroken SUSY, the bosonic and fermionic one-loop corrections cancel. However, during hybrid inflation SUSY is strongly broken and the cancellation between bosons and fermions becomes incomplete. This results in significantly large quantum corrections ΔV_{loop}, and the effective inflaton potential to use is

$$\widetilde{V}(\phi) \;=\; \widetilde{V}_{\text{tree}}(\phi) + \Delta V_{\text{loop}}(\phi). \tag{5.26}$$

Using this $\widetilde{V}(\phi)$ and accounting for the extra mass $\Delta m_\chi^2 = -\beta V_0$ for the waterfall field, SUSY hybrid inflation can then be analysed analogously to section 2.4.3.[5]

5.4.3 Comment on the η problem

Note that the scalar potentials in eqs. (5.21) and (5.23) contain an additional Hubble-sized mass term from the Kähler potential:

$$\Delta m_\phi^2 \;=\; \gamma V_0, \tag{5.27}$$

with $\gamma = -\beta$ in hilltop inflation and $\gamma = 4\kappa_S$ in hybrid inflation. Such a mass term contributes to the slow-roll parameter η given by eq. (2.18b):

$$\Delta\eta \;=\; \frac{\Delta V''(\phi)}{V(\phi)} \;\simeq\; \gamma. \tag{5.28}$$

If the coefficients in the Kähler potential are generic Planck-suppressed parameters, we might expect $\gamma \sim \mathcal{O}(1)$, and therefore a contribution $\Delta\eta \sim \mathcal{O}(1)$. However, slow-roll inflation requires $\eta \ll 1$, and the observed spectral index implies that $|\eta_*| \sim 10^{-2}$ barring finely tuned cancellations between different slow-roll parameters. The tension between the large generic SUGRA corrections from eq. (5.28) and the small required value $\eta \ll 1$ for slow-roll inflation is generally known as the η problem.

[5] Note that the perturbative effective potential $\widetilde{V}$ can be non-convex, and it can even have an imaginary component if the particle spectrum contains a tachyonic mass, whereas the non-perturbative full effective potential V_{eff} is always convex and real. It turns out [107] that the perturbative quantity $\operatorname{Re}\widetilde{V}$ is relevant for the evolution of semiclassical states with "well-defined" field values ϕ_i, and $\operatorname{Im}\widetilde{V}$ is related to a quantum decay rate of such semiclassical states. On the other hand, the non-perturbative V_{eff} applies to quantum superpositions of vacua with very different background fields ϕ_i. During inflation, it is therefore appropriate to use $\operatorname{Re}\widetilde{V}$ as the leading-order correction to the classical evolution of the background field, provided that the quantum decay rate due to $\operatorname{Im}\widetilde{V}$ is small compared to the Hubble rate.

The η problem is generic for SUGRA models of inflation [101, 108, 109], not just for the specific superpotentials of eqs. (5.17) and (5.22). It basically states that the relevant Kähler potential couplings for the inflaton must be tuned at the percent level to allow for slow-roll inflation.

Such tuning can be either accidental or due to some approximate symmetries. Many authors assume that the Kähler potential possesses an approximate shift symmetry [24, 110, 111] or a Heisenberg symmetry [31, 112–115] which enforces $\Delta\eta = 0$. But even without such symmetries, a percent-level tuning is not unreasonable: many proposed particle physics models have a large number of scalar fields, and therefore it is easily conceivable that some of them will have small Kähler masses just by chance, making them potential inflaton candidates.

In this thesis, we take an agnostic stance on the solution to the η problem. We will generally work with an expansion of the Kähler potential and tune the relevant Kähler potential coupling by hand, keeping in mind the possibility that such a tuning might ultimately be explained by some symmetry. We believe that this approach is generally useful, since the exact symmetry case can usually be recovered by choosing the Kähler potential coupling such that the Kähler mass vanishes exactly.

On the upside, the mechanism responsible for the η problem provides a simple way of stabilizing spectator fields Y_i during inflation, since even generic Planck-suppressed Kähler potential couplings will endow them with Hubble-sized extra mass terms during inflation. Such large masses quickly force the spectator fields towards $Y_i \to 0$ and suppress their quantum fluctuations during inflation.

Part III

Tribrid inflation in realistic particle physics models

Chapter 6

Introduction to tribrid inflation

After these preliminaries, we are now ready to analyse models of inflation in supergravity. In this thesis, we are interested in two related classes of small-field models which can potentially have close connections to particle physics: tribrid inflation and new inflation.

Both of these options can be realized with a "tribrid" superpotential. It features a symmetry breaking field H which acquires a vacuum expectation value after inflation, spontaneously breaking some high-scale particle physics symmetry like a GUT symmetry or a family symmetry. In addition, the symmetry breaking field H is coupled to another scalar field X which can be identified with a right-handed sneutrino or a D-flat MSSM direction.

With such a superpotential, either X or H can be the inflaton. As we will see, both possibilities allow for interesting connections to particle physics. We start with analysing tribrid inflation with X as the inflaton in chapters 6–8. New inflation with H as the inflaton is discussed later in chapters 9–11.

This chapter provides a general introduction to tribrid inflation and more detailed guidelines for building models of Kähler-driven tribrid inflation. We begin by introducing the tribrid superpotential and the different regimes of tribrid inflation. We then focus on Kähler-driven tribrid inflation for which we calculate the primordial spectrum and show that one of the inflaton potential parameters can be expressed entirely by $\alpha_{\rm s}$ and $n_{\rm s}$. This allows us to derive relations between $\alpha_{\rm s}$ and particle physics parameters like the symmetry breaking scale $\langle H\rangle$ and the inflaton's mass or Yukawa coupling after inflation.

As a next step towards a realistic model, we discuss how tribrid inflation can be realized in explicit particle physics models by replacing H and X by D-flat combinations of fields, e.g. D-flat MSSM directions, and the conditions under which the predictions of tribrid inflation remain unchanged under such generalizations of the tribrid superpotential.

This chapter constitutes a blueprint for model building: the second part contains the instructions on how to embed inflation in a given model, and the first part determines the relations between cosmological observables and model parameters that follow from such an embedding. This will be illustrated later in chapter 7 where we realize tribrid inflation in an explicit model of the leptonic flavour structure based on a spontaneously broken A_4 family symmetry.

6.1 Inflation with a tribrid superpotential

In this thesis, we study inflation with the "tribrid" superpotential

$$W_{\text{tribrid}} = \sqrt{V_0}\, S \left(1 - \frac{H^\ell}{\mu^\ell}\right) + \lambda\, H^m X^n \tag{6.1}$$

for the three complex scalar fields S, H and X. ℓ, m and n are integer numbers with $\ell \geq m \geq 2$ and $n \geq 2$. V_0, μ and λ are positive, real parameters, since a complex phase of these parameters can be absorbed in S, H and X via field redefinitions.

We can also write the superpotential in a different way which emphasizes the suppression scales of the non-renormalizable operators:

$$W_{\text{tribrid}} = S \left(\sqrt{V_0} - \frac{H^\ell}{\Lambda_H^{\ell-2}}\right) + \frac{H^m X^n}{\Lambda_X^{m+n-3}}, \tag{6.2}$$

with

$$\mu^\ell = \Lambda_H^{\ell-2}\sqrt{V_0}, \qquad \lambda = \Lambda_X^{3-m-n}, \tag{6.3}$$

where Λ_H, $\Lambda_X \gtrsim \mathcal{O}(1)$ for Planck-suppressed operators.[1]

The tribrid superpotential can usually be enforced by an $U(1)_R$ symmetry and one or more $\mathbb{Z}_p$ symmetries, though the precise charge assignment depends on how tribrid inflation is embedded in a realistic model. For example realizations of tribrid inflation with such symmetries, see sections 7.1 and 8.1.

Possible inflaton trajectories

Depending on the model parameters, any of the three scalar fields can be the inflaton:

- For $\ell = 2$, we can have hybrid inflation with S as the inflaton, since the first term in eq. (6.1) is then identical to the hybrid superpotential of eq. (5.22).
- For $\ell > 2$, we can have new inflation with H as the inflaton, since the first term in eq. (6.1) is then identical to the hilltop superpotential of eq. (5.17).
- For $\ell \geq m \geq 2$, we can have hybrid inflation with X as the inflaton; this case is usually called "tribrid inflation" in the literature.

Each of these possibilities can lead to inflation in agreement with the present experimental constraints, and they all allow for interesting connections to particle physics. In particular, for all of these possibilities, the scalar field H gets a vacuum expectation value

[1] For generic Planck-suppressed operators, one expects $\Lambda_{\text{suppr}} \sim \mathcal{O}(1)$, but there might be additional suppression mechanisms for any given operator beyond the mere energy scale suppression.

$\langle H\rangle = \mu$ after inflation. Therefore, these models can naturally connect inflation to spontaneous symmetry breaking of some particle physics symmetry,[2] e.g. of a GUT symmetry [29, 116–121] or a family symmetry [30].

The case of hybrid inflation with S as the inflaton has been widely studied in the literature [101–103, 116–122]. In this thesis, we focus on the less explored possibilities of tribrid inflation (chapters 6–8) and new inflation with a tribrid superpotential (chapters 9–11).

In addition to these single-inflaton cases, it is also possible to have multi-field inflation with any combination of S, H and X as inflaton fields. This is discussed in chapter 9 with the real and the imaginary components of H and in chapter 10 with H and X as inflaton fields.

Kähler potential

In principle, the tribrid superpotential allows both for small-field and for large-field models of inflation. An important theoretical difference between these options is that in small-field models, inflation is most sensitive to renormalizable operators in the potential, with operators of higher mass dimension being increasingly suppressed; in large-field models, the situation is exactly reversed. Since the low energy physics is dominated by the operators with low mass dimension, this makes small-field models particularly suitable for linking inflation to low-energy particle physics.

We therefore focus on small-field models throughout most of this thesis. This has the advantage that our models are insensitive to the details of the UV complete theory: we can generally expand all quantities in powers of $Y_i/m_{\rm Pl}$ and keep a limited number of terms, since higher-order terms are suppressed by the small field values.

In particular, we are able to consider a generic Kähler potential K and write it as a power series expansion. Throughout this thesis, we assume that the Kähler potential can be approximated by a power series in the modulus squared of the fields:

$$K = \sum_i |Y_i|^2 + \sum_{ij} \kappa_{ij}|Y_i|^2|Y_j|^2 + \sum_{ijk} \kappa_{ijk}|Y_i|^2|Y_j|^2|Y_k|^2 + ..., \tag{6.4}$$

with $Y = \{S, H, X\}$. We also assume that the higher-order operators in K are Planck-suppressed, i.e. $\kappa_{ij}, \kappa_{ijk} \lesssim \mathcal{O}(1)$. This guarantees that higher-order operators are suppressed in small-field models, i.e. for $Y_i \ll m_{\rm Pl}$.

The Kähler potential can generally include other terms like $\Delta K \propto {\rm Re}(H^\ell)$ which are irrelevant during Kähler-driven tribrid inflation. For some symmetry choices, it might also be possible to have operators linear in S, like $\Delta K \propto {\rm Re}(S^\dagger X^2)$, which can in principle disturb the inflationary dynamics. However, in all the models considered throughout this thesis, the most important of these operators are forbidden by symmetries, and we will generally assume that they are absent.

[2] All of these models require that H is charged under some symmetry, since otherwise the superpotential would contain terms like $\Delta W \propto SH$ which drastically change the dynamics.

6.2 Tribrid inflation

With the superpotential of eq. (6.1), tribrid inflation is defined as single-field inflation along $\phi := \sqrt{2}|X|$ while $H \simeq 0$ and $S \simeq 0$. Inflation ends with a waterfall transition in H, which is triggered when $|X|$ drops below a critical value $|X_c|$. The singlet field S is merely an auxiliary field which is approximately zero during and after inflation.[3]

The main difference between tribrid inflation and conventional SUSY hybrid inflation, which uses the singlet S as the inflaton, is that the tribrid inflaton X can be charged under symmetries, including gauge symmetries [25]. We can therefore use matter fields, e.g. D-flat MSSM directions, as inflaton directions. This connects inflation and particle physics more closely: inflation is most sensitive to the inflaton couplings, so if the inflaton is composed of observable matter fields, then the particle theory can more easily constrain inflationary predictions.

In tribrid inflation, the inflaton potential can be generated from three different sources: from the Kähler potential, from a non-zero $\langle H \rangle$ during inflation, and from one-loop quantum corrections. Depending on ℓ and m, the effective inflaton potential $V(\phi)$ is often dominated by one of these different contributions, leading to qualitatively different regimes:

- $\ell = m = 2$ ("loop-driven regime") [24–26, 114]: In this case, $V(\phi)$ is usually dominated by one-loop quantum corrections to the effective potential. The inflaton potential can receive dangerously large contributions from the Kähler potential, but these can be avoided either by symmetries in the Kähler potential [24, 114] or by a percent-level tuning of one Kähler potential parameter.

- $\ell \geq m = 2$ ("Kähler-driven regime") [23, 28]: In this case, $V(\phi)$ is generated mostly from Planck-suppressed operators in the Kähler potential.[4] For $\phi \ll m_{\rm Pl}$, for which the expansion of the Kähler potential in eq. (6.4) is valid, the resulting inflaton potential usually has a hilltop-type shape with only three relevant parameters. Kähler-driven tribrid inflation can produce an observably large $\alpha_s > 0$, which – if it should be measured – could fix the most important model parameter and also rule out the other regimes of tribrid inflation.

- $\ell \geq m > 2$ ("pseudosmooth regime") [27]: In this case, $V(\phi)$ is generated from the superpotential coupling $\lambda H^m X^n$, with $H \neq 0$ already during inflation. Inflation proceeds similar to smooth hybrid inflation [123] but ends with a waterfall. Note that because $H \neq 0$ already during inflation, no topological defects are formed during the waterfall transition. So far, the predictions have been calculated for $\ell = m$ only, so it

[3] S can get a super-Hubble mass from the Kähler potential during inflation. For $m = 2$, the auxiliary field is then stabilized at $S = 0$. For $m > 2$, $S \neq 0$ along the inflationary trajectory, but as long as it is heavy enough, we still have $S \ll X$ and $\dot{S} \ll \dot{X}$, which can be roughly approximated by $S \simeq 0$. [27]

[4] For $\ell = 2$, the loop potential is often dominant (loop-driven regime), except for some specific Kähler potentials for which even $\ell = 2$ can be Kähler-driven. For $\ell > 2$, loop corrections are strongly suppressed, and the Kähler-driven regime is the generic case.

is not yet clear whether models with $\ell > m > 2$ can generate primordial perturbations consistent with observations.

The generic predictions for small-field tribrid inflation are $r \lesssim 0.01$, $\mu \gtrsim O(10^{16}\,\mathrm{GeV})$ and $\alpha_s \gtrsim 0$. The small tensor-to-scalar ratio is typical for small-field models and the mass scale $\mu \sim M_{\mathrm{GUT}}$ is typical for hybrid inflation. Some of these are falsifiable predictions: an observable $\alpha_s > 0$ would exclude both the loop-driven and the pseudosmooth regimes, and an observable $\alpha_s < 0$ or $r > 0.01$ would exclude all three regimes of small-field tribrid inflation.

In addition to these generic predictions, tribrid inflation provides relations between CMB observables and model parameters, depending on the regime of tribrid inflation. For example, the Kähler-driven regime links the running of the spectral index α_s to the superpotential coupling λ and the symmetry breaking scale $\langle H \rangle$. These relations can connect cosmology and particle physics in explicit models.

In the following chapters, we focus on the Kähler-driven regime of tribrid inflation, which is most easily applicable to a wide range of particle physics models. For loop-driven tribrid inflation, the requirement that $\ell = m = 2$ makes it more difficult to find suitable symmetries which forbid troublesome extra terms: since both SH^2 and H^2X^n must be allowed superpotential operators, it is not clear how to forbid an X^n term in the superpotential. And in pseudosmooth tribrid inflation, due to $S \neq 0$ and $H \neq 0$, one must carefully consider not only couplings of additional fields to the inflaton X but also to S and H to check whether or not they affect the inflationary dynamics. As we will see, such considerations are much simpler in Kähler-driven tribrid inflation, and we will find useful model building guidelines for easily embedding Kähler-driven tribrid inflation in explicit models.

6.3 Kähler-driven tribrid inflation

We now discuss Kähler-driven tribrid inflation in greater detail. In particular, we consider inflation along $\phi = \sqrt{2}|X|$ with the superpotential of eq. (6.1), $\ell > m = 2$, and negligible one-loop corrections.[5] We start by deriving the inflaton potential and the slow-roll predictions and then explain how Kähler-driven tribrid inflation can be realized in realistic particle physics models, which allows us to relate particle physics couplings to the running of the spectral index in such models.

This section constitutes an updated version of the calculation in [28]. We improve on [28] by taking into account the leading order corrections due to ξ_*^2 and σ_*^3, by calculating κ_{s}, and by expressing the predictions in terms of α_{s} to find relations between cosmological and particle physics parameters.

[5] Though Kähler-driven tribrid inflation is possible for specific model parameters even for $\ell = 2$, the one-loop corrections to the inflaton potential are usually important in this case. For this reason, we only consider $\ell \geq 3$ when calculating the predictions for Kähler-driven tribrid inflation.

6.3.1 Inflaton potential

For a D-flat inflaton direction,[6] the inflaton potential $V_{\text{inf}}(\phi)$ is the F-term potential calculated from eq. (5.4). To find a simple expression for $V_{\text{inf}}(\phi)$, it is important to realize that $H = S = 0$ during inflation: H has a large positive mass from its coupling $\lambda H^2 X^n$ in the superpotential, and S gets a large mass from Kähler corrections due to the arguments given in section 5.4.3, with [28]

$$\Delta m_S^2 \;=\; -4\kappa_{SS} V_0, \tag{6.5}$$

for which we assume $(-\kappa_{SS}) \gg \frac{1}{12}$ so that $S = 0$ is stabilized with a super-Hubble mass term.

With $l > m = 2$ and $H = S = 0$, it follows that $W = W_X = W_H = 0$ and $W_S = \sqrt{V_0}$. The F-term potential of eq. (5.4) then becomes quite simple:

$$V_{\text{inf}} \;=\; e^K \left(W_S K^{S\overline{S}} W_S^\dagger \right) \;=\; V_0\, e^K K^{S\overline{S}}. \tag{6.6}$$

The inverse Kähler metric can be expanded as a Neumann series:

$$\left(K^{i\bar{j}}\right) = \left(K_{\bar{i}j}\right)^{-1} = \left(\mathbb{1}_3 - \left[\mathbb{1}_3 - \left(K_{\bar{i}j}\right) \right] \right)^{-1} = \sum_{k=0}^{\infty} \left[\mathbb{1}_3 - \left(K_{\bar{i}j}\right) \right]^k. \tag{6.7}$$

In this expression, $(K^{i\bar{j}})$ and $(K_{\bar{i}j})$ are 3×3 matrices, and powers of matrices are evaluated via matrix multiplication. Only terms proportional to $K_{\overline{S}S}$ contribute to $K^{S\overline{S}}$, as all other terms in this matrix multiplication (like $K_{\overline{S}Y_i} K_{\overline{Y}_i S}$) are proportional to $S^\dagger S = 0$. Therefore, $K^{S\overline{S}}$ has the very simple form

$$K^{S\overline{S}} = \sum_{k=0}^{\infty} \left(1 - K_{\overline{S}S}\right)^k = \frac{1}{K_{\overline{S}S}}. \tag{6.8}$$

With $\phi = \sqrt{2}|X|$, the inflaton potential is therefore

$$V_{\text{inf}}(\phi) \;=\; V_0 \left[\frac{e^K}{K_{\overline{S}S}} \right]_{S=H=0} \;=\; V_0 \left(1 \,+\, a\,\phi^2 \,+\, b\,\phi^4 \,+\, ...\right), \tag{6.9}$$

where the dots denote higher powers of ϕ/m_{Pl}.

The couplings a and b are given by sums and products of the κ_{ij} and κ_{ijk}. Their functional form (including the small canonical normalization effects as discussed in appendix B of [28]) is given by

$$a \;=\; \frac{1}{2}\left(1 - \kappa_{SX}\right), \tag{6.10a}$$

$$b \;=\; \frac{1}{8} + a^2 - \frac{a}{2} + \kappa_{XX}\left(\frac{1}{4} - \frac{2a}{3}\right) - \frac{\kappa_{SXX}}{4}. \tag{6.10b}$$

[6] See appendix C.1 for an estimate of corrections due to deviations from D-flatness.

To derive the predictions for Kähler-driven tribrid inflation, we assume that further Planck-suppressed operators like $c\phi^6$ are negligible, which is automatic for generic Planck-suppressed operators $|c| \sim |b| \sim \mathcal{O}(1)$ [28]. Then the only viable option for small-field inflation is $a > 0$ and $b < 0$ [28] and we can derive the predictions using the simple inflaton potential

$$V_{\text{inf}} \simeq V_0(1 + a\,\phi^2 - |b|\,\phi^4), \tag{6.11}$$

with $a \lesssim \mathcal{O}(1)$ and $|b| \lesssim \mathcal{O}(1)$ due to our assumption that the non-renormalizable operators in the Kähler potential are suppressed by the Planck scale.

6.3.2 End of inflation by waterfall transition

As in all models of hybrid inflation, inflation ends when the waterfall field's mass becomes tachyonic, which happens at small inflaton field values $\phi < \phi_{\text{c}}$, with

$$m_H^2(\phi_{\text{c}}) = 0. \tag{6.12}$$

The waterfall field's mass can be calculated from the F-term potential if we keep terms up to $\mathcal{O}(H^2)$ in eq. (5.4). For $\ell > 2$, this leads to [28]

$$m_H^2(\phi) \simeq V_0(1 - \kappa_{SH}) + 2^{2-n}\lambda^2\phi^{2n}, \tag{6.13}$$

from which we can calculate ϕ_{c} in terms of the model parameters:

$$\phi_{\text{c}}^{2n} \simeq \frac{V_0(\kappa_{SH} - 1)}{2^{2-n}\lambda^2}. \tag{6.14}$$

Note that with $\ell > 2$, H gets no tachyonic mass term from the superpotential. Instead, the tachyonic mass is generated entirely from the non-renormalizable Kähler potential term $K \supset \kappa_{SH}|S^2H^2|$. If these terms are Planck-suppressed as we assume throughout this thesis, i.e. $\kappa_{SH} \lesssim \mathcal{O}(1)$, then the tachyonic mass term in eq. (6.13) is not much larger than the Hubble scale: $|m_H(\phi \to 0)| \lesssim \mathcal{H}$.

It is known that waterfall transitions with a small tachyonic mass $|m_H| < \mathcal{H}$ are likely to overproduce primordial black holes [77], which could put a lower bound on the parameter κ_{SH}. The estimate in [77] suggests that black hole overproduction is avoided for $m_H \gtrsim \mathcal{H}$, which implies an estimated lower bound $(\kappa_{SH} - 1) \gtrsim 1/\sqrt{3}$.

6.3.3 Slow-roll predictions for primordial power spectra

We are now ready to calculate the slow-roll predictions for the inflaton potential $V_{\text{inf}}(\phi)$ given by eq. (6.11), using eqs. (3.24b)–(3.24e) and (3.25). Our goal is to derive the following results:

- Derive the generic predictions for the primordial spectra in Kähler-driven tribrid inflation: a positive running $\alpha_{\text{s}} > 0$ up to higher-order slow-roll corrections, negligible running of the running $\kappa_{\text{s}} \ll 10^{-2}$ and negligible tensor modes $r \ll 10^{-2}$.

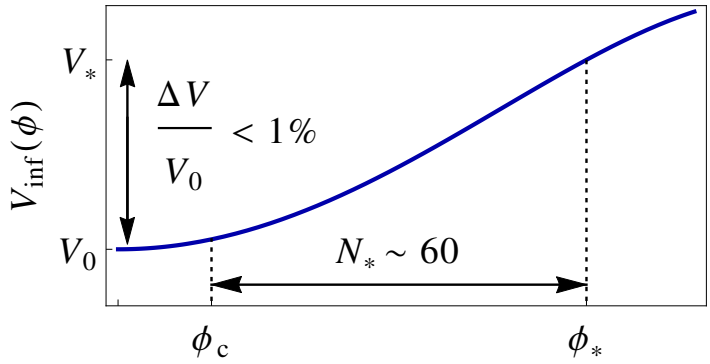

Figure 6.1: Inflaton potential $V_{\rm inf}(\phi)$ during Kähler-driven tribrid inflation, with the vertical axis zoomed in around V_0 so that the potential shape is visible despite $V_* \simeq V_0$. One can see that ϕ_* is close to the inflection point to allow for $(1 - n_{\rm s}) \simeq 2\eta_* \ll 1$; the precise location of ϕ_* determines the value of $n_{\rm s}$. We can thus determine ϕ_* by measuring $n_{\rm s}$, and in turn determine $\phi_{\rm c}$ as the inflaton value at N_* e-folds after ϕ_*.

- Express the inflaton potential parameter a as a function of the observables: $a = a(\alpha_{\rm s}, n_{\rm s})$.
- Find expressions for the superpotential parameters V_0 and λ in terms of $\alpha_{\rm s}$, $n_{\rm s}$ and $|b|$ to find relations between cosmological observables and the model's particle physics couplings.[7]

Like in other small-field models, we can use that $V_{\rm inf}(\phi) \simeq V_0$ during inflation (see [28]). Then the slow-roll parameters from eqs. (2.18a)–(2.18d) are

$$\varepsilon(\phi) \simeq \frac{1}{2}\left(\frac{V'}{V_0}\right)^2 = 2\phi^2\left(a - 2|b|\,\phi^2\right)^2, \tag{6.15a}$$

$$\eta(\phi) \simeq \frac{V''}{V_0} = 2a - 12|b|\,\phi^2, \tag{6.15b}$$

$$\xi^2(\phi) \simeq \frac{V'V'''}{V_0^2} = -48|b|\,\phi^2\left(a - 2|b|\,\phi^2\right), \tag{6.15c}$$

$$\sigma^3(\phi) \simeq \frac{(V')^2V''''}{V_0^3} = -48|b|\,\varepsilon(\phi). \tag{6.15d}$$

Horizon crossing inflaton value ϕ_*

To calculate the primordial spectrum, we need to evaluate the slow-roll parameters at the field value ϕ_* at horizon crossing, which can in principle be calculated from eq. (2.20) as the field value N_* e-folds before inflation ends at $\phi_{\rm c}$ as given by eq. (6.14).

[7] The range of the parameter $|b|$ can later be constrained by the requirement of small-field inflation $\phi_* \ll m_{\rm Pl}$, which imposes a lower bound on $|b|$, and by our assumption that the non-renormalizable operators are Planck-suppressed so that $|b| \lesssim \mathcal{O}(1)$.

However, since our tribrid model can account for any spectral index n_s, it will be more useful to reverse this logic: we can also consider n_s as a free input parameter and derive predictions for ϕ_* and ϕ_c as functions of n_s. We start by combining eqs. (3.24c) and (6.15b):

$$\begin{aligned} 24|b|\,\phi_*^2 - 4a \;\simeq\; -2\eta_* \;&=\; 1 - n_\mathrm{s} - 6\varepsilon_* + 2q_1\xi_*^2 + 2q_2\sigma_*^3 \\ &=\; 1 - n_\mathrm{s} - q_1\alpha_\mathrm{s} - (q_1^2 - q_2)\kappa_\mathrm{s} - \frac{3r}{8}, \end{aligned} \tag{6.16}$$

where we have replaced ε_*, ξ_*^2 and σ_*^3 with the observables r, α_s and κ_s using eqs. (3.24b)–(3.24e). With the definition

$$\begin{aligned} q_\mathrm{s} \;&:=\; 1 - n_\mathrm{s} - q_1\alpha_\mathrm{s} - (q_1^2 - q_2)\kappa_\mathrm{s} - \frac{3r}{8} \\ &\simeq\; 1 - n_\mathrm{s} - 1.06\,\alpha_\mathrm{s} - 0.92\,\kappa_\mathrm{s} - 0.38\,r, \end{aligned} \tag{6.17}$$

we can thus solve eq. (6.16) for ϕ_*:

$$\phi_*^2 \;=\; \frac{4a + q_\mathrm{s}}{24|b|}, \tag{6.18}$$

where a and b are the parameters of the inflaton potential and $q_\mathrm{s} \sim \mathcal{O}(10^{-2})$ is determined from the measured values of n_s, α_s, κ_s and r. (In fact, we will find that κ_s and r are negligible, and thus q_s only depends on n_s and α_s.)

This can be understood intuitively from the inflaton potential as shown in fig. 6.1. The curvature $V''(\phi)$ determines the spectral index n_s (or more precisely q_s). To get the small observed value of $q_\mathrm{s} \simeq (1 - n_\mathrm{s}) \sim 0.04$, we need to choose ϕ_* close to the inflection point at $\phi_\mathrm{inflect} = (\frac{a}{6|b|})^{1/2}$, with a small displacement from the inflection point determined by q_s.

Lower bound on a

Our approach so far hides the fact that we need a minimal a for reproducing the observed q_s: for very small a, the required ϕ_* calculated from eq. (6.18) lies beyond the local maximum of the potential at $\phi_\mathrm{max} = (\frac{a}{2|b|})^{1/2}$, and thus ϕ rolls towards larger field values and never reaches the critical inflaton field value ϕ_c. To have the inflaton field roll towards $\phi_\mathrm{c} < \phi_*$, we therefore require that $\phi_*^2 < \phi_\mathrm{max}^2$. This leads to a lower bound on a:

$$a > \frac{q_\mathrm{s}}{8}. \tag{6.19}$$

Slow-roll predictions for α_s and κ_s

To calculate the predictions for the primordial spectrum, we need to evaluate the slow-roll parameters at ϕ_*:

$$\varepsilon_* = \frac{4}{27|b|}\left(a+\frac{q_s}{4}\right)\left(a-\frac{q_s}{8}\right)^2, \tag{6.20a}$$

$$\xi_*^2 = -\frac{16}{3}\left(a+\frac{q_s}{4}\right)\left(a-\frac{q_s}{8}\right), \tag{6.20b}$$

$$\sigma_*^3 = -\frac{64}{9}\left(a+\frac{q_s}{4}\right)\left(a-\frac{q_s}{8}\right)^2 = \frac{4}{3}\left(a-\frac{q_s}{8}\right)\xi_*^2. \tag{6.20c}$$

Note that for large $a \gg q_s$, we have $\kappa_s \simeq 2\sigma_*^3 \sim \frac{128}{9}a^3$, so we need $a \lesssim 10^{-1}$ to get $|\kappa_s| \lesssim \mathcal{O}(10^{-2})$ as required by CMB constraints [9]. This in turn implies that $\sigma_*^3 \ll \xi_*^2$, and thus

$$\alpha_s \simeq -2\xi_*^2 = \frac{32}{3}\left(a^2+\frac{q_s}{8}a-\frac{q_s^2}{32}\right) > 0, \tag{6.21}$$

which is strictly positive due to $a > q_s/8$. Kähler-driven tribrid inflation therefore predicts a positive spectral index up to higher-order slow-roll corrections.

For large a, eq. (6.21) implies $\alpha_s \sim \frac{32}{3}a^2$, and thus an upper bound

$$a \lesssim \sqrt{\frac{3}{32}\,\alpha_s^{(\max)}} \sim 0.03 \tag{6.22}$$

for $\alpha_s < 0.01$ as implied by the Planck data [9].[8]

With this small value of a and $\alpha_s \lesssim \mathcal{O}(10^{-2})$, we find that

$$|\kappa_s| = |2\sigma_*^3| = \frac{4}{3}\left(a-\frac{q_s}{8}\right)\alpha_s \lesssim \mathcal{O}(10^{-4}), \tag{6.23}$$

which confirms that σ_*^3 and κ_s are negligible.

Note that eq. (6.21) allows us to eliminate the Kähler potential coupling a for the observable α_s, with

$$a(\alpha_s, q_s) = \frac{-q_s+\sqrt{9q_s^2+24\alpha_s}}{16}, \tag{6.24}$$

which can be combined with $q_s \simeq 1-n_s+1.06\alpha_s$ into a function $a(\alpha_s, n_s)$ to express other predictions in terms of α_s and n_s.

[8] Since tribrid inflation predicts small $\kappa_s \ll 10^{-2}$ and $r \ll 10^{-2}$ as we show in eqs. (6.23) and (6.25), the appropriate bounds on α_s are those for ΛCDM+α_s with $\kappa_s = r = 0$, for which $\alpha_s = -0.006 \pm 0.007$ at 68% CL for the Planck TT,TE,EE+lowP dataset [9]. Of course, it is possible to relax other model assumptions to weaken the bounds on α_s as discussed in appendix B. However, even in the 12-parameter extension of ΛCDM introduced in [124], the upper bound on α_s is only relaxed to $\alpha_s < 0.02$ at 95% CL, which still implies an upper bound of $a \lesssim 0.04$.

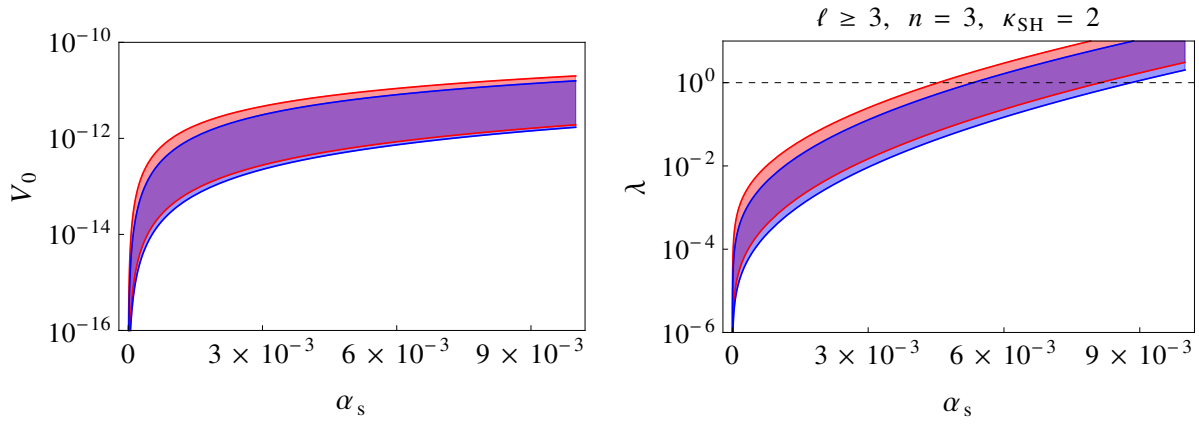

Figure 6.2: Predicted values for the vacuum energy V_0 and the superpotential coupling λ, for $n_s = 0.955$ (blue band) and $n_s = 0.974$ (red band), with $N_* = 55$. λ also depends on the exponent n of the inflaton term in the superpotential and weakly on the Kähler potential coupling κ_{SH}; we use $n = 3$ and $\kappa_{SH} = 2$ in this plot. The width of the bands is due to the Kähler potential coupling $|b|$, which we constrained from below by $\phi_* \leq 1/4$ in eq. (6.18) (to have small-field inflation) and from above by $|b| \leq 1$ (since we assume that non-renormalizable operators are suppressed by $m_{\rm Pl}$).

Slow-roll predictions for r and V_0

The tensor-to-scalar ratio r can be calculated from eq. (3.24b) as

$$r \;=\; 16\varepsilon_* \;=\; -\frac{4}{9|b|}\left(a - \frac{q_s}{8}\right)\xi_*^2 \;=\; \frac{2}{9|b|}\left(a - \frac{q_s}{8}\right)\alpha_s. \tag{6.25}$$

With $(a - q_s/8) < (a + q_s/4) \simeq 6|b|\phi_*^2$, this implies a tiny tensor-to-scalar ratio

$$r \;<\; \frac{4}{3}\,\phi_*^2\,\alpha_s \;\ll\; \alpha_s. \tag{6.26}$$

As expected for small-field models, Kähler-driven tribrid inflation cannot produce a significant amount of primordial gravity waves.

The prediction for V_0 then follows directly from eqs.(3.24b) and (3.25):

$$V_0 \;\simeq V_* \;=\; \frac{3\pi^2}{2}A_s\,r \;\simeq\; \frac{1}{|b|}\left(7.2 \times 10^{-9}\right)\left(a - \frac{q_s}{8}\right)\alpha_s, \tag{6.27}$$

with the amplitude of scalar perturbations fixed at $A_s \simeq 2.2 \times 10^{-9}$. V_0 is plotted as a function of α_s in fig. 6.2, where one can see that typical values are around $V_0 \sim 10^{-12}$, with smaller V_0 only for tiny running $\alpha_s \lesssim 10^{-3}$.

Critical inflaton value ϕ_c

As a next step, we can use eq. (2.20) to find the required value of ϕ_c at N_* e-folds after ϕ_*. With the approximation $V(\phi)/V'(\phi) \simeq V_0/V'(\phi)$, eq. (2.20) can be solved analytically

for $\phi_{\rm c}$ [28]:

$$\begin{aligned}\phi_{\rm c}^2 &\simeq \phi_*^2\left(\frac{a}{e^{4aN_*}(a-2|b|\phi_*^2)+2|b|\phi_*^2}\right)\\ &= \phi_*^2\left(\frac{12a}{(8a-q_{\rm s})e^{4aN_*}+4a+q_{\rm s}}\right),\end{aligned} \tag{6.28}$$

where we have used eq. (6.18) in the second step.

Superpotential coupling λ

As a final step, we can also derive the superpotential coupling $\lambda(\alpha_{\rm s}, n_{\rm s}, |b|)$ by plugging the results for $\phi_{\rm c}$ and V_0 into eq. (6.14):

$$\lambda^2 = \frac{V_0(\kappa_{SH}-1)}{2^{2-n}\phi_{\rm c}^{2n}}, \tag{6.29}$$

with $V_0(\alpha_{\rm s}, n_{\rm s}, |b|)$ and $\phi_{\rm c}(\alpha_{\rm s}, n_{\rm s}, |b|)$ given by eqs. (6.27) and (6.28), and $(\kappa_{SH}-1)\sim 1$ as explained in section 6.3.2. λ is shown as a function of $\alpha_{\rm s}$ in fig. 6.2; one can see that there is a strong correlation between λ and $\alpha_{\rm s}$. When we discuss how tribrid inflation can be embedded in realistic particle physics models in section 6.4, we will see how this allows us to predict relations between $\alpha_{\rm s}$ and a particle physics coupling, e.g. a Yukawa coupling or the seesaw mass scale.

6.4 Embedding Kähler-driven tribrid inflation in particle physics models

Now that we have analysed Kähler-driven tribrid inflation with the abstract fields S, H and X, we want to address the issue of how to embed this general structure in explicit particle physics models.

For this purpose, we discuss how to replace the abstract fields H and X with combinations of Higgs or matter fields, how we can derive relations between the cosmological observable $\alpha_{\rm s}$ and the mass or Yukawa coupling of the inflaton fields as well as the symmetry breaking scale $\langle H\rangle$, and some conditions which guarantee that tribrid inflation is not disturbed by other fields present in the full particle physics theory.

6.4.1 Composite waterfall and inflaton directions

Though we have so far analysed tribrid inflation with only three distinct fields S, H and X to keep the notation simple, tribrid inflation works just as well if H^ℓ, H^2 and X^n are D-flat combinations of different fields: $H^\ell \to H_1H_2\dots H_\ell$, $X^n \to X_1X_2\dots X_n$. We can, for example, use some D-flat MSSM direction as the inflaton by replacing $X^3 \to LH_dE$

or $X^2 \to LH_u$. Even for such composite D-flat inflaton directions, the inflaton potential retains the simple quartic form of eq. (6.9) (see appendix C.1 for details).

The predictions of section 6.3.3 remain almost unchanged, with a single exception: for $\lambda H^2 X^n \to \lambda H_1 H_2 X^n$, the predicted λ is doubled to compensate for the difference between $|W_H|^2 = |2\lambda H \Phi^n|^2$ and $|W_{H_2}|^2 = |\lambda H_1 \Phi^n|^2$.

Note that for $\ell \geq 3$, H^ℓ and H^2 can be partially composed of different fields as long as at least one of the fields in H^ℓ and H^2 is the same. For example, one could have

$$W_{\text{example}} = \sqrt{V_0}\, S(1 - \mu^{-3} \underbrace{H_1 H_2 H_3}_{\hat{=} H^\ell}) + \lambda \underbrace{H_1 N}_{\hat{=} H^2} X^n + ..., \tag{6.30}$$

where H_1 is the component of the waterfall field that appears both in H^ℓ and H^2. As long as H_2 and H_3 get a large mass from the superpotential or the Kähler potential, the waterfall can only start along the H_1 direction which is stabilized by $V_F \supset |\partial W/\partial N|^2 = |\lambda X^n H_1|^2$ during inflation.[9]

The field N which appears only in H^2 and not in H^ℓ will not get a vacuum expectation value after inflation. It should therefore not be identified with a Higgs field, but with a matter field like a right-handed sneutrino.

After inflation, tribrid inflation predicts either a mass or a Yukawa coupling for the inflaton direction, depending on n and on whether we use $H^2 \to H_1^2$ or $H^2 \to H_1 N$:

Coupling term	n	generated quantity	example application
$\lambda H_1^2 X^2$	2	$m_X = 2\lambda \langle H_1 \rangle^2$	neutrino Majorana mass term
$\lambda H_1^2 X^3$	3	$y_X = \lambda \langle H_1 \rangle^2$	quark or electron Yukawa coupling
$\lambda H_1 N X^2$	2	$y_{XN} = \lambda \langle H_1 \rangle$	neutrino Yukawa coupling

The examples mentioned in the table are

- generating a neutrino Majorana mass term from $\lambda H_1^2 X^2$, where the right-handed sneutrino X is the inflaton direction,
- generating a quark or charged lepton Yukawa coupling from e.g. $\lambda H_1^2 L H_d E$, where LH_dE is the inflaton direction,
- generating a neutrino Yukawa coupling from $\lambda H_1 L H_u N$, where LH_u is the inflaton direction and N is zero during and after inflation.

The factor 2 in the table for the generated mass applies only if a Majorana mass is generated. If one uses a composite inflaton direction $X^2 \to X_1 X_2$, one instead generates a Dirac mass term and the factor 2 is absent.

[9] The full theory can contain extra terms, which we denoted with "..." in eq. (6.30), that fix the ratios of the H_i to avoid massless directions in the $H_1 H_2 H_3$ hypersurface after inflation. An explicit example is given in chapter 7.

6.4.2 Relating particle physics couplings to α_s

In section 6.3.3, we have calculated the slow-roll predictions for the superpotential parameters V_0 and λ as functions of α_s, n_s and $|b|$, which can be translated into relations between α_s and the particle physics parameters that are derived from the superpotential.

Symmetry breaking scale $\langle H \rangle$

The prediction of V_0 from eq. (6.27) can be translated into constraints on the symmetry breaking scale $\langle H \rangle$ of the waterfall transition:

$$\langle H \rangle \;=\; \left(\Lambda_H^{\ell-2}\sqrt{V_0}\right)^{1/\ell}. \tag{6.31}$$

Note that Λ_H is a free parameter of the model, though we have $\Lambda_H \gtrsim \mathcal{O}(1)$ if we assume that non-renormalizable operators are Planck-suppressed. $\langle H \rangle$ is plotted in fig. 6.3 as a function of α_s for $\Lambda_H = 1$ and $\ell = 3$. For different Λ_H and ℓ, the predicted masses and Yukawa couplings scale according to eq. (6.31) with $V_0(\alpha_s)$ given in fig. 6.2.

Generated mass m_X or Yukawa coupling y_X after inflation

Together with the constraint on λ from eq. (6.29), the constraint on $\langle H \rangle$ can be translated into predictions for the generated mass m_X or Yukawa coupling y_X after inflation. These predictions are shown in fig. 6.3 for $\ell = 3$.[10]

Note that the m_X, y_X and y_{XN} scale with $(\kappa_{SH}-1)^{1/2}$ due to their dependence on λ.[11] The Yukawa coupling y_{XN} for $H^2 \to H_1 N$ also scales with $\Lambda_H^{(\ell-2)/\ell}$, and the mass m_X or Yukawa coupling y_X with $\Lambda_H^{2(\ell-2)/\ell}$ due to their respective dependencies on $\langle H \rangle$.

For $H^\ell \to H_1 H_2 \dots H_\ell$, eq. (6.31) holds for the geometric average of $\langle H_1 \rangle, ..., \langle H_\ell \rangle$. If $\langle H_1 \rangle$ deviates from this average, the predictions for m_X, y_X and y_{XN} must be adjusted accordingly.

Knowing the inflaton's mass or Yukawa coupling after inflation can be useful not just for constraining the low-energy particle physics of the model, but especially for analysing the reheating period. Both the initial preheating and the eventual perturbative decay are determined by the inflaton's mass and couplings which are related to α_s via the above considerations. Therefore, a study of the reheating phase after Kähler-driven tribrid inflation might eventually lead to relations also between α_s and reheating predictions like the reheat temperature, the baryon asymmetry or the non-thermal dark matter abundance.

[10] Fig. 6.3 includes the doubling of λ from replacing $\lambda H^2 \to \lambda H_1 N$ for y_{XN}, but not for m_X and y_X. If m_X or y_X are generated from $\lambda H_1 H_2$ instead of λH_1^2, their prediction in fig. 6.3 should be doubled.

[11] However, we need $(\kappa_{SH}-1) \gtrsim \mathcal{O}(1)$ to avoid overproduction of primordial black holes as discussed in section 6.3.2, and $\kappa_{SH} \lesssim \mathcal{O}(1)$ since we assume Planck-suppressed Kähler potential couplings, so that $(\kappa_{SH}-1) \sim 1$ cannot vary very much.

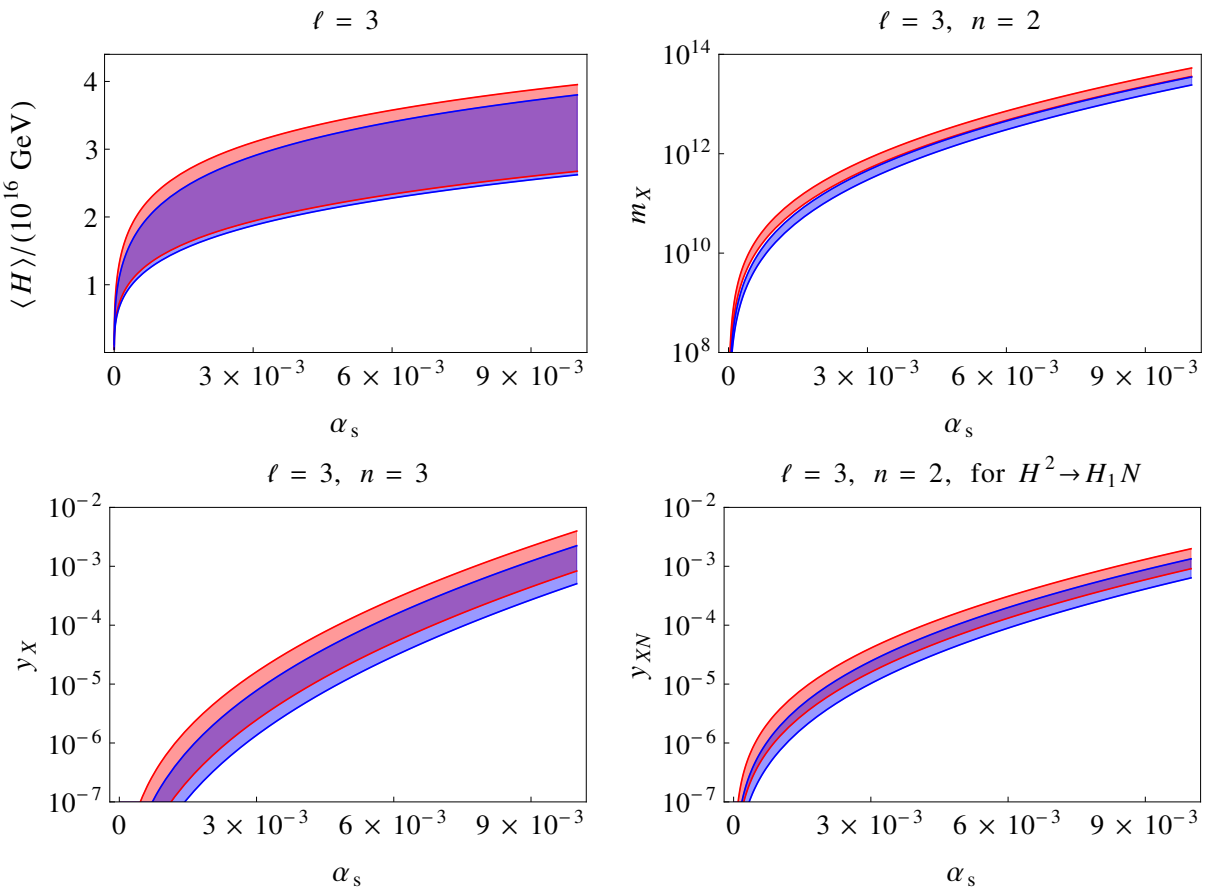

Figure 6.3: Predicted values for the waterfall field's vacuum expectation value $\langle H \rangle$ and the predicted inflaton mass m_X or Yukawa coupling y_X after inflation, for $n_\mathrm{s} = 0.955$ (blue band) and $n_\mathrm{s} = 0.974$ (red band), $N_* = 55$, $\ell = 3$, $\Lambda_H = 1$ and $\kappa_{SH} = 2$. For other values of the suppression scale Λ_H and of the Kähler potential coupling κ_{SH}, these predictions scale with $\langle H \rangle \propto \Lambda_H^{1/3}$ and $\lambda \propto (\kappa_{SH} - 1)^{1/2}$. The width of the bands is due to the Kähler potential coupling $|b|$, which we constrained from below by $\phi_* \leq 1/4$ in eq. (6.18) (to have small-field inflation) and from above by $|b| \leq 1$ (since we assume that non-renormalizable operators are suppressed by m_Pl). The equivalent relations for $\ell > 3$ can be inferred from eq. (6.31) and fig. 6.2.

6.4.3 Spectator fields

One important feature of realistic models is that they contain many fields. At the bare minimum, a realistic supersymmetric model contains the MSSM fields plus a supersymmetry breaking sector, and models based on GUT or family symmetries include additional symmetry breaking sectors for these symmetries. It is therefore important to understand how the presence of additional fields besides S, H and X affects the inflationary dynamics.

It turns out that Kähler-driven tribrid inflation is relatively robust against additional fields, provided that those extra fields' couplings satisfy a few simple conditions during

inflation. To understand this, recall that the dynamics during tribrid inflation only depends on three factors: the inflaton potential $V_{\rm inf}(\phi)$, the inflaton-dependent waterfall mass $m_H^2(\phi)$ responsible for the waterfall transition, and the stabilization of other fields with super-Hubble mass terms to ensure single-field inflation.

Inflaton potential

The tree-level inflaton potential in tribrid inflation is extremely robust since its calculation only depends on $W_S = \sqrt{V_0}$ and $W_{i\neq S} = W = 0$. Therefore, $V_{\rm inf}(\phi)$ is not affected by any new field Y_i which respects the simple condition $W_i = W = 0$.

In addition, quantum corrections to the inflaton potential are typically very small for $\ell > 2$,[12] and even if they are not completely negligible, they often have approximately polynomial form such that they can be absorbed in the inflaton potential couplings a and b (see section 8.3 for details).

Waterfall transition and stabilization of additional fields

When embedding tribrid inflation in an explicit model, we have to check that the spectator fields have positive masses and that they do not affect the mass terms of the waterfall field. The second condition mostly means we have to avoid mixed mass terms $\Delta W \propto HY_i$ and SUSY breaking mass splitting terms $\Delta W \propto SHY_i$ with the extra fields Y_i during inflation; otherwise the waterfall transition could be spoiled or the critical inflaton field value $\phi_{\rm c}$ and the related prediction for λ could be shifted.

To check the stabilization of the spectator fields, one has to calculate the scalar mass eigenvalues (with $\phi = \sqrt{2}|X| > \phi_{\rm c}$) to make sure they are all large and positive except for the inflaton direction. Note that during inflation, every field gets a supergravity mass term $\Delta m_i^2 = (1 - \kappa_{Si})V_0$ which can help with this stabilization.

The calculation of the scalar mass matrix can be simplified by appropriate power counting. Since the mass matrix depends only on the quadratic terms in the scalar potential, we can discard all terms which contain three or more powers of non-inflaton fields. This implies that we can immediately discard all superpotential terms which contain three or more fields except S or X, since such terms cannot generate quadratic terms in the F-term potential.[13] For example, terms like $\Delta W \propto H^3$ or $\Delta W \propto S^a X^b Y_i^3$ (with $Y_i \neq S, X$) cannot generate mass terms and can thus be ignored during inflation.

[12] Large logarithmic corrections can be generated if some field simultaneously has large inflaton-dependent mass terms (which typically occurs for couplings $\Delta W \propto Y_i Y_j X^a$ with $a \geq 1$) and large SUSY breaking mass splittings (which typically occurs for couplings $\Delta W \propto S Y_i Y_j$). In SUSY hybrid and tribrid inflation with $\ell = 2$, these conditions are both satisfied for the waterfall field, which is why the one-loop potential is generally important in those models.

[13] If there are more fields S_i which have a linear superpotential term just like S, then the S_i also do not count towards the power counting, since superpotential couplings $\Delta W \propto S_i(Y^2 - \Lambda^2)$ can generate mass terms for Y. Superpotential operators including S or S_i are only negligible if they contain at least three non-inflaton fields, e.g. SH^3 or $S_i X Y^3$.

For fields which have a vacuum expectation value during inflation, it is necessary to first do a shift $\delta Y_i = Y_i - \langle Y_i \rangle$ and then use the δY_i for the power counting. For example, a term like $\Delta W = \lambda Y Z^2 = (\lambda \langle Y \rangle Z^2 + ...)$ contributes a mass term for Z if Y has a vacuum expectation value.

6.5 Summary

In this chapter, we have introduced tribrid inflation with particular emphasis on Kähler-driven tribrid inflation. We started with a review of the inflationary dynamics and an updated calculation of the slow-roll predictions for the primordial spectrum. We confirmed the predictions of a positive running of the spectral index $\alpha_\mathrm{s} > 0$, a small tensor-to-scalar ratio $r \ll \alpha_\mathrm{s}$ and a symmetry breaking scale $\langle H \rangle \gtrsim \mathcal{O}(10^{16}\ \mathrm{GeV})$, and we found that $\kappa_\mathrm{s} \ll \alpha_\mathrm{s}$ is negligible.

We have shown how the most important inflaton coupling can be eliminated for α_s, allowing us to derive relations between α_s and the superpotential couplings V_0 and λ as shown in fig. 6.2 and the symmetry breaking scale $\langle H \rangle$ as shown in fig. 6.3. Furthermore, depending on the superpotential coupling between inflaton and waterfall field, we find relations between α_s and either the inflaton's mass or its Yukawa coupling after inflation, which are also shown in fig. 6.3.

Beyond constraining the low-energy particle physics of the model, these relations can be particularly useful for studies of the reheating period after inflation, since both preheating and reheating strongly depend on the inflaton's mass and couplings. In this way, α_s could eventually also be related to reheating observables like the baryon asymmetry or the non-thermal dark matter abundance.

As a next step, we have discussed how Kähler-driven tribrid inflation can be embedded in realistic models by identifying the abstract waterfall and inflaton fields with D-flat combinations of Higgs and matter fields. We have pointed out that the tribrid superpotential can be generalized easily without affecting the predictions, in particular by replacing the H^ℓ, H^m and X^n terms with different combinations of fields, which greatly broadens the scope of possible model applications.

Finally, we have pointed out that the inflaton potential is robust against the presence of any additional fields Y_i provided that $W = W_i = 0$, and thus predictions derived from the simple tribrid superpotential can be retained when tribrid inflation is realized in a realistic model with many additional fields. However, one must still check that the extra fields are stabilized during inflation, and that they do not affect the waterfall field's mass.

The considerations in this chapter provide a framework for realizing Kähler-driven tribrid inflation in realistic models. We are now ready to construct a realistic example model to demonstrate how these results can be applied in practice.

Chapter 7

Tribrid inflation in an A_4 lepton flavour model

After the general analysis of Kähler-driven tribrid inflation in the last chapter, we now demonstrate in an explicit example how tribrid inflation can be realized in a realistic particle physics model. For this purpose, we present a lepton flavour model based on [17] which employs a discrete A_4 family symmetry[1] and a CP symmetry to predict the structure of the leptonic Yukawa couplings and neutrino masses.

As we will see, one can easily realize Kähler-driven tribrid inflation in this model using either the D-flat LH_u direction or a right-handed sneutrino direction. The model then predicts a relationship between the running of the spectral index α_s and the neutrino Yukawa coupling or the heavy neutrino mass as shown in fig. 6.3.

Interestingly, we find one particular inflaton direction for which the waterfall field is slightly shifted already during inflation. This has the advantage that the production of topological defects during the waterfall transition may be avoided. We analyse this trajectory in greater detail to confirm that the shifts in the non-inflaton fields do not disturb the inflationary dynamics, and we discuss the conditions on the waterfall field and its alignment potential which can lead to such shifts.

7.1 Lepton flavour model with A_4 family symmetry

We start by introducing the lepton flavour model in which we will eventually realize tribrid inflation. We first discuss the representations of discrete A_4 symmetries, and then we introduce the superpotential and the symmetry breaking sector for the A_4 family symmetry which lead to predictions for two of the leptonic mixing angles and the leptonic Dirac CP phase.

7.1.1 A_4 symmetry: representations and notation

Since the model is based on a discrete A_4 symmetry, we first introduce the representations of A_4. There are four irreducible representations of A_4, which we call $\mathbf{1}$, $\mathbf{1}'$, $\mathbf{1}''$ for the one-dimensional representations and $\mathbf{3}$ for the three-dimensional representation. The A_4 transformations can then be characterized by the two generators S and T. We use the

[1] For early models with A_4 family symmetry, see e.g. [14–16].

Ma-Rajasekaran basis [16] for which the generators in the one-dimensional representations are [125]

$$S_{\mathbf{1}} = S_{\mathbf{1}'} = S_{\mathbf{1}''} = T_{\mathbf{1}} = 1, \qquad T_{\mathbf{1}'} = \omega, \qquad T_{\mathbf{1}''} = \omega^2, \tag{7.1}$$

with $\omega = \exp(2\pi i/3)$. In the $\mathbf{3}$ representation, S and T are [125]

$$S_{\mathbf{3}} = \begin{pmatrix} -1 & 0 & 0 \\ 0 & 1 & 0 \\ 0 & 0 & -1 \end{pmatrix}, \qquad T_{\mathbf{3}} = \begin{pmatrix} 0 & 1 & 0 \\ 0 & 0 & 1 \\ 1 & 0 & 0 \end{pmatrix}. \tag{7.2}$$

To construct the A_4 invariant superpotential, we need to contract these representations such that their product is invariant, i.e. transforms as a $\mathbf{1}$. For products of one-dimensional representations, the transformation properties in eq. (7.1) imply that

$$\mathbf{1}' \times \mathbf{1}'' = \mathbf{1}, \tag{7.3}$$
$$\mathbf{1}' \times \mathbf{1}' = \mathbf{1}'', \tag{7.4}$$
$$\mathbf{1}'' \times \mathbf{1}'' = \mathbf{1}', \tag{7.5}$$

so we can form invariants as products of three $\mathbf{1}'$, three $\mathbf{1}''$ or a product of $\mathbf{1}'$ with $\mathbf{1}''$.

For products of three-dimensional representations, one finds the different contractions [16]

$$\mathbf{3} \times \mathbf{3} = \mathbf{1} + \mathbf{1}' + \mathbf{1}'' + \mathbf{3} + \mathbf{3}, \tag{7.6}$$

with the contractions of two triplets $x = (x_1, x_2, x_3)$ and $y = (y_1, y_2, y_3)$ given by

$$(x\,y)_{\mathbf{1}} = x_1y_1 + x_2y_2 + x_3y_3 =: x \cdot y, \tag{7.7a}$$
$$(x\,y)_{\mathbf{1}'} = x_1y_1 + \omega^2 x_2y_2 + \omega\, x_3y_3, \tag{7.7b}$$
$$(x\,y)_{\mathbf{1}''} = x_1y_1 + \omega\, x_2y_2 + \omega^2 x_3y_3, \tag{7.7c}$$
$$(x\,y)^+_{\mathbf{3}} = \begin{pmatrix} x_2y_3 + x_3y_2 \\ x_3y_1 + x_1y_3 \\ x_1y_2 + x_2y_1 \end{pmatrix} =: x \star y, \tag{7.7d}$$
$$(x\,y)^-_{\mathbf{3}} = \begin{pmatrix} x_2y_3 - x_3y_2 \\ x_3y_1 - x_1y_3 \\ x_1y_2 - x_2y_1 \end{pmatrix} =: x \times y. \tag{7.7e}$$

We can then use eqs. (7.7a)–(7.7e) to form the cubic invariants $(\mathbf{3} \times \mathbf{3}) \cdot \mathbf{3}$, $(\mathbf{3} \star \mathbf{3}) \cdot \mathbf{3}$, $(\mathbf{3} \times \mathbf{3})_{\mathbf{1}'} \times \mathbf{1}''$ and $(\mathbf{3} \times \mathbf{3})_{\mathbf{1}''} \times \mathbf{1}'$, which implies that two A_4 triplets plus any other field always have an A_4 invariant contraction.

We will also need the quartic invariants involving a single triplet field $\Theta = (x, y, z)$. Since $\Theta \times \Theta = 0$, the only possible combinations are

$$(\Theta \cdot \Theta)^2 = x^4 + y^4 + z^4 + 2(x^2y^2 + x^2z^2 + y^2z^2), \tag{7.8a}$$
$$(\Theta \star \Theta) \cdot (\Theta \star \Theta) = 4(x^2y^2 + x^2z^2 + y^2z^2), \tag{7.8b}$$
$$(\Theta\Theta)_{\mathbf{1}'}(\Theta\Theta)_{\mathbf{1}''} = x^4 + y^4 + z^4 - (x^2y^2 + x^2z^2 + y^2z^2), \tag{7.8c}$$

where we used $\omega+\omega^2=-1$ in eq. (7.8c). Note that we can express any of these by a linear combination of the other two, so we will drop the first of these terms in the superpotential.

As a shorthand, we will also write $[\Theta]^n$ for all possible A_4 contractions with n powers of Θ, and $\Theta_i\Theta_j := \Theta_i\cdot\Theta_j$ as well as $\Theta^2 := \Theta\cdot\Theta$ and $\Theta^3 := \frac{1}{6}\Theta\cdot(\Theta\star\Theta)$ for the corresponding unique invariant contractions.

7.1.2 Superpotential and field content

The model is based on the A_4 invariant superpotential

$$\begin{aligned} W = {}& \lambda_i\,\Theta_i\cdot LH_uN_i + \gamma_{ij}(\Theta_i\cdot\Theta_j)\Theta_S N_iN_j \\ & + \lambda_4\Theta_4\cdot LH_dE_1 + \lambda_5\Theta_5\cdot LH_dE_2 + \lambda_6\Theta_3\cdot LH_dE_3 + W_{\text{fl}} + W_{\text{misc}}, \end{aligned} \tag{7.9}$$

where summation over $i,\ j=1,\ 2$ is implied. The left-handed slepton doublets L and the flavons Θ_n are A_4 triplets, while the right-handed sleptons E_i and N_i, the electroweak Higgs doublets H_u and H_d and the flavon Θ_S are A_4 singlets.

In this expression, the first terms are the lepton Yukawa couplings and the right-handed neutrino masses. W_{fl} is the flavon alignment superpotential that enforces the correct breaking of the A_4 and CP symmetries via vacuum expectation values $\langle\Theta_n\rangle$. W_{misc} contains the quark Yukawa couplings and possibly additional interactions which are not relevant for our purpose. How this model relates to the simple tribrid superpotential from eq. (6.1) will be explained in section 7.2.

The flavon alignment superpotential of our model has the form[2]

$$\begin{aligned} W_{\text{fl}} = {}& S_1\left([\Theta_1]^{n_1}-\Lambda_1^2\right) + \kappa S_2\left(\Theta_2^3-\Lambda_2^2\right) + S_3\left([\Theta_3]^{n_3}-\Lambda_3^2\right) + S_4\left([\Theta_4]^{n_4}-\Lambda_4^2\right) \\ & + S_5\left([\Theta_5]^6-\Lambda_5^2\right) + S_6\left([\Theta_6]^{n_6}-\Lambda_6^2\right) + S_7\left(\Theta_S^{n_7}-\Lambda_7^2\right) \\ & + P_{12}\Theta_1\Theta_2 + P_{16}\Theta_1\Theta_6 + P_{34}\Theta_3\Theta_4 + P_{35}\Theta_3\Theta_5 + P_{36}\Theta_3\Theta_6 + P_{46}\Theta_4\Theta_6 \\ & + A_3\Theta_3\star\Theta_3 + A_4\Theta_4\star\Theta_4 + D_5\left\{(\Theta_5^2)_{\mathbf{1}'}(\Theta_5^2)_{\mathbf{1}''} + k_5(\Theta_5\star\Theta_5)^2\right\} \\ & + \alpha_1 D_2'(\Theta_2^2)_{\mathbf{1}''} + \alpha_2 D_2''(\Theta_2^2)_{\mathbf{1}'}, \end{aligned} \tag{7.10}$$

where we introduced additional chiral fields S_i, P_{ij}, A_i, D_5, D_2' and D_2'' which are expected to be stabilized at zero during inflation just like S in the minimal tribrid superpotential of eq. (6.1).

Prefactors which are not needed in the later calculations are dropped for brevity. κ, Λ_2, α_1 and α_2 are real in a suitable basis due to the assumed CP symmetry (before family symmetry breaking). n_1, n_3, n_4 and n_6 can take even integer values and n_7 any integer value greater than two, and we assume $k_5\geq 3$.[3]

The symmetries and charge assignments for the entire superpotential are discussed in appendix C.2.

[2]The flavon alignment potential of eq. (6.1) is based on [17] for Θ_i with $i=1,...,5$, extended by alignment terms for Θ_6 which enforce $\langle\Theta_3\rangle\perp\langle\Theta_6\rangle\perp\langle\Theta_4\rangle$.

[3]For a discussion of the case $k_5<3$, see appendix A of [17].

7.1.3 Flavon vacuum expectation values

The flavon alignment potential fixes the vacuum expectation values in the true vacuum to [17]

$$\langle\Theta_1\rangle = c_1 \begin{pmatrix} 0 \\ 1 \\ \pm 1 \end{pmatrix}, \quad \langle\Theta_2\rangle = c_2 \begin{pmatrix} \pm 1 \\ \pm 1 \\ 1 \end{pmatrix}, \quad \langle\Theta_3\rangle = c_3 \begin{pmatrix} 0 \\ 0 \\ 1 \end{pmatrix},$$
$$\langle\Theta_4\rangle = c_4 \begin{pmatrix} 0 \\ 1 \\ 0 \end{pmatrix}, \quad \langle\Theta_5\rangle = \begin{pmatrix} c_5 \sin(\vartheta_5) \\ \mathrm{i}\, c_5 \cos(\vartheta_5) \\ 0 \end{pmatrix}, \quad \langle\Theta_6\rangle = c_6 \begin{pmatrix} 1 \\ 0 \\ 0 \end{pmatrix}, \quad \langle\Theta_S\rangle = c_7, \tag{7.11}$$

where the $\pm$ can be chosen independently from each other with the constraint that $\langle\Theta_1\rangle \perp \langle\Theta_2\rangle$, and $c_i \in \mathbb{R}$, with global phases of the $\langle\Theta_i\rangle$ absorbed by field redefinitions of the Θ_i and the P_{ij}, A_i, D_5, D_2' and D_2''.

The phase difference of $\pi/2$ between the two components of $\langle\Theta_5\rangle$ is predicted for $k_5 \geq 3$, and the value of ϑ_5 is given by the precise value of k_5.

7.1.4 Predictions for leptonic mixing parameters

Following [17], we choose the vacuum in which $\langle\Theta_2\rangle = c_2(1,1,1)^T$. In this vacuum, we get leptonic Yukawa matrices of the form

$$y_\nu = \begin{pmatrix} 0 & \varepsilon_2 \\ \varepsilon_1 & \varepsilon_2 \\ -\varepsilon_1 & \varepsilon_2 \end{pmatrix}, \quad y_e = \begin{pmatrix} 0 & \varepsilon_5 \sin(\vartheta_5) & 0 \\ \varepsilon_4 & \mathrm{i}\,\varepsilon_5 \cos(\vartheta_5) & 0 \\ 0 & 0 & \varepsilon_6 \end{pmatrix}, \tag{7.12}$$

and a diagonal right-handed neutrino mass matrix[4]

$$M_R = \begin{pmatrix} M_1 & 0 \\ 0 & M_2 \end{pmatrix}, \quad M_i = 2\gamma_{ii}\langle\Theta_i^2\rangle\langle\Theta_S\rangle. \tag{7.13}$$

y_ν and M_R generate the light neutrino masses via the seesaw mechanism [126, 127]:

$$m_\nu \;=\; \langle H_u^2\rangle y_\nu M_R^{-1} y_\nu^T, \tag{7.14}$$

which leads to a real symmetric mass matrix

$$m_\nu = \langle H_u^2\rangle \begin{pmatrix} A & A & A \\ A & A+B & A-B \\ A & A-B & A+B \end{pmatrix}, \quad A \;=\; \frac{\varepsilon_2^2}{M_2}, \quad B \;=\; \frac{\varepsilon_1^2}{M_1}. \tag{7.15}$$

[4]The off-diagonal contribution from $\gamma_{12}\langle\Theta_S\Theta_1\Theta_2\rangle N_1 N_2$ vanishes because $\langle\Theta_1\rangle \perp \langle\Theta_2\rangle$.

Diagonalizing the light neutrino mass matrix of eq. (7.15), we find that mixing in the neutrino sector is "tri-bi-maximal" [128], with

$$\theta_{13}^{\nu} = 0, \qquad \theta_{12}^{\nu} = 35.3^{\circ}, \qquad \theta_{23}^{\nu} = 45^{\circ} \tag{7.16}$$

in the notation of [129]. For the charged lepton mixing, we get

$$\theta_{12}^{e} \simeq |\vartheta_5|, \quad \theta_{13}^{e} = \theta_{23}^{e} = 0, \tag{7.17}$$

to leading order in ϑ_5 [130].

With $\theta_{23}^{e} = 0$ in the charged lepton sector, the leptonic 2-3 mixing $\theta_{23}^{\mathrm{PMNS}}$ is [129]

$$\theta_{23}^{\mathrm{PMNS}} \;=\; \theta_{23}^{\nu} = 45^{\circ}. \tag{7.18}$$

The leptonic 1-3 mixing receives a contribution from the 1-2 charged lepton mixing, inducing a non-zero $\theta_{13}^{\mathrm{PMNS}}$ [129]:

$$\theta_{13}^{\mathrm{PMNS}} \;\simeq\; \frac{\theta_{12}^{e}}{\sqrt{2}} \;\simeq\; \left|\frac{\vartheta_5}{\sqrt{2}}\right|. \tag{7.19}$$

The leptonic Dirac CP phase is almost maximal due to the phase difference in the two components of $\langle\Theta_5\rangle$:[5]

$$\delta^{\mathrm{PMNS}} \;\simeq\; 270^{\circ}. \tag{7.20}$$

Since the 1-3 mixings in both the neutrino and the charged lepton mass matrices are zero in this model, we can also use the lepton mixing sum rule [129, 132, 133]

$$\theta_{12}^{\mathrm{PMNS}} \;\simeq\; \theta_{13}^{\mathrm{PMNS}} \cos(\delta^{\mathrm{PMNS}}) + \theta_{12}^{\nu} \;\simeq\; 35^{\circ}. \tag{7.21}$$

Thus, for the vacuum with $\langle\Theta_2\rangle = c_2(1,1,1)^T$, the model predicts the leptonic mixings $\theta_{12}^{\mathrm{PMNS}} \simeq 35^{\circ}$, $\theta_{23}^{\mathrm{PMNS}} \simeq 45^{\circ}$, and an almost maximal $\delta^{\mathrm{PMNS}} \simeq 270^{\circ}$. The value of $\theta_{13}^{\mathrm{PMNS}}$ can be fitted by the choice of ϑ_5.[6]

7.2 Inflaton directions for tribrid inflation

The first step for implementing tribrid inflation in any model is to find suitable inflaton and waterfall directions in the superpotential. In our A_4 flavour model, possible waterfall directions are given by the flavon directions Θ_i and possible inflaton directions are given by D-flat combinations of matter fields.

As we have mentioned in section 6.4, Kähler-driven tribrid inflation requires a superpotential term of the form $\lambda H^2 X^n$ or $\lambda H N X^n$, where H is the waterfall field, X^n is a D-flat inflaton direction and N is some matter field with $N \simeq 0$ during and after inflation. In the superpotential (7.9), the candidate terms are

[5] While there are some corrections due to the non-zero $\theta_{13}^{\mathrm{PMNS}}$, we have numerically confirmed that these are small using the publicly available MPT package [131].

[6] When a model of this type is embedded into a GUT, then the parameter ϑ_5 is linked to the quark sector, which can lead to a prediction also for $\theta_{13}^{\mathrm{PMNS}}$ [17].

1. $\lambda_j \Theta_j \cdot LH_u N_j$, with $H \to \Theta_j$, $X^2 \to LH_u$ and $N \to N_j$,
2. $\gamma_{jj}\langle\Theta_S\rangle N_j^2 \Theta_j^2$, with $H^2 \to \Theta_j^2$, $X^2 \to N_j^2$,

for any $j \in \{1, 2\}$, without implied summation over j.

In the first case, $N_j = 0$ during inflation, and tribrid inflation predicts the Yukawa coupling $y_{\nu_j} = \lambda_j\langle\Theta_j\rangle$ as a function of α_s (fig. 6.3). In the second case, the right-handed sneutrino N_j is the inflaton and tribrid inflation predicts its mass $m_{N_j} = 2\gamma_{jj}\langle\Theta_S\Theta_j^2\rangle$ as a function of α_s (fig. 6.3).

We assume that Θ_S and all Θ_i ($i = 1, ..., 6$) except Θ_j have already settled at their minimum 60 e-folds before the end of inflation,[7] so that only the dynamics of the inflaton X^n and the chosen waterfall field Θ_j are important.

7.2.1 Sneutrino inflation

Using $N_j^2 =: X^2$ as the inflaton direction is straightforward, as N_j does not have any A_4 structure, and the superpotential operator $\langle\Theta_S\rangle\Theta_j^2 N_j^2$ stabilizes all components of the A_4 triplet flavon Θ_j during inflation. The relevant terms during inflation exactly reduce to the simple structure of eq. (6.1); the superpotential term $\gamma_{12}\langle\Theta_S\Theta_i\rangle \cdot \Theta_j N_1 N_2$ does not generate an extra mass for Θ_j during inflation because $\Theta_1 \perp \Theta_2$ is enforced by the flavon alignment potential (7.10). We thus expect that the usual results for Kähler-driven tribrid inflation apply.

7.2.2 Lepton-Higgs inflation

Using LH_u as the inflaton direction, we must account for the possibility that the $\langle\Theta_i\rangle$, $i \neq j$, can induce a large F-term potential for the inflaton:

$$\left|\frac{\partial W}{\partial N_i}\right|^2 = |\lambda_i \Theta_i \cdot LH_u + 2\gamma_{ii}\langle\Theta_S\rangle\Theta_i^2 N_i + \gamma_{ij}\langle\Theta_S\rangle\Theta_i\Theta_j N_j|^2. \tag{7.22}$$

During inflation, these terms can generate a large inflaton potential except if $L \perp \langle\Theta_i\rangle$.[8] This means that the inflaton component with $L \parallel \langle\Theta_i\rangle$ will be quickly driven to zero. If inflation lasts more than the bare minimum of 60 e-folds, we can therefore assume that $L \perp \langle\Theta_i\rangle$ throughout the last 60 e-folds of inflation.

For $j = 1$, the model then again reduces to eq. (6.1), with $LH_u =: \hat{e}_\phi X^2$, where $\hat{e}_\phi \perp \langle\Theta_{i\neq j}\rangle$ is the inflaton direction in A_4 space, normalized to $|\hat{e}_\phi|^2 = 1$. The case $j = 2$ is more complicated and will be discussed below.

[7] Otherwise, we would have multi-field inflation with several waterfalls. Only after the last waterfall will the vacuum energy be zero, so we expect that inflation continues until the last flavon field moves towards its minimum.

[8] The F-term in eq. (7.22) could also be minimised by $N_i = \lambda_i\Theta_i \cdot LH_u/(2\gamma_{ii}\langle\Theta_S\rangle\Theta_i^2)$. This ambiguity disappears if we include Hubble-scale mass terms for N_i which can be naturally generated from the Kähler potential.

7.2.3 Unique inflaton direction for preventing topological defects

Many models of hybrid inflation can produce dangerous topological defects at the end of inflation, and the above model is no exception. In our case, the waterfall transition for the Θ_j usually generates $\mathbb{Z}_{n_j}$ domain walls. The model therefore needs some mechanism to either prevent their production or to remove the domain walls after they are formed.

In tribrid inflation, the problem is alleviated by the fact that the inflaton can be charged under the symmetries of the waterfall field, and therefore those symmetries are usually already broken during inflation. If the symmetry breaking is transmitted to the waterfall field, e.g. via additional inflaton-waterfall field couplings, the formation of topological defects at the end of inflation may be avoided [25].

However, in this chapter's A_4 model there is one unique inflaton direction for which the production of domain walls is avoided automatically: the LH_u direction with Θ_2 as the waterfall field ($j = 2$). We want to discuss this case in more detail in the next section.

7.3 Inflationary trajectory without topological defects

As we have discussed in section 7.2.3, one can use different mechanisms to avoid the overproduction of topological defects at the end of inflation. In this section, we discuss a particular inflaton trajectory for which topological defects are avoided automatically, because the waterfall field has a small shift during inflation. In our model, this naturally occurs for inflation along the LH_u direction with Θ_2 as the waterfall field. We restrict our analysis to that special case throughout this section.

We will need to keep track of the different A_4 triplet components of both the inflaton and the waterfall field, so it will be useful to introduce the notation

$$\Theta_2 = \begin{pmatrix} x \\ y \\ z \end{pmatrix}, \quad LH_u = \Phi^2 \begin{pmatrix} 1 \\ 0 \\ 0 \end{pmatrix}, \tag{7.23}$$

where we chose an inflaton direction which satisfies the condition $LH_u \perp \langle\Theta_1\rangle$ which we have explained in section 7.2.2.[9]

We should also note that during inflation Θ_1 can have any value

$$\Theta_1 = \begin{pmatrix} 0 \\ u \\ v \end{pmatrix}, \quad \text{with } u^2 + v^2 = \Lambda_1^2. \tag{7.24}$$

The flavon alignment potential (7.10) only fixes u and v when Θ_2 has a sufficiently large vacuum expectation value, i.e. after the waterfall transition. During inflation, u and v are instead determined by their initial conditions.

[9] This inflaton direction is not unique, one can choose any direction perpendicular to $\langle\Theta_1\rangle$. We focus on one specific direction, which suffices to demonstrate how the proposed mechanism works.

7.3.1 Shift in Θ_2

To see that Θ_2 is non-zero during inflation, we need to minimize its scalar potential during inflation. The relevant superpotential terms are

$$\begin{aligned} W \supset\ & \lambda_2\, \Theta_2 \cdot L H_u N_2 + \gamma_{22} \langle \Theta_S \rangle N_2^2 \Theta_2^2 + \kappa S_2 \left(\Theta_2^3 - \Lambda_2^2 \right) \\ & + \alpha_1 D_2' (\Theta_2^2)_{\mathbf{1}''} + \alpha_2 D_2'' (\Theta_2^2)_{\mathbf{1}'} + \alpha_3 P_{12} \Theta_1 \Theta_2. \end{aligned} \tag{7.25}$$

We use the A_4 contractions, with $\omega = e^{2\pi i/3}$:

$$\begin{aligned} (\Theta_2^2)_{\mathbf{1}'} &= x^2 + \omega^2 y^2 + \omega z^2, & \Theta_2^2 &= x^2 + y^2 + z^2, \\ (\Theta_2^2)_{\mathbf{1}''} &= x^2 + \omega y^2 + \omega^2 z^2, & \Theta_2^3 &= xyz. \end{aligned} \tag{7.26}$$

When calculating the F-term potential, we must include the Kähler potential coupling

$$\Delta K \ =\ (\kappa_\Theta + 1) |\Theta_2^2 S_2^2| + ... \tag{7.27}$$

The F-term potential then becomes

$$\begin{aligned} V_F^{(\Theta_2)} \ &=\ \left| \frac{\partial W}{\partial N_2} \right|^2 + \left| \frac{\partial W}{\partial S_2} \right|^2 + \left| \frac{\partial W}{\partial D_2'} \right|^2 + \left| \frac{\partial W}{\partial D_2''} \right|^2 + \left| \frac{\partial W}{\partial P_{12}} \right|^2 - \kappa_\Theta V_0 |\Theta_2|^2 \\ &=\ \left| \lambda_2 x \Phi^2 + 2\gamma_{22} \langle \Theta_S \rangle N_2 (x^2 + y^2 + z^2) \right|^2 + \kappa^2 \left| xyz - \Lambda_2^2 \right|^2 - \kappa_\Theta V_0 (|x|^2 + |y|^2 + |z|^2) \\ &\quad + \alpha_1^2 \left| x^2 + \omega y^2 + \omega^2 z^2 \right|^2 + \alpha_2^2 \left| x^2 + \omega^2 y^2 + \omega z^2 \right|^2 + \alpha_3^2 \left| \Theta_1 \cdot \Theta_2 \right|^2 . \end{aligned} \tag{7.28}$$

The last term enforces $\Theta_1 \perp \Theta_2$, which implies that

$$y = \varepsilon v, \quad z = -\varepsilon u, \quad \text{(for some } \varepsilon \in \mathbb{C}) \tag{7.29}$$

and which also guarantees that we can ignore the operator $\gamma_{12} \langle \Theta_S \rangle \Theta_1 \Theta_2 N_1 N_2$ throughout this calculation.

Shift in y and z

To find the shifts in y and z, we approximate $x \simeq 0$ and $N_2 \simeq 0$. We will later see under which conditions this approximation is valid. With this approximation and eq. (7.29), the potential (7.28) simplifies to

$$\begin{aligned} V_F^{(\Theta_2)} \ \simeq\ & V_0 - \kappa_\Theta V_0 (|u|^2 + |v|^2) |\varepsilon|^2 + (\alpha_1^2 + \alpha_2^2)(|u|^4 + |v|^4) |\varepsilon|^4 \\ & + 2\,|uv|^2 \left\{ \alpha_1^2 \cos\left(2 \arg(u/v) + \frac{2\pi}{3} \right) + \alpha_2^2 \cos\left(2 \arg(u/v) - \frac{2\pi}{3} \right) \right\} |\varepsilon|^4. \end{aligned} \tag{7.30}$$

Minimizing the potential with respect to $|\varepsilon|^2$ gives

$$|\varepsilon|^2 \ \simeq\ \frac{|u|^2 + |v|^2}{2(\alpha_1^2 + \alpha_2^2)(|u|^4 + |v|^4) + 4\gamma |uv|^2}\, \kappa_\Theta V_0, \tag{7.31}$$

with

$$\gamma := \alpha_1^2 \cos\left(2\arg(u/v) + \frac{2\pi}{3}\right) + \alpha_2^2 \cos\left(2\arg(u/v) - \frac{2\pi}{3}\right). \tag{7.32}$$

For $\alpha_i = \mathcal{O}(1)$, one can show that eq. (7.31) implies $\max(|y|, |z|) = \mathcal{O}(1)\sqrt{\kappa_\Theta V_0}$.

Note that the potential is not minimized with respect to $\Theta_1 = (0, u, v)$. Instead, u and v are constants given by the initial conditions, because in general their potential is very flat compared to the inflaton potential, and therefore the fields can be treated as constant during inflation.[10]

Shift in x

Using the shifts in y and z, but still assuming that $S_2 = N_2 = 0$, we can find the minimum for x by minimizing eq. (7.28):

$$\begin{aligned} V_F^{(x)} \;=\; & (\lambda_2^2|\Phi|^4 - \kappa_\Theta V_0)|x|^2 - 2\kappa^2\Lambda_2^2 \operatorname{Re}(xyz) + (\alpha_1^2 + \alpha_2^2)|x|^4 \\ & + 2\alpha_1^2 \operatorname{Re}\left\{(x^*)^2(\omega y^2 + \omega^2 z^2)\right\} + 2\alpha_2^2 \operatorname{Re}\left\{(x^*)^2(\omega^2 y^2 + \omega z^2)\right\}. \end{aligned} \tag{7.33}$$

The two dominant terms are $\lambda_2^2|\Phi|^4$ and the linear term in x. The other mass terms for x are negligible during inflation because $\lambda_2^2|\Phi|^4 \gg \lambda_2^2|\Phi_\mathrm{c}|^4 = \kappa_\Theta V_0$, and y^2, $z^2 \lesssim \kappa_\Theta V_0$. The x^4 term is also negligible, as we will find that $x^2 \ll \kappa_\Theta V_0$.

We can therefore minimize the simple potential

$$V_F^{(x)} \;\simeq\; \lambda_2^2|\Phi|^4|x|^2 - 2\kappa^2\Lambda_2^2 \operatorname{Re}(xyz) \tag{7.34}$$

with respect to x. The result is

$$|x| \;\simeq\; \frac{\kappa|yz|}{\lambda_2^2|\Phi|^4} \underbrace{\kappa\Lambda_2^2}_{\sqrt{V_0}} \;\leq\; \frac{\kappa \max(|y|,|z|)^2}{\lambda_2^2|\Phi|^4}\sqrt{V_0} \;=\; \mathcal{O}(1)\,\kappa\frac{\kappa_\Theta V_0}{\lambda_2^2|\Phi|^4}\sqrt{V_0}. \tag{7.35}$$

During inflation, we have $\lambda_2^2\Phi^4 \gg \lambda_2^2\Phi_\mathrm{c}^4 = \kappa_\Theta V_0$, and therefore $|x|^2 \ll V_0$, so x is suppressed with respect to y, $z \sim \sqrt{\kappa_\Theta V_0}$. This justifies our assumption in section 7.3.1, where we set $x \simeq 0$ for the calculation of the shifts in y and z.

Near the critical point, we find that x is no longer suppressed with respect to y and z: $x \simeq \mathcal{O}(1)\sqrt{V_0}$. In this case, y and z are no longer stabilized by $|\partial W/\partial D_2'|^2$ and $|\partial W/\partial D_2''|^2$, and we expect Θ_2 to roll down the potential along the direction $x \simeq y \simeq z$. Therefore, near the critical inflaton value, we could have a smooth transition towards the minimum

[10] u and v initially minimize the F-term potential for $\Theta_2 = 0$, so the only term which induces a potential for u and v is the interaction term $\alpha_3^2|\Theta_1 \cdot \Theta_2|^2$, which creates a potential for Θ_1 and Θ_2 when they are not perpendicular to each other. However, this potential for each field is proportional to the vacuum expectation value of the other field, and due to $\Theta_1 \sim \Lambda_1 \gg \Theta_2 \sim \mathcal{H}$, the potential will generally be much greater for Θ_2 and thus be minimized by an adjustment in Θ_2.

of the waterfall field instead of a sudden waterfall at $\Phi = \Phi_c$. Anyway, as the waterfall potential is steep, we expect inflation to end quickly near $\Phi \simeq \Phi_c$, so that the model still approximately acts as a model of Kähler-driven tribrid inflation.

We expect that the slow-roll predictions for α_s and $\langle H \rangle$ are not influenced by the shift in Θ_2, as they depend only on the inflaton potential far away from the critical point. However, λ_2 (and the derived y_{ν_2}) might be changed by a factor of about $\exp(\pm\delta N/10)$, where δN is the number of e-folds before the critical point at which the shift in Θ_2 becomes relevant.[11]

Shifts in other fields

S_2 and N_2 also get small shifts due to the shift in x. However, these are completely negligible if S_2 and N_2 also get positive Hubble-size masses from the Kähler potential: in that case, one can easily show that $S_2 \ll N_2 \ll |x|$. We therefore set S_2, $N_2 \simeq 0$ in this chapter.

7.3.2 Inflaton potential

The shift in Θ_2 induces a small correction to the inflaton potential from

$$\begin{aligned} V_F \supset |\lambda_2 \Theta_2 \cdot L H_u|^2 &= \lambda_2^2 |x|^2 |\Phi|^4 \lesssim \lambda_2^2 \kappa^2 V_0 \left(\frac{\kappa_\Theta V_0}{\lambda_2^2 |\Phi|^4} \right)^2 |\Phi|^4 \\ &\ll \mathcal{O}(1)\, V_0 |\Phi|^4 . \quad (\text{for } \Phi \gg \Phi_c) \end{aligned} \tag{7.36}$$

For $\Phi \gg \Phi_c$, the extra inflaton potential that is induced by $\Theta_2 \neq 0$ is therefore much smaller than the inflaton potential $V_\phi \simeq V_0(1 + a\,\phi^2 + b\,\phi^4)$.

We conclude that despite the shift in Θ_2, inflation is mostly Kähler-driven, except possibly near $\Phi \simeq \Phi_c$ around which we expect inflation to end anyway. Therefore we can approximately use the predictions for $y_{\nu_2} \mathrel{\hat{=}} y_\nu$ and $\langle \Theta_2 \rangle \mathrel{\hat{=}} \langle H \rangle$ from fig. 6.3, which have been calculated for purely Kähler-driven tribrid inflation.

7.3.3 Possible variant: $S_2(\Theta_2^5 - \Lambda_2^2)$

A simple variant of this model can be obtained by replacing the vacuum energy term for Θ_2 in the superpotential:

$$W \supset \kappa S_2(\Theta_2^3 - \Lambda_2^2) \;\to\; \kappa S_2 \left(\Theta_2^3\, \Theta_2^2 - \Lambda_2^2 \right). \tag{7.37}$$

The replacement suppresses the shift in x during inflation by another power of $y^2 + z^2 \sim V_0 \sim 10^{-12}$, which makes it completely negligible. This improves the quality of our approximations and we expect that the model will behave more exactly like purely Kähler-driven

[11] This change in λ_2 happens if the shift in Θ_2 either accelerates or delays the phase transition, because λ_2 must be adjusted to get the correct number of e-folds between Φ_* and the end of inflation. A precise prediction of λ_2 therefore requires an analysis of the complete multi-field model near $\Phi \simeq \Phi_c$ including all components of Θ_2, and possibly a quantitative treatment of the tachyonic preheating phase.

tribrid inflation, even very close to $\Phi \simeq \Phi_c$. Nevertheless, this setup may still remove domain walls during the waterfall transition, as the potential still prefers a specific phase for x when x, y and z grow during the waterfall transition.

However, it is not clear whether the preference is sufficiently large to either prevent the production of domain walls or to efficiently remove them if they are produced. To answer this question, the preheating phase must be studied in detail, which is beyond the scope of this chapter.

7.4 Conditions for the shift in the waterfall field

We have seen that if the flavon Θ_2 is identified with the waterfall field and LH_u with the inflaton, the waterfall field obtains a small shift during inflation, which can prevent the formation of topological defects during the waterfall transition.[12] However, if we had used Θ_1 as the waterfall field or N_2 as the inflaton, no such shift would have occurred during inflation.

In this section, we briefly want to sketch which characteristics of the superpotential determine whether the waterfall field can obtain a shift during Kähler-driven tribrid inflation:

1. The waterfall field H consists of several fields, e.g. it is a multiplet under some symmetry.

2. At least one of the multiplet components of H does not receive a mass from the inflaton.

3. The same multiplet component of H does not receive a mass term from the alignment potential, but is instead stabilized by higher-order terms only.[13]

Let us apply these considerations to our example model: The first condition restricts the range of waterfall fields for which this mechanism can work. In our model it is satisfied because we use an A_4 triplet flavon as the waterfall field.

The second condition explains why we do not get a shifted waterfall field when we use N_2 as the inflaton: the superpotential term $W^{(N)} = \gamma_{22}\langle\Theta_S\rangle\Theta_2^2 N_2^2 = \gamma_{22}\langle\Theta_S\rangle(x^2+y^2+z^2)N_2^2$ provides masses for all three A_4 components of Θ_2 as long as $N_2 > \Phi_c$, so the waterfall field is stabilized exactly at zero during inflation.

The third condition explains why using Θ_1 does not lead to shifted waterfall trajectories. Although an LH_u inflaton only provides masses for one of the three A_4 components of Θ_1, the other two components acquire mass terms from the flavon alignment potential via the

[12] Even if the production of domain walls is not totally prevented, it might be sufficient to bias the occupation fraction such that domains of one vacuum are more abundant than those of other vacua, since such biased initial conditions lead to an exponential decay of the domain wall network [134].

[13] There must be stabilizing terms, otherwise the waterfall will happen immediately along the unstabilized direction.

terms $W_{\text{fl}} \supset P_{12}\Theta_1\Theta_2 + P_{16}\Theta_1\Theta_6$. Therefore, all three A_4 directions of the waterfall field are stabilized at zero during inflation, and no shift can occur.

7.5 Summary

As an explicit example for tribrid inflation in a realistic particle physics model, we have analysed a particular flavour model based on a spontaneously broken A_4 family symmetry. The inflaton can be either a right-handed sneutrino or a D-flat LH_u direction, and tribrid inflation predicts a relation between the running of the spectral index α_s and either the right-handed neutrino mass m_N or the neutrino Yukawa coupling y_ν as shown in fig. 6.3. For the considered range of parameters, the model also predicts leptonic mixing angles $\theta_{12}^{\text{PMNS}} \simeq 35^\circ$ and $\theta_{23}^{\text{PMNS}} \simeq 45^\circ$, and an almost maximal leptonic Dirac CP phase $\delta^{\text{PMNS}} \simeq 270^\circ$.

For a particular inflaton trajectory along the LH_u direction, the waterfall field gets a slight shift already during inflation, which might prevent the formation of topological defects at the end of inflation. We have calculated the shifts of the waterfall field's components and shown that their effect on the inflaton dynamics is small, so that the predictions of Kähler-driven tribrid inflation should still apply with a possible small change in the predicted value of the neutrino Yukawa coupling y_ν.

We also discussed the specific properties of our flavon alignment potential and of the inflaton-waterfall coupling which are responsible for the waterfall field's shift. These properties can be reproduced in other tribrid inflation models to identify alignment potentials and inflaton directions for which the production of topological defects can be avoided.

Chapter 8

Tribrid inflation from renormalizable couplings to messenger fields

In chapters 6 and 7, we have discussed small-field tribrid inflation with the assumption that all non-renormalizable operators are suppressed by the Planck scale. This allowed us not only to expand the scalar potential in powers of $Y_i/m_{\rm Pl}$, but also to use effective field theory (EFT) without worrying about its validity since all the energy scales involved in tribrid inflation were small compared to the Planck scale.

However, many realistic particle physics embeddings of tribrid inflation extend the MSSM not only by the tribrid fields S, H, and X, but also by other new physics at a scale $\Lambda_{\rm NP} < m_{\rm Pl}$, e.g. some additional particles of mass $m_A \sim \Lambda_{\rm NP}$. In principle, we can always account for such particles by analysing the inflationary dynamics in the full model including all of the new particles explicitly in the superpotential W and the Kähler potential K as we did for the A_4 lepton flavour model in chapter 7. For energies below $\Lambda_{\rm NP}$, we can also use a simpler approach: we can integrate out the messenger particles and work with the resulting EFT which then includes various non-renormalizable operators suppressed by powers of $Y_i/\Lambda_{\rm NP}$.

In general, such an EFT is only valid for energies below the cutoff scale $\Lambda_{\rm cutoff} \sim \Lambda_{\rm NP}$. However, it is not immediately clear how this translates into bounds on the inflaton field displacement $\Delta\phi$ during inflation. For $\Delta\phi \gtrsim \Lambda_{\rm cutoff}$, it is not possible to deduce the most relevant operators by a truncated expansion in $\Delta\phi/\Lambda_{\rm cutoff}$. However, if there are symmetry arguments to limit the number and field content of non-renormalizable operators, the EFT might still work for larger $\Delta\phi$ as long as the relevant energy scale (e.g. the Hubble scale $\mathcal{H}$ in inflation) is smaller than $\Lambda_{\rm cutoff}$.

In tribrid inflation, this question is particularly relevant, as its waterfall phase transition can naturally be related to some new physics at high but sub-Planckian scales $\Lambda_{\rm NP} \ll m_{\rm Pl}$. At the same time, typical inflaton field displacements $\Delta\phi$ during tribrid inflation are about $M_{\rm GUT} \lesssim \Delta\phi \ll m_{\rm Pl}$, and many potentially interesting tribrid models have $\Delta\phi \gtrsim \Lambda_{\rm NP}$. It is therefore important to understand whether tribrid inflation in such models can be studied in the effective field theory framework with non-renormalizable operators suppressed by $\Lambda_{\rm cutoff} \sim \Lambda_{\rm NP}$, or if one needs to explicitly include all relevant particles with masses up to almost $m_{\rm Pl}$.

In this chapter, we study this question for tribrid inflation by comparing the predictions of a non-renormalizable Kähler-driven tribrid model to an explicit UV completion in which

	S	H	N	X
$U(1)_R$	2	0	1	1/2
$\mathbb{Z}_{4n}$	0	n	$n-2$	$n+1$

Table 8.1: One possible set of symmetries and charge assignments for the superpotential in eq. (8.1), for any integer $n \geq 3$.

the effective superpotential operators are replaced by renormalizable couplings to heavy messenger fields. We discuss one particular case in detail and show that the tree-level quantities match even for $\Delta\phi > \Lambda_{\rm cutoff}$ up to small corrections of order $\mathcal{H}/\Lambda_{\rm cutoff}$. We then analyse the one-loop corrections which can be different between effective and renormalizable superpotential, and finally discuss how one can generate different effective tribrid models by different choices for the messenger sector, providing guidelines for tribrid inflation model building in the presence of sub-Planckian new particles coupled to the S, H or X fields of tribrid inflation.

Throughout this chapter, we generally keep the powers of $m_{\rm Pl}$ instead of setting $m_{\rm Pl} = 1$ to emphasize the relevant suppression scales.

8.1 Tribrid inflation with non-renormalizable superpotential

Let us initially focus on the specific choice $\ell = 4$, $m = n = 2$ for the tribrid superpotential of eq. (6.1), i.e.

$$W_{\rm eff} \,=\, S\left(\Lambda^2 - \frac{H^4}{\Lambda_H^2}\right) + \frac{1}{\Lambda_\phi} HNX^2 + ..., \tag{8.1}$$

where we defined $\Lambda := V_0^{1/4}$ and the dots denote terms which are irrelevant for inflation.[1] Our analysis can be extended to tribrid superpotentials with $\ell > 4$ and/or $n > 2$ as we will briefly discuss in section 8.4. However, the analysis will be much easier to follow for a particular example, and therefore we will do most of our analysis for the explicit superpotential in eq. (8.1). The given form of the superpotential can be enforced e.g. by an $U(1)_R$ and a $\mathbb{Z}_{4n}$ symmetry with charge assignments given in table 8.1. We also assume that the Kähler potential can be expanded in the modulus squared of the fields as in eq. (6.4).

[1] Such extra terms can give a mass to N after inflation, e.g. via $\Delta W \propto H^3N^2$ if one chooses a $\mathbb{Z}_{16}$ symmetry ($n = 4$) in table 8.1.

The resulting scalar potential has the form

$$V = \Lambda^4 \left| \frac{H^4}{\Lambda_H^2 \Lambda^2} - 1 \right|^2 + \left(\frac{|X|^4}{\Lambda_\phi^2} + \Delta m_H^2 \right) |H|^2 + \Delta V_{\rm inf}(X) + \left(\frac{|X|^4}{\Lambda_\phi^2} + \Delta m_N^2 \right) |N|^2 + \Delta m_S^2 |S|^2 + ..., \tag{8.2}$$

where $\Lambda^4 + \Delta V_{\rm inf}(X)$ is the inflaton potential during inflation and Δm_H^2, Δm_N^2 and Δm_S^2 are additional squared masses for H, N and S due to Kähler potential operators for which we assume $\Delta m_H^2 \lesssim -\mathcal{H}^2$ and Δm_N^2, $\Delta m_S^2 \gtrsim \mathcal{H}^2$.[2]

Inflation happens for $|X| > |X_{\rm c}| \equiv |\Delta m_H \Lambda_\phi|^{1/2}$ and $H = N = S = 0$, with the inflaton slowly rolling towards smaller values while $H = N = S = 0$ due to their positive mass terms, and the universe expands due the large false vacuum energy $V \simeq \Lambda^4$. Eventually, $|X|$ drops below $|X_{\rm c}|$, at which time H develops a tachyonic mass and quickly falls towards its minimum, terminating inflation.

As explained in chapter 6, Kähler-driven tribrid inflation is equivalent to single-field inflation with the canonically normalized[3] real inflaton field $\phi \simeq \sqrt{2}|X|$ with the inflaton potential $V_{\rm inf}(\phi)$ given by eq. (6.9):

$$V_{\rm inf}(\phi) = V_0 \left(1 + \frac{a}{m_{\rm Pl}^2} \phi^2 + \frac{b}{m_{\rm Pl}^4} \phi^4 + ... \right). \tag{8.3}$$

Inflation ends by a waterfall transition at

$$\phi_{\rm c} = \sqrt{|2\Lambda_\phi \Delta m_H|}, \tag{8.4}$$

after which the waterfall field acquires a vacuum expectation value

$$\langle H \rangle^2 = \pm \Lambda_H \Lambda. \tag{8.5}$$

The predictions of Kähler-driven tribrid inflation were calculated in chapter 6 based only on the three eqs. (8.3)–(8.5). It is therefore sufficient to show that a model reproduces these three equations to conclude that its predictions will be identical to those of Kähler-driven tribrid inflation.

8.2 Generating W from renormalizable couplings

In the tribrid inflation model discussed above, the inflaton field traverses distances $\Delta\phi \sim \mathcal{O}(m_{\rm Pl}/10)$ during inflation. While this is sufficiently small to allow expanding the potential

[2] The sign of $\Delta m_{Y_i}^2$ depends on κ_{iS}. We assume that κ_{iS} is chosen such that tribrid inflation is possible; for $\Delta m_S^2 < 0$, $S = 0$ would not be stable during inflation, and for $\Delta m_H^2 > 0$, H would not develop a tachyonic instability for any ϕ.

[3] The small difference between ϕ and $\sqrt{2}|X|$ is due to canonical normalization, because X has a non-canonical kinetic term $K_{\overline{X}X}(\partial_\mu X)^\dagger(\partial^\mu X)$.

	S	H	N	X	A_1	A_2	B_1	B_2
$U(1)_R$	2	0	1	1/2	2	0	3/2	1/2
$\mathbb{Z}_{4n}$	0	n	$n-2$	$n+1$	$2n$	$2n$	$2n-1$	$2n+1$

Table 8.2: One possible set of symmetries and charge assignments for the superpotential in eq. (8.6), for any integer $n \geq 3$.

in powers of $\phi^2/m_{\rm Pl}^2$, it is not clear whether the model remains valid for $\Lambda_H \ll m_{\rm Pl}$ or $\Lambda_\phi \ll m_{\rm Pl}$: this would lead to $\Delta\phi \gtrsim \Lambda_H$ or $\Delta\phi \gtrsim \Lambda_\phi$, which suggests that the inflaton field value might be above the cutoff scale of the EFT during inflation.

To study this question, we construct an explicit UV completion of the above model by replacing the non-renormalizable superpotential operators with renormalizable couplings to heavy messenger fields A_i and B_i which have masses much greater than the Hubble scale.[4] We then study inflation with the renormalizable superpotential and show that it leads to the same tree-level predictions as the EFT even for $\Delta\phi > \Lambda_H$ and $\Delta\phi > \Lambda_\phi$ up to small corrections. The one-loop quantum corrections to the inflaton potential and the effects of different choices for the messenger sector will be discussed in sections 8.3 and 8.4, respectively.

8.2.1 W and K with renormalizable couplings to messenger fields

We can generate the two non-renormalizable operators in eq. (8.1) from renormalizable couplings to messengers A_1, A_2, B_1 and B_2 via the diagrams shown in fig. 8.1. The superpotential for the theory including the heavy messengers is

$$W = g_1 H^2 A_1 + m_A A_1 A_2 + S\left(g_2 A_2^2 - \Lambda^2\right) + g_H X H B_1 + g_N X N B_2 + m_B B_1 B_2 + ..., \tag{8.6}$$

where the dots again denote terms which are irrelevant for inflation. A possible choice of symmetries and charge assignments for all fields including the messengers is given in table 8.2.

The Kähler potential is again expanded in powers of $Y_i/m_{\rm Pl}$, see eq. (6.4), with $Y = \{S, H, N, X, A_1, A_2, B_1, B_2\}$.

We will now in turn calculate the inflaton potential $V_{\rm inf}$, the critical inflaton field value $\phi_{\rm c}$ and the vacuum expectation value $\langle H\rangle^2$ after inflation to compare this models' predictions to the tribrid model of section 8.1.

8.2.2 Inflaton potential $V_{\rm inf}$

The inflaton potential $V = V_F$ can be calculated from eq. (5.4) with $V_D = 0$, because the D-term potential enforces that the inflaton trajectory is D-flat as discussed in appendix C.1.

[4] If the messenger fields' masses are below the Hubble scale, they need to be taken into account as dynamical degrees of freedom. Their quantum fluctuations can affect the primordial spectrum of perturbations and the predictions must be calculated using a multi-field formalism such as the δN formalism.

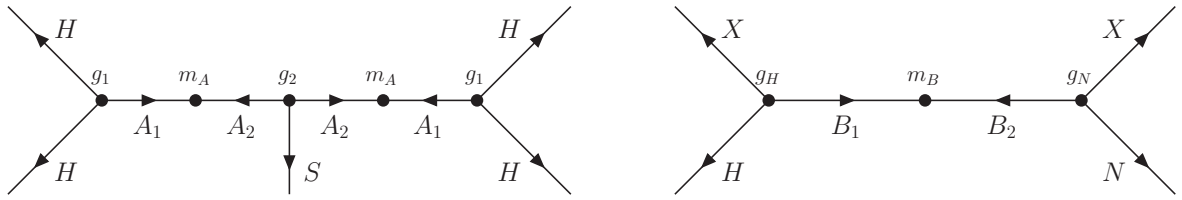

Figure 8.1: Diagrams for generating the non-renormalizable operators of the superpotential in eq. (8.1) from renormalizable superpotential couplings to heavy messenger fields A_i and B_i.

During inflation, all non-inflaton fields are stabilized at zero, so the inflaton potential is given by the scalar potential from eq. (5.4) with $S = H = N = A_i = B_i = 0$. As before, we have $W = 0$, $W_i = 0$ for all $i \neq S$, and $W_S = \Lambda^2$, and therefore

$$V_{\text{inf}} \;=\; e^{K/m_{\text{Pl}}^2}\left(W_S K^{S\overline{S}} W_S^\dagger\right) \;=\; \Lambda^4 e^{K/m_{\text{Pl}}^2} K^{S\overline{S}}. \tag{8.7}$$

With the same arguments as in section 6.3.1 we arrive at the inflaton potential:

$$V_{\text{inf}} \;=\; \Lambda^4 \left[\frac{e^{K/m_{\text{Pl}}^2}}{K_{\overline{S}S}}\right]_{S=H=\ldots=0} \simeq\; \Lambda^4\left(1 \;+\; \frac{a}{m_{\text{Pl}}^2}\phi^2 \;+\; \frac{b}{m_{\text{Pl}}^4}\phi^4 \;+\; \ldots\right). \tag{8.8}$$

This tree-level inflaton potential is identical to that in eq. (6.9) for the non-renormalizable superpotential. The underlying reason is that during inflation, both models have $W = 0$, $|W_S| = \Lambda^2$, and $W_i = 0$ for all $i \neq S$. No matter how the superpotential is changed, as long as it contains the term $W \supset \Lambda^2 S$ and all other terms have at least two powers of non-inflaton fields (which are stabilized at zero during inflation), the inflaton potential will always reduce to eq. (6.9) during inflation.

8.2.3 Critical inflaton field value ϕ_{c}

We now want to find the critical inflaton field value ϕ_{c}, which is defined as the inflaton field value below which the waterfall field develops a tachyonic mass:

$$m_H^2(\phi_{\text{c}}) = 0. \tag{8.9}$$

The first step will be to find the waterfall fields' mass matrix and the second step will be to solve eq. (8.9) for ϕ_{c}.

Calculation of the waterfall fields' mass terms

To determine the waterfall fields' mass terms, we need to keep terms in the scalar potential given by eq. (5.4) up to quadratic order in H. We also need to keep terms up to quadratic order in B_2 because we will find mixing between H and B_2, and we keep terms up to

leading order in X to find the correct dependence of the mass terms on the inflaton field value.

The renormalizable contributions to the mass matrix can be calculated from $V_F^{(\mathrm{ren})} = |W_i|^2$. The relevant terms are:

$$|W_N|^2 = |g_N X B_2|^2 , \tag{8.10a}$$

$$|W_{B_1}|^2 = |g_H X H + m_B B_2|^2 = |m_B B_2|^2 + |g_H X|^2 |H|^2 + 2\,\mathrm{Re}\left(g_H m_B^\dagger X H B_2^\dagger\right). \tag{8.10b}$$

The non-renormalizable corrections to these masses can be calculated starting with the full formula from eq. (5.4), expanding K as in eq. (6.4) and keeping only terms up to quadratic order in Y_i/m_{Pl}. Their main effect is generating additional Hubble-sized diagonal mass terms for all fields during inflation (see appendix C.3 for details):

$$V_{\mathrm{SUGRA}} \simeq \frac{c_i \Lambda^4}{m_{\mathrm{Pl}}^2} |Y_i|^2 \equiv \Delta m_i^2 |Y_i|^2, \tag{8.11}$$

where the c_i are functions of the Kähler potential coupling constants κ_{ij}.

Waterfall fields' mass matrix

Due to the mixing term in eq. (8.10b), we must consider the entire H-B_2 mass matrix to determine for which ϕ the lowest mass eigenvalue becomes tachyonic.

To make the calculation less cumbersome, we choose g_H, g_N, m_B and X to be real; their phases can be absorbed into H, N, B_1 and B_2 by field redefinitions. We then decompose the fields into real and imaginary parts:

$$B_2 = \frac{1}{\sqrt{2}} (b_R + i b_I) , \quad H = \frac{1}{\sqrt{2}} (h_R + i h_I) , \quad X = \frac{\phi}{\sqrt{2}}. \tag{8.12}$$

The potential for H and B_2 is now

$$\begin{aligned} V_{HB_2} = {} & \frac{1}{2}\left(m_B^2 + \Delta m_{B_2}^2 + \frac{g_N^2 \phi^2}{2}\right)\left(b_R^2 + b_I^2\right) + \frac{1}{2}\left(\Delta m_H^2 + \frac{g_H^2 \phi^2}{2}\right)\left(h_R^2 + h_I^2\right) \\ & + \frac{g_H \phi}{\sqrt{2}} m_B \left(b_R h_R + b_I h_I\right). \end{aligned} \tag{8.13}$$

The mass matrices for the field pairs (b_R, h_R) and (b_I, h_I) are

$$m_{HB_2}^2 = \begin{pmatrix} m_B^2 + \Delta m_{B_2}^2 + \frac{g_N^2 \phi^2}{2} & \frac{g_H \phi}{\sqrt{2}} m_B \\ \frac{g_H \phi}{\sqrt{2}} m_B & \Delta m_H^2 + \frac{g_H^2 \phi^2}{2} \end{pmatrix}. \tag{8.14}$$

For large inflaton field values, this mass matrix is dominated by the diagonal entries proportional to ϕ^2:

$$m_{HB_2}^2 \xrightarrow{\phi \to \infty} \begin{pmatrix} \frac{g_N^2 \phi^2}{2} & 0 \\ 0 & \frac{g_H^2 \phi^2}{2} \end{pmatrix} + \ldots, \tag{8.15}$$

so that all mass eigenvalues are positive for very large inflaton field values.[5]

Solving for ϕ_c

For small inflaton field values below ϕ_c, one of the mass eigenvalues becomes negative. We can determine ϕ_c from the condition $m^2_{HB_2,\pm}(\phi_c) = 0$, where $m^2_{HB_2,\pm}$ are the eigenvalues of the waterfall fields' mass matrix in eq. (8.14). To find a zero eigenvalue, we just have to set the determinant of the matrix to zero:

$$\begin{aligned} 0 \;&=\; \det \begin{pmatrix} m_B^2 + \Delta m_{B_2}^2 + \frac{g_N^2 \phi_c^2}{2} & \frac{g_H \phi_c}{\sqrt{2}} m_B \\ \frac{g_H \phi_c}{\sqrt{2}} m_B & \Delta m_H^2 + \frac{g_H^2 \phi_c^2}{2} \end{pmatrix} \\ &=\; \left(\frac{g_N^2 \phi_c^2}{2} + m_B^2 + \Delta m_{B_2}^2 \right) \left(\frac{g_H^2 \phi_c^2}{2} + \Delta m_H^2 \right) - \frac{g_H^2 \phi_c^2}{2} m_B^2. \end{aligned} \tag{8.16}$$

We can easily solve this for ϕ_c^2. The exact result looks somewhat messy, but we find a simple leading-order result by expanding in powers of $\Delta m_i / m_B \sim \mathcal{H}/m_B$:

$$\phi_c^2 \;\simeq\; \frac{2 m_B}{g_N g_H} |\Delta m_H| + ... \tag{8.17}$$

Up to corrections suppressed by powers of $\mathcal{H}/m_B$, which we denoted by "...", eq. (8.17) coincides with eq. (8.4) from the non-renormalizable theory if we identify

$$\Lambda_\phi \;=\; \frac{m_B}{g_N g_H}, \tag{8.18}$$

just as one would expect from integrating out the heavy B_i fields in the renormalizable theory.

8.2.4 Vacuum expectation values after inflation

The SUSY-preserving global minimum can be determined by setting all W_i to zero. A straightforward calculation shows that this requires

$$\langle A_2 \rangle^2 \;=\; \frac{\Lambda^2}{g_2}, \tag{8.19a}$$

$$\langle H \rangle^2 \;=\; -\frac{m_A}{g_1} \langle A_2 \rangle \;=\; \pm \frac{m_A \Lambda}{g_1 \sqrt{g_2}}. \tag{8.19b}$$

Eq. (8.19b) coincides with eq. (8.5) from the non-renormalizable tribrid model if

$$\Lambda_H \;=\; \frac{m_A}{g_1 \sqrt{g_2}}, \tag{8.20}$$

[5] One can also check that $N_* \sim 50$ e-folds before the end of inflation, when CMB scales cross the horizon, the H-B_2 mass eigenvalues are large compared to the Hubble scale, so that the waterfall field's perturbations can be neglected for computing the spectrum of primordial curvature perturbations.

just as one would expect from integrating out the heavy A_i fields in the renormalizable theory.

Most of the other fields are automatically stabilized at zero after inflation. Only two directions do not gain a mass from the operators explicitly shown in eq. (8.6), but they can easily be made massive by extra operators which are irrelevant during inflation, e.g. $\Delta W \propto A_2 N^2$ and $\Delta W \propto D B_2 A_2$ with an extra chiral superfield D.[6]

8.2.5 Stabilization of messenger fields during inflation

We have shown that the renormalizable model reproduces the non-renormalizable model as characterized by eqs. (6.9), (8.4) and (8.5), assuming that $S = N = B_1 = A_1 = A_2 = 0$ during inflation. We should now check that this assumption is consistent. Note that we have already shown that $H = B_2 = 0$ for $\phi > \phi_c$, see eq. (8.15).

For N and B_1, we find mixing just as for H and B_2:

$$|W_H|^2 = |g_H X B_1 + 2 g_1 H A_1|^2 = |g_H X B_1|^2 + ..., \tag{8.21a}$$

$$|W_{B_2}|^2 = |g_N X N + m_B B_1|^2 = |m_B B_1|^2 + |g_N X|^2 |N|^2 + 2\,\mathrm{Re}\left(g_N m_B^\dagger X N B_1^\dagger\right). \tag{8.21b}$$

The calculation of the eigenvalues works analogously to the discussion for the H-B_2 mass matrix. For large ϕ, the mass matrix is nearly diagonal with very large masses $m^2_{NB_1} \propto \phi^2$. For smaller ϕ, a positive supergravity mass $\Delta m_N^2 \gtrsim \mathcal{H}^2$ is sufficient to stabilize all N-B_1 directions even for $\phi \leq \phi_c$.

The mass terms for S, A_1 and A_2 also take the form $\sum_i (|W_i|^2 + \Delta m_i^2)$ during inflation, where $\Delta m_i^2 \sim \mathcal{O}(\mathcal{H}^2)$ (see appendix C.3):

$$m_S^2 = \Delta m_S^2, \tag{8.22a}$$

$$m_{A_1}^2 = m_A^2 + \Delta m_{A_1}^2, \tag{8.22b}$$

$$m_{A_2}^2 = m_A^2 \pm 2 g_2 \Lambda^2 + \Delta m_{A_2}^2, \tag{8.22c}$$

where the $\pm$ sign for A_2 is "$-$" for the real and "$+$" for the imaginary component. We see that $A_2 = 0$ is stable if

$$m_A > \sqrt{2 g_2}\,\Lambda, \tag{8.23}$$

or if $g_2 \lesssim \mathcal{O}(\Lambda^2/m_{\mathrm{Pl}}^2)$ so that $2 g_2 \Lambda^2 < \Delta m_{A_2}^2 \sim \mathcal{O}(\Lambda^4/m_{\mathrm{Pl}}^2)$.

A_1 is strictly heavier than the real component of A_2, and S can always have a super-Hubble mass depending on the Kähler potential (as usual in tribrid inflation).

In summary, we find that if eq. (8.23) is satisfied or if g_2 is very small, all non-inflaton fields can be stabilized at zero during inflation.

[6] As a general rule, such superpotential terms should contain at least three non-inflaton fields and no power of S (which makes them negligible during inflation), and one should check that they do not generate unwanted operators after inflation when H and A_2 acquire vacuum expectation values.

8.3 One-loop corrections to the inflaton potential

In section 8.2, we have shown that the renormalizable superpotential given by eq. (8.6) including heavy messenger fields A_i and B_i leads to the same tree-level predictions for inflation as the non-renormalizable tribrid superpotential defined in eq. (8.1), up to corrections of order $\mathcal{H}/m_A$, $\mathcal{H}/m_B$. In particular, we demonstrated that both models reduce to hybrid inflation with the same inflaton potential given by eq. (6.9), ending with a waterfall at the same critical inflaton field value given by eq. (8.4), after which the waterfall field acquires a vacuum expectation value given by eq. (8.5).

In this section, we want to compare the one-loop corrections to the effective inflaton potential for the non-renormalizable and the renormalizable superpotential. In particular, we want to show that for small inflaton field values $\phi^2 \ll \Lambda_\phi m_B$, the loop corrections are practically identical, up to small shifts that can be absorbed in the tree-level Kähler potential couplings κ_{XS} and κ_{XX} or κ_{SXX}, whereas for larger field values the loop corrections can take on a different functional form. However, for Kähler-driven tribrid inflation, they turn out to be subdominant in both cases, so that our tree-level result remains valid and the inflationary dynamics are identical for both cases even for large $\phi^2 \gtrsim \Lambda_\phi m_B$.

8.3.1 One-loop potential in tribrid inflation

The loop effects can be studied using the one-loop effective potential as given in eq. (5.25). In tribrid inflation, the one-loop contribution to the inflaton potential is suppressed by two mechanisms:

1. Fermions contribute with a minus sign, so in unbroken SUSY, where one has equal numbers of bosonic and fermionic degrees of freedom with identical masses, $\Delta V_{\text{loop}} = 0$. During inflation, SUSY is broken by $|W_S|^2 \simeq \Lambda^4$, which leads to some mass splittings between scalars and fermions. The resulting loop potential is nevertheless strongly suppressed by partial cancellations between bosonic and fermionic contributions.

2. Some fields have no ϕ-dependent mass terms from the superpotential, but only get some Planck-suppressed ϕ-dependent mass terms from the Kähler potential. In this case, the inflaton-dependent part of the one-loop potential must also be Planck-suppressed.

For S and A_1, both suppression mechanisms work simultaneously, and their contribution to the inflaton potential is negligible. The contributions from the inflaton-dependent inflaton mass can also generally be ignored, because the inflaton mass must be small throughout slow-roll: $m_\phi^2 \ll \mathcal{H}^2 \simeq \Lambda^4/(3m_{\text{Pl}}^2)$, and therefore $\Delta V_{\text{loop}} \ll \Lambda^8/m_{\text{Pl}}^4$.

For the non-renormalizable superpotential given by eq. (8.1), H and N have strongly ϕ-dependent masses, so the second suppression mechanism does not apply, and the one-loop

potential is

$$\Delta V_{\text{loop}}^{(EFT)} \simeq \frac{(\Delta m_H^2 + \Delta m_N^2)}{64\pi^2} \frac{\phi^4}{\Lambda_\phi^2} \ln\left(\frac{\phi^4}{4eQ^2\Lambda_\phi^2}\right). \tag{8.24}$$

For a large part of parameter space, these loop corrections are subdominant to the tree-level inflaton potential of eq. (6.9) [28].

We now want to calculate the one-loop corrections for the renormalizable superpotential of eq. (8.6). We discuss the corrections due to the A_2 masses first, and those due to the H-B_2 and N-B_1 mass eigenvalues afterwards. We do not discuss the contributions from S, A_1 and X, which are negligible for the reasons mentioned above.

8.3.2 Weakly inflaton dependent mass: A_2

For A_2, the mass splitting between scalar and fermionic components is large, which makes the first suppression mechanism less effective. The scalar and fermionic masses are approximately:

$$m_{A_2}^{(S)\,2}(\phi) \simeq \mathcal{N}_A(\phi)\left(m_A^2 \pm 2g_2\Lambda^2 + \frac{c\Lambda^4}{m_{\text{Pl}}^2}\right), \tag{8.25a}$$

$$m_{A_2}^{(F)\,2}(\phi) \simeq \mathcal{N}_A(\phi)\, m_A^2, \tag{8.25b}$$

where the $\pm$ sign is "$-$" for the real and "$+$" for the imaginary scalar component, and

$$\mathcal{N}_A(\phi) = \frac{e^{K/m_{\text{Pl}}^2}}{K_{\overline{A}_1 A_1} K_{\overline{A}_2 A_2}} = 1 + \mathcal{O}(\phi^2/m_{\text{Pl}}^2) \tag{8.26}$$

is a multiplicative mass rescaling from non-renormalizable Kähler potential contributions (see appendix C.3 for details).

To understand the qualitative behaviour of $\Delta V_{\text{loop}}^{(A_2)}$ for these masses, we observe that

1. $\Delta V_{\text{loop}}^{(A_2)} = 0$ for $\Lambda = 0$.
2. $\Delta V_{\text{loop}}^{(A_2)}$ is an even function of Λ^2: $\Delta V_{\text{loop}}^{(A_2)}(\Lambda^2) = \Delta V_{\text{loop}}^{(A_2)}(-\Lambda^2)$.

This implies that $\Delta V_{\text{loop}}^{(A_2)}$ can be expanded in powers of Λ^4, with no term containing less than one power of Λ^4.

The only inflaton dependence arises from expanding $\mathcal{N}(\phi)$ in powers of ϕ^2/m_{Pl}^2, so the inflaton-dependent part of ΔV_{loop} generally has the form[7]

$$\Delta V_{\text{loop}}^{(A_2)} = \Lambda^4\left(\tilde{a}\frac{\phi^2}{m_{\text{Pl}}^2} + \tilde{b}\frac{\phi^4}{m_{\text{Pl}}^4} + ...\right), \tag{8.27}$$

[7]Higher powers of Λ^4, like Λ^8/m_A^4, can be absorbed in the coefficients $\tilde{a}$ and $\tilde{b}$.

which has the same form as the tree-level expansion in eq. (6.9). The loop corrections can therefore be absorbed in the tree-level couplings, replacing $a \to a_{\text{eff}} = (a + \tilde{a})$ and $b \to b_{\text{eff}} = (b + \tilde{b})$, which is equivalent to small shifts in the Kähler potential couplings κ_{XS} and κ_{XX} or κ_{XXS} in the tree-level calculation.

The numeric factors $\tilde{a}$ and $\tilde{b}$ are also suppressed by the loop factor $\log(...)/64\pi^2$. For the one-loop approximation to be valid, this loop factor must be small (otherwise two and more loops would be expected to give even larger corrections), and one generally finds $\tilde{a}, \tilde{b} \ll 1$. However, even small corrections $\tilde{a} \sim 10^{-2}$ lead to measurable changes in the predictions, as the predictions of tribrid inflation are very sensitive to the precise value of a.

8.3.3 Strongly inflaton dependent mass: H, N and B_i

We now want to discuss the H-B_2 and N-B_1 directions whose masses are strongly ϕ-dependent due to their renormalizable couplings involving the inflaton field. We can focus on the H-B_2 direction with the mass matrix given in eq. (8.14); the calculation for N-B_1 is identical except for a substitution $g_H \leftrightarrow g_N$, $\Delta m_H^2 \leftrightarrow \Delta m_N^2$ and $\Delta m_{B_1}^2 \leftrightarrow \Delta m_{B_2}^2$.

The masses take a form similar to eqs. (8.25a)–(8.25b), but without the large splitting between the real and imaginary scalar components. We write

$$m_i^{(F)\,2}(\phi) \;=\; M_i^2(\phi), \tag{8.28a}$$

$$m_i^{(S)\,2}(\phi) \;=\; M_i^2(\phi) \,+\, \delta_i^2, \tag{8.28b}$$

where $\delta_i^2 \sim \mathcal{O}(\Lambda^4/m_{\text{Pl}}^2)$ is the SUSY breaking mass splitting term. During inflation, the masses are large compared to the Hubble scale[8], so we can expand $V_{\text{loop}}^{(i)}$ (the contribution of the i-th superfield to V_{loop}) in powers of δ_i^2/M_i^2:

$$\begin{aligned}
\Delta V_{\text{loop}}^{(i)} \;&=\; \frac{1}{64\pi^2} \sum_{\text{s, f}} (-1)^{2s_i}\, m_i^4(\phi) \left[\ln\left(\frac{m_i^2(\phi)}{Q^2} \right) - \frac{3}{2} \right] \\
&=\; \frac{1}{32\pi^2} \left\{ \left(M_i^2 + \delta_i^2 \right)^2 \ln\left(\frac{M_i^2 + \delta_i^2}{e^{3/2} Q^2} \right) - M_i^4 \ln\left(\frac{M_i^2}{e^{3/2} Q^2} \right) \right\} \\
&=\; \frac{M_i^2 \delta_i^2}{16\pi^2} \ln\left(\frac{M_i^2}{e Q^2} \right) \,+\, \mathcal{O}(\delta_i^4),
\end{aligned} \tag{8.29}$$

[8]Very close to the critical point, $\phi \simeq \phi_{\text{c}}$, two of the masses become small just before the tachyonic instability develops at $\phi = \phi_{\text{c}}$, but during most of inflation the masses are very large. In particular, at the time when CMB scales leave the horizon, $m_{HB_2} \gg \mathcal{H}$ is a very good approximation. This is important because predictions for the primordial spectrum depend most strongly on the potential around the time of horizon crossing, so that is the time when we want our calculation of the loop corrections to be most accurate.

where the sum in the first line goes over both scalar and fermionic degrees of freedom corresponding to the i-th superfield.

We now want to evaluate eq. (8.29) for the H-B_2 mass matrix. As the M_i^2 and δ_i^2 for the mass eigenvalues look quite complicated, we will consider the limits of small and large inflaton field values, expanding M_i^2 and δ_i^2 in powers of ϕ^2/m_B^2 for small ϕ and in powers of m_B^2/ϕ^2 for large ϕ. For $g_N \sim g_H$, these two cases correspond to $\phi^2 \ll \Lambda_\phi m_B$ and $\phi^2 \gg \Lambda_\phi m_B$.

Small field values: $\phi^2 \ll \Lambda_\phi m_B$

For $\phi \ll m_B/g_N$ and $\phi \ll m_B/g_H$, the mass eigenvalues can be expanded in powers of ϕ. The leading order terms are

$$M_1^2 \simeq \frac{\phi^4}{4\Lambda_\phi^2}, \qquad \delta_1^2 \simeq \Delta m_H^2, \tag{8.30a}$$

$$M_2^2 \simeq m_B^2 + \frac{g_H^2 + g_N^2}{2}\phi^2, \qquad \delta_2^2 \simeq \Delta m_{B_2}^2 + \frac{g_H^2\phi^2}{2m_B^2}\left(\Delta m_H^2 - \Delta m_{B_2}^2\right), \tag{8.30b}$$

and eq. (8.29) becomes, to leading order in ϕ^2/m_B^2:

$$\Delta V_{\text{loop}}^{(1)} \simeq \frac{\Delta m_H^2}{64\pi^2}\frac{\phi^4}{\Lambda_\phi^2}\ln\left(\frac{\phi^4}{4eQ^2\Lambda_\phi^2}\right), \tag{8.31a}$$

$$\Delta V_{\text{loop}}^{(2)} \simeq \frac{\phi^2}{32\pi^2}\left[g_H^2\left(\Delta m_{B_2}^2 - \Delta m_H^2\right) + \left(g_N^2\Delta m_{B_2}^2 + g_H^2\Delta m_H^2\right)\ln\left(\frac{m_B^2}{Q^2}\right)\right]. \tag{8.31b}$$

The smaller mass eigenvalue in this limit is identical to the mass of H for the non-renormalizable superpotential from eq. (8.1), up to corrections suppressed by higher powers of $\phi^2/(m_B\Lambda_\phi)$. For this reason, eq. (8.31a) reproduces the loop potential for the non-renormalizable tribrid superpotential as given in eq. (8.24).[9]

The corrections due to the heavy B_2 field, given by eq. (8.31b), can be made small by choosing a suitable renormalization scale $Q \sim m_B$. In principle, Q can be chosen such that the entire bracket is zero (in that case, the leading term is $\mathcal{O}(\phi^4/m_B^4)$). Even if it provides a contribution to the effective inflaton potential, it takes the same functional form as eq. (8.27), and could therefore be absorbed in the inflaton potential terms a_{eff} and b_{eff} as discussed for $\Delta V_{\text{loop}}^{(A_2)}$ in section 8.3.2.

[9] We also reproduce the term proportional to Δm_N^2 when we consider the contribution of the N-B_1 mass eigenvalues.

Large field values: $\phi^2 \gg \Lambda_\phi m_B$

For very large ϕ, the mass eigenvalues asymptote to eq. (8.15), with δ^2 given by Δm_H^2 or $\Delta m_{B_2}^2$. This leads to a loop potential of the form

$$\Delta V_{\text{loop}}^{(1,2)} = \frac{g_{H,N}^2 \Delta m_i^2}{32\pi^2} \phi^2 \ln\left(\frac{g_{N,H}^2 \phi^2}{2eQ^2}\right), \tag{8.32}$$

with a functional form $\Delta V \propto \phi^2 \ln(\phi)$ which is qualitatively different from that of the EFT loop potential in eq. (8.24), and which cannot be absorbed in the tree-level couplings a and b due to the logarithmic dependence. Note that this loop potential is suppressed by $(m_B^2/\phi^2) \ll 1$ compared to the EFT loop potential in eq. (8.24), so it is negligible in cases where even the EFT loop corrections are subdominant.

8.3.4 Conclusion on one-loop corrections

The above calculations indicate that for small inflaton field values $\phi^2 \ll \Lambda_\phi m_B$, the one-loop corrections are almost identical for the non-renormalizable EFT superpotential and the renormalizable superpotential involving heavy messenger fields. Though the heavy messenger fields can introduce some corrections to the effective inflaton potential, the deviations have the same form as the tree-level potential and can be absorbed in the tree-level couplings as small shifts in the Kähler potential couplings κ_{XS} and κ_{XX} or κ_{XXS}.

For large inflaton field values $\phi^2 \gg \Lambda_\phi m_B$, the logarithmic one-loop corrections have a different functional form for the renormalizable and non-renormalizable superpotentials, with ΔV_{loop} for the renormalizable superpotential suppressed by $\mathcal{O}(m_B^2/\phi^2) \ll 1$ compared to the EFT.

In general, this shows that the one-loop corrections for inflaton field values above the cutoff scale can deviate between the renormalizable and the non-renormalizable superpotential, which could be relevant when constructing explicit models. However, in the many cases where even the (larger) EFT one-loop corrections are small compared to the tree-level inflaton potential, our analysis indicates that the inflationary dynamics for both superpotentials are determined by their tree-level predictions and therefore identical up to $\mathcal{O}(\mathcal{H}/m_A)$.

8.4 Generalisation to other superpotentials and messenger topologies

In the previous section, we have discussed how to generate the specific non-renormalizable tribrid superpotential defined in eq. (8.1) using the renormalizable superpotential in eq. (8.6), such that both superpotentials lead to the same inflationary dynamics even for large field values ϕ above the suppression scales Λ_ϕ and Λ_H of the non-renormalizable superpotential.

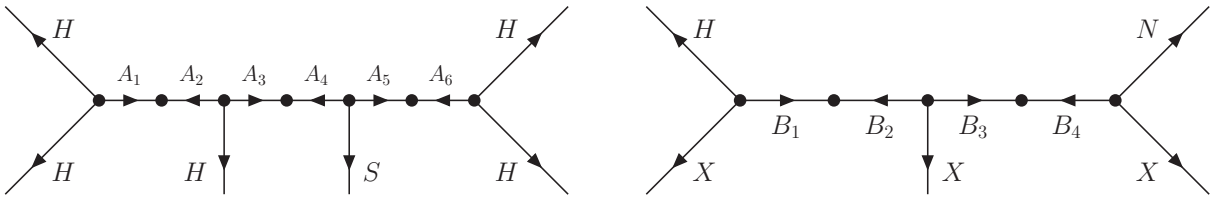

Figure 8.2: Diagrams for generating the non-renormalizable operators of the superpotential in eq. (8.33) from renormalizable superpotential couplings to heavy messenger fields A_i and B_i for $\ell = 5$ (left) and $n = 3$ (right).

In this section, we briefly discuss how this explicit worked-out example can be generalized to more general tribrid superpotentials and how different choices for the messenger sector can affect the inflationary predictions.

8.4.1 More general superpotentials

It is possible to extend our analysis to more general Kähler-driven tribrid superpotentials of the form

$$W \;=\; S\left(\frac{H^\ell}{\Lambda_H^{\ell-2}} - \Lambda^2\right) \;+\; \frac{1}{\Lambda_\phi^{n-1}} HNX^n, \tag{8.33}$$

with $\ell \geq 4$ and $n \geq 2$. The last term can also be replaced by $H^2X^n/\Lambda_\phi^{n-1}$ without changing the inflationary dynamics, except for a numerical factor of 2 in the waterfall mass. It is also straightforward to replace X^n by a D-flat direction of multiple fields, e.g. $X^2 \to LH_u$ or $X^3 \to LH_dE$.

For these more general tribrid superpotentials, it is possible to proceed analogously to the discussion in section 8.2 using diagrams like those shown in fig. 8.2 (with the caveat discussed in section 8.4.3). From the diagrams, one can read off the messengers' symmetry charges, as the total charge of the fields connected to each vertex must be 2 for an $U(1)_R$ symmetry, 0 for $U(1)$ symmetries and some multiple of n for $\mathbb{Z}_n$ symmetries.

Higher $\ell > 4$ can generally be achieved by adding more external H legs to the left diagram in fig. 8.2. For this kind of messenger topology, the inflationary dynamics is unaffected except for the vacuum expectation value after inflation, which is $\langle H\rangle^\ell \sim c\Lambda^2$ with a constant c composed of the A_i fields' masses and their couplings to S and H. The basic reason is that such diagrams are based only on superpotential couplings mA_iA_j, HA_iA_j and H^2A_i, which have no effect during inflation, and SA_iA_j, which generates a mass splitting for A_i and A_j only, but no mass terms for H which is the field responsible for initiating the waterfall instability.

Larger n can be achieved by adding more external X legs to the right diagram in fig. 8.2. This leads to more complicated mixing. In the example given in fig. 8.2, we find mixing terms between H, B_2 and B_4, so that the calculation of the mass eigenvalues is

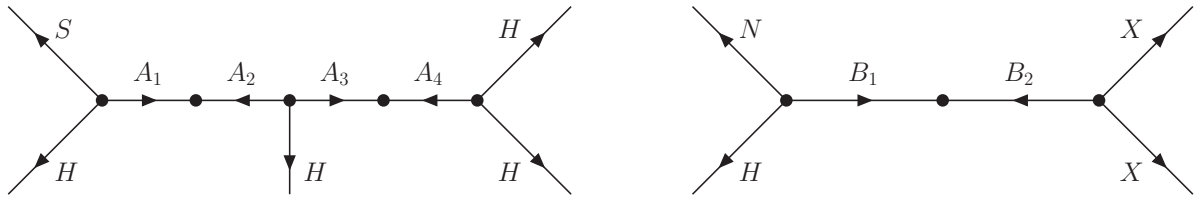

Figure 8.3: Alternative diagrams for generating the non-renormalizable operators of the superpotential defined in eq. (8.1) from different renormalizable couplings to heavy messenger fields A_i and B_i. These choices introduce stronger deviations from the predictions of the EFT superpotential in eq. (8.1). The left diagram introduces significant H-A_1 mixing, which can change both ϕ_c and ΔV_{loop}. The right diagram changes the dynamics even more drastically, as it destabilizes the B_1 field during inflation, which would lead to multi-field inflation involving X and B_1.

more involved, and therefore both the calculation of ϕ_c and the estimation of the one-loop corrections are more difficult.

8.4.2 Effect of different messenger topologies

In our analysis, we have focused on a particular choice for the messenger sector which leads to matching predictions between the renormalizable and non-renormalizable superpotential. One could also think of generating the non-renormalizable operators in eq. (8.1) with different messenger sectors, e.g. using the diagrams shown in fig. 8.3. However, these alternative messenger sectors introduce stronger deviations from the predictions of the non-renormalizable superpotential defined in eq. (8.1).

The left diagram in fig. 8.3 depicts an alternative way to generate the coupling SH^4/Λ_H^2. The main difference is that it contains a vertex SHA_1, which introduces a large H-A_1 mixing term in the scalar mass matrix. This mixing affects the mass eigenvalues of the waterfall directions and thus changes both ϕ_c and ΔV_{loop}.

The right diagram in fig. 8.3, which one might expect to generate $\Delta W \supset HNX^2/\Lambda_\phi$, changes the dynamics even more drastically, as it destabilizes B_1 during inflation (the F-term $|W_{B_2}|^2$ is minimized only for $B_1 \sim X^2/m_B$). In general, this will lead to multi-field inflation involving X and B_1.[10]

We do not want to discuss these models in detail, but we want to emphasize that for messenger sectors like those in fig. 8.3, the predictions for inflation must be calculated carefully for the model including all the messengers, and the results will generally differ from those expected for the non-renormalizable tribrid superpotentials defined in eq. (8.33).

[10]Even if B_1 is heavy during inflation, so that it tracks its minimum at $B_1 \sim X^2/m_B$, the effective inflation potential is changed by canonical normalization of the adiabatic direction along the two-field trajectory, which is a large effect at least for $X \gtrsim \mathcal{O}(m_B)$.

8.4.3 Checking for additional operators allowed by the symmetries

When constructing explicit models including the messenger sector, it is necessary to check that no unwanted additional operators are allowed by the symmetries. This puts some constraints on the possibilities for building messenger sectors. As an example, consider constructing a messenger sector for the superpotential

$$W_{\rm EFT} \,=\, S\left(\frac{H^4}{\Lambda_H^2}-\Lambda^2\right) \,+\, \frac{1}{\Lambda_\phi}H^2X^2. \tag{8.34}$$

This is the same superpotential as in eq. (8.1), apart from replacing $HN \to H^2$, so one might try to construct a messenger sector using the diagrams in fig. 8.1 with N replaced by H:

$$W_{\rm ren} \,=\, g_1H^2A_1 + m_AA_1A_2 + S\left(g_2A_2^2-\Lambda^2\right) + g_HXHB + \frac{m_B}{2}B^2 + ... \tag{8.35}$$

However, any choice of $U(1)_R$ and $\mathbb{Z}_n$ symmetries consistent with eq. (8.35) also allows the troublesome operator

$$\Delta W_{\rm trouble} \,\propto\, A_2X^2, \tag{8.36}$$

which destabilizes A_1 during inflation and generates a tree-level contribution to the inflaton potential.

To be safe, one should always check that the symmetries of the model including the messenger sector do not allow for any additional superpotential operators with less than three powers of non-inflaton, non-S fields. In that case, the extra operators cannot generate any mass terms during inflation, so that no fields can be destabilized and $\phi_{\rm c}$ is unchanged.

8.5 Summary

In this chapter, we have studied whether tribrid inflation can be successfully realized even in the presence of superpotential operators with low cutoff scales $\Lambda_H, \Lambda_\phi \lesssim \Delta\phi \ll m_{\rm Pl}$, or if inflation must be studied in a more UV complete model explicitly including all particles with masses $m_i \lesssim \Delta\phi$.

We started by constructing a particular UV extension in which the non-renormalizable operators with sub-Planckian suppression scales $\Lambda_{\rm cutoff}$ are replaced by renormalizable couplings to heavy messenger fields. We found that at tree level, the inflationary dynamics for both superpotentials could be reduced to eqs. (6.9), (8.4) and (8.5), even for $\Delta\phi > \Lambda_H, \Lambda_\phi$. In particular, this implies that the tree-level predictions are identical regardless of whether one uses the non-renormalizable superpotential (with messenger fields already integrated out) or the renormalizable superpotential (explicitly including all messenger fields), apart from small corrections of order $\mathcal{H}/m_A$.

However, the one-loop quantum corrections to the effective inflaton potential are different when calculated with the renormalizable superpotential. Most importantly, the logarithmic corrections due to the waterfall field's mass are suppressed by (m_B^2/ϕ^2) for large field values $\phi^2 \gg \Lambda_\phi m_B$ compared to the non-renormalizable superpotential. The heavy messengers' masses also generate small polynomial corrections to the inflaton potential, but those can easily be accounted for by small shifts of the tree-level Kähler potential couplings κ_{XS} and κ_{XX} or κ_{XXS}. Our results imply that in the cases in which one-loop corrections are subdominant even for the non-renormalizable superpotential, they will generally be negligible for the renormalizable superpotential as well, so inflation is well-described by the tree-level predictions which are identical for both superpotentials. However, for models in which the one-loop corrections are important, e.g. loop-driven tribrid inflation [24–26, 114], it is important to explicitly include all messengers with masses $m_i \lesssim \Delta\phi$.

Finally, we also discussed how our analysis can be extended to more general tribrid superpotentials given by eq. (8.33). We discussed how one can systematically construct a messenger sector to generate the non-renormalizable superpotential operators analogously to our explicit example. We also discussed which qualitative differences occur when using the different messenger topologies given in fig. 8.3, and why it is important to check explicitly that the messenger sector does not generate additional unwanted operators which might disturb the inflationary dynamics.

In summary, we have shown that it is possible to realize Kähler-driven tribrid inflation in particle physics models even when the superpotential contains non-renormalizable operators with suppression scales $\Lambda_{\text{cutoff}} \lesssim \Delta\phi$, and we have outlined how a messenger sector can be constructed such that the full theory including the messenger sector leads to the same predictions as the non-renormalizable superpotential. For loop-driven tribrid inflation, our results suggest that the messenger sector must be included explicitly, and that the inflaton potential generally depends on the details of the messenger fields' couplings. These results have important implications for embedding tribrid inflation within realistic particle physics theories that sponsor some intermediate scale $\Lambda_{\text{NP}} \ll m_{\text{Pl}}$, and they provide useful guidelines for whether it is sufficient to use the simpler effective theory with cutoff scale Λ_{NP} or whether it is necessary to include the messenger sector explicitly to study tribrid inflation within any given model.

Part IV

New inflation with a tribrid superpotential

Chapter 9

New inflation in supergravity

In the next few chapters, we discuss new inflation with the tribrid superpotential of eq. (6.1). As we will see, both the supergravity embedding of new inflation and the coupling between H and X can have important consequences. The SUGRA embedding can turn new inflation into a two-field model with possible effects on the primordial curvature perturbation. On the other hand, the coupling between H and X affects the dynamics before and after new inflation: it allows for dynamically generating the initial conditions for new inflation with a preceding period of "preinflation", and it also opens up a decay channel for reheating and preheating which can allow e.g. for successful non-thermal leptogenesis if X is a right-handed sneutrino field.

In this chapter, we start with the effects of the SUGRA embedding. When models of new inflation are implemented in supergravity [29–36], the inflaton is a complex and not a real scalar field. As a complex scalar field has two independent components, supersymmetric models of new inflation are naturally two-field models. In this chapter, we analyse how this two-field behaviour modifies the usual single-field predictions. We discuss for which model parameters the model reduces to the well-known single-field model, and how the predictions are affected otherwise.

The chapter is structured as follows. First we introduce the inflaton potential of SUGRA new inflation including both the real and the imaginary component of the inflaton field, and we review the single-field predictions for the case that the imaginary component is negligible. Afterwards, we analytically study the initial conditions and field trajectories to understand under which conditions the model reduces to a single-field model, and under which conditions we expect that the multi-field dynamics should influence the inflationary predictions. Finally, we use the δN formalism to numerically calculate the primordial spectrum in the two-field model.

9.1 Scalar potential of supersymmetric new inflation

Throughout this chapter, we work with the scalar potential of SUGRA new inflation:

$$V = V_0 \left\{ \left| 1 - \frac{(\phi + i\psi)^\ell}{v^\ell} \right|^2 - \frac{\beta}{2} \left(\phi^2 + \psi^2 \right) \right\} \tag{9.1}$$

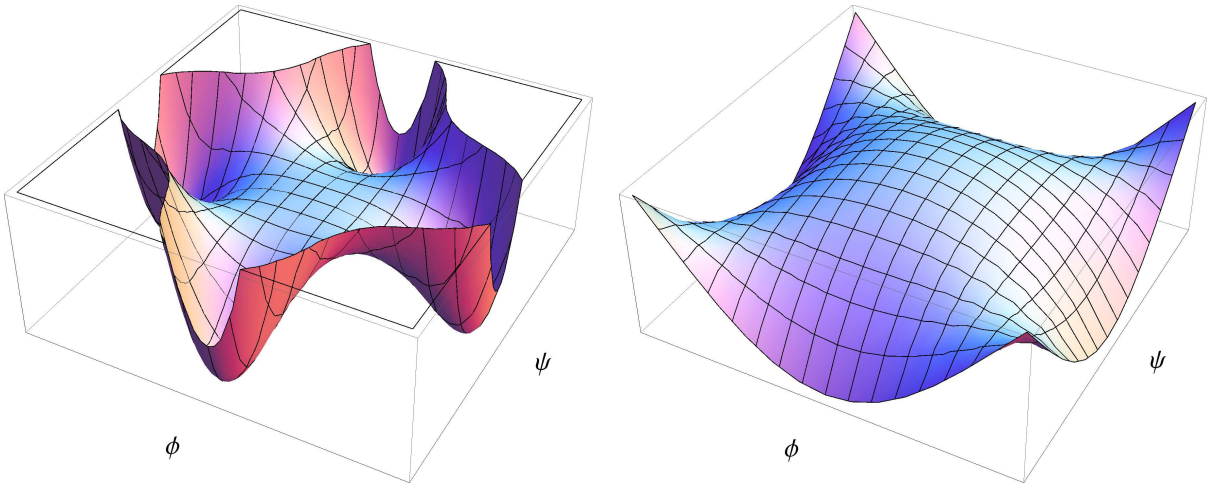

Figure 9.1: Qualitative form of the potential (9.1) for $\ell = 4$ on large scales (left) and zoomed in near the origin (right). It is easy to see that the potential is symmetric and that we can restrict our discussion to the half-quadrant $\phi \geq \psi \geq 0$.

for the real components ϕ and ψ of the complex scalar field $H = \frac{1}{\sqrt{2}}(\phi + i\psi)$. We require that $\ell \geq 3$, $v \ll 1$ and $\beta \ll 1$ so that small-field new inflation is possible, and $\beta \geq 0$ so that the inflaton can roll away from $H = 0$ without tunnelling.

Inflaton potentials of the form of eq. (9.1) can be constructed from different superpotentials and Kähler potentials, e.g. from the new inflation superpotential of eq. (5.17), proceeding analogously to section 5.4.1 without assuming that $\psi = 0$.

Throughout this chapter, we only use the inflaton potential (9.1) for the calculations, so our results are also valid for other superpotentials and Kähler potentials which lead to an effective inflaton potential of the form (9.1), e.g. for [32, 33, 36], and for [35] (in the limit $c \to 0$ in the last cited paper).

Note that the inflaton potential (9.1) is invariant under transformations $H \to H^*$ and $H \to e^{2i\pi/\ell}H$. These symmetries are also obvious in fig. 9.1 where the potential is plotted for $\ell = 4$. Due to these symmetries, we can assume that $0 \leq \psi \leq \phi \tan(\pi/\ell)$ without loss of generality, and we will do so throughout this chapter.[1]

9.2 Predictions in the single-field limit

As a first step, we calculate the predictions for ϕ_e, ϕ_*, n_s and V_0 in the single-field limit $\psi = 0$. The predictions for $\psi \neq 0$ will be derived in later sections.

[1]For any ϕ and ψ, we can do a symmetry transformation $H \to e^{2i\pi(n/\ell)}H$ to get $\phi > 0$ and $-\phi\tan(\pi/\ell) < \psi \leq \phi\tan(\pi/\ell)$. If $\psi \geq 0$, our assumption is now valid. Otherwise, we can follow up with a symmetry transformation $H \to H^*$ to get $\psi > 0$.

Since $\phi \ll v$ during inflation, we can neglect the term $V_0(\phi/v)^{2\ell}$ in the inflaton potential:

$$V(\phi) \simeq V_0 \left(1 - \frac{2}{v^\ell}\,\phi^\ell - \frac{1}{2}\beta\phi^2\right). \tag{9.2}$$

With $V(\phi) \simeq V_0$ during new inflation, the slow-roll parameters ε and η as defined in eqs. (2.18a)–(2.18b) are

$$\varepsilon(\phi) \simeq \frac{1}{2}\left(\frac{2\ell}{v^\ell}\,\phi^{\ell-1} + \beta\phi\right)^2, \qquad \eta(\phi) \simeq -\frac{2\ell(\ell-1)}{v^\ell}\,\phi^{\ell-2} - \beta. \tag{9.3}$$

For reasonable values of ℓ, i.e. $\ell \ll \beta^{-1}$, one can easily show that $\xi^2 \ll \eta$ and $\sigma^3 \ll \eta$, so we neglect ξ^2 and σ^3 in this chapter.

Inflaton field values ϕ_e and ϕ_*

Eq. (9.3) implies $\varepsilon \ll |\eta|$, and thus slow-roll inflation ends at $\eta(\phi_\mathrm{e}) = -1$:

$$\phi_\mathrm{e}^{\ell-2} \simeq \frac{(1-\beta)v^\ell}{2\ell(\ell-1)}. \tag{9.4}$$

Note that for sub-Planckian $v \ll 1$, we find $\phi_\mathrm{e} \ll v$, so our assumption that $\phi \ll v$ during inflation is consistent.

To calculate the inflaton field value ϕ_* at horizon crossing, we use eq. (2.20):

$$N_* \simeq \int_{\phi_*}^{\phi_\mathrm{e}} \frac{d\phi}{\frac{2\ell}{v^\ell}\phi^{\ell-1} + \beta\phi} = \frac{1}{\beta(\ell-2)} \ln\left(\frac{2\ell + v^\ell\beta\phi_*^{2-\ell}}{2\ell + v^\ell\beta\phi_\mathrm{e}^{2-\ell}}\right), \tag{9.5}$$

which can be solved for

$$\phi_*^{\ell-2} \simeq \frac{\beta v^\ell}{2\ell\left(\left(\frac{1+(\ell-2)\beta}{1-\beta}\right)e^{(\ell-2)\beta N_*} - 1\right)}. \tag{9.6}$$

Predictions for n_s and V_0

The spectral index can be calculated from eq. (3.24c), using $\xi^2 \ll \eta$ and $\sigma^3 \ll \eta$:

$$n_\mathrm{s} \simeq 1 + 2\eta_* \simeq 1 - 2\beta - \frac{2(\ell-1)\beta}{\frac{1+\beta(\ell-2)}{1-\beta}e^{(\ell-2)\beta N_*} - 1}. \tag{9.7}$$

n_s is shown in fig. 9.2 as a function of β for various $\ell \geq 4$. $\ell = 3$ is not shown because it predicts $n_\mathrm{s} < 0.94$ for any choice of β. As one can see in the plots, for $\ell \geq 5$ it is always possible to get a spectral index in agreement within the Planck constraints of $n_\mathrm{s} = 0.965 \pm 0.005$ at a 68% CL [9].

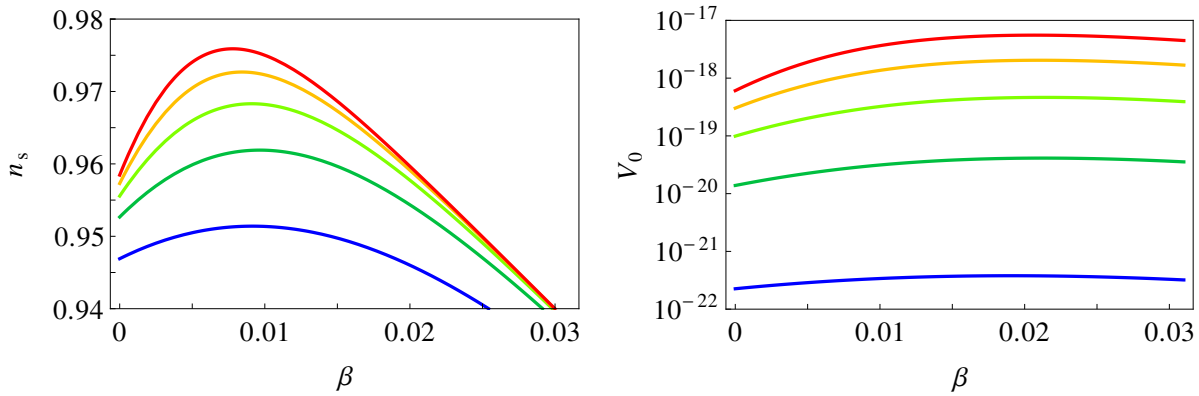

Figure 9.2: Spectral index n_s and vacuum energy V_0 in the single-field limit as functions of β for various ℓ from $\ell = 4$ (blue) to $\ell = 8$ (red). The plots are done for $N_* = 55$ and $v = 10^{-2}$. Changing v only introduces an overall factor in V_0 but does not change its β-dependence, and n_s is completely independent of v.

The inflationary vacuum energy V_0 can be calculated from eqs. (3.25), (9.3) and (9.6). The result has the form

$$V_0 \;=\; f(\beta, \ell, N_*) \times v^{2\ell/(\ell-2)}. \tag{9.8}$$

f is a non-trivial function of β, ℓ and N_*, but the proportionality $V_0 \propto v^{2\ell/(\ell-2)}$ is independent of β. V_0 is plotted for various ℓ and $v = 10^{-2}$ in fig. 9.2.

r can be deduced from $V_0 \simeq V_*$ via eq. (3.27); for small-field new inflation, r is generally negligible.

9.3 Initial conditions for real and imaginary inflaton component

In a multi-field model of inflation, the predictions can depend on the initial conditions. In this section, we discuss the initial conditions that we use for the analysis of the two-field effects in SUGRA new inflation.

9.3.1 Quantum diffusion boundary

We start from the assumption that at some point in time, the field is very close to $H = 0$, e.g. due to a previous phase of preinflation during which H is driven to zero by its coupling to another scalar field (see chapter 10 for an extended discussion).

When $H = 0$, the classical equations of motion imply that the field does not move away from $H = 0$ at all. However, the field H has quantum fluctuations which can be thought of

as moving H randomly over time.[2] Near $H = 0$, these quantum fluctuations dominate over the classical evolution; we call this area the quantum diffusion region. After some time, however, H has randomly moved into some region where the potential is steep enough for the classical evolution to take over and the inflaton rolls away from $H = 0$, down the potential gradient towards the nearest minimum. We therefore choose initial conditions on the boundary where the classical evolution starts to dominate over the quantum diffusion, and calculate the evolution with the classical field equations from there.

The boundary between the quantum diffusion region and the region of classical field evolution can be estimated by comparing the classical evolution $\Delta H_{\rm cl}$ per Hubble time $t_{\mathcal{H}} = \mathcal{H}^{-1}$ to the growth of quantum fluctuations $\Delta H_{\rm qu}$ per Hubble time. For this purpose, $|\Delta H_{\rm qu}|^2 = \frac{1}{2}\langle \delta\phi^2 + \delta\chi^2\rangle$ is estimated from the de Sitter space vacuum fluctuations of a massless real scalar field φ [41]:

$$\langle \delta\varphi^2\rangle = \left(\frac{\mathcal{H}}{2\pi}\right)^2 N(t), \tag{9.9}$$

where $N = \mathcal{H}t$ grows by $\Delta N = 1$ per Hubble time. With the classical slow-roll eqs. (2.15)–(2.16) for ϕ, ψ and $\mathcal{H}$, the quantum diffusion boundary can be estimated as

$$|\Delta H_{\rm cl}|^2 \,=\, |\dot{H}|^2\, t_{\mathcal{H}}^2 \,=\, \frac{1}{2V^2}\left[\left(\frac{\partial V}{\partial\phi}\right)^2 + \left(\frac{\partial V}{\partial\psi}\right)^2\right] \stackrel{!}{=} |\Delta H_{\rm qu}|^2 \,=\, \left(\frac{\mathcal{H}}{2\pi}\right)^2. \tag{9.10}$$

To solve eq. (9.10), it is more useful to work in polar coordinates for H, with a radius φ and an angle θ:

$$H \,=\, \frac{1}{\sqrt{2}}(\phi + i\psi) \,=\, \frac{\varphi}{\sqrt{2}}\, e^{i\theta}. \tag{9.11}$$

With these conventions, the scalar potential (9.1) is

$$V \,=\, V_0\left\{1 - \frac{2}{v^\ell}\varphi^\ell\cos(\ell\theta) + \frac{\varphi^{2\ell}}{v^{2\ell}} - \frac{\beta}{2}\varphi^2\right\}. \tag{9.12}$$

We must also be careful to note that

$$\left(\frac{\partial V}{\partial\phi}\right)^2 + \left(\frac{\partial V}{\partial\psi}\right)^2 \,=\, \left(\frac{\partial V}{\partial\varphi}\right)^2 + \left(\frac{1}{\varphi}\frac{\partial V}{\partial\theta}\right)^2, \tag{9.13}$$

where the factor $1/\varphi$ appears in front of the derivative with respect to θ because θ is not a canonically normalized field. In these polar coordinates, and using the fact that $V \simeq V_0$ during new inflation, eq. (9.10) can be written as

$$\left(\frac{1}{V_0}\frac{\partial V}{\partial\varphi}\right)^2 + \left(\frac{1}{V_0}\frac{1}{\varphi}\frac{\partial V}{\partial\theta}\right)^2 \,=\, \left(\frac{\mathcal{H}}{\sqrt{2}\pi}\right)^2. \tag{9.14}$$

We want to solve this equation for the initial field values $\phi_{\rm i}$ and $\psi_{\rm i}$ separately for the cases $\beta = 0$ and $\beta \neq 0$.

[2] During inflation, perturbation modes continuously cross the horizon and freeze out, after which they can be treated as part of the classical background field within the local Hubble patch [41].

9.3.2 Diffusion boundary for $\beta = 0$

For $\beta = 0$, the relevant derivatives are[3]

$$\frac{1}{V_0}\frac{\partial V}{\partial \varphi} = -\frac{2\ell}{v^\ell}\varphi^{\ell-1}\cos(\ell\theta), \tag{9.15a}$$

$$\frac{1}{V_0}\frac{\partial V}{\partial \theta} = \frac{2\ell}{v^\ell}\varphi^{\ell}\sin(\ell\theta). \tag{9.15b}$$

With these ingredients, eq. (9.14) becomes very simple

$$\left(\frac{2\ell}{v^\ell}\varphi_\mathrm{i}^{\ell-1}\right)^2 = \left(\frac{\mathcal{H}}{\sqrt{2}\pi}\right)^2, \tag{9.16}$$

so the diffusion boundary is a circle in field space with the squared radius

$$\left(\phi_\mathrm{i}^2 + \psi_\mathrm{i}^2\right) = \left(\frac{v^\ell \mathcal{H}}{\sqrt{8}\pi\ell}\right)^{\frac{2}{\ell-1}}. \tag{9.17}$$

9.3.3 Diffusion boundary for $\beta > 0$

For sufficiently small H, the mass term from β dominates over the other inflaton potential terms which are of higher order in the fields. Therefore, we can neglect the other interactions at the diffusion boundary,[4] and eq. (9.14) simplifies to

$$\left(\phi_\mathrm{i}^2 + \psi_\mathrm{i}^2\right) = \left(\frac{\mathcal{H}}{\sqrt{2}\pi\beta}\right)^2. \tag{9.18}$$

We find that the diffusion boundary is a circle around the origin with radius $\mathcal{H}/(\sqrt{2}\pi\beta)$.

To find out how large β must be so that we can neglect the other inflaton interactions, we can compare the size of the two interactions at the diffusion boundary given by eq. (9.18):

$$\frac{\left[\left(\frac{\partial V}{\partial \varphi}\right)^2 + \left(\frac{1}{\varphi}\frac{\partial V}{\partial \theta}\right)^2\right]_{\beta=0}}{\left[\left(\frac{\partial V}{\partial \varphi}\right)^2 + \left(\frac{1}{\varphi}\frac{\partial V}{\partial \theta}\right)^2\right]_{\beta>0}} = \frac{\left(\frac{2\ell}{v^\ell}\varphi_\mathrm{i}^{\ell-1}\right)^2}{\beta^2\varphi_\mathrm{i}^2} = \frac{4\ell^2}{\beta^2 v^{2\ell}}\left(\frac{\mathcal{H}}{\sqrt{2}\pi\beta}\right)^{2\ell-4} \ll 1$$

$$\Leftrightarrow \quad \beta \gg \left[\frac{4\ell^2}{v^{2\ell}}\left(\frac{V_0}{6\pi^2}\right)^{\ell-2}\right]^{\frac{1}{2\ell-2}}. \tag{9.19}$$

[3] We drop the term $\varphi^{2\ell}/v^{2\ell}$ in the potential because it is negligible during inflation.

[4] If β is so small that it does not dominate even at the diffusion boundary, it can be neglected completely for the purpose of inflation, and the results for $\beta = 0$ can be used.

For an order-of-magnitude estimate, we can insert the vacuum energy for single-field new inflation with $\beta \simeq 0$, which is

$$V_0 \sim 12\pi^2 A_\mathrm{s} \left(\frac{v^\ell}{2\ell}\right)^{\frac{2}{\ell-2}} \left[(\ell-2)N_*\right]^{-\left(2+\frac{2}{\ell-2}\right)}. \tag{9.20}$$

Then the condition (9.19) becomes

$$\beta \gg \frac{(2A_\mathrm{s})^{\frac{\ell-2}{2\ell-2}}}{(\ell-2)N_*}, \tag{9.21}$$

and we find that eq. (9.18) is valid for any $\beta \gg 10^{-5}$ if $\ell = 4$. For larger ℓ, the threshold for β is even lower.

9.4 Analytic estimate of two-field trajectory

In this section, we analyse the dynamics of the ϕ and ψ fields during inflation to estimate for which parameters the model reduces to the well-known single-field model of new inflation.

We can rewrite the fields ϕ, ψ as φ, θ according to eq. (9.11). Using the partial derivatives

$$\frac{\partial\varphi}{\partial\phi} = \cos(\theta), \qquad \frac{\partial\varphi}{\partial\psi} = \sin(\theta), \qquad \frac{\partial\theta}{\partial\phi} = -\frac{\sin(\theta)}{\varphi}, \qquad \frac{\partial\theta}{\partial\psi} = \frac{\cos(\theta)}{\varphi}, \tag{9.22}$$

and ignoring the negligible term proportional to $\varphi^{2\ell}$ in the potential, we can calculate the partial derivatives of the scalar potential (9.12) during inflation:

$$\begin{aligned}
\partial_\phi V &= -V_0 \left\{\beta\phi + \frac{2}{v^\ell}\frac{\partial}{\partial\phi}(\varphi^\ell\cos(\ell\theta))\right\} \\
&= -V_0\,\phi\left\{\beta + \frac{2\ell\varphi^{\ell-2}}{v^\ell}\left(\cos(\ell\theta) + \sin(\ell\theta)\tan(\theta)\right)\right\}, &\text{(9.23a)}\\
\partial_\psi V &= -V_0 \left\{\beta\psi + \frac{2}{v^\ell}\frac{\partial}{\partial\psi}(\varphi^\ell\cos(\ell\theta))\right\} \\
&= -V_0\,\psi\left\{\beta + \frac{2\ell\varphi^{\ell-2}}{v^\ell}\left(\cos(\ell\theta) - \sin(\ell\theta)\cot(\theta)\right)\right\}. &\text{(9.23b)}
\end{aligned}$$

Using eq. (2.16), we can calculate the inflaton trajectory in field space:

$$\frac{\partial\psi}{\partial\phi} = \frac{\dot\psi}{\dot\phi} = \frac{-\partial_\psi V}{-\partial_\phi V} = \left(\frac{\psi}{\phi}\right)\frac{\beta v^\ell + 2\ell\varphi^{\ell-2}\left(\cos(\ell\theta) - \sin(\ell\theta)\cot(\theta)\right)}{\beta v^\ell + 2\ell\varphi^{\ell-2}\left(\cos(\ell\theta) + \sin(\ell\theta)\tan(\theta)\right)}. \tag{9.24}$$

We will discuss the behaviour of the field trajectory for two distinct cases: for a vanishing mass term ($\beta = 0$), for which we will recover the single-field new inflation limit, and for a large mass term ($\beta \gtrsim 10^{-2}$), for which we show that the imaginary inflaton component cannot generally be neglected.

9.4.1 Supergravity mass term vanishes ($\beta = 0$): single-field limit

If $\beta = 0$, the tachyonic mass term for H exactly vanishes.[5] In this case, we can show that the imaginary component ψ decays before the observable primordial fluctuations leave the horizon, and inflation reduces to single-field new inflation.

With $\beta = 0$, eq. (9.24) simplifies to

$$\frac{\partial(\log\psi)}{\partial(\log\phi)} = \frac{\cos(\ell\theta) - \sin(\ell\theta)\cot(\theta)}{\cos(\ell\theta) + \sin(\ell\theta)\tan(\theta)}. \tag{9.25}$$

As explained in section 9.1, we can assume that $0 \leq \theta \leq \pi/\ell$. Moreover, for large $\theta > \theta_{\rm thr}$, we have $\partial_\phi V > 0$, so for such large θ, ϕ is rolling back towards 0 until the inflaton is so close to $\phi = \psi = 0$ that quantum diffusion dominates. Eventually, the inflaton will randomly diffuse out of this diffusion region. Every time it leaves the diffusion region with $\theta > \theta_{\rm thr}$, it is pushed back, until it eventually leaves the diffusion region with $\theta < \theta_{\rm thr}$.

Assuming $0 < \theta < \theta_{\rm thr}$, we find that

$$\frac{\partial(\log\psi)}{\partial(\log\phi)} = \frac{\cos(\ell\theta) - \sin(\ell\theta)\cot(\theta)}{\cos(\ell\theta) + \sin(\ell\theta)\tan(\theta)} = \frac{\tan((1-\ell)\theta)}{\tan\theta} < -(\ell - 1). \tag{9.26}$$

This implies that ψ drops off faster than $1/\phi^{\ell-1}$:

$$\psi(\phi) < \psi_0 \left(\frac{\phi_0}{\phi}\right)^{\ell-1} \tag{9.27}$$

for any initial values ψ_0 and ϕ_0. If the initial displacement from $\psi = \phi = 0$ is due to quantum fluctuations as in eq. (9.17), then eq. (9.27) implies that ψ is always negligible at horizon crossing. We can estimate this from the single-field results for new inflation, where the normalization of $\mathcal{P}_\zeta(k_*)$ ensures that between the quantum diffusion boundary and horizon crossing, ϕ grows by a factor of $\left(\phi_*/\phi_{\rm i}\right)^{\ell-1} = A_{\rm s}^{-1/2}$. Then eq. (9.27) implies that $(\psi_*/\psi_{\rm i}) < A_{\rm s}^{1/2}$, and so $(\psi_*/\phi_*) < A_{\rm s}^{\frac{1}{2}+\frac{1}{2\ell-2}} \sim 10^{-5}$, so at horizon crossing ψ is already negligible compared to ϕ.

We conclude that for $\beta = 0$, the model reduces to single-field new inflation in ϕ.

9.4.2 Supergravity mass term relevant ($\beta \gtrsim 10^{-3}$)

If $\beta > 0$, ψ grows during the early stages of inflation. For sufficiently large β, ψ can be significantly large when the primordial fluctuations leave the horizon, and therefore the dynamics of ψ is expected to have an effect on the primordial spectrum.

For small field values $\varphi^{\ell-2} \ll \beta v^\ell/(2\ell)$, ψ grows proportionally with ϕ, as we can see from eq. (9.24):

$$\frac{\partial\psi}{\partial\phi} \to \frac{\psi}{\phi} \qquad \Rightarrow \quad \psi \simeq \left(\frac{\psi_0}{\phi_0}\right)\phi. \qquad (\text{for } 2\ell\varphi^{\ell-2} \ll \beta v^\ell) \tag{9.28}$$

[5] This can naturally happen if such a mass term is forbidden by a symmetry of the Kähler potential, e.g. a Heisenberg symmetry [31].

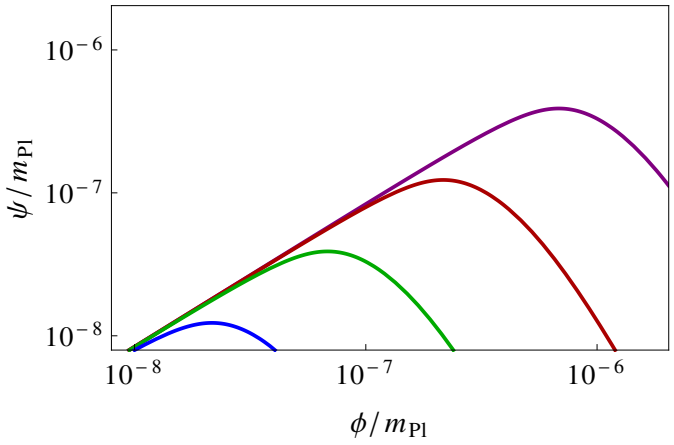

Figure 9.3: Field trajectories $\psi(\phi)$ for $\beta = 10^{-4}$ (blue), $\beta = 10^{-3}$ (green), $\beta = 10^{-2}$ (red) and $\beta = 10^{-1}$ (purple). The plots are shown for $\ell = 4$, $v = 10^{-2.5}$ and $\psi_{\rm i} = (\tan 40°)\phi_{\rm i}$. We can clearly see both the growing phase, where β dominates and ψ grows linearly with ϕ, and the decaying phase, where β can be neglected and ψ falls off rapidly. Not surprisingly, the size of β determines where the transition between the two phases takes place: for larger β, the growing phase lasts longer. Therefore, we can expect that deviations from single-field new inflation occur for large β, when the field ψ does not decay before cosmological scales leave the horizon.

This linear growth of ψ with ϕ continues until the fields grow large enough to make the higher-order interactions dominate over the tachyonic mass term from β. From that point onwards, the dynamics are approximately given by eq. (9.27): ψ starts decaying faster than $\phi^{-(\ell-1)}$ while ϕ rolls towards the minimum at $\phi = v$. Both the growing and the decaying phase for ψ can be clearly seen in fig. 9.3.

If ψ decays before cosmological scales leave the horizon, then we recover the single-field inflation limit with ϕ as the inflaton. We can use this to estimate for which values of β we can expect significant deviations from the single-field limit. The transition from the growing to the decaying phase occurs at approximately $\phi_{\rm trans}^{\ell-2} \sim \varphi_{\rm trans}^{\ell-2} \sim \beta v^{\ell}/(2\ell)$, as can be seen from eq. (9.24). Calculating the field value ϕ_* at which cosmological scales leave the horizon is more involved. For a rough estimate, we assume that it is given by its single-field new inflation value as stated in eq. (9.6). Setting $\phi_* \lesssim \phi_{\rm trans}$, we find that multi-field effects are expected to become important for β above the threshold value

$$\beta \gtrsim \frac{\ln(2)}{(\ell-2)N_*} \sim \frac{10^{-2}}{\ell-2}. \tag{9.29}$$

We therefore recover the single-field limit for $\beta \ll 10^{-2}/(\ell-2)$, whereas for $\beta \gtrsim 10^{-2}/(\ell-2)$ the predictions should be calculated in a multi-field formalism. This is done numerically in section 9.5.

9.4.3 Generalization to initial field values outside the diffusion region

So far, we have assumed that inflation starts at $H_\mathrm{i} \simeq 0$ inside the diffusion region given by eq. (9.17) or (9.18). Due to the field dynamics, our results can be immediately generalized to initial field values H_i outside the diffusion region, as long as H_i remains sufficiently small.

For $\beta > 0$, we have $\psi \propto \phi$ and therefore $\theta = \text{const}$ for small field values. This implies that our results, which depend on θ_i, are valid even when the initial value H_i is outside of the diffusion region, as long as H_i starts in the growing phase in which $\psi \propto \phi$. A sufficient condition for the validity of our results is $\varphi_\mathrm{i}^{\ell-2} \ll \frac{\beta v^\ell}{2\ell}$.

For $\beta = 0$, no growing phase exists. However, because ψ quickly decays according to eq. (9.27), we recover the single-field limit even for larger initial field values. We expect significant deviations from the single-field results only for initial values close to the horizon crossing scale, such that ψ has very little time to decay between the start of inflation and horizon crossing.

9.5 Numerical results for primordial spectrum

In the last section, we have discussed that the inflationary predictions can be changed by the imaginary inflaton component for $\beta \gtrsim 10^{-2}/(\ell - 2)$. In this section, we present a numerical calculation of the primordial curvature perturbation using the δN formalism introduced in section 3.3.

9.5.1 Numerical approach

For calculating the predictions for any set of parameters and initial conditions $(\phi_\mathrm{i}, \psi_\mathrm{i})$, we took the following steps:

1. We integrated the slow-roll equations of motion starting from $(\phi_\mathrm{i}, \psi_\mathrm{i})$ forward in time until slow-roll inflation ends at $|\eta_{\phi\phi}| = 1$. From this trajectory, we determined the end-of-inflation energy density ρ_end and the background field values (ϕ_*, ψ_*) at $N_* = 55$ e-folds before the end of inflation.

2. For very small displacements $\Delta\phi$ and $\Delta\psi$, we integrated the equations of motion without using the slow-roll approximation, starting from $(\phi_* \pm \Delta\phi, \psi_* \pm \Delta\psi)$ and ending on the final uniform-density hypersurface with $\rho = \rho_\mathrm{end}$, to determine the number N of e-folds along these trajectories.

3. We calculated the first and second derivatives of N from the difference quotients, e.g. $N_\phi = \frac{N(\phi_*+\Delta\phi,\psi_*)-N(\phi_*-\Delta\phi,\psi_*)}{2\Delta\phi}$.

4. We used eqs. (3.32)–(3.34) to calculate the primordial spectrum from the N_i, N_{ij}, ϕ_* and ψ_*.

Note that $\rho_{\rm end}$ is recalculated for each initial condition $(\phi_{\rm i}, \psi_{\rm i})$ because for different initial conditions inflation can end at slightly different energy densities.

This algorithm calculates $\mathcal{P}_\zeta$ at the end of inflation on the uniform-density hypersurface with $\rho = \rho_{\rm end}$. To compare this spectrum to the constraints on $A_{\rm s}$, $n_{\rm s}$ and $f_{\rm NL}$, we must calculate $\mathcal{P}_\zeta$ at a sufficiently late time that the adiabaticity condition (3.28) is satisfied, which is automatic in the single-field limit but not in a multi-field model. However, we have checked for each data point that $\psi \ll \phi$ at the end of inflation, so that at $\rho_{\rm end}$ we are already close to a single-field (and thus adiabatic) limit and ζ is conserved on superhorizon scales.[6]

9.5.2 Numerical results

Using the approach outlined in section 9.5.1, we have numerically calculated the spectral index $n_{\rm s}$, the amplitude of the reduced bispectrum $f_{\rm NL}$ and the vacuum energy V_0 during inflation. We assumed that inflation starts on the circle given by eq. (9.18) where the classical evolution starts to dominate over the quantum diffusion of the inflaton fields.[7] We calculated the predictions for various points on this initial surface, parametrized by the angle

$$\theta \,=\, \arctan(\psi_i/\phi_i), \tag{9.30}$$

where the maximum angle is

$$\theta_{\rm max} \,=\, \pi/\ell \tag{9.31}$$

because as we explained in section 9.1, larger angles are related to angles in the range $0 \leq \theta \leq \theta_{\rm max}$ by symmetry transformations, so we can restrict ourselves to angles between 0 and $\theta_{\rm max}$.

The results for $n_{\rm s}$ and V_0 are shown in fig. 9.4 for $N_* = 55$ and $v^\ell = 10^{-10}$. The numerical results confirm that we recover the single-field limit for $\beta \to 0$, while for larger β the imaginary inflaton component reduces both $n_{\rm s}$ and V_0. Note that the green curve, which is quite close to the black single-field result, corresponds to $\theta = \frac{2}{3}\theta_{\rm max}$. Therefore, even though the deviations become large for maximal θ, most initial conditions give results similar to the single-field limit.

$f_{\rm NL}$ is shown in fig. 9.5. It is generally in the range $-1 < f_{\rm NL} < 0$ which is too small to be observed, even for close-to-maximal θ.

We have checked that the β-dependence of our results is insensitive to changes in v. As in the single-field case, different choices of v only give a constant factor for V_0, while $n_{\rm s}$ does not depend on v at all.

Note that while the results depend sensitively on $\theta_{\rm i}$, they are valid for any initial $\varphi_{\rm i} = \sqrt{\phi_{\rm i}^2 + \psi_{\rm i}^2}$ as long as it is sufficiently close to zero (see section 9.4.3).

[6] As explained in section 3.3.1, adiabaticity requires not only that ψ is small, but also that the decay rate of ψ into radiation is not much smaller than that of ϕ. Since ϕ and ψ are both components of H, this condition is also generally satisfied.

[7] Eq. (9.18) is valid only for $\beta \gg 10^{-5}$, which is satisfied for all points in figs. 9.4 and 9.5. For smaller β, one recovers the single-field limit, and no numerical calculation is needed.

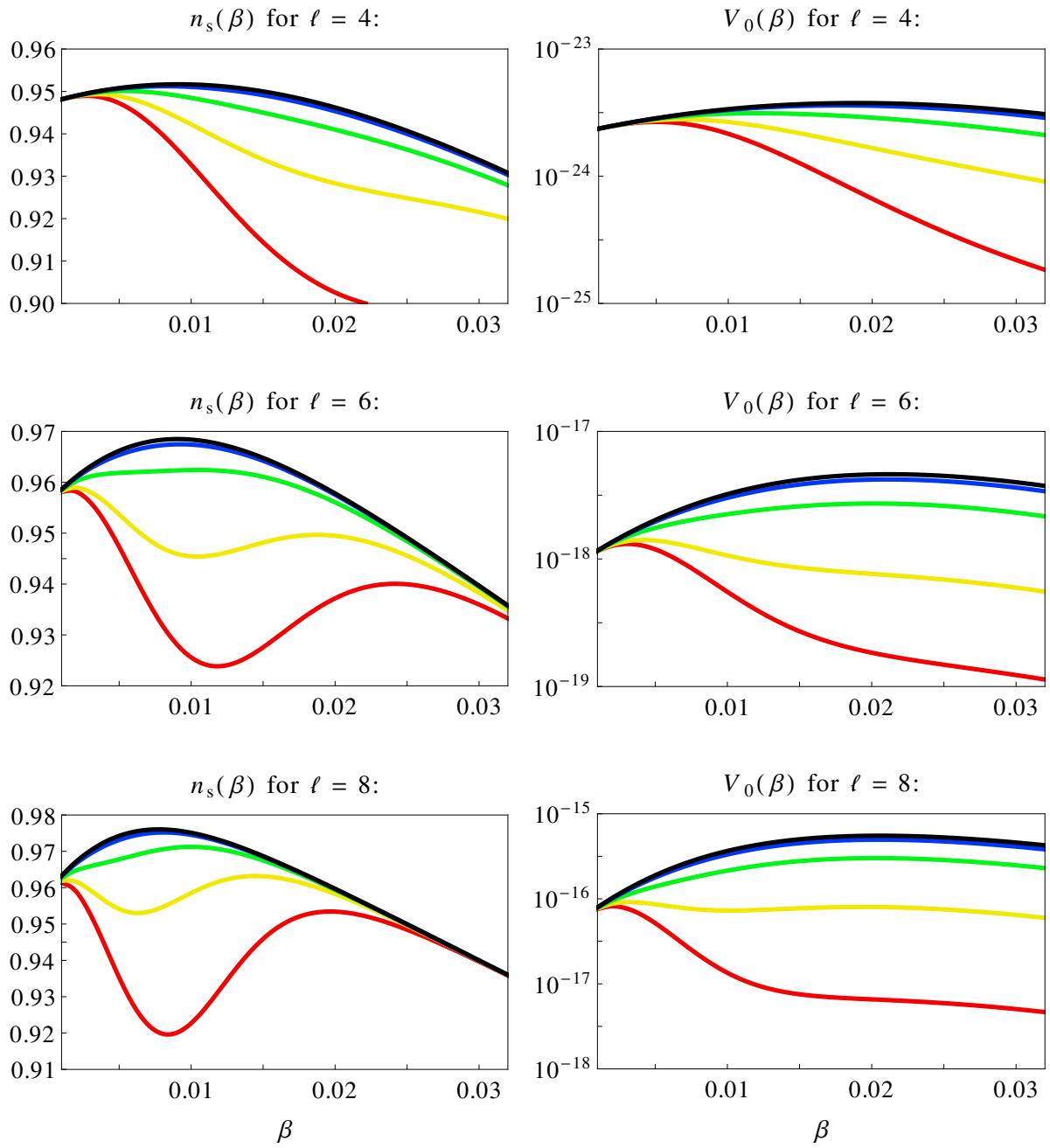

Figure 9.4: Spectral index n_s and vacuum energy V_0 as functions of β for $\ell = 4$ (upper row), $\ell = 6$ (middle row) and $\ell = 8$ (bottom row). All plots are done for $N_* = 55$ and $v^\ell = 10^{-10}$; changing v only introduces an overall factor in V_0 but does not change its β-dependence, while n_s is completely independent of v. The differently coloured curves correspond to different initial angles θ in the ϕ-ψ-plane: black is the single-field limit ($\theta = 0°$) and red is close to the maximum angle ($\theta = 180°/\ell$). The angles shown are 0°, 15°, 30°, 40° and 44° (for $\ell = 4$), 0°, 10°, 20°, 27° and 29° (for $\ell = 6$) and 0°, 7.5°, 15°, 20° and 22° (for $\ell = 8$). We see that increasing θ reduces n_s and V_0, except for $\beta \simeq 0$ which always reproduces the single-field result. The effect is mild for most angles but becomes very large close to the maximum angle.

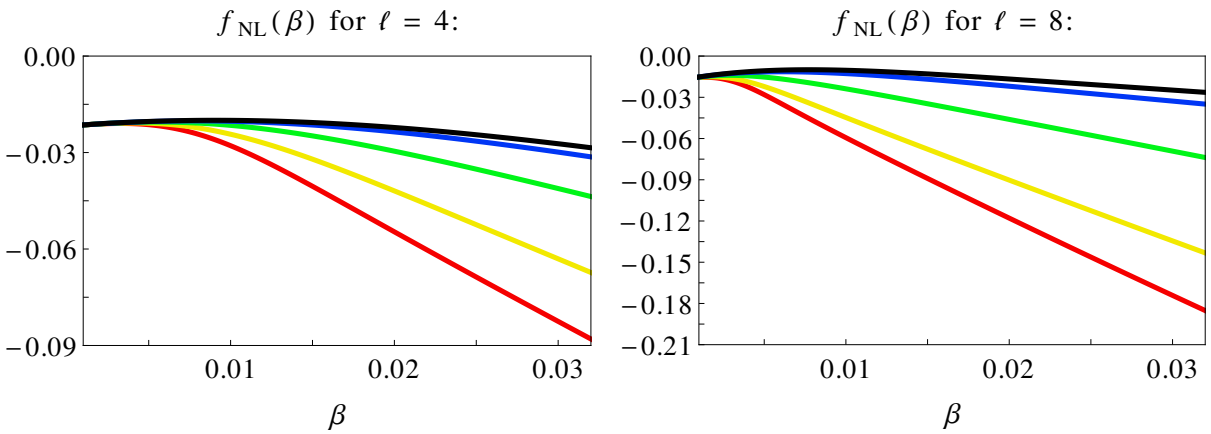

Figure 9.5: Reduced bispectrum f_{NL} as a function of β for $N_* = 55$, $v^\ell = 10^{-10}$ and $\ell = 4$ (left) or $\ell = 8$ (right). The differently coloured curves correspond to different initial angles θ in the ϕ-ψ-plane: black is the single-field limit ($\theta = 0°$) and red is close to the maximum angle ($\theta = 180°/\ell$). The angles shown are 0°, 15°, 30°, 40° and 44° (for $\ell = 4$) and 0°, 7.5°, 15°, 20° and 22° (for $\ell = 8$). Independently of v, we generally find $|f_{\mathrm{NL}}| < 1$, which makes it practically indistinguishable from zero.

9.6 Summary

In this chapter, we have studied the effects of the multi-field dynamics of the complex scalar inflaton field in supersymmetric new inflation, presenting both analytical considerations and numerical calculations. We have found that for most of the parameter space, the model is well described by the usual single-field approximation, where only the real component of the inflaton is considered and its imaginary component is set to zero. In particular, this is the case if the mass term from the Kähler potential is very small or absent, in which case the imaginary component is quickly driven to zero before cosmological scales leave the horizon.

For a sufficiently large mass term, the results become sensitive to the initial conditions. For these cases, we have numerically calculated the predictions using the δN formalism. For most initial conditions, we find that the results are still similar to the single-field results, but the deviations become significant for large initial values of the imaginary inflaton component (see fig. 9.4). Those deviations generally reduce the spectral index n_{s} and the inflationary vacuum energy V_0 compared to the single-field case. The reduced bispectrum is within the range $-1 < f_{\mathrm{NL}} < 0$, which is in good agreement with the current constraints, but probably too small to ever be observed.

Our conclusions are twofold. First, we want to emphasize that new inflation in supergravity is well-approximated by a single-field model if either

- the inflaton mass is very small compared to the Hubble scale, i.e. $\beta \ll 10^{-2}/(\ell - 2)$, or

- the initial displacement of the imaginary component is small (up to about 1/2 of its maximum value).

Second, if both of these conditions are violated (if both the inflaton mass term and the initial value of the imaginary inflaton component are sufficiently large), the spectral index n_{s} and the vacuum energy V_0 depend sensitively on the initial conditions, and the single-field results should be interpreted as upper limits on n_{s} and V_0 only.

Chapter 10

Preinflation and reheating from coupling to matter field

In the previous chapter, we have discussed new inflation with H as the inflaton, assuming the usual new inflation superpotential of eq. (5.17). In this chapter, we look at the effects of embedding new inflation in the tribrid superpotential of eq. (6.1). With such an embedding, the inflaton H has an additional superpotential coupling to X^n, where X^n can be a D-flat MSSM direction like a right-handed sneutrino or an LH_u direction as in chapter 7.

Such a coupling can have important effects especially before and after new inflation. Before new inflation, it can lead to a period of "preinflation" during which H is driven towards $H = 0$, dynamically generating the correct initial conditions for subsequent new inflation. After inflation, the same H-X coupling can open up a decay channel for the inflaton into MSSM fields which allows for efficient reheating of the universe.

We start with the discussion of preinflation. The basic idea is explained in section 10.1. In section 10.2, we calculate the initial conditions arising from quantum fluctuations near $H = X = 0$ and derive a simple condition for whether or not the last $N_* \sim 60$ e-folds are well-described by new inflation with H as the inflaton. The different regimes of single- and multi-field inflation in this model are discussed in section 10.3 along with a comparison of our results to numerical calculations. We close with a discussion of reheating in this setup in section 10.4. In particular, we study perturbative reheating for a specific example in which X is identified with a right-handed sneutrino, and demonstrate that in this case the model can generate the observed baryon asymmetry through non-thermal leptogenesis.

10.1 Initial conditions for new inflation from preinflation

New inflation starts with peculiar initial conditions: at early times, the inflaton field rests very close to its local maximum at $H = 0$. One might wonder how the universe has reached such a state.

One possibility for explaining these initial conditions is generating them dynamically through a period of "preinflation" during which H has a large mass term and is driven to zero. Usually, this involves adding a new sector of singlet fields which are decoupled from

the visible sector (e.g. in [29, 33, 135]).[1]

When realizing new inflation with a tribrid superpotential, preinflation can be achieved using the coupling of H to the matter field direction X^n, which can be identified e.g. with a D-flat direction of MSSM scalar fields. The purpose of this section is to introduce the scalar potential for such a model and qualitatively describe the dynamics of preinflation leading to the right initial conditions for new inflation.

Throughout this chapter, we analyse preinflation and new inflation with the tribrid superpotential of eq. (6.1) and $m = n = 2$:

$$W \;=\; \sqrt{V_0} S \left(1 - \frac{H^\ell}{\mu^\ell}\right) + \lambda H^2 X^2, \tag{10.1}$$

and assuming a power series expansion of the Kähler potential as in eq. (6.4).

The F-term scalar potential for H and X can be calculated from eq. (5.4).[2] The calculation is analogous to that for tribrid inflation with the difference that we cannot set $H = 0$ during inflation. We assume that κ_{SS} generates a sufficiently large mass term such that $S \simeq 0$ during inflation. In that case, the scalar potential is approximately given by eq. (5.6) plus supergravity induced mass terms, up to corrections suppressed by additional powers of X^2, H^2 or $(H/\mu)^\ell$:

$$\begin{aligned} V \;&\simeq\; |W_S|^2 + |W_H|^2 + |W_X|^2 - \beta V_0 \,|H|^2 + \alpha V_0 \,|X|^2 \\ &\simeq\; V_0 \left|1 - \frac{H^\ell}{\mu^\ell}\right|^2 + 4\lambda^2 |X^2 H^2| \left(|X|^2 + |H|^2\right) - \beta V_0 \,|H|^2 + \alpha V_0 \,|X|^2 , \end{aligned} \tag{10.2}$$

with $\alpha = 1 - \kappa_{SX}$ and $\beta = \kappa_{SH} - 1$. For new inflation, we need $\beta \ll 1$ to allow for slow-roll in H and $\beta \lesssim 0.03$ to get a correct prediction for the spectral index.

Throughout most of this chapter, we neglect the imaginary component of H; we briefly comment on its effects later in section 10.3.3. With $S = \mathrm{Im}(H) = 0$, the potential V can be expressed in terms of the real scalar fields $\phi = \sqrt{2}\,\mathrm{Re}(H)$ and $\chi = \sqrt{2}|X|$:

$$V(\phi, \chi) \;\simeq\; V_0 \left(1 - \frac{\phi^\ell}{v^\ell}\right)^2 + \frac{\lambda^2}{2} \phi^2 \chi^2 \left(\phi^2 + \chi^2\right) - \frac{\beta V_0}{2}\, \phi^2 + \frac{\alpha V_0}{2}\, \chi^2, \tag{10.3}$$

with $v = \sqrt{2}\mu$.

We assume that at some point in time, χ has a sufficiently large vacuum expectation value.[3] Then inflation happens in several stages:

- **Preinflation**: Due to the large value of χ, the inflaton ϕ gets a large mass $m_\phi^{(\mathrm{eff})} \sim \lambda\chi^2$ which drives it towards zero. The preinflaton χ gets a smaller mass $m_\chi^{(\mathrm{eff})} \sim \lambda\phi^2$,

[1] A similar function is performed by a coupling of the inflaton to the energy density as proposed in [136]. Alternative approaches to the initial conditions problem include [137–139].

[2] We do not consider the D-term scalar potential because we assume that inflation happens along a D-flat direction.

[3] χ must be large enough so that $\phi \to 0$ faster than $\chi \to \chi_\mathrm{c}$ during preinflation.

so it rolls towards zero more slowly. Eventually, $\phi \simeq 0$ and we get single-field slow-roll inflation in χ with the potential $V_{\rm pre} \simeq V_0 + \frac{1}{2}\alpha V_0 \chi^2$.

- **Quantum diffusion:** Eventually, χ drops below $\chi_{\rm c} = (\beta V_0/\lambda^2)^{1/4}$. At that time, ϕ is no longer stabilized at zero by a positive mass term, and it starts growing due to quantum fluctuations while χ continues to roll towards zero. This continues until ϕ grows large enough for its classical motion to take over, such that ϕ starts to slow-roll towards large values.

- **New inflation:** If the growth of ϕ during the quantum diffusion stage is slow enough, χ has rolled close to zero before ϕ starts its classical slow-roll motion. In this case, the last $N_* \sim 60$ e-folds of inflation are well-described by single-field new inflation with $\chi \simeq 0$ and $V \simeq V_0(1 - \phi^\ell/v^\ell)^2 - \frac{1}{2}\beta V_0 \phi^2$.

- **Reheating:** After single-field new inflation, ϕ decays into Standard Model particles to reheat the universe.[4] Depending on the model parameters, the coupling between ϕ and χ can provide an efficient inflaton decay channel. If χ is identified with a matter particle, e.g. a D-flat direction of MSSM scalars, this can lead to predictions for reheating observables. In section 10.4, we illustrate this using an example model of sneutrino preinflation, for which we derive predictions for the reheat temperature and non-thermal leptogenesis.

The above description of the inflationary dynamics mentions an important condition: single-field new inflation is reached only if the quantum fluctuations of ϕ grow sufficiently slowly compared to the classical motion of χ. Otherwise, χ is still large during the final N_* e-folds and we get multi-field inflation with ϕ and χ as inflaton fields.

To clarify the situation, we study the quantum diffusion stage in section 10.2 to derive the condition on the coupling constants which determines whether or not the single-field new inflation limit is reached. Afterwards, we discuss the multi-field effects for non-negligible χ in section 10.3.

10.2 On the initial conditions near the instability

During preinflation with $\chi \gg \chi_{\rm c}$, the inflaton field ϕ is driven to zero by its large mass $(m_\phi^{(\rm eff)})^2 \simeq (\lambda^2\chi^4 - \beta V_0)$. However, when χ approaches the instability at $\chi = \chi_{\rm c}$, the inflaton field ϕ becomes massless and $\langle\phi^2\rangle$ grows due to quantum fluctuations. As explained in section 9.3.1, quantum diffusion dominates when the classical displacement $\delta\phi_{\rm cl}$ of the field per Hubble time is smaller than the growth of quantum fluctuations $\delta\phi_{\rm qu}$ per Hubble time $\mathcal{H}^{-1}$:

$$\delta\phi_{\rm qu} = \frac{\mathcal{H}}{2\pi} \stackrel{!}{>} \delta\phi_{\rm cl} = \mathcal{H}^{-1}|\dot{\phi}| \simeq \left|\frac{\partial_\phi V}{V}\right|. \tag{10.4}$$

[4] This process often involves non-perturbative preheating effects, see chapter 11.

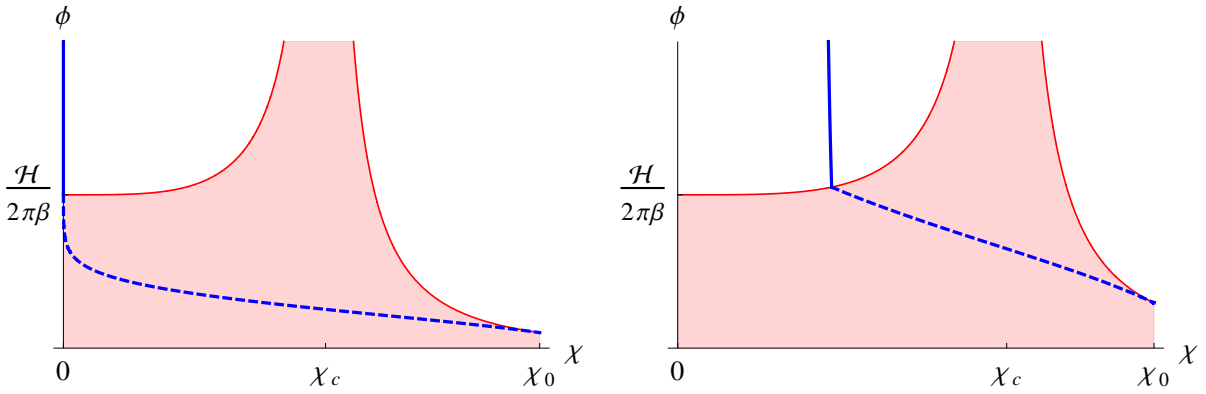

Figure 10.1: Field trajectory (blue curve) for $\beta = 0.03$ through the diffusion region (red area) for $\alpha = 10^{-2}$ (left) and $\alpha = 10^{-3}$ (right). The red curve is the diffusion boundary $\phi_{\rm b}(\chi)$ given in eq. (10.8). The field trajectory enters the diffusion region at (ϕ_0, χ_0) and leaves it at (ϕ_1, χ_1). The aim of this section is to calculate (ϕ_1, χ_1) which we identify as the initial conditions for the observable part of inflation. The left plot is the generic result for $\beta^2 \ll \alpha$, in which case $\chi_1 \to 0$ and inflation proceeds as single-field inflation in ϕ. Only for $\beta^2 \gtrsim \alpha$, χ_1 can be significantly large, in which case inflation should be analysed in a multi-field framework like the δN formalism.

In this section, we discuss how the fields evolve during this phase to find expressions for the field values ϕ_1 and χ_1 at the end of the quantum diffusion regime. To do this, we take the following steps (see fig. 10.1):

1. We find the boundary $\phi_{\rm b}(\chi)$ of the diffusion region inside which quantum diffusion dominates over the classical slow-roll field evolution for ϕ.

2. Inside this boundary, we assume that ϕ grows due to quantum fluctuations. We estimate the value of ϕ in this region via the expectation value $\phi_{\rm diff} \sim \sqrt{\langle\phi^2\rangle}$.[5] Outside the boundary, we calculate the trajectory of ϕ from the slow-roll equations of motion.

3. Assuming that initially we start from $\chi \gg \chi_{\rm c}$ (which quickly drives $\phi \to 0$), we find the values (ϕ_0, χ_0) at which ϕ enters the diffusion region and the values (ϕ_1, χ_1) at which it leaves the diffusion region. ϕ_1 and χ_1 are then the initial condition for inflation using the classical slow-roll equations of motion.

[5]Of course, quantum fluctuations are random, so the realized value of ϕ can be different for different patches of the universe. We use the expectation value only for an estimate of the likely magnitude of ϕ. This is sufficient because our conclusions will only depend on the order of magnitude of ϕ. The precise initial conditions are less important as the trajectories exhibit an attractor behaviour towards single-field new inflation.

10.2.1 Approximate potential during quantum diffusion phase

To keep the calculation of the diffusion region simple, we only keep terms of lowest order in ϕ, i.e.

$$\partial_\phi V \simeq \left(-\beta V_0 + \lambda^2 \chi^4\right) \phi = -\beta V_0 \left(1 - \frac{\chi^4}{\chi_\mathrm{c}^4}\right) \phi, \tag{10.5a}$$

$$\partial_\chi V \simeq \alpha V_0 \, \chi. \tag{10.5b}$$

This approximation usually works well because ϕ is very small in this region, as it is generated from quantum fluctuations only. Note that in this case, the initial conditions from quantum diffusion become independent of ℓ, v and λ.

One must include the higher-order terms in the calculation only if α or β are very small. In that case, the following calculation can be performed numerically using the exact scalar potential. The exact values for α and β for which this is necessary depend on ℓ, v and λ, but they are typically smaller than about 10^{-4}. The exact threshold is determined by the condition that eqs. (10.5a)–(10.5b) are the dominant contributions to the potential gradients at the diffusion boundary given by eq. (10.4).

As we will discuss below, the single-field limit is generic for $\beta^2 \ll \alpha$; this result can be generalized if either α or β is significantly large, in which case $\beta \simeq 0$ leads to the single-field limit and $\alpha \simeq 0$ suggests non-trivial multi-field dynamics. Only if both α and β are very small, the higher-order terms need to be considered explicitly and the result becomes dependent on ℓ, v and λ. This is discussed in appendix D.2 for the example $\ell = 6$ and $v = 10^{-2}$.

10.2.2 Boundary ϕ_b of the diffusion region

We find a formula for the boundary between the diffusion region and the classical region by inserting the scalar potential $\partial_\phi V$:

$$\frac{\mathcal{H}}{2\pi} \stackrel{!}{=} \left|\frac{\partial_\phi V}{V}\right|_{\phi_\mathrm{b}} = \beta \left|1 - \frac{\chi^4}{\chi_\mathrm{c}^4}\right| \phi_\mathrm{b}. \tag{10.6}$$

In the following, it will be useful to substitute the field χ with its quartic displacement from χ_c:

$$\Delta(\chi) \equiv \frac{\chi^4}{\chi_\mathrm{c}^4} - 1. \tag{10.7}$$

Using this variable, the diffusion boundary can be written as

$$\phi_\mathrm{b}(\Delta) = \left(\frac{\mathcal{H}}{2\pi}\right) \frac{1}{\beta|\Delta|}. \tag{10.8}$$

10.2.3 Trajectory ϕ_{diff} inside the diffusion region

After the fields enter the diffusion region at some $\Delta_0 > 0$, the expectation value for $\langle\phi^2\rangle$ grows linearly with $N = \mathcal{H}t$ [41].[6] Inside the diffusion region, $\langle\phi^2\rangle$ is thus given by

$$\phi^2_{\text{diff}}(\Delta) \;=\; \phi^2_{\text{b}}(\Delta_0) + \left(\frac{\mathcal{H}}{2\pi}\right)^2 N(\Delta). \tag{10.9}$$

The function $N(\Delta)$ can be inferred from the slow-roll equation of motion for χ, which is dominated by the term proportional to α:

$$0 \;\simeq\; 3\mathcal{H}^2\chi'(N) + \partial_\chi V \;\simeq\; V_0\left[\chi'(N) + \alpha\chi(N)\right]. \tag{10.10}$$

This differential equation can be solved for $\chi(N)$:

$$\chi(N) \;=\; \chi_0\, e^{-\alpha N}, \tag{10.11}$$

which implies, using eq. (10.7):

$$N(\Delta) \;=\; \frac{1}{\alpha}\ln\left(\frac{\chi_0}{\chi}\right) \;=\; \frac{1}{4\alpha}\ln\left(\frac{\Delta_0+1}{\Delta+1}\right). \tag{10.12}$$

Combining eqs. (10.8), (10.9) and (10.12) we find

$$\phi^2_{\text{diff}}(\Delta) \;=\; \left(\frac{\mathcal{H}}{2\pi}\right)^2\left[\frac{1}{\beta^2\Delta_0^2} + \frac{1}{4\alpha}\ln\left(\frac{\Delta_0+1}{\Delta+1}\right)\right]. \tag{10.13}$$

10.2.4 Diffusion region entry at Δ_0 and exit at Δ_1

Eq. (10.13) still depends on the point Δ_0 where the diffusion region is entered. This is determined from the condition that the diffusion region should not be exited immediately (otherwise, the field will travel at the boundary between the two regions):

$$\left|\frac{\partial\phi^2_{\text{b}}}{\partial\Delta}\right|_{\Delta_0} \;=\; \left(\frac{\mathcal{H}}{2\pi}\right)^2\frac{2}{\beta^2\Delta_0^3} \;\overset{!}{\geq}\; \left|\frac{\partial\phi^2_{\text{diff}}}{\partial\Delta}\right|_{\Delta_0} \;=\; \left(\frac{\mathcal{H}}{2\pi}\right)^2\frac{1}{4\alpha(\Delta_0+1)}. \tag{10.14}$$

The field stops travelling near the boundary when the inequality starts to be satisfied:[7]

$$\frac{\Delta_0^3}{1+\Delta_0} \;=\; \frac{8\alpha}{\beta^2}. \tag{10.15}$$

[6] We approximate $\langle\phi^2\rangle$ by the de Sitter space fluctuations of a massless field and neglect the small corrections due to the non-zero mass of ϕ.

[7] For arbitrary initial conditions, the fields could enter the diffusion region for any value $\Delta \leq \Delta_0$. However, when we assume that the fields approach along a trajectory where $\chi \gg \chi_{\text{c}}$ and $\phi \simeq 0$, we know it will move along the boundary until it enters the region at the largest possible value $\Delta = \Delta_0$.

The fields then travel along the trajectory $\phi_{\rm diff}(\Delta)$ until they exit the diffusion region at Δ_1 where $\phi_{\rm diff}(\Delta)$ and the diffusion boundary $\phi_{\rm b}(\Delta)$ intersect again:

$$\phi_{\rm b}^2(\Delta_1) \,=\, \left(\frac{\mathcal{H}}{2\pi}\right)^2 \frac{1}{\beta^2\Delta_1^2} \,\stackrel{!}{=}\, \phi_{\rm diff}^2(\Delta_1) \,=\, \left(\frac{\mathcal{H}}{2\pi}\right)^2 \left[\frac{1}{\beta^2\Delta_0^2} + \frac{1}{4\alpha}\ln\left(\frac{\Delta_0+1}{\Delta_1+1}\right)\right]. \quad (10.16)$$

We find an equation to determine Δ_1 from Δ_0:

$$\frac{1}{\Delta_1^2} - \frac{1}{\Delta_0^2} + \frac{\beta^2}{4\alpha}\ln\left(\frac{\Delta_1+1}{\Delta_0+1}\right) \,=\, 0. \quad (10.17)$$

10.2.5 Single-field limit for $\beta^2/\alpha \ll 1$

Let us now consider the special case $\beta^2/\alpha \ll 1$. Eq. (10.15) then has the approximate solution

$$\Delta_0^2 \,\simeq\, \frac{8\alpha}{\beta^2} \,\gg\, 1, \quad (10.18)$$

which we can plug into eq. (10.17) to find

$$\frac{1}{\Delta_1^2} \,\simeq\, \frac{\beta^2}{4\alpha}\left[-\ln\left(\Delta_1+1\right) + \frac{1}{2}\ln\left(\frac{8\alpha}{\beta^2}\right) + \frac{1}{2}\right]. \quad (10.19)$$

Since $0 < \chi_1 < \chi_{\rm c}$, eq. (10.7) implies that $-1 < \Delta_1 < 0$, so the left-hand side of eq. (10.19) is greater than 1. On the other hand, for $\beta^2/\alpha \to 0$, the last terms in eq. (10.19) both go to zero. Therefore, we know that $-\ln(1+\Delta_1) \gtrsim 4\alpha/\beta^2 \gg 1$, and therefore $\Delta_1 \simeq -1$. To lowest order in α/β^2, we thus find

$$\frac{\chi_1}{\chi_{\rm c}} \,\equiv\, (1+\Delta_1)^{1/4} \,\simeq\, \exp(-\alpha/\beta^2), \qquad \phi_1 \,\simeq\, \frac{\mathcal{H}}{2\pi\beta}. \quad (10.20)$$

For $\beta^2/\alpha \ll 1$, χ_1 is exponentially suppressed, usually down to the level of quantum fluctuations. The classical equations of motion only drive χ to smaller values, so it remains small, while ϕ is growing over time. As a consequence, ϕ is the only relevant field at horizon crossing, and we recover the single-field new inflation limit with ϕ as the inflaton.

10.2.6 Multi-field dynamics for $\beta^2/\alpha \gtrsim 1$

For arbitrary β^2/α, eqs. (10.15) and (10.17) can be solved numerically for Δ_0 and Δ_1. The result for Δ_1 can then be translated to χ_1 and ϕ_1 using eqs. (10.7) and (10.8).[8] The results

[8]Note that χ_1 also has a lower bound due to quantum fluctuations. The diffusion region for χ is given by $\chi < \chi_{\rm b} = \frac{\mathcal{H}}{2\pi\alpha}$. Below this value, χ is no longer decaying exponentially but instead behaves as a random variable of order $\chi_{\rm b}$. However, $\chi_{\rm b}$ is so small that it is negligible for the dynamics during inflation, so this lower bound has no practical relevance in our model.

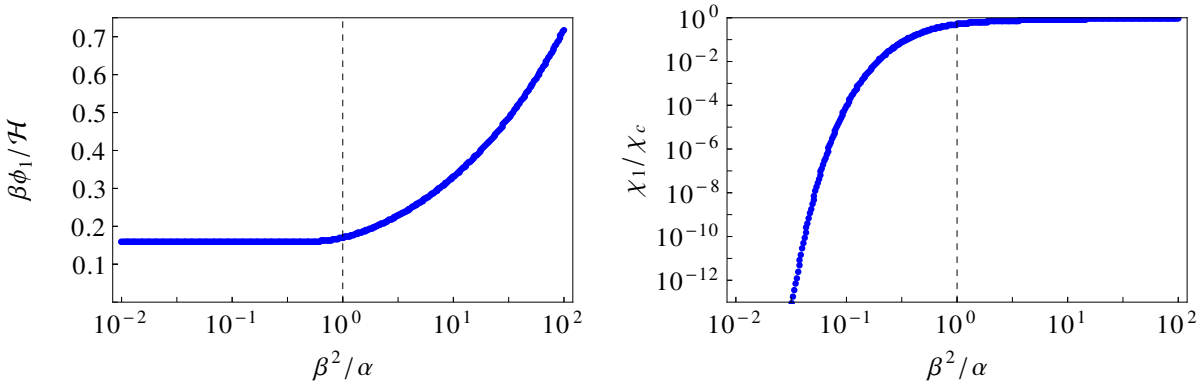

Figure 10.2: Values for ϕ_1 and χ_1 as functions of β^2/α. We see that for $\beta^2 \ll \alpha$, the value of the preinflaton χ_1 after preinflation is exponentially suppressed in agreement with eq. (10.20), down to the level of vacuum fluctuations for sufficiently small β^2/α. This implies that for $\beta^2 \ll \alpha$, preinflation generally leads to single-field new inflation with ϕ as the only inflaton. Only for $\beta^2 \gtrsim \alpha$, the preinflaton can have an influence during the observable last 60 e-folds, in which case inflation should be studied as a two-field model using e.g. the δN formalism (see section 10.3).

for ϕ_1 and χ_1 are shown in fig. 10.2. As expected, we see an exponential suppression of χ_1 for $\beta^2/\alpha \ll 1$. However, for larger values of β^2/α, we can initially have $\chi_1 \sim \chi_c \gg \phi_1$. In this case, the matter field χ can have an effect on the spectrum of primordial perturbations. This case is discussed in the next section.

10.3 Single-field and multi-field regimes

As we have seen in the last section, whether or not $\chi \simeq 0$ after preinflation depends on β^2/α. If χ is large, then it cannot be neglected during inflation, and we generically get multi-field inflation in ϕ and χ. In this case, the dynamics also depend on the coupling λ between ϕ and χ. Our model thus supports three different regimes of inflation which we now discuss in turn.

10.3.1 Discussion of the different regimes

Depending on β^2/α and λ, we find three qualitatively different regimes:

1. The limit of **single-field new inflation** ($\beta^2/\alpha \ll 1$), where $\chi \sim 0$ and inflation happens as single-field inflation in ϕ.

2. The limit of **quasi-single-field new inflation** ($\beta^2/\alpha \gtrsim 1$, small λ), where $\chi \sim$ constant and slow-roll inflation happens as single-field inflation in ϕ, with the inflaton potential $V(\phi)$ modified by the nearly constant background field χ.

3. Non-trivial **multi-field inflation** ($\beta^2/\alpha \gtrsim 1$, large λ), where both χ and ϕ are dynamic fields during slow-roll inflation.

Single-field inflation for $\beta^2/\alpha \ll 1$

As we discussed in section 10.2, the initial conditions for $\beta^2/\alpha \ll 1$ converge towards $\phi_\mathrm{i} \to \mathcal{H}/(2\pi\beta)$, $\chi_\mathrm{i} \to 0$. This means that inflation happens along the single-field new inflation trajectory with $\chi \simeq 0$. The predictions in this limit reproduce the results of chapter 9, and they do not depend on the preinflaton couplings α and λ.

Quasi-single-field inflation for $\beta^2/\alpha \gtrsim 1$ and small λ

When β^2/α is not small, the initial preinflaton field value χ_i is large enough for χ to have an impact during inflation. Therefore, the dynamics during inflation depends on the preinflaton coupling λ.

For small λ, the preinflaton potential is extremely flat; note that $\alpha \lesssim \beta^2$ implies that the preinflaton mass term is tiny, so that a sizeable potential for χ can only be generated from the coupling λ. We therefore expect that for sufficiently small λ, χ is nearly constant throughout slow-roll inflation: $\chi(t) \simeq \chi_* \simeq \chi_\mathrm{e}$.

In this limit for small λ, the slow-roll dynamics are equivalent to single-field slow-roll inflation in ϕ in the presence of a constant background field χ_*, which leads to an inflaton potential

$$\begin{aligned} V(\phi) &\simeq V_0 \left(1 - 2\frac{\phi^\ell}{v^\ell} - \frac{\beta}{2}\phi^2\right) + \frac{1}{2}\lambda^2\chi_*^2\phi^4 + \frac{1}{2}\lambda^2\chi_*^4\phi^2 \\ &= V_0 \left(1 - 2\frac{\phi^\ell}{v^\ell} - \frac{\beta_\mathrm{eff}}{2}\phi^2\right) + \frac{1}{2}\lambda^2\chi_*^2\phi^4, \end{aligned} \tag{10.21}$$

with

$$\beta_\mathrm{eff} = \beta\left(1 - \frac{\chi_*^4}{\chi_\mathrm{c}^4}\right). \tag{10.22}$$

We therefore recover the single-field new inflation limit with a redefined parameter $\beta \to \beta_\mathrm{eff}$ and an additional quartic term $\frac{1}{2}\lambda^2\chi_*^2\phi^4$. This term is negligible for sufficiently small λ, in which case we recover the predictions of chapter 9 with a rescaled β_eff.

If λ is too large to neglect the extra quartic term, the predictions must be calculated explicitly including the additional quartic term, leading to λ-dependent deviations from the results of chapter 9.

However, the curvature perturbation in this quasi-single-field regime is not necessarily constant at the end of inflation. Since the preinflaton field χ has not reached its minimum at that time, the universe has not yet reached the adiabatic limit. Therefore, the spectrum of primordial curvature perturbations could still be changed during the reheating period

after inflation (see e.g. [140–142] for perturbative reheating and [143] for non-equilibrium effects). As the reheating process is model dependent, these effects cannot be addressed in our general framework and must be checked for each specific model.

Two-field inflation for $\beta^2/\alpha \gtrsim 1$ and large λ

When λ is large, the preinflaton χ gets mass and self-coupling terms $\frac{1}{2}\lambda^2\phi^2\chi^2(\phi^2+\chi^2)$. As they are proportional to ϕ^2 and ϕ^4, these couplings start out small, so χ usually does not roll to zero before horizon crossing (if it did, we would end up in the single-field new inflation limit discussed above). However, when ϕ grows to larger values during inflation, the potential for χ becomes increasingly steep, and $\chi \to 0$.

In this regime, slow-roll inflation happens along a non-trivial multi-field trajectory and the predictions depend on the model parameters v and λ. If λ is sufficiently large, the preinflaton χ usually reaches the minimum before the end of inflation, so the evolution at the end of inflation should already be adiabatic. Otherwise, the spectrum of curvature perturbations could be affected by reheating in the same way as discussed for the small λ regime above.

10.3.2 Comparison with numerical results

Our results are confirmed by the numerical results shown in figs. 10.3 and 10.4, which have been calculated by Stefano Orani [3] using the δN formalism analogously to section 9.5.1.

For $\beta^2/\alpha \ll 1$, we recover the single-field predictions which are independent of α. For $\beta^2/\alpha \gtrsim 1$, the predictions change depending on λ. For large λ as shown in fig. 10.3, we are in the true multi-field regime and the predictions change non-trivially due to the two-field dynamics. For small λ as shown in fig. 10.4, the numerical calculation confirms that we indeed find a quasi-single-field regime for $\beta^2/\alpha \gtrsim 1$, with $\beta \to \beta_{\text{eff}}$, where β_{eff} scales monotonously with α as expected from eq. (10.22) and fig. 10.2.

10.3.3 Effect of $\mathrm{Im}(H)$

So far, we have ignored the imaginary inflaton component $\mathrm{Im}(H)$. It has been shown in chapter 9 that the imaginary inflaton component can reduce the spectral index n_{s} and the vacuum energy V_0 in supersymmetric new inflation, depending on the inflaton mass parameter β. For small $\beta \ll 10^{-2}/(2\ell)$, this effect is negligible, whereas for larger β, the magnitude of the reduction in n_{s} and V_0 depends on the initial ratio $\mathrm{Im}(H)/\mathrm{Re}(H)$, which is a random variable given by quantum fluctuations.

For the single-field and the quasi-single-field regimes (with sufficiently small λ in the latter case), these results are directly applicable, as the last $N_* \sim 60$ e-folds of inflation are well-described by supersymmetric new inflation with the complex inflaton field H. Only for large λ, the effect of the imaginary inflaton component may be different. In this case, it must generally be included in the numerical calculation, with the initial condition $\mathrm{Im}(H)/\mathrm{Re}(H)$ as an additional free parameter.

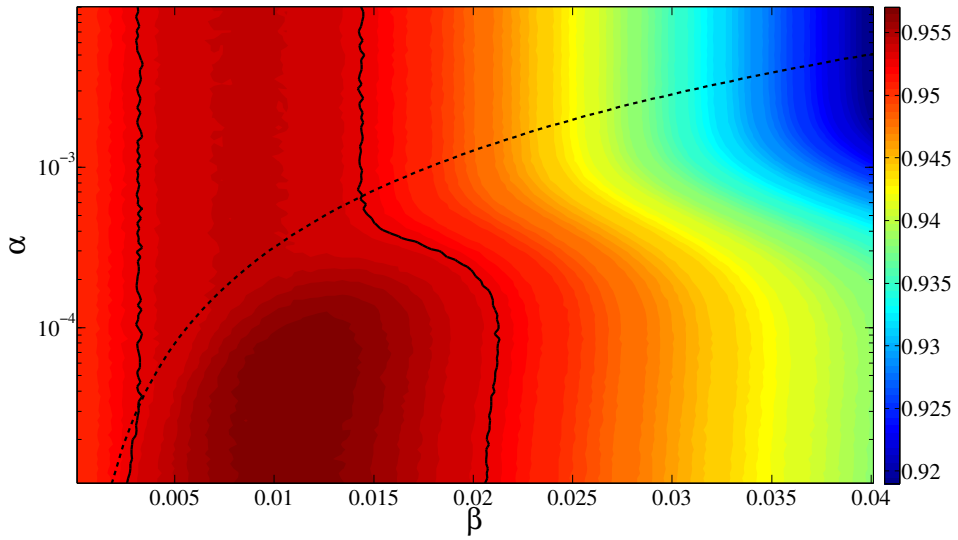

Figure 10.3: Numerical result by Stefano Orani [3] for the spectral index n_{s} as a function of α and β with $\lambda = 1$, $\ell = 4$ and $v = 10^{-2.5}$, using the initial field values from eqs. (10.15) and (10.17). The numerical result confirms our analytic arguments: for $\beta^2/\alpha \ll 1$, the predictions approach the single-field limit where $\chi \simeq 0$ during inflation and the predictions reproduce those of chapter 9 independently of α and λ. For $\beta^2/\alpha \gtrsim 1$, we are in the multi-field regime where predictions change non-trivially with α, β and λ. The two regimes are separated by the black dashed line which corresponds to $\alpha/\beta^2 = 1.4$.

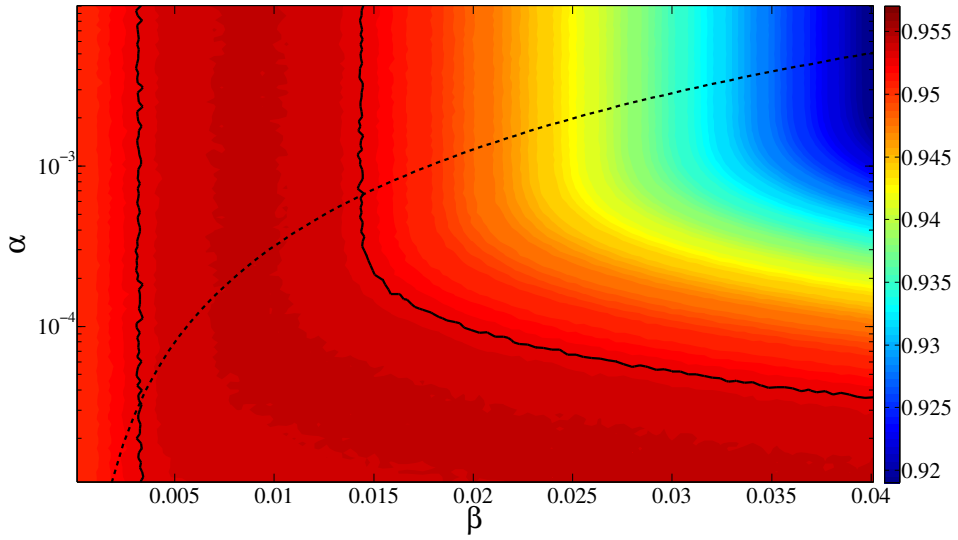

Figure 10.4: This plot is the equivalent of fig. 10.3 for $\lambda = 10^{-3}$. For $\beta^2/\alpha \ll 1$, the predictions again approach the single-field limit, whereas for $\beta^2/\alpha \gtrsim 1$, we are in the quasi-single-field limit where the predictions change according to eq. (10.22).

10.4 Reheating and leptogenesis from coupling to matter field

Using matter fields for preinflation is not only economical, it also provides an interesting decay channel for reheating. The inflaton-matter coupling used for preinflation allows decays of the inflaton particle ϕ into the matter field χ. The matter field can then decay further into Standard Model particles to reheat the universe. As the couplings within the matter sector are related to particle physics observables, this can lead to relations between particle physics and reheating observables.

To illustrate the benefits of using matter fields for preinflation, we discuss an explicit example in which one of the right-handed sneutrinos takes the role of the preinflaton.[9] For this example, we calculate the reheat temperature and the lepton asymmetry that is generated from out-of-equilibrium decays during reheating. Demanding that the generated baryon asymmetry from nonthermal leptogenesis matches the observed value, we can then constrain the masses of both the inflaton and the lightest right-handed neutrino.

10.4.1 Example model: sneutrino preinflation

The superpotential for our example model is

$$W = \sqrt{V_0}S\left(1-\frac{4H^4}{v^4}\right)+\sum_i \lambda_i H^2 X_i^2+\sum_{i,j} y_{ji} L_j H_u X_i, \tag{10.23}$$

which is a sum of the tribrid superpotential from eq. (6.1) and neutrino Yukawa couplings including the left-handed slepton doublets L_j, the electroweak up-type Higgs doublet H_u and the right-handed sneutrinos X_i. The right-handed neutrino masses are generated from the vacuum expectation value of the inflaton H after inflation. We assume that $L_j = H_u = 0$ during inflation, so the Yukawa couplings have no effect on inflation.[10]

With this superpotential, the inflaton can decay into right-handed sneutrinos and right-handed neutrinos which then continue to decay into left-handed (s)leptons and electroweak up-type Higgs(ino) particles.

A tree-level decay of the inflaton into right-handed (s)neutrinos requires $m_\phi > 2m_{X_i}$ for at least one of the X_i. In this example, we assume for simplicity that $m_\phi > 2m_{X_i}$ is satisfied for exactly one of the right-handed sneutrinos. We drop the index i from now on both on this right-handed sneutrino X and its superpotential coupling λ. The calculation can be generalized easily to the more general case that the inflaton can decay into more than one of the X_i.

[9] For a discussion of using the sneutrino as the inflaton, see e.g. [144, 145] for chaotic inflation or [23] for hybrid inflation.

[10] The left-handed sleptons and the electroweak Higgs can get Hubble-sized mass terms from the Kähler potential which stabilize them at zero.

10.4.2 Decay rates

To calculate the reheat temperature and baryon asymmetry, we need to calculate the inflaton decay rate Γ_ϕ into right-handed (s)neutrinos. We also need the decay rates of right-handed (s)neutrinos into (s)leptons and Higgs(ino) particles, which are assumed to thermalize quickly due to their gauge interactions.

Assuming $m_\phi > 2m_X$ so that the inflaton can decay into pairs of right-handed (s)neutrinos, we find the tree-level decay rate for the inflaton ϕ

$$\Gamma_\phi \;=\; \frac{\lambda}{8\pi} m_\phi m_X \left(1 + 12\frac{m_X^2}{m_\phi^2}\right)\left(1 - 4\frac{m_X^2}{m_\phi^2}\right)^{1/2} \tag{10.24}$$

and the tree-level decay rates for the right-handed neutrino ψ_X and the two sneutrino components χ, $\overline{\chi}$

$$\Gamma_\chi \;=\; \Gamma_{\overline{\chi}} \;=\; \Gamma_{\psi_X} \;=\; \frac{\sum_j |y_{ji}|^2}{4\pi} m_X. \tag{10.25}$$

The calculation of these decay rates is discussed in appendix D.1.

As reheating happens through the decay chains $\phi \to \chi + \chi \to$ MSSM, $\phi \to \overline{\chi} + \overline{\chi} \to$ MSSM and $\phi \to \psi_X + \psi_X \to$ MSSM, the relevant decay rate for the entire decay chain will be the minimum of Γ_ϕ and $\Gamma_\chi = \Gamma_{\overline{\chi}} = \Gamma_{\psi_X}$. In our model, we find the ratio

$$\frac{\Gamma_\phi}{\Gamma_\chi} \;=\; \frac{\lambda m_\phi}{2\sum\limits_j |y_{ji}|^2}\left(1 + 12\frac{m_X^2}{m_\phi^2}\right)\left(1 - 4\frac{m_X^2}{m_\phi^2}\right)^{1/2} \;\sim\; \frac{\lambda m_\phi}{2\sum\limits_j |y_{ji}|^2}. \tag{10.26}$$

For the following discussion, we will assume that $\Gamma_\phi \ll \Gamma_\chi$, which is generally the case if the neutrino Yukawa couplings are sufficiently large. We will later show that our results are consistent with this assumption (see section 10.4.6).

If the Yukawa couplings were very small, so that $\Gamma_\phi \gg \Gamma_\chi$, the calculation would be identical to [26], where the ϕ field decays quickly and reheating can be studied by only considering the sneutrino and neutrino decays via their Yukawa coupling. However, for our model the case with $\Gamma_\phi \ll \Gamma_\chi$ is more generic because with our superpotential (10.23) the mass m_ϕ is smaller than in the model studied in [26]. We therefore focus on the case $\Gamma_\phi \ll \Gamma_\chi$ for the rest of this chapter.

In the simplest case, reheating happens via perturbative inflaton decays and the decay products thermalize quickly due to the efficient gauge interactions. In that case, the reheat temperature and the produced lepton asymmetry can be estimated from the inflaton decay rate Γ_ϕ and the inflaton and sneutrino masses m_ϕ and m_X as outlined below.

For a detailed analysis, one should also consider non-perturbative effects from tachyonic preheating and parametric resonance. We will show in chapter 11 that, depending on the model parameters, preheating can lead to early explosive production of ϕ and χ particles such that the energy densities for both particle species are of the same order. However,

since the decay rates in our model are very hierarchical with $\Gamma_\chi \gg \Gamma_\phi$, χ particles produced during preheating will decay much earlier than ϕ particles, at a time when $\Gamma_\chi \sim \mathcal{H}$. The radiation produced by these decays redshifts faster than the energy density in the (almost) non-relativistic ϕ particles, so that the energy density is dominated by ϕ at the time when ϕ decays at $\Gamma_\phi \sim \mathcal{H}$. For this reason, we expect that our estimates for reheating derived from perturbative ϕ decays are reasonable estimates even in the case of efficient preheating.[11]

Rapid thermalization of the decay products is also not guaranteed if some D-flat MSSM directions develop large vacuum expectation values during inflation [146]. The calculations in this section assume that thermalization happens fast compared to the inflaton decay rate.

10.4.3 Inflaton and (s)neutrino masses

The inflationary vacuum energy V_0 is fixed by the amplitude A_s of scalar perturbations. As V_0 does not depend very much on α and β [3], we estimate V_0 from the single-field new inflation limit for $\beta = 0$ as given in eq. (9.20) with $N_* \simeq 60$ and $A_\mathrm{s} \simeq 2.2 \times 10^{-9}$.

The inflaton mass m_ϕ and the right-handed sneutrino mass m_X at the global minimum can be calculated in terms of the model parameters v and λ:

$$m_\phi = 16\frac{\sqrt{V_0}\langle H\rangle^3}{v^4} = 2^{5/2}\frac{\sqrt{V_0}}{v} \simeq \left(\frac{6\pi^2 A_\mathrm{s}}{N_*^3}\right)^{\frac{1}{2}} v \simeq (8\times 10^{-7})\, v, \tag{10.27a}$$

$$m_X = 2\lambda\langle H\rangle^2 = \lambda v^2. \tag{10.27b}$$

The right-handed neutrino fermion mass is equal to the sneutrino mass m_X because the global minimum of the inflaton potential does not break SUSY.[12]

We can invert eqs. (10.27a) and (10.27b) to express v and λ in terms of m_ϕ and m_X:

$$v = \left(\frac{N_*^3}{6\pi^2 A_\mathrm{s}}\right)^{\frac{1}{2}} m_\phi \simeq \left(1.3\times 10^6\right) m_\phi, \tag{10.28a}$$

$$\lambda = \left(\frac{6\pi^2 A_\mathrm{s}}{N_*^3}\right)\frac{m_X}{m_\phi^2} \simeq \left(6\times 10^{-13}\right)\frac{m_X}{m_\phi^2}. \tag{10.28b}$$

We can use eqs. (10.28a) and (10.28b) to express all results in terms of the physical masses m_X and m_ϕ or in terms of m_X and v.

[11] Preheating might still have some effect on the generated lepton asymmetry, as the lepton number density produced from χ decays is only diluted with $n_L \propto a^{-3}$, just like the inflaton field's energy density.

[12] We neglect soft SUSY breaking terms because these are expected to be much smaller than the energy scales relevant for reheating.

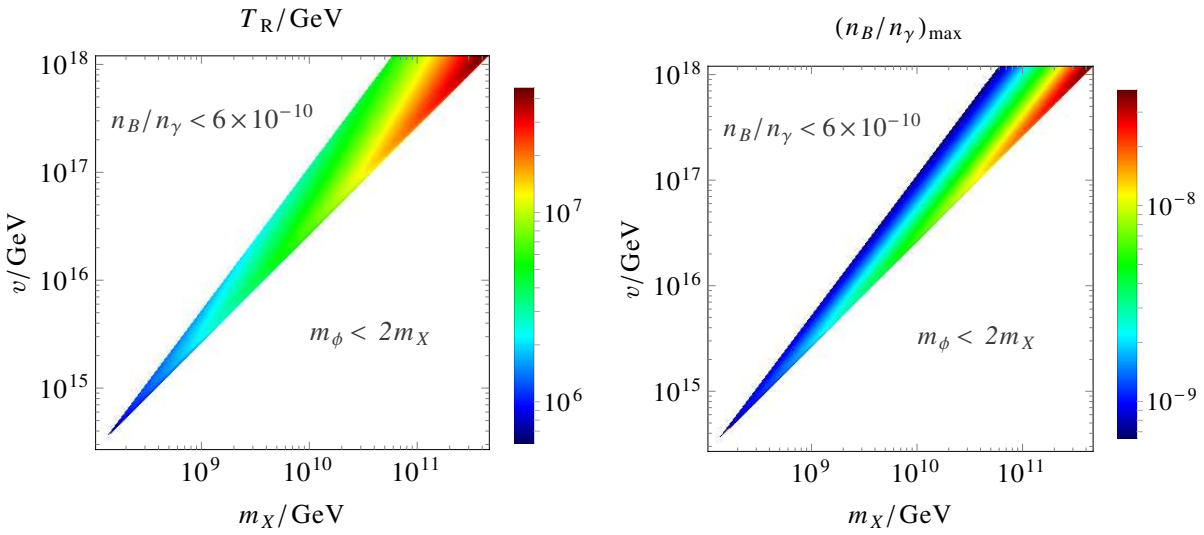

Figure 10.5: Reheat temperature T_R and upper bound on the baryon asymmetry $\frac{n_B}{n_\gamma}$ as functions of the right-handed neutrino mass m_X and inflaton vacuum expectation value v. We see that a sufficiently large baryon asymmetry can be generated for $m_X > 10^8\,\mathrm{GeV}$ if $v \sim 10^7\, m_X$.

10.4.4 Reheat temperature

Assuming that $\Gamma_\phi \ll \Gamma_\chi$ as discussed above, the reheat temperature can be estimated from eq. (4.15):

$$T_\mathrm{R} = \frac{1.2}{g_*^{1/4}}\sqrt{\Gamma_\phi} = \frac{0.24}{g_*^{1/4}}\left(\lambda m_\phi m_X\right)^{\frac{1}{2}}\left(1+12\frac{m_X^2}{m_\phi^2}\right)^{\frac{1}{2}}\left(1-4\frac{m_X^2}{m_\phi^2}\right)^{\frac{1}{4}}, \tag{10.29}$$

with $g_* = 228.75$ in the MSSM for temperatures above the mass of the heaviest visible sector sparticle [48].

For a simpler estimate, we can set $\left(1+12m_X^2/m_\phi^2\right)^{1/2}\left(1-4m_X^2/m_\phi^2\right)^{1/4} \sim 1$; the actual value is between 2/3 and 4/3 for $m_X/m_\phi < 0.497$. With this approximation, the reheat temperature is

$$T_\mathrm{R} \sim \frac{0.24}{g_*^{1/4}}\left(\frac{6\pi^2 A_\mathrm{s}}{N_*^3}\right)^{\frac{1}{2}}\frac{m_X}{\sqrt{m_\phi}} \sim \left(\frac{10^4\,\mathrm{GeV}}{m_\phi}\right)^{\frac{1}{2}} m_X. \tag{10.30}$$

In particular, this result implies that the right-handed (s)neutrinos are out of equilibrium during reheating ($T_\mathrm{R} \ll m_X$) for $m_\phi \gg 10^4\,\mathrm{GeV}$.

The reheat temperature as a function of m_X and v is shown in fig. 10.5 for the range of parameters for which the baryon asymmetry can be produced by nonthermal leptogenesis (see below) and $v < 1$. In this region, the reheat temperature is generally between $10^6\,\mathrm{GeV}$

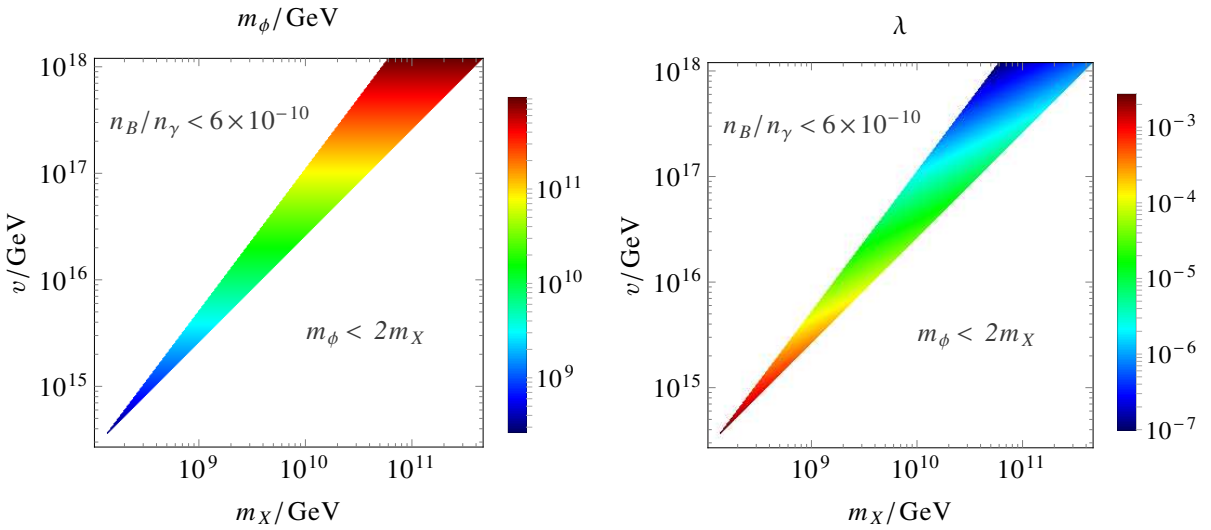

Figure 10.6: Inflaton mass m_ϕ after inflation and superpotential parameter λ as functions of the right-handed neutrino mass m_X and inflaton vacuum expectation value v.

and 10^8 GeV, which can be low enough to evade the bounds on thermal gravitino production depending on the gravitino mass $m_{3/2}$ [83–85].

10.4.5 Nonthermal leptogenesis

The inflaton particles decay into pairs of right-handed neutrinos and sneutrinos whose out-of-equilibrium decay generates a lepton asymmetry. The generated lepton asymmetry can be estimated analogously to [26] as

$$\left|\frac{n_L}{s}\right| \simeq \frac{5}{2}\frac{\epsilon T_\mathrm{R}}{m_\phi}. \tag{10.31}$$

ϵ quantifies the CP violation per (s)neutrino decay:

$$\epsilon \equiv \frac{\Gamma - \Gamma^{(\mathrm{CP})}}{\Gamma + \Gamma^{(\mathrm{CP})}}, \tag{10.32}$$

where Γ denotes the neutrino or sneutrino decay process and $\Gamma^{(\mathrm{CP})}$ the CP conjugate of that decay process. As an estimate for ϵ, we use its upper bound for the decay of right-handed neutrinos with a hierarchical spectrum [147–149]:

$$\epsilon < \frac{3}{8\pi}\frac{\sqrt{\Delta m^2_{\mathrm{atm}}}m_X}{\langle H_u\rangle^2}. \tag{10.33}$$

The lepton asymmetry is converted into a baryon asymmetry by sphaleron processes, which introduce a conversion factor $n_B = \frac{C}{C-1}n_L$ with $C \simeq 1/3$ in the MSSM [91], and $s = 7.04\, n_\gamma$

[37]:

$$\left|\frac{n_B}{n_\gamma}\right| \;=\; 7.04\left|\frac{C}{C-1}\frac{n_L}{s}\right| \;\simeq\; 8.8\,\frac{\epsilon T_\mathrm{R}}{m_\phi}. \tag{10.34}$$

Using the bound from eq. (10.33) with $\langle H_u\rangle \sim 174\,\mathrm{GeV}$ and $\Delta m^2_\mathrm{atm} \simeq 3\times10^{-3}\,\mathrm{eV}^2$, we find an upper bound on the baryon asymmetry (fig. 10.5). For a simple estimate, we can approximate T_R with eq. (10.30):

$$\left|\frac{n_B}{n_\gamma}\right| \;\lesssim\; 6\times10^{-10}\frac{(2m_X)^2}{\sqrt{(2\times10^8\,\mathrm{GeV})m_\phi^3}}. \tag{10.35}$$

If we demand that nonthermal leptogenesis generates the observed baryon asymmetry $n_B/n_\gamma = 6\times10^{-10}$, eq. (10.35) together with $m_\phi > 2m_X$ implies a lower bound on the inflaton mass: $m_\phi > 2\times10^8\,\mathrm{GeV}$. Also, one can see in fig. 10.5 that this condition relates the right-handed neutrino mass m_X and the symmetry breaking scale v, which must be related roughly by $v \sim 10^7\,m_X$.

10.4.6 Consistency of $\Gamma_\phi \ll \Gamma_\chi$

For our calculations, we have assumed that $\Gamma_\phi \ll \Gamma_\chi$, which according to eq. (10.26) means that the Yukawa coupling must be sufficiently large. We can estimate the size of the Yukawa coupling from the seesaw formula for the light neutrino mass m_ν:

$$m_\nu \;\sim\; \frac{y^2\langle H_u\rangle^2}{m_X}, \tag{10.36}$$

which implies that the Yukawa coupling is

$$y^2 \;\sim\; \left(\frac{m_\nu}{1\,\mathrm{meV}}\right)\left(\frac{m_X}{3\times10^{16}\,\mathrm{GeV}}\right). \tag{10.37}$$

If we insert this in eq. (10.26) and use eq. (10.28b), we find

$$\frac{\Gamma_\phi}{\Gamma_\chi} \;\sim\; \frac{\lambda m_\phi}{2y^2} \;\sim\; \left(\frac{10^{-4}\,\mathrm{meV}}{m_\nu}\right)\left(\frac{10^8\,\mathrm{GeV}}{m_\phi}\right). \tag{10.38}$$

With $m_\phi > 2\times10^8\,\mathrm{GeV}$, the assumed decay rate hierarchy holds if the light neutrino mass generated by the seesaw mechanism is much bigger than about 10^{-4} meV, which is true for at least two of the three light neutrinos.

10.5 Summary

In this chapter, we have studied the effects of realizing supergravity new inflation with a tribrid superpotential as given in eq. (6.1). In such a setup, the inflaton H is coupled to another scalar field direction X^n, where X^n can be any D-flat combination of scalar fields. Such a coupling has two main effects: it can generate the initial conditions for new inflation dynamically during a period of preinflation, and it can provide an efficient decay channel for reheating after inflation.

We first discussed the mechanism for preinflation. During preinflation, X has a large vacuum expectation value which induces a mass for H, driving $H \to 0$. Eventually, the preinflaton rolls to small values $|X| < |X_c|$, where its stabilising effect on H ends and the fields enter a "diffusion region" in which quantum fluctuations have to be included.

We have calculated the initial conditions after this phase in section 10.2 and found that there are two cases depending on the ratio of Kähler potential couplings α and β for X and H. If $\beta^2 \ll \alpha$, then $X \to 0$ during this quantum diffusion phase, and the subsequent final phase of inflation is well-described by supergravity new inflation with H as the inflaton as discussed in chapter 9.

For $\beta^2 \gtrsim \alpha$, X can be non-negligible during the last N_* e-folds of inflation. We have shown in section 10.3 that depending on the coupling λ between H and X, this leads either to a quasi-single-field regime where X acts as a constant background field, or to a non-trivial two-field regime which has to be studied in a multi-field formalism like the δN formalism. We also compared our analytical results to numerical computations and found that they are in excellent agreement with each other.

Finally, we discussed reheating in this class of models in section 10.4. In particular, we calculated the reheat temperature and non-thermally produced lepton asymmetry for an example model where one of the right-handed sneutrinos acts as the preinflaton. We found that successful nonthermal leptogenesis is indeed possible and imposes a relation between the symmetry breaking scale v and the mass m_X of the lightest right-handed neutrino after inflation, as well as lower bounds on both quantities.

Chapter 11

Preheating in new inflation

As we have illustrated in section 10.4 for an example model of sneutrino preinflation, reheating can provide additional constraints on the model parameters when inflation is embedded in a realistic particle physics model. In that example model, the analysis is simplified by the very hierarchical decay rates $\Gamma_\chi \gg \Gamma_\phi$: χ particles are expected to decay long before ϕ, and thus the final phase of reheating generically starts with an energy density dominated by ϕ particles. Therefore, we could estimate the reheating observables just from analysing the decay of ϕ particles.

In general, the decay rates can be less hierarchical. In that case, we must also consider the effects of the preheating stage. During preheating, the oscillations of the inflaton field can source explosive particle growth which affects the initial conditions for the subsequent reheating phase. Understanding the preheating period is therefore a prerequisite for calculating reheating observables in many models.

In this chapter, we discuss preheating in the new inflation model of chapter 10 which was derived from the tribrid superpotential. We start with a brief overview, listing the different phases of preheating and their qualitative effects. We then focus on preheating of the inflaton ϕ, showing that preheating can quickly make ϕ very inhomogeneous within a few oscillations of the inflaton condensate. Finally, we consider the effects of the coupling between ϕ and χ, and show that χ can be resonantly amplified even by the already inhomogeneous ϕ field such that the abundances of ϕ and χ particles become comparable.

The contents of this chapter were originally part of team projects involving numerical lattice simulations by Stefano Orani and Francesco Cefalà [6, 150]. My own results are complementary to the lattice simulations in that they motivate the choice of parameters and initial conditions for the lattice simulations and help to interpret the lattice results. This thesis focuses on my own work and only briefly summarizes the related lattice results which are presented more completely in [6, 150].

11.1 Preheating in new inflation with coupling to matter field

In this chapter, we study preheating with the scalar potential

$$V(\phi,\chi) = V_0\left(1-\frac{\phi^\ell}{v^\ell}\right)^2 + \frac{\lambda^2}{2}\phi^2\chi^2(\phi^2+\chi^2), \tag{11.1}$$

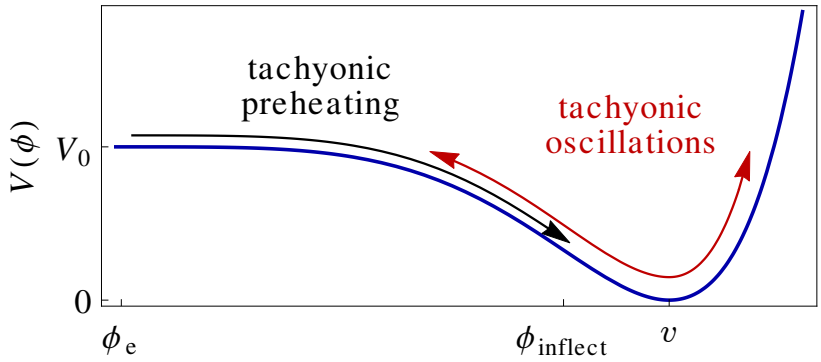

Figure 11.1: Phases of preheating in new inflation. After slow-roll inflation ends at ϕ_e, the inflaton field rolls down a part of its potential with $V''(\phi) < -\mathcal{H}^2$ which triggers a phase of tachyonic preheating. Afterwards, the inflaton field oscillates around its minimum with large amplitude which periodically brings it back into the tachyonic region. For $v \lesssim 10^{-2}$, ϕ becomes strongly inhomogeneous after a few of these tachyonic oscillations. In that case, there can be a third stage of preheating during which χ grows exponentially due to its coupling to the inhomogeneous ϕ field.

with the inflaton field ϕ and the preinflaton field χ. Throughout this chapter, we assume that $\langle\chi\rangle = 0$ at the beginning of preheating; the effect of non-zero initial $\langle\chi\rangle$ will be discussed briefly in section 11.3.5.

This scalar potential is identical to the preinflation model of chapter 10; it is derived from the tribrid superpotential of eq. (6.1) by neglecting $\mathrm{Im}(H)$ and S. The growth of S during preheating in the full tribrid model is briefly discussed in appendix D.3. We also set $\alpha = \beta = 0$ throughout this chapter, as preheating happens in a much steeper region of the potential compared to slow-roll inflation, and we expect the effects of α and β to be negligible for preheating.

Preheating in this model happens in three qualitatively different stages (see fig. 11.1):

1. **Tachyonic preheating:** During the initial descent of ϕ towards its minimum, the infrared modes of ϕ grow exponentially due to its large tachyonic mass $V''(\phi) < -\mathcal{H}^2$. For $v \lesssim 10^{-6}$, this growth is strong enough to make ϕ very inhomogeneous with $\langle\delta\phi^2\rangle \sim v^2$, so that linear preheating ends already during this stage [151].

2. **Tachyonic oscillations:** For $v \gtrsim 10^{-5}$, the perturbations of ϕ remain linear during tachyonic preheating, and the inflaton field performs large amplitude oscillations around the minimum which periodically bring it back into the tachyonic region of its potential. During these oscillations, perturbations grow rapidly at a characteristic peak scale k_{peak} [151]. For $10^{-5} \lesssim v \lesssim 10^{-2}$, the oscillations grow so fast that the perturbations become non-linear after a few oscillations. Only for $v \gtrsim 10^{-1}$, the growth is limited by Hubble damping and the perturbations always remain small.

3. **Parametric resonance of χ:** If ϕ has become inhomogeneous during the tachyonic oscillation stage, then the inhomogeneous ϕ can still trigger exponential amplification of χ fluctuations similar to a parametric resonance.[1]

In this chapter, we discuss these different stages in turn. The first two stages are studied in section 11.2. We review the analytic results of [151] and perform numerical calculations of the linear perturbations for various model parameters, showing that ϕ indeed becomes inhomogeneous with a sharply peaked spectrum within a few oscillations for $10^{-5} \lesssim v \lesssim 10^{-2}$, and we briefly discuss the subsequent stage of hill crossing and oscillon formation in these cases. Afterwards, the resonant amplification of χ is studied in section 11.3. We perform a generalized Floquet analysis which highlights the similarities between this inhomogeneous resonance and a usual parametric resonance, and we comment on the lattice results which confirm the existence and parametric dependence of this resonance.

11.2 Preheating and hill crossing of ϕ

In this section, we study the tachyonic preheating and tachyonic oscillations of ϕ, neglecting the χ field for now. Since ϕ is homogeneous up to tiny vacuum fluctuations during inflation, the initial phase of preheating can be studied using linear perturbation theory as discussed in section 4.2.

We first summarize the analytic results from [151] for these two phases and then show numerical results for the linear perturbation spectra produced by preheating. We then discuss how these power spectra suggest that for $10^{-5} \lesssim v \lesssim 10^{-2}$, the perturbations could push the inflaton field above the hilltop towards $\phi(x) < 0$ and create bubbles of vacuum with $\phi < 0$ separated by a typical distance $d \sim 2\pi/k_{\rm peak}$.

11.2.1 Tachyonic preheating

When $V''(\phi) < 0$, all modes with $k/a < \sqrt{-V''(\phi)}$ experience exponential growth. This period of tachyonic growth lasts the longest for modes with $k/a \lesssim \mathcal{H}_0$, which are already tachyonic at the end of inflation. Modes with larger k become tachyonic later. Therefore, they grow for a shorter time and achieve a smaller final amplitude. Modes above $k_{\rm m}/a = \max_{\phi} \sqrt{-V''(\phi)}$ are not amplified at all.

After tachyonic preheating[2], the power spectrum for small wavenumbers $k_{\rm IR} \lesssim a\mathcal{H}_0$ can be estimated as [151]

$$\mathcal{P}_\phi(k_{\rm IR}) \sim 10 A_{\rm s} \left(\frac{1}{N_*^2}\right)^{\frac{\ell-1}{\ell-2}}, \tag{11.2}$$

[1] Fields coupled to the inflaton such as χ generically exhibit some linear or power-law growth from driven turbulence after preheating [78], but not exponential growth as during a parametric resonance.

[2] The value of the power spectrum in eq. (11.2) is evaluated at $\phi = v$ at which time the tachyonic peak takes on its maximum.

so for $50 \lesssim N_* \lesssim 60$ the infrared part of the tachyonic preheating spectrum is

$$10^{-13} \lesssim \mathcal{P}_\phi(k_{\rm IR}) \lesssim 10^{-11}, \tag{11.3}$$

with $\mathcal{P}_\phi(k_{\rm IR}) \sim 10^{-13}$ for $\ell = 4$. For $a\mathcal{H}_0 < k < k_{\rm m}$, the power spectrum falls off rapidly with k, and for $k > k_{\rm m}$, the spectrum is just the vacuum spectrum $\mathcal{P}_\phi \simeq k^2/(4\pi^2 a^2)$.

The variance of the inflaton field is dominated by the large contribution from the infrared modes:

$$\langle \delta\phi^2(x) \rangle \;=\; \int (d\log k)\, \mathcal{P}_\phi(k) \;\sim\; \mathcal{P}_\phi(k_{\rm IR}). \tag{11.4}$$

For very small $v \lesssim 10^{-6}$, this implies $\langle \delta\phi^2(x) \rangle \gtrsim v^2$, so the perturbations become non-linear during tachyonic preheating – the inflaton field becomes very inhomogeneous and the description in terms of a background field plus perturbations breaks down. For larger $v \gtrsim 10^{-5}$, eq. (11.4) implies $\langle \delta\phi^2 \rangle \ll v^2$ and the linear approximation should remain viable.

11.2.2 Tachyonic oscillations

For $v \gtrsim 10^{-5}$, tachyonic preheating is followed by a phase of tachyonic oscillations during which the background field oscillates around the minimum. For $v \lesssim 10^{-1}$, these oscillations take the inflaton back into the tachyonic region. In this case, one can estimate the inflaton field value after j complete oscillations as [151]

$$\frac{\phi_j}{v} \;\sim\; (jv)^{1/\ell}\,. \tag{11.5}$$

These oscillations trigger strong growth of perturbations at a characteristic peak scale [151]

$$k_{\rm peak} \;\sim\; \ell\, v^{-\frac{\ell+2}{2\ell}}\, a\mathcal{H}_0. \tag{11.6}$$

For small $v \lesssim 10^{-2}$, the perturbations grow by many orders of magnitude and become non-linear within a few oscillations around the minimum. For large $v \gtrsim 10^{-1}$, however, the oscillations are quickly damped due to Hubble damping (see fig. 11.2). After a few oscillations, the amplitude decreases so much that the inflaton field never re-enters the tachyonic region, which makes preheating much less efficient. In this case, the perturbations remain so small that the linear approximation remains valid throughout the entire preheating phase.[3]

Note that the perturbations with $k \ll k_{\rm peak}$, which are amplified most during tachyonic preheating, do not continue to grow during the oscillation phase. Even though they are amplified every time that the inflaton field rolls down the tachyonic part of the potential, this amplification is exactly cancelled by an exponential damping every time the field rolls back up. The infrared part of the spectrum therefore oscillates: it is very large near the minimum at $\phi \sim v$, and it is negligible at ϕ_j (i.e. near the hilltop).

[3]There is some non-adiabatic growth of the inflaton perturbations during the subsequent non-tachyonic oscillations around the minimum, but red-shifting and Hubble damping make the perturbations decay before they can grow non-linear.

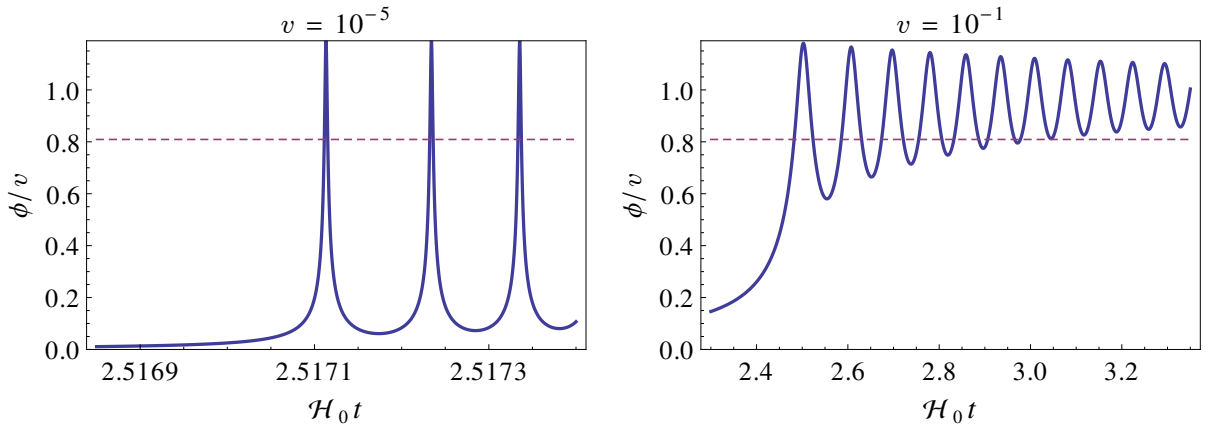

Figure 11.2: Oscillations of the inflaton background field around the minimum as a function of $\mathcal{H}_0 t$, plotted for $v = 10^{-5}$ and $v = 10^{-1}$ with $\ell = 4$. The dashed horizontal line denotes the inflaton value $\phi_{\text{inflect}} \simeq 0.81v$ below which $V''(\phi) < 0$. We see that for small $v \ll 10^{-1}$, the oscillations continue to bring ϕ deeply into the tachyonic region for several oscillations. For large $v = 10^{-1}$, however, Hubble damping quickly dampens the oscillation amplitude so that after a few oscillations, the inflaton field never re-enters the tachyonic region. Preheating is much less efficient in this case: the perturbations remain small and are eventually redshifted away as the inflaton field oscillates around the quadratic part of its potential.

11.2.3 Numerical results for the power spectra

Integrating the mode equations (4.3) numerically, we can calculate the power spectrum $\mathcal{P}_\phi(k)$ of the inflaton perturbations. As initial conditions, we match ϕ_k and $\dot{\phi}_k$ for each k to eq. (3.6) at a sufficiently early time such that $\mathcal{H}$ is still approximately constant and $(k/a)^2 \gg |V''(\phi)|$. This initial matching time is chosen differently for each k, since the smallest k need much earlier matching than the largest k.

Fig. 11.3 shows $\mathcal{P}_\phi/\overline{\phi}^2$ for $\ell = 4$ and various values of v evaluated at the time when the inflaton crosses the minimum ($\overline{\phi} = v$ and $\dot{\overline{\phi}} > 0$), while fig. 11.4 shows the power spectra closest to the hilltop at the end of each full oscillation, where $\dot{\overline{\phi}} = 0$.

All of the plots show the strong growth of power for modes with $k \sim k_{\text{peak}}$ with each successive oscillation. For $v \leq 10^{-2}$, it only takes a few oscillations for the perturbations to grow non-linear (i.e., $\mathcal{P}_\phi(k_{\text{peak}}) \gtrsim \overline{\phi}^2$). Only for large $v = 10^{-1}$, the perturbations remain small due to Hubble damping as explained above.

For the infrared modes, fig. 11.3 clearly shows the tachyonic preheating spectrum with $\mathcal{P}_\phi(a\mathcal{H}_0) \sim 10^{-13}$. The infrared modes do not continue to grow during the tachyonic oscillation phase: for $v \leq 10^{-2}$, the infrared parts of the spectra after the j-th oscillation lie on top of each other. For $v = 10^{-1}$, we even see that the infrared modes slowly decay due to Hubble damping and redshifting. Near the hilltop, the tachyonic preheating spectrum almost vanishes, as one can see in fig. 11.4. The infrared part of the spectrum actually oscillates during the tachyonic oscillation phase, growing to maximum values at

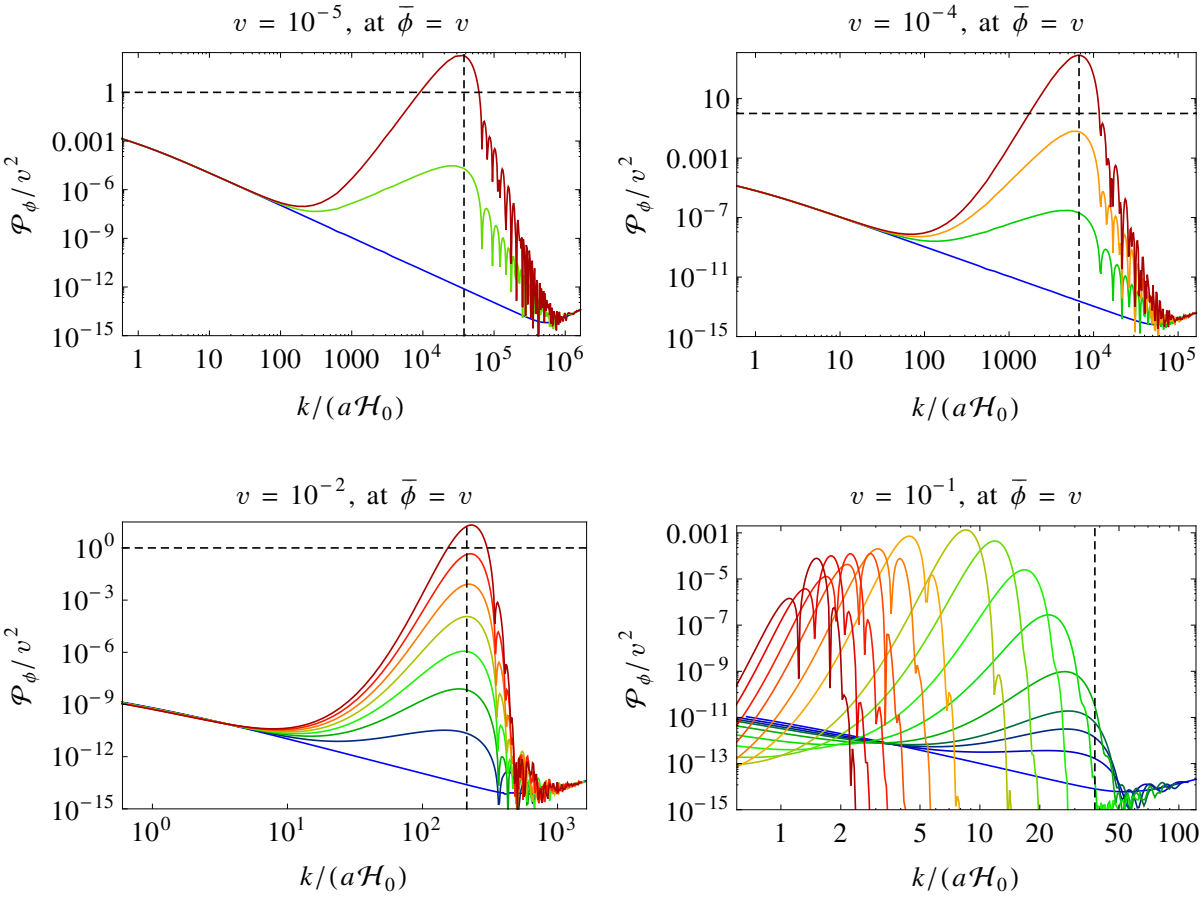

Figure 11.3: Linear power spectra evaluated at $\bar{\phi} = v$ and $\dot{\bar{\phi}} > 0$ for the first few oscillations (first to last oscillation: blue to red), for $\ell = 4$. Tachyonic preheating most strongly enhances the infrared modes ($k \lesssim a\mathcal{H}_0$), whereas the oscillations enhance modes with much larger momenta around the peak scale $k_{\rm peak} \simeq 7v^{-3/4}a\mathcal{H}_0$, which is denoted by a vertical dashed line. For $v = 10^{-1}$, we do not show every oscillation, because linear preheating lasts for very many oscillations; the dark red line in this case corresponds to over 1000 oscillations.

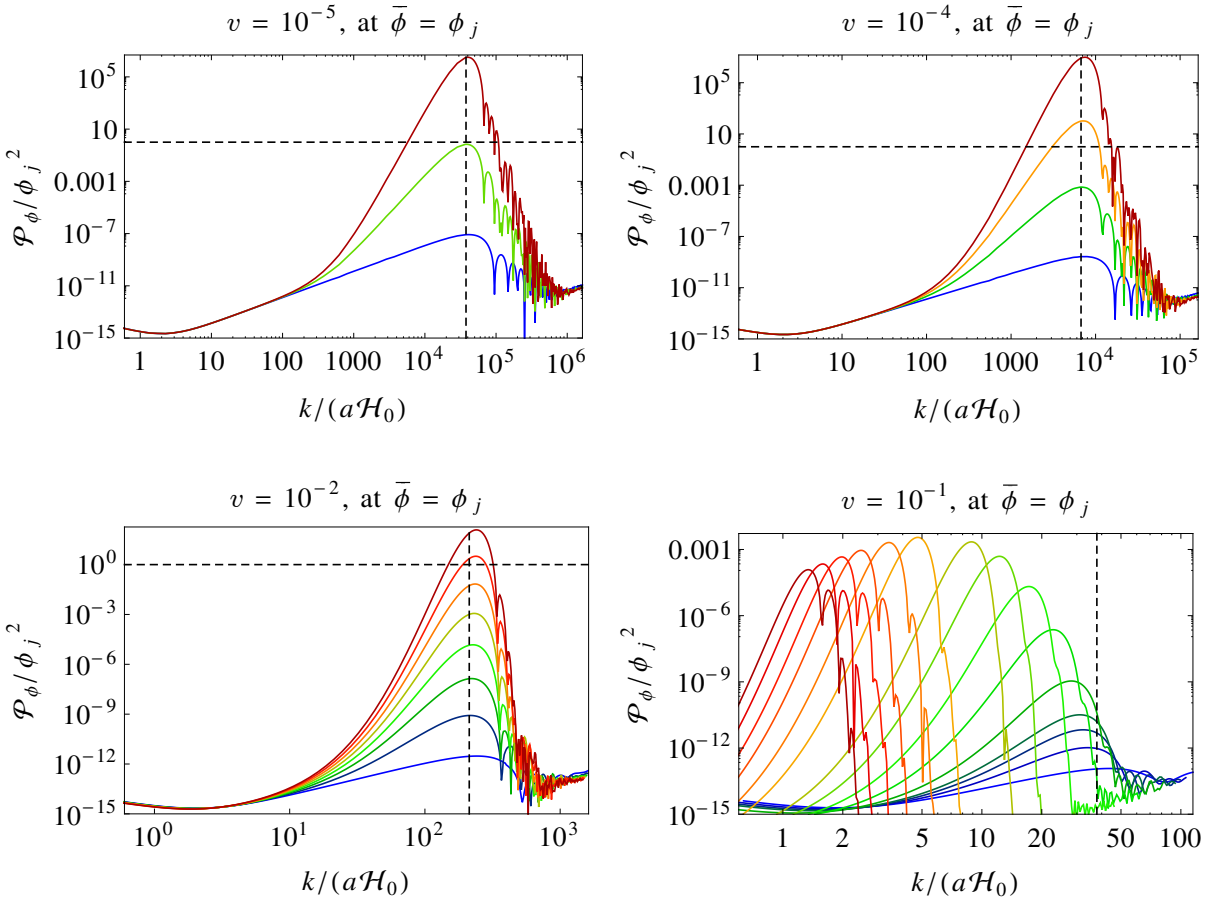

Figure 11.4: Linear power spectra normalized to the mean inflaton value $\overline{\phi} = \phi_j$, evaluated at the end of each oscillation when the inflaton is closest to the hilltop (first to last oscillation: blue to red), for $\ell = 4$. We see that the infrared peak from tachyonic preheating is negligible near the hilltop, whereas the perturbations around the peak scale $k_{\rm peak}$ (vertical dashed line) can grow to amplitudes larger than ϕ_j, indicating that on these scales, the perturbations can push the inflaton towards $\phi(x) < 0$. For $v = 10^{-1}$, we do not show every oscillation, because linear preheating lasts for very many oscillations; the dark red line in this case corresponds to over 1000 oscillations.

$\overline{\phi} \simeq v$ and shrinking to minimal values at $\overline{\phi} \simeq \phi_j$, whereas $\mathcal{P}_\phi(k_{\rm peak})/\overline{\phi}^2$ continuously grows throughout each oscillation[4] until the evolution becomes non-linear.

11.2.4 End of linear preheating and hill crossing

Linear preheating predicts that for $10^{-5} \lesssim v \lesssim 10^{-2}$, there is a rapid growth of perturbations at the scale $k_{\rm peak}$, producing a large fluctuation amplitude

$$\langle \delta\phi^2(\vec{x}) \rangle \;=\; \int (d\ln k) \mathcal{P}_\phi(k) \;\sim\; \mathcal{P}_\phi(k_{\rm peak}) \;\gtrsim\; \overline{\phi}^2. \tag{11.7}$$

This could indicate either that the fluctuations become large enough to push the inflaton field over the hilltop towards $\phi(\vec{x}) < 0$, or that linear perturbation theory breaks down and non-linear interactions stop the growth of perturbations before this happens. To find out which of these options is realized, we must perform a non-linear calculation, e.g. a lattice simulation as discussed in section 4.3.

Such lattice simulations have been performed for our model by Stefano Orani in [6], using the results from our numerical calculations of the linear preheating phase to set the initial conditions and choose suitable lattice parameters. The key result of these simulations is shown in fig. 11.5. It turns out that the fluctuations can really push $\phi(\vec{x})$ to negative values at some points in space, and the potential subsequently drives $\phi(\vec{x}) \to -v$ in these regions. Afterwards, these regions form localized, roughly spherical bubbles oscillating between $\phi = \pm v$, which can be interpreted as oscillons [152].

As expected from the strongly peaked form of the linear power spectra in figs. 11.3 and 11.4, oscillon formation is dominated by fluctuations at the peak scale $k_{\rm peak}$, which leads to a typical distance between oscillons of about $d \sim 2\pi/k_{\rm peak}$ [6]. The power spectra during this phase remain peaked around $k_{\rm peak}$, though the spectra gradually get flatter. For details on the formation and subsequent evolution of the oscillons, see [6, 153].

[4] To be precise, $\mathcal{P}_\phi(k_{\rm peak})/\overline{\phi}^2$ temporarily drops when $\overline{\phi} > v$, but it grows both on its way up and down the hilltop for $\overline{\phi} < v$.

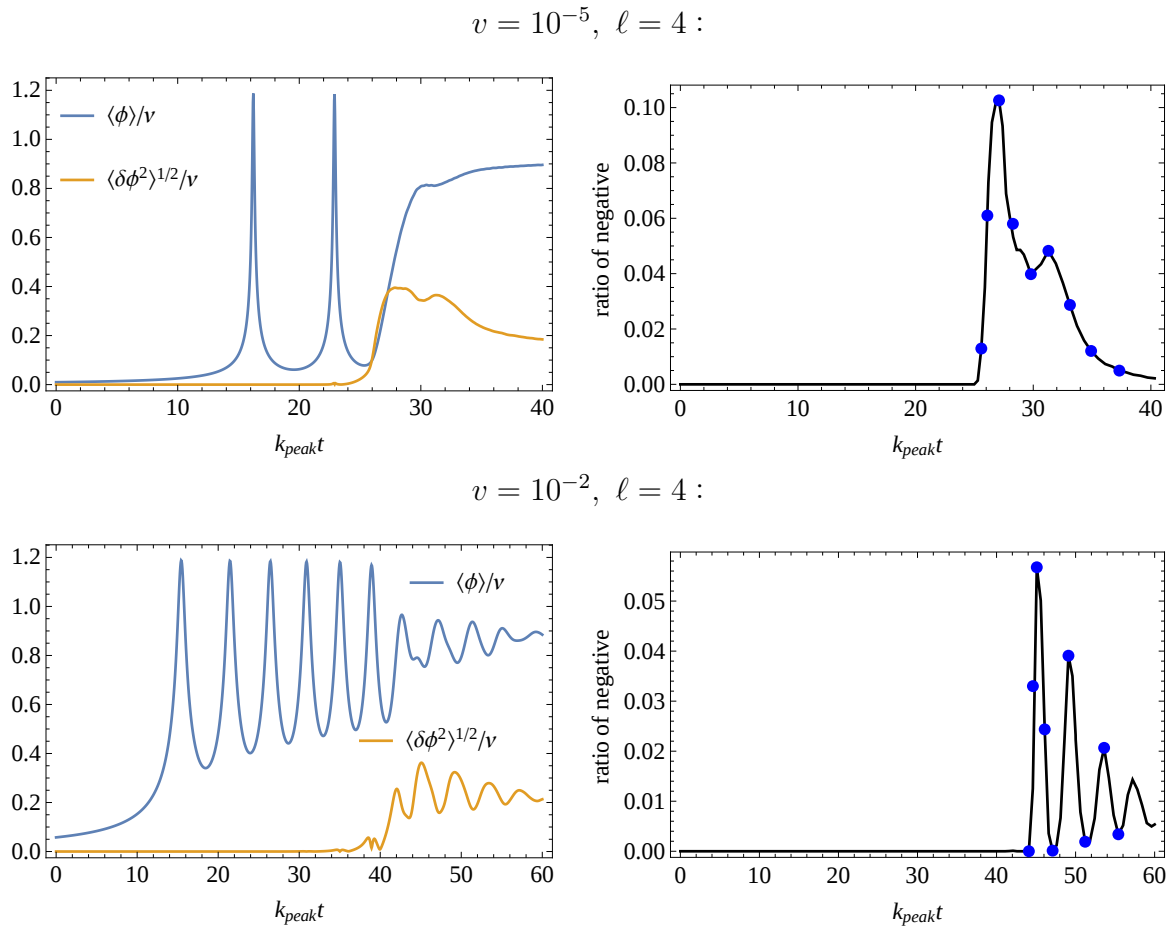

Figure 11.5: Numerical results by Stefano Orani [6] from (2+1)-dimensional lattice simulations as described in section 4.3 for single-field new inflation with $\ell = 4$ and $v = 10^{-5}$ (above) or $v = 10^{-2}$ (below).
The left plots show the variance and the mean of ϕ in units of v as functions of $k_{\text{peak}}t$. We can clearly see how the mean performs two or six oscillations, respectively, before the variance grows to values $\langle\delta\phi^2\rangle \sim \langle\phi - v\rangle^2$ and non-linearities become important, which agrees with our results from linear preheating in figs. 11.3 and 11.4.
The right plots show the fraction of lattice points for which $\phi(x) < 0$ as a function of $k_{\text{peak}}t$. These plots clearly show that the perturbations push the inflaton field over the hilltop towards the other vacuum at $\phi \to -v$. These hilltop-crossing regions form localized bubbles which oscillate between $\phi \sim -v$ and $\phi \sim v$. The behaviour of these "oscillons" has been studied further in [6, 153].

11.3 Parametric resonance of χ from inhomogeneous ϕ background

When a homogeneous inflaton field ϕ oscillates around the minimum of its potential, this generates a nearly periodic variation in the masses of the fields coupled to the inflaton, e.g. the χ field in our model. Such a time-dependent mass can lead to efficient non-perturbative production of χ particles. This effect is called "parametric resonance" [43, 44, 90, 154].

In our new inflation model, the situation is different. During the phase of tachyonic oscillations, the homogeneous mode of ϕ decays into perturbations peaked around the characteristic scale k_{peak} for $10^{-5} \lesssim v \lesssim 10^{-2}$. A priori, it is not clear whether parametric resonance for χ can also work after this has occurred: the usual mode eqs. (4.4) do not apply, because they assume a homogeneous background field $\phi(t)$, but the χ field gets a locally time-dependent mass term due to the time evolution of $\phi(\vec{x}, t)$ and could therefore be non-perturbatively amplified.[5]

In this section, we want to understand how χ might undergo a parametric resonance even for a strongly inhomogeneous inflaton field. We start with a semi-analytical analysis based on four simplifying assumptions:

1. We assume that $\delta\phi := (\phi - v) \ll v$. This assumption becomes valid briefly after the end of tachyonic oscillations, as Hubble damping reduces the amplitude of perturbations $\delta\phi$.[6]

2. We assume $\delta\chi \ll \delta\phi$. This assumption is valid initially, as $\delta\chi$ is not strongly amplified during the homogeneous oscillations of ϕ. It can be violated later if there is efficient $\delta\chi$ production due to preheating. In that case, our formalism breaks down at the time when $\delta\chi \sim \delta\phi$.

3. We approximate $\delta\phi(\vec{x}, t)$ as a standing wave with wavenumber $|\vec{k}| = k_{\text{peak}}$, motivated by the observation that the spectrum of ϕ is strongly peaked around k_{peak}.

4. We neglect the expansion of the universe because the timescales considered below are much shorter than $\mathcal{H}^{-1}$.

These assumptions are based on the main qualitative features of our system, and they allow us to derive simple equations that can be analysed using Floquet theory. We therefore believe that they provide a useful starting point for discussing how we can have a parametric resonance even with an inhomogeneous inflaton background field.

[5] In principle, χ can be amplified by a conventional parametric resonance before the tachyonic oscillations make ϕ inhomogeneous. In this chapter, we are interested in the range of parameters for which this conventional parametric resonance is not efficient, so that ϕ becomes inhomogeneous before χ is amplified to significant abundances.

[6] This assumption makes our analysis inapplicable during the earlier stage of preheating, when $\delta\phi \sim v$. To decide whether χ can grow non-perturbatively during this early phase, a non-linear calculation is required, e.g. lattice simulations as discussed in section 11.3.4.

11.3.1 Equations of motion

The equation of motion for $\chi(\vec{x},t)$ is

$$\ddot{\chi} - \vec{\nabla}^2\chi + 3\mathcal{H}\dot{\chi} + \frac{\partial V}{\partial \chi} = 0, \tag{11.8}$$

with V given by eq. (11.1).

As discussed above, we can neglect $\mathcal{H}$ for the purposes of this section. For small perturbations $\delta\chi$ and $\delta\phi = (\phi - v)$, we can also expand eq. (11.8) to leading order in $\delta\chi$ and $\delta\phi$:

$$\delta\ddot{\chi} - \vec{\nabla}^2\delta\chi + \left[\left.\frac{\partial^2 V}{\partial\chi^2}\right|_{\rm min} + \left.\frac{\partial^3 V}{\partial\chi^2\partial\phi}\right|_{\rm min}\delta\phi\right]\delta\chi = 0, \tag{11.9}$$

where the derivatives of V are evaluated at the global minimum $\phi = v$, $\chi = 0$:

$$\delta\ddot{\chi}(\vec{x},t) - \vec{\nabla}^2\delta\chi(\vec{x},t) + \left[\lambda^2 v^4 + 4\lambda^2 v^3\,\delta\phi(\vec{x},t)\right]\delta\chi(\vec{x},t) = 0. \tag{11.10}$$

We can Fourier transform this equation by multiplying with $e^{-i\vec{k}\vec{x}}$ and integrating over $d\vec{x}$:

$$\ddot{\chi}_{\vec{k}} + \left(k^2 + \lambda^2 v^4\right)\chi_{\vec{k}} + 4\lambda^2 v^3 \int d\vec{x}\; e^{-i\vec{k}\vec{x}}\delta\phi(\vec{x},t)\delta\chi(\vec{x},t) = 0, \tag{11.11}$$

where $\chi_{\vec{k}}(t)$ is the Fourier transform of $\delta\chi(\vec{x},t)$. To evaluate the last term, we approximate $\delta\phi$ as a standing wave with wavenumber $|\vec{k}_{\rm p}| = k_{\rm peak}$:

$$\delta\phi(\vec{x},t) = \delta\phi_0\,\cos\left(\vec{k}_{\rm p}\vec{x}\right)\cos\left(\omega_\phi t\right), \qquad \text{with } \omega_\phi = \sqrt{k_{\rm peak}^2 + m_\phi^2}. \tag{11.12}$$

Note that eq. (11.12) is a solution to the linearised equation of motion for $\delta\phi(\vec{x},t)$, so the approximation as a standing wave is consistent given our assumption that $\delta\phi \ll v$. Assuming this form of $\delta\phi$, eq. (11.11) can be simplified to

$$\ddot{\chi}_{\vec{k}} + \left(k^2 + \lambda^2 v^4\right)\chi_{\vec{k}} + 2\lambda^2 v^3\delta\phi_0\cos(\omega_\phi t)\left(\chi_{\vec{k}+\vec{k}_{\rm p}} + \chi_{\vec{k}-\vec{k}_{\rm p}}\right) = 0. \tag{11.13}$$

This is similar to the usual Mathieu equation for parametric resonance, with the important difference that the time-dependent term couples modes with different $\vec{k}$.[7] For each $\vec{k}$, eq. (11.13) actually describes a ladder of differential equations involving all $\chi_{\vec{k}+n\cdot\vec{k}_{\rm p}}$ for every integer number n.

We cannot solve these infinitely many equations simultaneously, so we have to apply a cutoff, setting $\chi_{\vec{k}} = 0$ for all $|\vec{k}| > k_{\rm cutoff}$ or equivalently for all $|n| > N$.[8]

[7] For another generalisation of the Mathieu equation with inhomogeneous background fields in the context of colliding domain walls, see [155].

[8] Applying a cutoff is consistent with our lattice results, where we see that the spectrum of χ is peaked at values $k \lesssim k_{\rm peak}$, so we do not expect Fourier modes χ_k with $k \gg k_{\rm peak}$ to be involved in preheating. We have also checked that if we solve eq. (11.13) numerically using such a cutoff, the eigenfunctions of eq. (11.13) are peaked around one or two neighbouring values of k and quickly fall off for larger k. In addition, we reproduced fig. 11.6 with lower resolution for $k_{\rm cutoff} = 6k_{\rm peak}$ and found that the result does not change significantly.

11.3.2 Equations of motion in matrix form

Imposing such a cutoff, eq. (11.13) can be written in matrix form. We use the short notation

$$\chi_{n} := \chi_{\vec{k}_n}, \qquad \vec{k}_n := \vec{k}_0 + n \cdot \vec{k}_{\mathrm{p}}, \tag{11.14}$$

for any arbitrary momentum vector $\vec{k}_0$, and

$$f(t) \;:=\; 2\lambda^2 v^3 \delta\phi_0 \cos(\omega_\phi t). \tag{11.15}$$

In this notation, eq. (11.13) becomes

$$\begin{pmatrix} \ddot{\chi}_N \\ \ddot{\chi}_{N-1} \\ ... \\ \ddot{\chi}_{-(N-1)} \\ \ddot{\chi}_{-N} \end{pmatrix} \;=\; \mathcal{F} \begin{pmatrix} \chi_N \\ \chi_{N-1} \\ ... \\ \chi_{-(N-1)} \\ \chi_{-N} \end{pmatrix}, \tag{11.16}$$

with the matrix

$$\mathcal{F}(t) = -\lambda^2 v^4 \mathbb{1} - \begin{pmatrix} k_N^2 & f(t) & 0 & 0 & ... & 0 \\ f(t) & k_{N-1}^2 & f(t) & 0 & ... & 0 \\ 0 & f(t) & k_{N-2}^2 & f(t) & ... & 0 \\ 0 & 0 & f(t) & k_{N-3}^2 & ... & 0 \\ ... & ... & ... & ... & ... & f(t) \\ 0 & 0 & 0 & 0 & f(t) & k_{-N}^2 \end{pmatrix}. \tag{11.17}$$

As a last step, we transform eq. (11.16) into a first order differential equation, introducing extra variables

$$\pi_n \;:=\; \dot{\chi}_n. \tag{11.18}$$

Then, for the vector

$$y(t) := (\chi_N, \chi_{N-1}, ..., \chi_{-N}, \pi_N, \pi_{N-1}, ..., \pi_{-N})^T, \tag{11.19}$$

eq. (11.16) can be written as

$$\dot{y}(t) \;=\; U(t) y(t), \tag{11.20}$$

with

$$U(t) \;=\; \begin{pmatrix} \mathbb{0} & \mathbb{1} \\ \mathcal{F}(t) & \mathbb{0} \end{pmatrix}, \tag{11.21}$$

where $\mathbb{1}$ and $\mathbb{0}$ are the unit matrix and the zero matrix with the same dimensions as $\mathcal{F}(t)$.

11.3.3 Floquet analysis

Eq. (11.20) is formally equivalent to equations of parametric resonance in a multi-field system, with different modes $\chi_{\vec{k}_0+n\cdot\vec{k}_\mathrm{p}}$ in place of different fields φ_n. We can thus perform a Floquet analysis analogously to multi-field parametric resonance [44].[9]

The Floquet theorem implies that we can find the growing solutions of eq. (11.20) using the differential equation for the square matrix $\mathcal{O}(t)$:

$$\dot{\mathcal{O}}(t) \;=\; U(t)\mathcal{O}(t), \tag{11.22}$$

with $U(t)$ from eq. (11.21).

The Floquet exponents can be determined using the following algorithm [44]:

1. Solve eq. (11.22) with the initial value $\mathcal{O}(0) = \mathbb{1}$ up to time $T = 2\pi/\omega_\phi$.
2. Find the eigenvalues σ of $\mathcal{O}(T)$.
3. The Floquet exponents are $\mu = \frac{1}{T}\log\sigma$. Exponential growth happens for $\mathrm{Re}(\mu) = \frac{1}{T}\log|\sigma| > 0$. Taking into account Hubble damping, effective growth is possible for $\mathrm{Re}(\mu) \gg \mathcal{H}$.

The eigenvalues σ describe how much the corresponding eigenstates grow during each oscillation of $\delta\phi$. Fig. 11.6 shows the numerical results for the eigenvalues and eigenstates assuming $v = 10^{-2}$, $\ell = 6$ and different m_χ/m_ϕ and $\delta\phi_0$. The left side of the plot shows the maximum Floquet exponent (for the fastest growing eigenfunction), and the right-hand side shows the average wavenumber $\langle k\rangle$ of the corresponding eigenfunction.

To generate the plots, we scanned over 41 different $\vec{k}_0$ with $|\vec{k}_0| \in [0, k_\mathrm{peak}/2]$ and $\vec{k}_0 \parallel \vec{k}_\mathrm{p}$.[10] As eq. (11.13) couples each $\vec{k}_0$ to all other $\vec{k}_0 + n\cdot\vec{k}_\mathrm{p}$, and because the equations are symmetrical under $\vec{k}_0 \to -\vec{k}_0$, this is equivalent to scanning over all $|\vec{k}_0| \le k_\mathrm{cutoff}$ for $\vec{k}_0 \parallel \vec{k}_\mathrm{p}$.

Discussion of the results

For each of the k_0, we find a series of thin resonance bands for specific m_χ/m_ϕ. Plotting all of these thin resonance bands in one plot (plotting the maximum eigenvalue), we find that they combine into very broad bands with strongest amplification close to $m_\chi/m_\phi \in \{0.5, 1, 1.5, 2\}$. These broad bands extend towards smaller m_χ/m_ϕ, with the exponentially growing modes for smaller m_χ/m_ϕ having increasingly larger k, and the growth getting weaker the further we go away from half-integer values of m_χ/m_ϕ. Also, the strongest amplification happens for $m_\chi/m_\phi \lesssim 0.5$. The band at $m_\chi/m_\phi \simeq 1$ already has much

[9] Fundamentally, Floquet theory can be applied because the explicit time-dependence in $U(t)$ is periodic.

[10] We have also performed the Floquet analysis with angles of 30° and 90° between $\vec{k}_0$ and $\vec{k}_\mathrm{p}$, with $|\vec{k}_0| \le 1.5k_\mathrm{peak}$. Such non-parallel $\vec{k}_0$ lead to a very similar band structure, just with slightly broader bands.

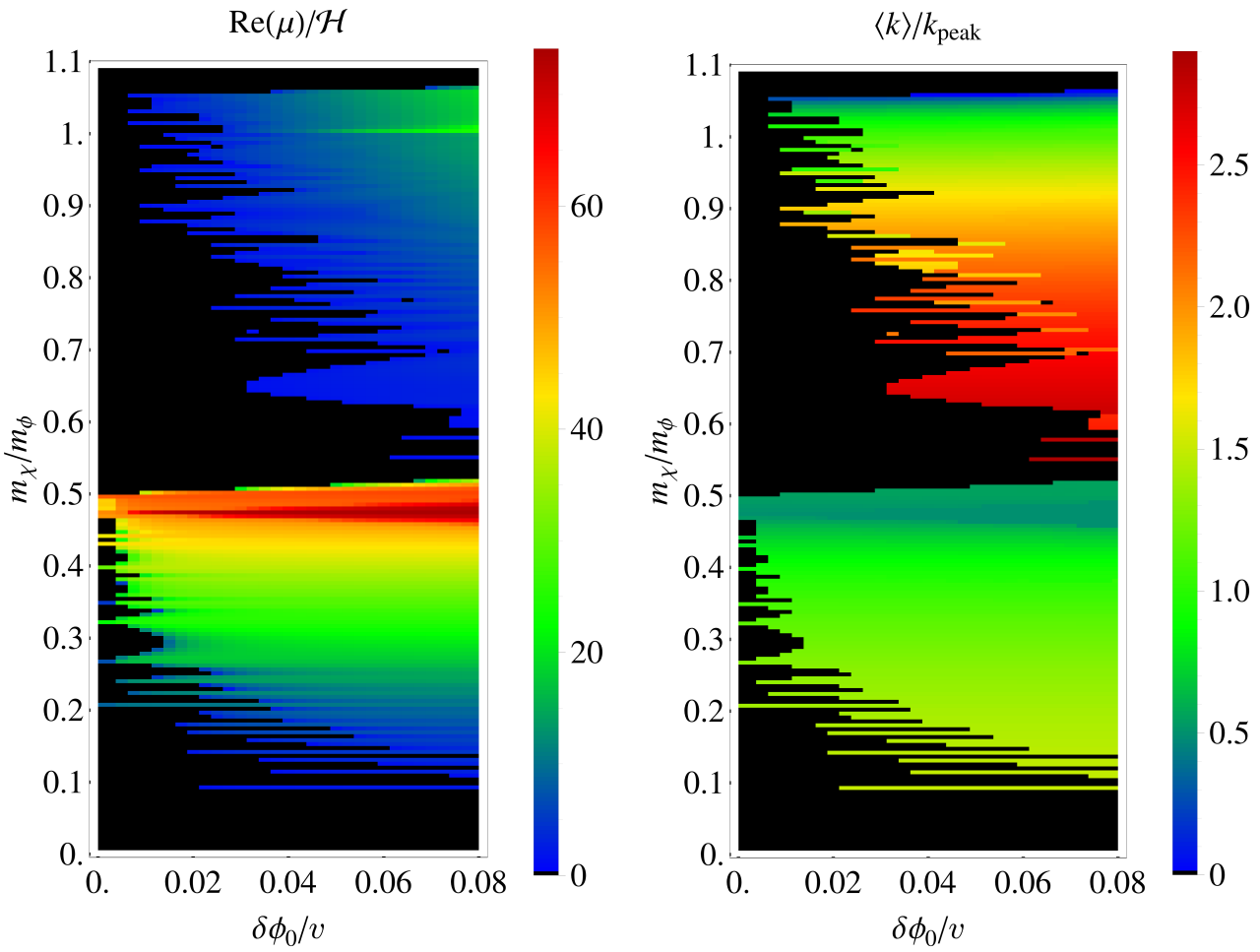

Figure 11.6: Results of Floquet analysis for $v = 10^{-2}$ and $\ell = 6$, using a cutoff $k_{\text{cutoff}} = 3.5k_{\text{peak}}$. The left plot shows the largest Floquet exponent for a given mass ratio m_χ/m_ϕ and inflaton perturbation amplitude $\delta\phi_0$, indicating how strongly the fastest-growing χ perturbations are growing. Black regions indicate no growth (only oscillatory solutions), while in the coloured regions χ perturbations grow exponentially. The right plot shows the average wavenumber $\langle k\rangle$ of the fastest-growing linear combination of χ_k. The eigenvector generally includes noticeable contributions from up to three neighbouring wavenumbers separated by $\Delta k = k_{\text{peak}}$, but the contributions to the eigenvector quickly fall off with larger k, justifying the use of a cutoff for solving the coupled eqs. (11.13). Further faint bands can be found at $m_\chi/m_\phi \simeq 3/2$ and $m_\chi/m_\phi \simeq 2$, but the Floquet exponents are much smaller for those bands.
The presence of thin resonance bands is an artefact of our finite resolution in k-space, as we have only scanned over 41 different k_0, and the value of k_0 determines the position of the individual resonance bands. Including more k_0, the individual resonance bands combine into continuous broad bands.

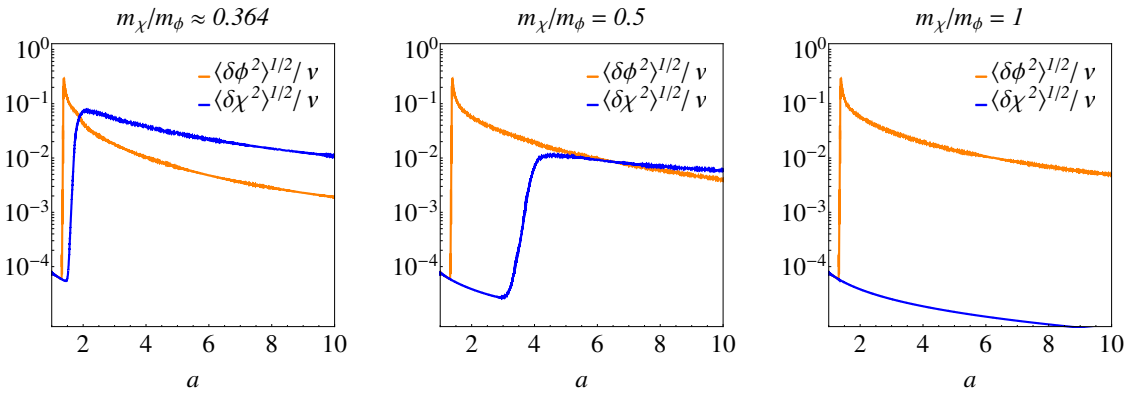

Figure 11.7: Lattice results for the variances of ϕ and χ by Francesco Cefalà [150] for $v = 10^{-2}$, $\ell = 6$ and different mass ratios m_χ/m_ϕ. They confirm that χ grows exponentially in the mass range $0.25 \lesssim m_\chi/m_\phi \lesssim 0.5$ where the inhomogeneous Floquet analysis predicts the strongest resonance band, see fig. 11.6. The growth starts after ϕ perturbations have become non-linear, and as such it is not a usual parametric resonance driven by a homogeneous background field.

smaller Floquet exponents, and the bands at $m_\chi/m_\phi \simeq 1.5$ and $m_\chi/m_\phi \simeq 2$ only exhibit extremely weak amplification.

Note that our plane-wave approximation for $\delta\phi$ requires $V(\delta\phi) \simeq \frac{1}{2}m_\phi^2\delta\phi^2$. For this reason, the results of our Floquet analysis will be most trustworthy for small $\delta\phi_0$, i.e. on the left side of the plots in fig. 11.6. The lower band at $m_\chi/m_\phi \lesssim 0.5$ extends to small $\delta\phi_0$, with $\mathrm{Re}(\mu)/\mathcal{H} > 20$ even for $\delta\phi_0/v < 0.01$ where the potential is very close to harmonic. However, the band at $m_\chi/m_\phi \simeq 1$ becomes very faint already for $\delta\phi_0/v \sim 0.05$ where our actual potential (10.3) for $\delta\phi$ is still significantly skewed. For this reason, it is not clear whether the conditions for our Floquet analysis are satisfied sufficiently well for this upper band given the anharmonic hilltop potential of eq. (10.3).

Our Floquet analysis demonstrates that, in principle, exponential growth of χ due to parametric resonance might happen even for a strongly inhomogeneous background field ϕ with a sharp peak around some k_{peak}, and that such growth sensitively depends on the coupling λ or equivalently the mass ratio m_χ/m_ϕ. However, since our analysis is based on a harmonic approximation of the inflaton potential and on simpler initial conditions for ϕ compared to the hilltop model of eq. (10.3), we need to resort to lattice simulations to assess whether or not this mechanism is effective in our hilltop model.

11.3.4 Comparison to results from lattice simulations

To check the results of the semi-analytical Floquet analysis of section 11.3.3, we compare them to lattice simulations of preheating in our model which were performed by Francesco Cefalà in [150]. The lattice results for the variances of ϕ and χ for three different values of m_χ/m_ϕ are shown in fig. 11.7. As the first two plots show, $\delta\chi$ indeed grows exponentially in the mass range for which our inhomogeneous Floquet analysis predicts the strongest

resonance band, and this growth starts well after the homogeneous mode of ϕ has decayed into sub-Hubble perturbations. As such, the results of [150] confirm our prediction of a parametric resonance of χ due to an inhomogeneous ϕ background. In fact, a scan over lattice simulations for different m_χ/m_ϕ shows that resonant growth occurs in a band with $0.25 \lesssim m_\chi/m_\phi \lesssim 0.5$ [150], which fits very well to the mass range of the strong resonance band predicted by our Floquet analysis.

At larger mass ratios $m_\chi/m_\phi > 0.5$, the lattice simulations show no noticeable growth of $\delta\chi$. As we already mentioned in section 11.3.3, the resonances at those mass ratios only show up in the Floquet analysis for large inflaton amplitudes $\delta\phi_0/v \gtrsim 0.05$ where the approximations leading to eq. (11.13) are not satisfied as well. We conclude that the faint resonance bands at larger mass ratios are an artefact of our approximations and are absent in the full non-linear model.

11.3.5 Possible effect of initial $\langle\chi\rangle$

Throughout this chapter, we have assumed that $\langle\chi\rangle = 0$ at the end of inflation. However, $\langle\chi\rangle$ can also be non-negligible throughout new inflation, especially if no mass term for χ is generated from Kähler potential couplings. In that case, the energy in the initial $\langle\chi\rangle$ can provide additional χ particles on top of those produced from $\delta\phi$ by preheating, and the results of this chapter might be interpreted as a lower bound on the abundance of χ particles after preheating.

A calculation of the possible initial values of $\langle\chi\rangle$ is given in appendix D.2 for $\ell = 6$, $v = 10^{-2}$ and $\alpha = \beta = 0$, where we find that the maximal $\langle\chi\rangle$ at the beginning of preheating depends on the mass ratio m_χ/m_ϕ, see fig. D.4. For $m_\chi/m_\phi \gtrsim 0.5$, the maximal initial $\langle\chi\rangle$ is so small that the results of this chapter remain unchanged. For small m_χ/m_ϕ, the initial $\langle\chi\rangle$ can extend the range of parameters for which $\delta\chi$ can be large after preheating towards smaller $m_\chi/m_\phi < 0.25$.

11.4 Summary

In this chapter, we have studied preheating after new inflation, first focusing on the perturbations of the inflaton field ϕ itself and then on the perturbations of another scalar field χ coupled to it with a tribrid superpotential coupling.

For the inflaton perturbations, we reviewed the phases of tachyonic preheating and tachyonic oscillations and numerically calculated the spectra during the linear preheating stage for various values of the inflaton field's vacuum expectation value v. We confirmed that for $v \geq 10^{-1}$, preheating is ineffective due to Hubble damping, whereas for $10^{-5} \leq v \leq 10^{-2}$, the perturbations of ϕ quickly grow around a characteristic peak scale $k_{\text{peak}} \gg a\mathcal{H}$. We explained how in this case, the large perturbations at sub-Hubble scales might indicate that the inflaton field could be locally pushed over the maximum of the potential from $\phi > 0$ to $\phi < 0$.

Since the perturbations are already non-linear at that point, the study of this phase requires numerical lattice simulations, which were performed by Stefano Orani [6] based on the parameters given by my numerical calculations for the linear preheating phase. Those lattice simulations show that ϕ indeed crosses the maximum of its potential, forming localized bubbles oscillating between $\phi = \pm v$. The spectrum during this phase remains peaked around k_{peak}, though the peak gets flatter during this stage as one expects for non-linear evolution.

In the second part of this chapter, we considered preheating with an additional scalar field χ, assuming the coupling to the inflaton field that would result from realizing new inflation with a tribrid superpotential as in chapter 10.

In particular, we focused on the case $10^{-5} \lesssim v \lesssim 10^{-2}$ for which the inflaton field rapidly becomes inhomogeneous with a power spectrum sharply peaked around k_{peak}. In this case, we argued that a parametric resonance for χ might be driven by the inhomogeneous inflaton field, in contrast to the usual parametric resonance driven by a homogeneous inflaton background. To illustrate this idea, we performed a generalized Floquet analysis for inhomogeneous backgrounds with $\ell = 6$ and $v = 10^{-2}$ for which we found a broad resonance band at $m_\chi/m_\phi \lesssim 0.5$. We also saw some weaker indications for faint resonance bands at other half-integer values of m_χ/m_ϕ, though only in regions where the assumptions underlying the Floquet analysis are less well satisfied.

This semi-analytical analysis was complemented with lattice simulations by Francesco Cefalà [150] based on parameters and initial conditions from my linear preheating calculations. They confirmed the existence of the resonance band at $0.25 \lesssim m_\chi/m_\phi \lesssim 0.5$ for which the χ fluctuations can be amplified to amplitudes even exceeding those of the inflaton field. This resonant growth of χ occurs when ϕ is already strongly inhomogeneous; the precise time at which the amplification starts depends on m_χ/m_ϕ. The simulations did not show any amplification around $m_\chi/m_\phi \sim 1$, clarifying that the faint resonance which is visible in the Floquet analysis at this mass ratio is not realized in the full non-linear model.

These results have important implications for the calculation of reheating observables. The oscillons produced after the tachyonic oscillation stage could have a significant effect especially if they are very long-lived. This can depend on the specific particle physics model embedding; for example, a tribrid coupling of the inflaton to another field can either reduce or extend the oscillons' lifetime depending on the model parameters [153].

The production of χ perturbations from an inhomogeneous inflaton background has even more important consequences, as it directly affects the relative particle abundances at the beginning of reheating. Therefore, a study of reheating which assumes that the energy density is dominated by the inflaton field at the beginning of reheating will generally not lead to correct results unless χ has a much greater decay rate than ϕ such that any χ generated from preheating will decay early enough to be negligible.

Part V

Implications of large r for small-field inflation

Chapter 12

Implications of large r for slow-roll model building

In chapters 6–11, we studied small-field models of inflation within an effective field theory framework. The assumption of small field values allowed us to expand the scalar potential in powers of $Y_i/m_{\rm Pl}$ and to keep only the leading terms in this expansion, such that the predictions depend on a limited number of relevant coupling constants.

Small field values $Y_i \ll m_{\rm Pl}$ are required for getting predictive models from specifying all fields' charges under $U(1)_R$ and $\mathbb{Z}_n$ symmetries. Since $|Y_i|^2$ is always invariant under such symmetries, the Kähler potential K can be an arbitrary function of the $|Y_i|^2$. For $Y_i \gtrsim \mathcal{O}(m_{\rm Pl})$, this leads to scalar potentials which are mostly determined by arbitrary choices for K. Small field values are therefore a critical prerequisite for the framework used throughout this thesis.

A well-known property of small-field models of inflation is that they generically predict tiny amplitudes of primordial gravity waves [156, 157]. When BICEP2 detected an indication for large gravity waves with $r \sim 0.2$ [158], this triggered lively discussions on whether such large r would rule out the entire framework of small-field inflation or whether small-field models could remain viable with suitable adjustments.

Though it has turned out that the original BICEP2 measurement was dominated by foregrounds, a discovery of large r within the present bounds of $r < 0.09$ remains possible [51]. In this chapter, we discuss how such a discovery could constrain or exclude small-field models of inflation like those discussed in chapters 6–11.

We start with a review of the famous Lyth bound relating the inflaton field excursion $\Delta\phi$ to the tensor-to-scalar ratio r, and revisit proposals for avoiding the Lyth bound using suitable inflaton potentials. We then discuss how to reconstruct the inflaton potential from the primordial power spectra to highlight the importance of higher-order runnings of the spectral index for evading the Lyth bound. Finally, we derive a model-independent field range bound for slow-roll models of inflation to clarify whether or not a large r could rule out the small-field framework employed throughout this thesis.

12.1 Lyth bound

The Lyth bound [156] provides a popular estimate for the length of the inflaton trajectory

$$\Delta\phi \equiv |\phi_* - \phi_\mathrm{e}| \tag{12.1}$$

depending on the tensor-to-scalar ratio r. In this section, we review the derivation of the Lyth bound and proposals for how it might be evaded in specific models.

12.1.1 Derivation of the Lyth bound

The Lyth bound is based on the slow-roll eqs. (2.20) and (3.24b) together with the assumption that ε remains constant or grows during inflation:

$$\varepsilon(\phi) \gtrsim \varepsilon_*. \tag{12.2}$$

Eq. (12.2) corresponds to the typical shape of inflaton potentials, where slow-roll inflation happens around a flat region of the potential with $\varepsilon_* \ll 1$ and ends when the potential becomes too steep for slow-roll.

Eq. (12.2) can be combined with the slow-roll eqs. (2.18a), (2.20) and (3.24b):

$$N_* \simeq \int_{\phi_\mathrm{e}}^{\phi_*} \mathrm{d}\phi \, \frac{1}{\sqrt{2\varepsilon(\phi)}} \lesssim \frac{|\phi_* - \phi_\mathrm{e}|}{\sqrt{2\varepsilon_*}} \simeq \frac{\Delta\phi}{\sqrt{r/8}}, \tag{12.3}$$

where we assumed $\phi_* > \phi_\mathrm{e}$ without loss of generality. Solving eq. (12.3) for $\Delta\phi$ leads to the Lyth bound:

$$\Delta\phi \gtrsim N_* \sqrt{\frac{r}{8}} \simeq \left(\frac{N_*}{60}\right) \sqrt{\frac{r}{0.002}}. \tag{12.4}$$

According to the Lyth bound, tensor-to-scalar ratios $r \gtrsim 10^{-3}$ imply $\Delta\phi \gtrsim m_\mathrm{Pl}$.

The Lyth bound can be weakened if we assume that only the first $\Delta N = 8$ e-folds for which we observe a roughly scale-invariant spectrum happen due to slow-roll inflation. However, even in this case $\Delta\phi$ is estimated to be close to or above the Planck scale for $r > 10^{-2}$.

12.1.2 Evading the Lyth bound with non-monotonous $\varepsilon(\phi)$

Though the assumption of a roughly monotonous $\varepsilon(\phi) \geq \varepsilon_*$ is realized in many explicit models, it is not required for slow-roll inflation. It has thus been suggested that the Lyth bound can be evaded by using an inflaton potential for which $\varepsilon(\phi) < \varepsilon_*$ for some ϕ during inflation [159–161].

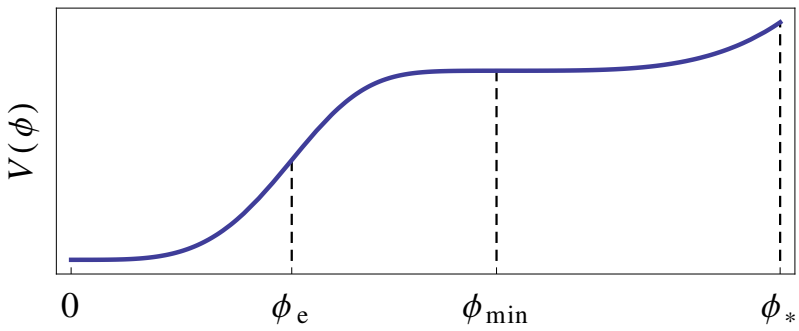

Figure 12.1: Schematic shape of the inflaton potential required to evade the Lyth bound. A large $r = 16\varepsilon_*$ is generated around ϕ_*. The potential then becomes flat very quickly so that $\varepsilon \ll \varepsilon_*$, and the N_* e-folds of inflation are generated mostly around the flattest part of the inflaton potential.

To understand how a non-monotonous ε helps to evade the Lyth bound, we rewrite eqs. (2.20) and (3.24b) as

$$r = 8\left[\frac{V'(\phi_*)}{V(\phi_*)}\right]^2, \qquad \Delta\phi = \int \mathrm{dN}\left|\frac{V'}{V}\right|. \tag{12.5}$$

For large r, these equations impose conflicting requirements on small-field models:

- The initial slope V'/V at ϕ_* must be large to generate large $r \simeq 8(V'_*/V_*)^2$.
- During inflation, the slope V'/V must be small to have $\Delta\phi \ll m_{\rm Pl}$ within N_* e-folds of inflation.

To get large r in a small-field model, we must decouple these requirements by satisfying them at different field values ϕ: $V(\phi)$ must start with a large slope $V'_*/V_* \sim \sqrt{r/8}$, but quickly become flat ($V'/V \ll \sqrt{r/8}$). Since $\varepsilon = (V'/V)^2/2$, this is equivalent to demanding a non-monotonous $\varepsilon(\phi) \ll \varepsilon_*$.

The qualitative shape of such a potential is depicted in fig. 12.1. The large r is generated around ϕ_* where ε is large, and the N_* e-folds of inflation are generated in the flat region around $\phi_{\rm min}$. Afterwards, inflation ends at $\phi_{\rm e} \leq \phi_{\rm min}$ either due to a waterfall transition or because the potential becomes too steep for slow-roll.

Such potentials have been discussed, using the constraints available at that time, in a number of insightful earlier papers [159, 160]. They find that a large tensor-to-scalar ratio $r > 0.01$ with $\Delta\phi \lesssim m_{\rm Pl}$ requires a scale-dependent running of the spectral index, and they generally do not find that $\Delta\phi \ll m_{\rm Pl}$ is possible: their field values lie in the range $m_{\rm Pl}/2 \lesssim \Delta\phi \lesssim m_{\rm Pl}$, which is already too large to reliably use expansions in powers of $\phi/m_{\rm Pl}$. However, their analysis is limited to specific potentials, so they cannot exclude small-field inflation with $r > 0.01$ in general.

The goal of this chapter is to understand how much the Lyth bound can be evaded for arbitrary inflaton potentials and what the conditions on the runnings of the spectral index are. For this purpose, we first perform a reconstruction of the inflaton potential in terms of the CMB observables in section 12.2 and then derive a very general field range bound for slow-roll inflation in section 12.3.

12.2 Inflaton potential reconstruction

As a first step towards understanding the relation between $\Delta\phi$, r and the runnings of the spectral index, we consider a reconstruction of the inflaton potential around ϕ_* from the constraints on the primordial spectrum [162]. This reconstruction will lead to estimates for how much the Lyth bound can be evaded depending on α_s, κ_s and higher order runnings.

12.2.1 Inflaton potential reconstruction from primordial power spectrum

We start with a Taylor expansion of $V(\phi)$ around ϕ_*:

$$V(\phi) = V(\phi_*) + V'(\phi_*)\delta\phi + \frac{1}{2}V''(\phi_*)\delta\phi^2 + \frac{1}{6}V'''(\phi_*)\delta\phi^3 + \frac{1}{24}V''''(\phi_*)\delta\phi^4 + ..., \tag{12.6}$$

with $\delta\phi \equiv (\phi - \phi_*)$. Without loss of generality, we can assume that $V'(\phi) > 0$.[1] We can then rewrite eq. (12.6) in terms of the slow-roll parameters using eqs. (2.18a)–(2.18d):

$$\frac{V(\phi)}{V_*} = 1 + \sqrt{2\varepsilon_*}\,\delta\phi + \frac{\eta_*}{2}\delta\phi^2 + \frac{\xi_*^2}{6\sqrt{2\varepsilon_*}}\delta\phi^3 + \frac{\sigma_*^3}{48\varepsilon_*}\delta\phi^4 + ... \tag{12.7}$$

At leading order in the slow-roll approximation, the slow-roll parameters at ϕ_* are related to the observables via eqs. (3.24b)–(3.24e). We can thus express eq. (12.7) in terms of the observables:

$$\begin{aligned}\frac{V}{V_*} = 1 + \sqrt{\frac{r}{8}}\,\delta\phi + \frac{1}{4}\left(n_\mathrm{s} - 1 + \frac{3r}{8} + q_1\alpha_\mathrm{s} + (q_1^2 - q_2)\kappa_\mathrm{s}\right)\delta\phi^2 \\ - \left(\frac{\alpha_\mathrm{s} + q_1\kappa_\mathrm{s}}{3\sqrt{2}r}\right)\delta\phi^3 + \frac{\kappa_\mathrm{s}}{6r}\,\delta\phi^4 + ...\end{aligned} \tag{12.8}$$

Terms of $\mathcal{O}(\delta\phi^5)$ are proportional to even higher order slow-roll parameters, or equivalently higher order runnings [69, 70]. For now, we assume that all runnings beyond α_s and κ_s are zero so that the potential is described by the 4th order polynomial given in eq. (12.8). We comment on the effects of higher-order runnings later in section 12.2.3.

[1] We can always redefine the inflaton field as $\tilde{\phi} = -\phi$ so that the assumption is satisfied for the field $\tilde{\phi}$, which we then relabel as ϕ. With the opposite assumption $V'(\phi) < 0$, the calculation is identical except for $V'/V = -\sqrt{2\varepsilon}$ which changes the sign in front of the odd powers in eqs. (12.7) and (12.8).

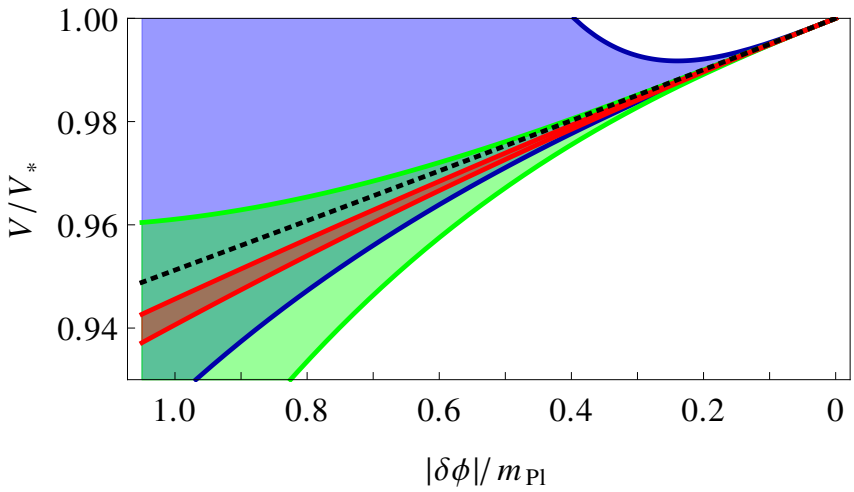

Figure 12.2: Reconstructed inflaton potential for $r = 0.02$ in various cosmological models: ΛCDM+r (red), ΛCDM+r+α_s (green) and ΛCDM+r+α_s+κ_s (blue). The width of the bands corresponds to twice the range of the 68% CL Planck constraints [9].
The dashed black line marks $\varepsilon = \varepsilon_*$ for which the Lyth bound is exact. To evade the Lyth bound, the potential must be much flatter than this line. We find that a significant flattening for $|\delta\phi| \ll m_{\rm Pl}$ is only possible if we allow for both α_s and κ_s, in which case a flat plateau can be reached at $|\delta\phi| \gtrsim m_{\rm Pl}/4$.

12.2.2 Required running for evading the Lyth bound

The reconstructed potential from eq. (12.8) is shown in fig. 12.2 for the example case of $r = 0.02$ and various cosmological models: ΛCDM is shown in red, ΛCDM+α_s is shown in green, and ΛCDM+α_s+κ_s is shown in blue. The width of the bands corresponds to twice the width of the 68% CL Planck constraints [9] quoted in table B.1.[2]

The black dashed line corresponds to $\varepsilon(\phi) = \varepsilon_*$ for which the Lyth bound eq. (12.4) becomes exact. Evading the Lyth bound requires that the potential becomes much flatter than this black dashed line.

We see that for $\kappa_s = 0$, the potential shape of fig. 12.1 required to evade the Lyth bound is excluded by the constraints on the observables. In fact, the ΛCDM curve with $\alpha_s = \kappa_s = 0$ is always steeper than $\varepsilon = \varepsilon_*$, so that the field range bound in this case is even stronger than the conventional Lyth bound. This result is consistent with the calculations in [163, 164] which have shown that accounting for a constant spectral index $n_s < 1$ significantly tightens the Lyth bound.

Adding a running α_s but keeping $\kappa_s = 0$, the Lyth bound is only slightly relaxed. The main reason is that relaxing the Lyth bound requires a positive $\alpha_s > 0$ which is very constrained for ΛCDM+α_s, as $\alpha_s = -0.006 \pm 0.007$ at 68% CL if $\kappa_s = 0$.

Only when we allow for a running of the running κ_s, a flat plateau can be generated for $\delta\phi \ll m_{\rm Pl}$, so that the Lyth bound might be weakened. This has two reasons: a positive

[2]The applicability of these bounds for $r = 0.02$ is discussed in appendix B.

κ_s makes $V(\phi)$ flatter, and it relaxes the bounds on $\alpha_\mathrm{s} > 0$ which also contributes to a flatter potential.

These results also hold up for other values of $r \gtrsim 10^{-2}$. The main difference is that for larger r, all of the curves in fig. 12.2 become steeper and the plateau for the ΛCDM+α_s+κ_s case is shifted towards larger $|\delta\phi|$.

12.2.3 Effects of higher-order runnings

Our reconstruction of the inflaton potential in eq. (12.8) is based on the assumption that higher-order runnings beyond κ_s, i.e. all $\left[(d/d\ln k)^n \mathcal{P}_\zeta(k)\right]_{k=k_*}$ with $n > 3$, are negligible. As such higher-order runnings are proportional to the $(n+1)$-th derivatives of the inflaton potential $V(\phi)$, this assumption ensures that the inflaton potential can be approximated by a fourth-order polynomial in $\delta\phi$. If one allows for higher-order runnings beyond κ_s, higher-order terms $\delta\phi^{n+1}$ with $n > 3$ need to be taken into account.[3]

As we discussed in section 12.1.2, to evade the Lyth bound it is necessary that V' changes rapidly from its large value at horizon crossing to a small value at ϕ_min. This change must be driven by higher-order derivatives of the potential, be it the third and fourth only as in (12.8) or higher-order derivatives also. Including higher than fourth-order terms and choosing their value at horizon crossing to minimize $\Delta\phi$ would presumably lead to weaker constraints on $\Delta\phi$ than those indicated by the analysis in section 12.2.2. However, as we will show in section 12.3, the Lyth bound cannot be evaded to an arbitrary degree even if we allow for any number of higher-order runnings.

Note that if the higher-order runnings of the spectral index are not negligible, one cannot rely on cosmological parameter constraints that were derived under the assumption that these runnings are zero (see appendix B). In the same way in which the upper bound on α_s is relaxed when allowing for $\kappa_\mathrm{s} \neq 0$, adding large higher-order runnings will likely change the bounds on α_s and κ_s. Higher-order terms also give additional contributions to eqs. (3.24c)–(3.24e), which change the prefactors of the $\delta\phi^2$, $\delta\phi^3$ and $\delta\phi^4$ terms in eq. (12.8) by terms proportional to the additional higher-order runnings.

It may therefore be possible to evade the Lyth bound even for small κ_s, but with large higher-order running parameters. In any case, it requires sizeable running of the spectral index beyond α_s, e.g. $\kappa_\mathrm{s} > 0$ or some higher-order running.

12.3 General field range bound in slow-roll inflation

In sections 12.1.2 and 12.2, we have discussed how the Lyth bound can be weakened by assuming a non-monotonous evolution of $\varepsilon(\phi)$ during inflation. We have explained how such a non-monotonous ε can be achieved with potentials that have the qualitative form shown

[3] These arguments are only exact to leading order in the slow-roll parameters or equivalently in r, $(n_\mathrm{s}-1)$, α_s and κ_s. At higher order in the slow-roll expansion, higher order runnings are induced not only by slow-roll parameters involving higher derivatives, but also by higher powers of the first few slow-roll parameters.

in fig. 12.1, and we have shown that such potentials can be consistent with observations if we allow for a scale-dependent running of the spectral index (e.g. $\kappa_\mathrm{s} > 0$).

While the potential shape is constrained by cosmological observations, these constraints depend on the arbitrary choice of priors for the primordial spectrum $\mathcal{P}_\zeta(k)$, and they can be relaxed if we allow for runnings α_s, κ_s or even an arbitrary number of higher-order runnings.

In this section, we derive a slow-roll bound on $\Delta\phi$ that applies generally assuming only the slow-roll eqs. (2.16) and (3.24b), to show that the Lyth bound cannot be evaded arbitrarily strongly and that a large $r \sim 0.1$ could indeed rule out the small-field slow-roll framework employed in this thesis.

12.3.1 Field range bound for single-field slow-roll inflation

To evade the Lyth bound, we need a potential that is very steep at ϕ_* and quickly becomes flat. However, in slow-roll inflation, $V'(\phi)/V(\phi)$ cannot vary arbitrarily quickly. This follows from the definition of the slow-roll parameters in eqs. (2.18a)–(2.18b):

$$\frac{\mathrm{d}}{\mathrm{d}\phi}\frac{V'}{V} = \frac{V''}{V} - \left(\frac{V'}{V}\right)^2 = \eta - 2\varepsilon. \tag{12.9}$$

During slow-roll, one has $\varepsilon \ll 1$ and $\eta \ll 1$. Therefore, eq. (12.9) tells us that V'/V can only change slowly during slow-roll inflation. We will show that this constraint makes it impossible to have slow-roll inflation with large $r \sim 0.1$ and $\Delta\phi \ll m_\mathrm{Pl}$, independently of the form of the potential.

As in fig. 12.1, we define ϕ_* as the field value at horizon crossing, ϕ_e as the field value at the end of inflation, and ϕ_min as the field value where ε has its minimum in the interval between ϕ_* and ϕ_e. We can assume that $\phi_\mathrm{e} \leq \phi_\mathrm{min} \leq \phi_*$.[4] According to the slow-roll eq. (2.16), this implies $V'(\phi) > 0$ along the entire inflaton trajectory.

Integrating eq. (12.9) over ϕ from ϕ_min to ϕ_*, we find

$$\left(\frac{V'}{V}\right)_* - \left(\frac{V'}{V}\right)_\mathrm{min} = \int_{\phi_\mathrm{min}}^{\phi_*} \mathrm{d}\phi \, \frac{\mathrm{d}}{\mathrm{d}\phi}\frac{V'}{V} = \int_{\phi_\mathrm{min}}^{\phi_*} \mathrm{d}\phi \, (\eta - 2\varepsilon) = (\phi_* - \phi_\mathrm{min}) \, \langle \eta - 2\varepsilon \rangle, \tag{12.10}$$

where $\langle \eta - 2\varepsilon \rangle$ is the mean of $(\eta - 2\varepsilon)$ between ϕ_min and ϕ_*.

As a next step, we find expressions for $(V'/V)_*$ and $(V'/V)_\mathrm{min}$ from eq. (12.5). For $(V'/V)_*$, we get

$$\left(\frac{V'}{V}\right)_* = \sqrt{\frac{r}{8}}. \tag{12.11}$$

[4] If this is not the case for some inflaton field $\tilde{\phi}$, we can always perform a field redefinition $\tilde{\phi} = -\phi$, so that our assumption is correct for the field ϕ.

We can also derive a bound on $(V'/V)_{\min}$ from eq. (12.5):

$$\Delta\phi \;=\; \int_0^{N_*} \mathrm{dN} \left|\frac{V'}{V}\right| \;>\; N_* \left(\frac{V'}{V}\right)_{\min}, \tag{12.12}$$

where N_* is the number of e-folds between ϕ_* and ϕ_e.

Plugging eqs. (12.11) and (12.12) into eq. (12.10), we get

$$(\phi_* - \phi_{\min}) \langle \eta - 2\varepsilon \rangle \;>\; \sqrt{\frac{r}{8}} - \frac{\Delta\phi}{N_*}. \tag{12.13}$$

With $\phi_\mathrm{e} \leq \phi_{\min}$, we also have

$$\Delta\phi \;\geq\; \phi_* - \phi_{\min}, \tag{12.14}$$

so that eq. (12.13) also holds for $\Delta\phi$ instead of $(\phi_* - \phi_{\min})$:

$$\Delta\phi \langle \eta - 2\varepsilon \rangle \;>\; \sqrt{\frac{r}{8}} - \frac{\Delta\phi}{N_*}. \tag{12.15}$$

Solving this for $\Delta\phi$, we arrive at a general slow-roll bound for $\Delta\phi$:

$$\Delta\phi \;>\; \frac{0.11}{\langle \eta - 2\varepsilon \rangle + \frac{1}{N_*}} \sqrt{\frac{r}{0.09}}. \tag{12.16}$$

Eq. (12.16) clearly shows that generating $r \sim 0.09$ from single-field slow-roll inflation requires inflaton field excursions close to or above the Planck scale (recall that both ε and η must be small during slow-roll inflation). The derivation only relies on the slow-roll eqs. (2.20) and (3.24b), so this field range bound cannot be circumvented by any particular choice for the inflaton potential, even if the evolution of ε is not monotonous.

Note on canonical normalization

Our result applies to the canonically normalized inflaton field ϕ. When talking about large- and small-field models, it is useful to use the canonically normalized inflaton field, as this makes the categorization independent of arbitrary field redefinitions. Otherwise, every model could be interpreted as a "small-field" model by e.g. replacing the inflaton field ϕ with a rescaled inflaton field $\tilde{\phi} = \phi/\alpha$ with $\alpha \gg \Delta\phi$. For models with non-canonical kinetic terms, eq. (12.16) is applicable only after the inflaton field has been redefined to have canonical kinetic terms.

Note on multi-stage inflation

The assumption of slow-roll inflation is usually motivated by the observation of a nearly scale-invariant spectrum on CMB scales. In principle, one can require slow-roll inflation only throughout the $\Delta N \sim 8$ e-folds of inflation for which the primordial spectrum has been probed by CMB observations.[5] In this case, N_* must be replaced by ΔN in eq. (12.16),

[5]The remaining $(N_* - \Delta N)$ e-folds must be generated by another mechanism, e.g. a second phase of slow-roll inflation or thermal inflation.

and the average $\langle \eta - 2\varepsilon \rangle$ must be evaluated only over these ΔN e-folds [165]. While this weakens the bound noticeably, $r \simeq 0.09$ still requires either $\Delta\phi \gtrsim 0.4$ or relatively large slow-roll parameters $\langle \eta - 2\varepsilon \rangle > 1/6$.

12.3.2 Implications of this bound for model building

Eq. (12.16) shows that a discovery of r close to its maximally allowed value $r \simeq 0.09$ would have dramatic implications for inflationary model building. In particular, it has the potential to rule out the entire framework of small-field slow-roll inflation used throughout chapters 6–11 of this thesis.

Even for smaller $r \gtrsim 10^{-2}$, eq. (12.16) implies relatively large $\Delta\phi$ or $\langle \eta - 2\varepsilon \rangle$, which means that it might be necessary to include higher orders in the small-field expansion or in the slow-roll approximation.[6]

This conclusion can only be avoided by changing one of the three fundamental assumptions leading to eq. (12.16): the assumption of slow-roll inflation, the equation of motion for ϕ, or the slow-roll prediction for the tensor amplitude. Each of these options would require drastic changes to the usual paradigm of small-field slow-roll inflation beyond the choice of specific inflaton potentials.

12.3.3 Generalization to multi-field slow-roll inflation

Note that the arguments leading to eq. (12.16) are also valid for multi-field models if V' and V'' are replaced by derivatives of V along the field trajectory and $\Delta\phi$ by the length of the trajectory in field space. Thus, the bound (12.16) is also applicable to multi-field models of slow-roll inflation.

However, one can in principle avoid the conclusion that individual fields must have super-Planckian excursions. There are two possibilities to realize this. The first one is to have very curved field trajectories that spiral [166–168] or zig-zag within a small sphere with radius $\phi_{\max} \ll m_{\mathrm{Pl}}$, so that the length of the trajectory is much larger than the radius $\phi_{\max}$. As the slow-roll trajectory always moves along the gradient of the potential, this requires very non-trivial scalar potentials. The other possibility is to use a large number $\mathcal{N}$ of inflaton fields [169]; then by the Pythagorean theorem, each field only needs to travel a shorter distance $\Delta\phi_i \sim \Delta\phi/\sqrt{\mathcal{N}} \ll \Delta\phi$.

[6] In the case of larger slow-roll parameters, a more promising approach might be to drop the slow-roll approximation altogether and calculate the predictions for $\mathcal{P}_\zeta(k)$ for each k from directly integrating the Mukhanov-Sasaki eq. (3.7), using a numerical solution of eqs. (2.13) and (2.14) for the background field $\overline{\phi}(t)$ and the Hubble parameter $\mathcal{H}(t)$.

12.4 Summary

In this chapter, we have studied the implications that a discovery of a large tensor-to-scalar ratio r would have for building small-field models of slow-roll inflation.

We started with a discussion of the Lyth bound, which implies that small-field models would be excluded for $r \gtrsim 10^{-2}$, and proposals for how the Lyth bound could be evaded by choosing a suitable inflaton potential for which $\varepsilon(\phi)$ is not monotonous.

To understand the implications of such an approach to evading the Lyth bound, we reconstructed the inflaton potential from the spectra of primordial perturbations. This reconstruction proves that the required potential shape can only be realized with a large scale-dependent running of the spectral index, i.e. if one allows for $\kappa_\mathrm{s} > 0$ or even higher-order runnings. The Lyth bound cannot be weakened very much in ΛCDM+r or in ΛCDM+r+α_s.

To determine how strongly the Lyth bound can be evaded independently of arbitrary choices of the cosmological model, we derived a general slow-roll bound on $\Delta\phi$ for any given r, see eq. (12.16). This bound clearly demonstrates that a discovery of large $r \sim 0.09$ has the potential to rule out slow-roll small-field inflation, and that even smaller $r \gtrsim 10^{-2}$ would imply that higher-order terms in Y_i/m_Pl and in the slow-roll parameters are likely to become relevant.

The derivation of the bound is based on only three basic assumptions: the validity of the slow-roll approximation, the equation of motion for ϕ, and the slow-roll prediction for the tensor amplitude. It is therefore valid very generally and does not depend on any assumptions about the inflaton potential.

We also briefly discussed how this bound can be generalized to multi-field slow-roll inflation. In this case, the bound applies to the length of the inflaton trajectory, and the conclusion that any individual field takes large field values can be avoided even for large r.

We conclude that a discovery of any observable tensor-to-scalar ratio r would have important implications for inflationary model building. For very large $r \sim 0.09$, slow-roll small-field models would be ruled out entirely. For smaller $r \gtrsim 10^{-2}$, they still generally require a scale-dependent running of the spectral index, so that small-field models are strongly constrained.

Part VI

Summary and conclusions

Chapter 13

Summary and conclusions

In this thesis, we have studied supersymmetric models of tribrid inflation and new inflation with tribrid superpotentials. We not only calculated their cosmological predictions, but also discussed their possible connections to models of high energy particle physics, and how such connections can relate cosmological and particle physics observables.

The thesis had three main parts: a first part on tribrid inflation, a second part on new inflation, and a third part on primordial gravity waves in small-field inflation.

Tribrid inflation in realistic particle physics models

In the first part, we studied tribrid inflation, with particular focus on the Kähler-driven regime which can most easily be embedded in realistic particle physics models. In chapter 6, we calculated the predictions for the primordial spectrum. We found that $\kappa_{\rm s} \ll \alpha_{\rm s}$, and we confirmed that the model can account for any spectral index $n_{\rm s} < 1$ but predicts a positive running $\alpha_{\rm s} > 0$.

Most importantly, we derived relations between the cosmological observable $\alpha_{\rm s}$ and the superpotential couplings V_0 and λ as shown in fig. 6.2 and the symmetry breaking scale $\langle H \rangle$ as shown in fig. 6.3. Furthermore, depending on the superpotential coupling between the inflaton and the waterfall field, we found relations between $\alpha_{\rm s}$ and either the inflaton's mass or its Yukawa coupling after inflation, which are also shown in fig. 6.3. Beyond constraining the low-energy particle physics of the model, these relations can be particularly useful for studies of the reheating period after inflation, since both preheating and reheating strongly depend on the inflaton's mass and couplings. In this way, $\alpha_{\rm s}$ could eventually also be related to reheating observables like the baryon asymmetry or the non-thermally produced dark matter abundance.

We also provided simple guidelines for how Kähler-driven tribrid inflation can be embedded in realistic models by identifying the abstract waterfall and inflaton fields with D-flat combinations of Higgs and matter fields.

As an example application, we demonstrated how tribrid inflation can be realized in a model of the leptonic flavour structure based on a spontaneously broken A_4 family symmetry in chapter 7. In this model, either a right-handed sneutrino or a D-flat LH_u direction can be used as the inflaton field, and tribrid inflation predicts a relation between the running of the spectral index α_s and either the right-handed neutrino mass m_N or the neutrino Yukawa coupling y_ν as shown in fig. 6.3. For the considered range of parameters, the model

also predicts leptonic mixing angles $\theta_{12}^{\mathrm{PMNS}} \simeq 35^\circ$ and $\theta_{23}^{\mathrm{PMNS}} \simeq 45^\circ$, and a leptonic Dirac CP phase $\delta^{\mathrm{PMNS}} \simeq 270^\circ$.

When a particular LH_u direction is chosen as the inflaton field, the waterfall field in this model gets a slight shift already during inflation, which could prevent the formation of topological defects at the end of inflation. We calculated this shift explicitly and showed that its effect on the inflaton potential is small, such that the predictions of Kähler-driven tribrid inflation should still approximately apply. We also discussed the specific properties of our flavon alignment potential and of the inflaton-waterfall coupling which are responsible for the waterfall field's shift. These properties can be reproduced in other models of tribrid inflation to identify alignment potentials and inflaton directions for which the production of topological defects can be avoided.

Finally, in chapter 8, we considered the possibility of generating the non-renormalizable operators of the tribrid superpotential with sub-Planckian suppression scales $\Lambda_i \ll m_{\mathrm{Pl}}$ from renormalizable couplings to messenger fields. We were particularly interested in inflaton field excursions $\Delta\phi \gtrsim \Lambda_i$, for which it is not clear whether the EFT that arises from integrating out the messenger fields is applicable during inflation.

We have calculated the inflationary dynamics both for the renormalizable superpotential including messenger fields, and for the non-renormalizable superpotential where the messenger fields have been integrated out. For messenger topologies that satisfy certain criteria, the tree-level predictions are identical up to $\mathcal{O}(\mathcal{H}/\Lambda_i)$ even when the inflaton field takes values above the messenger scale, i.e. $\Delta\phi \gtrsim \Lambda_i$.

The one-loop quantum corrections to the effective inflaton potential can be different when calculated with the renormalizable superpotential. However, in those cases, the quantum corrections are smaller than for the non-renormalizable superpotential. In Kähler-driven tribrid inflation, where they are negligible even for the non-renormalizable superpotential, inflation is thus well-described by the tree-level predictions which are identical for both superpotentials.

For Kähler-driven tribrid inflation, these results extend the applicability of tribrid inflation to some models with intermediate mass scales $\mathcal{H} \ll \Lambda_i \ll m_{\mathrm{Pl}}$: if the particles with mass Λ_i satisfy the conditions of our messenger topology, they can be integrated out during inflation even if $\Delta\phi > \Lambda_i$.

New inflation with a tribrid superpotential

In the second part, we studied supersymmetric new inflation. In chapter 9, we have calculated the effects of the multi-field dynamics of the complex scalar inflaton field in supersymmetric new inflation. For most of the parameter space, the model is well described by the usual single-field approximation, where only the real component of the inflaton is considered and its imaginary component is set to zero. In particular, this approximation is valid if the mass $\Delta m_\phi^2 = -\beta V_0$ from the Kähler potential is very small or absent, i.e. $\beta \ll 10^{-2}/(\ell - 2)$, in which case the imaginary component is quickly driven to zero before cosmological scales leave the horizon.

For sufficiently large Δm_ϕ^2, the results are sensitive to the initial conditions (see fig. 9.4). Non-Gaussianities remain small with $-1 < f_{\rm NL} < 0$, but the multi-field effects generally reduce the spectral index $n_{\rm s}$ and the inflationary vacuum energy V_0 compared to the single-field case. Thus, for $\beta \gtrsim 10^{-2}/(\ell-2)$, the single-field results should be interpreted as upper limits on $n_{\rm s}$ and V_0 only.

In chapter 10, we have studied the effects of realizing new inflation with a tribrid superpotential, which implies a coupling of the inflaton to another scalar field, the "preinflaton". Such a coupling has two main effects: it can generate the initial conditions for new inflation dynamically through a period of preinflation, and it can provide an efficient decay channel for reheating after inflation.

During preinflation, the inflaton is quickly driven to zero by its coupling to the slow-rolling preinflaton. Eventually, the preinflaton also rolls to very small values, and the fields enter a "diffusion region" in which quantum fluctuations have to be included. The qualitative behaviour in this region depends on the ratio of the Kähler potential couplings α and β for the two fields. If $\beta^2 \ll \alpha$, then the preinflaton rolls to zero, and the subsequent final phase of inflation is well-described by supersymmetric new inflation as discussed in chapter 9. Otherwise, the preinflaton can be non-negligible during the last N_* e-folds of inflation. Depending on the superpotential coupling between both fields, this leads either to a quasi-single-field regime where the preinflaton acts as a constant background field, or to a non-trivial two-field regime.

To demonstrate how the tribrid coupling can open up a suitable decay channel for reheating, we considered an example model where one of the right-handed sneutrinos acts as the preinflaton. By demanding that the correct baryon asymmetry is produced by non-thermal leptogenesis, we find a relation between the symmetry breaking scale v and the mass m_X of the lightest right-handed neutrino after inflation, as well as lower bounds on both quantities.

Finally, we studied the different stages of preheating in such models in chapter 11. We confirmed that preheating is ineffective for $v \gtrsim 10^{-1}$ due to Hubble damping, whereas for $10^{-5} \lesssim v \lesssim 10^{-2}$, the inflaton field's perturbations grow non-linear within a few oscillations of the field around its minimum. In this case, the spectrum of perturbations is sharply peaked around some peak scale $k_{\rm peak}/a \gg \mathcal{H}$ (see figs. 11.3 and 11.4), and the large perturbations locally push the inflaton field over the maximum of the scalar potential from $\phi > 0$ to $\phi < 0$, forming localized bubbles oscillating between $\phi = \pm v$.

We also considered resonant production of the scalar preinflaton field by the inflaton oscillations, focusing on the case $10^{-5} \lesssim v \lesssim 10^{-2}$ for which the inflaton field rapidly becomes inhomogeneous with a power spectrum sharply peaked around $k_{\rm peak}$. In this case, we explained how a parametric resonance for χ can be driven by the inhomogeneous inflaton field, in contrast to the usual parametric resonance driven by a homogeneous inflaton background. We performed a generalized Floquet analysis for inhomogeneous backgrounds with $\ell = 6$ and $v = 10^{-2}$, and we found a broad resonance band at $0.25 \lesssim m_\chi/m_\phi \lesssim 0.5$

for which χ perturbations can grow approximately up to the level of ϕ fluctuations even after the preheating of ϕ has been terminated by non-linear interactions.

These results have important implications for the calculation of reheating observables. The oscillons produced after the tachyonic oscillation stage could have a significant effect especially if they are very long-lived. More importantly, the production of χ perturbations during preheating affects the relative particle abundances at the beginning of the final reheating phase, which can affect the predictions for the reheat temperature and for the non-thermal production of relics like baryon number or dark matter.

Implications of large r for small-field inflation

In chapter 12, we considered the implications that a discovery of a large tensor-to-scalar ratio r would have for small-field models of slow-roll inflation like those studied in chapters 6–11.

While the Lyth bound implies that small-field models would be disfavoured or excluded for $r \gtrsim 10^{-2}$, there have been proposals for how the Lyth bound could be evaded by choosing a suitable inflaton potential for which $\varepsilon(\phi)$ is not monotonous. To understand the implications of such an approach to evading the Lyth bound, we reconstructed the inflaton potential from the spectra of primordial perturbations. This reconstruction proves that the required potential shape can only be realized with a large scale-dependent running of the spectral index, i.e. if one allows for $\kappa_\mathrm{s} > 0$ or even higher-order runnings.

To determine how strongly the Lyth bound can be evaded, we derived a general slow-roll bound on $\Delta\phi$ for any given r, see eq. (12.16), which is based on only three basic assumptions: the validity of the slow-roll approximation, the equation of motion for ϕ, and the slow-roll prediction for the tensor amplitude. Our bound clearly demonstrates that a discovery of large $r \sim 0.09$ has the potential to rule out slow-roll small-field inflation, and that even smaller $r \gtrsim 10^{-2}$ would imply that higher-order terms in Y_i/m_Pl or in the slow-roll parameters become non-negligible during inflation.

Conclusions and outlook

The results of this thesis confirm that tribrid superpotentials offer exciting possibilities for realizing inflation in close connection with high energy particle physics, particularly for theories in which masses or Yukawa couplings are generated by spontaneous symmetry breaking at a high energy scale.

Tribrid inflation is particularly interesting as it can predict relations between α_s and particle physics couplings. However, even in new inflation, a tribrid coupling to right-handed sneutrinos or visible sector fields can lead to useful constraints from reheating.

In the future, more predictions and constraints could be derived from a more detailed study of the preheating and reheating periods of both tribrid inflation and new inflation, e.g. concerning the production of primordial black holes, gravitino dark matter or topological defects. Since these processes depend particularly strongly on the particle physics

embedding, such studies could eventually offer further insights into both cosmology and particle physics.

Part VII

Appendix

Appendix A

Notations and conventions

This appendix lists the conventions used throughout this thesis.

We use natural units

$$c = \hbar = m_{\mathrm{Pl}} = (8\pi G)^{-1/2} = 1, \tag{A.1}$$

where c is the speed of light in vacuum, $\hbar$ is the reduced Planck constant, $m_{\mathrm{Pl}} = 2.4 \times 10^{18}$ GeV is the reduced Planck mass and G is the gravitational constant.

The metric signature is $(+,-,-,-)$. Four-vector indices are denoted by lowercase Greek letters and take the values $0, 1, 2, 3$. Other numeric indices are denoted by lowercase Latin letters. If an index appears as an upper and lower index in the same expression, summation over that index is implied.

Derivatives with respect to physical time are denoted by an overdot: $\dot{a} = \frac{\mathrm{d}}{\mathrm{d}t} a$. Other derivatives are sometimes denoted by a prime; in that case, the argument is either given explicitly, e.g. $V'(\phi) = \frac{\mathrm{d}}{\mathrm{d}\phi} V$, or it is mentioned in the text.

Complex scalar fields are denoted by uppercase letters, real scalar fields are denoted by lowercase letters, and the fermionic superpartner of a complex scalar field X is denoted by ψ_X.

In some cases, the full notation is used if it helps clarity, e.g. summation over repeated indices is made explicit in some formulas, and the reduced Planck mass m_{Pl} is sometimes reinserted to emphasize the mass scales.

A list of the abbreviations used in this thesis is given in table A.1.

BAO	Baryon acoustic oscillations
BBN	Big Bang nucleosynthesis
BSM	Beyond the Standard Model (of particle physics)
CL	Confidence level
CMB	Cosmic microwave background
EFT	Effective field theory
FRW	Friedmann-Robertson-Walker
GUT	Grand Unified Theory
IR	Infrared
LSP	Lightest supersymmetric particle
MSSM	Minimal Supersymmetric Standard Model
ODE	Ordinary differential equation
QFT	Quantum field theory
SM	Standard Model (of particle physics)
SUGRA	Supergravity
SUSY	Supersymmetry, supersymmetric
UV	Ultraviolet

Table A.1: List of abbreviations used in this thesis.

Appendix B

Experimental constraints on primordial perturbations

Every model of slow-roll inflation predicts a specific spectrum of primordial curvature and tensor perturbations from inflaton quantum fluctuations. Since these primordial perturbations are the seeds for both the CMB anisotropies and the matter density inhomogeneities, they can be constrained from observations of the CMB [8, 9, 50, 51] and of the large scale structure of the observable universe, particularly the BAO peak in the matter power spectrum [52–54].

However, to extract information about the primordial perturbations from observations of the current universe, one has to account for the evolution of the primordial perturbations. This time evolution depends on the cosmological model (e.g. on the expansion history of the universe), and for this reason the inferred constraints on the primordial quantities depend on which cosmological model is assumed.

Constraints on primordial perturbations in ΛCDM

The conventional baseline scenario is the 6-parameter ΛCDM model [49], which assumes that the universe is filled with cold dark matter, baryonic matter, photons and a cosmological constant Λ, with Λ chosen such that the total energy density is exactly equal to the critical density (i.e. the universe is flat). Reionization is parametrized by a single parameter τ. Apart from these assumptions on the post-inflationary universe, the spectrum of the primordial curvature perturbation from eq. (3.20a) is assumed to have the simple form

$$\mathcal{P}_\zeta(k) \,=\, A_\mathrm{s} \left(\frac{k}{k_*}\right)^{n_\mathrm{s}-1} , \tag{B.1}$$

with the runnings $\alpha_\mathrm{s} = \kappa_\mathrm{s} = ... = 0$ by assumption, and the tensor power spectrum is assumed to be completely negligible ($r = 0$). Given these assumptions, CMB temperature and polarization data strongly constrain the six free model parameters, with $A_\mathrm{s} = (2.13 \pm 0.05) \times 10^{-9}$ and $n_\mathrm{s} = 0.965 \pm 0.005$ at 68% CL [9].

Primordial perturbations in extensions of ΛCDM

There are many ways to relax the assumptions, introducing more parameters which can be constrained by observations. However, introducing more parameters typically leads

	n_s	α_s	κ_s
ΛCDM	0.965 ± 0.005	-	-
ΛCDM + α_s	$\sim 0.965 \pm 0.005$	-0.006 ± 0.007	-
ΛCDM + α_s + κ_s	0.959 ± 0.006	0.009 ± 0.010	0.025 ± 0.013

Table B.1: 68% CL constraints for ΛCDM and for extended models allowing for a running α_s and a running of the running κ_s, using Planck's TT,TE,EE+lowP dataset [9]. The spectral index n_s for ΛCDM+α_s is not given in [9], but [170] shows that n_s is virtually identical in ΛCDM and ΛCDM+α_s, so we use $n_\mathrm{s} = 0.965 \pm 0.005$ in both cases.

to weaker constraints for all parameters, including the usual six ΛCDM parameters.[1] In this sense, the usually-quoted experimental bounds on cosmological parameters are model-dependent: a 95% confidence interval only means that if all the model assumptions were known to be certainly and exactly true, the parameter would have a 95% chance to lie within the cited interval.

The ΛCDM model can be extended in two ways:

- Allow for more generic primordial spectra, e.g. for a non-zero primordial tensor-to-scalar ratio r or for a running spectral index with α_s, κ_s and possibly even further runnings (see table B.1 for constraints on such models).

- Change the late-time cosmology, e.g. allowing for an equation-of-state parameter $w_\Lambda \neq -1$ for the dark energy (or assuming an even more complicated evolution of dark energy as in quintessence models), assuming a non-standard number of neutrinos N_eff (or other light particles which have similar effects), allowing for deviations $\Omega_\mathrm{k} \neq 0$ from the critical energy density, and many other possibilities.

In this thesis, we only explicitly consider the first kind of extension with non-zero r, α_s and κ_s. However, it is important to keep in mind that extensions of the second kind can also considerably weaken the constraints on the primordial spectra. Though the current data are consistent with ΛCDM, they do not rule out such extensions, and it might be premature to rule out specific models of inflation just because they are in mild tension with the restrictive 6-parameter ΛCDM constraints.

Which constraints should be applied to models of inflation?

Since constraints depend on the cosmological model, which cosmological model should be assumed to constrain models of inflation?

Many models of inflation predict negligible r, α_s and κ_s. In this case, the 6-parameter ΛCDM constraints can be applied consistently. For other models that predict large values

[1] See e.g. the recent constraints on a 12-parameter extension of ΛCDM [124] for which $n_\mathrm{s} = 0.972 \pm 0.024$, which is much less constraining than the $n_\mathrm{s}^{(\Lambda\mathrm{CDM})} = 0.966 \pm 0.008$ of the 6-parameter ΛCDM model (using the Planck+BAO dataset of [124] in both cases).

for any of these parameters, it is necessary to use the constraints for a suitable extension of the ΛCDM model.

The uncertainties about the correct cosmological model mean that the true model might have more parameters in which case the ΛCDM constraints are overly tight. However, since the ΛCDM model describes the current observations so well it is reasonable to assume that it is at least a reasonably good approximation to the true cosmological model, so that constraints derived for ΛCDM and its simple extensions might still provide useful guides towards the correct model of inflation.

Constraints used in this thesis

In this thesis, we generally consider the constraints given in table B.1, assuming ΛCDM for new inflation and ΛCDM+α_s for Kähler-driven tribrid inflation. For the case of large r discussed in chapter 12, we use the bounds quoted in table B.1 as an estimate.

The precise bounds for $r > 0$ can in principle be calculated using Bayesian parameter estimation techniques. We have performed such calculations for Planck 2013 data using the software packages Monte Python [171] and CLASS [172, 173], and we found that a large r generally reduces α_s and increases κ_s [5]. However, the effect is small for $r \leq 0.1$. Since the results of chapter 12 are not sensitive to the precise choice of the constraints, we decide to use the bounds for $r = 0$ quoted in table B.1 as an estimate.

Appendix C

Tribrid inflation supplement

In this appendix, we present additional technical details related to our work on tribrid inflation which were left out of the main text for brevity. In particular, we derive the inflaton potential for multi-component inflaton directions, we show that deviations from D-flatness are negligible for $\mathcal{O}(1)$ gauge couplings, and we discuss the choice of symmetries for the A_4 family symmetry based model of chapter 7. Finally, we show how to calculate the mass terms for tribrid inflation including the non-renormalizable supergravity corrections using appropriate power counting.

C.1 Multi-component inflaton directions

When we use a D-flat composite inflaton direction $X^n = X_1 X_2 \cdots X_n$, e.g. $X^2 := LH_u$, the inflaton potential $V(\phi_1, \phi_2, ..., \phi_n)$ depends on all ϕ_i independently. In this section, we show that, if the D-term potential fixes the ratios between all of the X_i, the inflaton trajectory during Kähler-driven tribrid inflation has the same inflaton potential as if it were a single scalar field. This ensures that the predictions for the single-field case still apply even when we replace $X^n \to X_1 X_2 \cdots X_n$.

Multi-field inflaton potential from the Kähler potential

As in chapter 6, we assume that the Kähler potential depends only on the modulus squared of the fields:

$$K = |H|^2 + |S|^2 + \sum_i \left(|X_i|^2 + \kappa_{iS}|X_i S|^2\right) + \sum_{i \leq j} \left(\kappa_{ij}|X_i X_j|^2 + \kappa_{ijS}|X_i X_j S|^2\right) + ... \quad \text{(C.1)}$$

The inflaton potential can then be calculated by expanding eq. (6.6) in powers of the real scalar fields $\phi_i = \sqrt{2}|X_i|$:

$$V(\phi_1, ..., \phi_n) \;=\; V_0 \left(1 + \sum_i a_i \phi_i^2 + \sum_{i \leq j} b_{ij} \phi_i^2 \phi_j^2 + ...\right) \;+\; V_D, \quad \text{(C.2)}$$

with the coefficients[1]

$$a_i = \frac{1}{2}\left(1 - \kappa_{iS}\right), \tag{C.3a}$$

$$b_{ii} = \frac{1}{4}\left(\frac{1}{2} + \kappa_{ii} - \kappa_{iiS} + \kappa_{iS}^2 - \kappa_{iS}\right) =: b_i, \tag{C.3b}$$

$$b_{ij} = \frac{1}{4}\left(1 + \kappa_{ij} - \kappa_{ijS} + 2\kappa_{iS}\kappa_{jS} - \kappa_{iS} - \kappa_{jS}\right). \quad (\text{for } i < j) \tag{C.3c}$$

These coefficients depend entirely on the Kähler potential, and if the cutoff scale is around the Planck scale, we find that a_i, $b_{ij} \lesssim O(1)$.

Furthermore, if the D-term potential fixes the ratio between the different ϕ_i, we can express them all by a single quantity ϕ. This leads to an effective single-field potential $V(\phi) = V_0(1 + a\,\phi^2 + b\,\phi^4 + ...)$ as in the non-composite inflaton case.

Deviation from D-flatness

In this section, we work with only two fields $X_1 = L$ and $X_2 = H_u$ and with the renormalizable V_D from eq. (5.10) to keep the discussion simple:

$$V(\phi_1, \phi_2) = V_0\left(1 + a_1\phi_1^2 + a_2\phi_2^2 + b_1\phi_1^4 + b_2\phi_2^4 + b_{12}\phi_1^2\phi_2^2\right) + \frac{1}{2}\sum_a g_a^2\Big(X^\dagger T^a X\Big)^2. \tag{C.4}$$

From this function, we want to derive the one-dimensional inflaton potential $V(\phi)$ along the inflaton trajectory.

The D-term will generally depend on the gauge charges of the ϕ_i. In our example with $X_1 = L$ and $X_2 = H_u$:

$$\begin{aligned} V_D &= \frac{g_1^2}{8}\left[\left(L^\dagger, H_u^\dagger\right)\begin{pmatrix}-1 & 0\\ 0 & 1\end{pmatrix}\begin{pmatrix}L\\ H_u\end{pmatrix}\right]^2 + \frac{g_2^2}{8}\sum_{i=1}^{3}\left[\left(L^\dagger, H_u^\dagger\right)\begin{pmatrix}\sigma^i & 0\\ 0 & \sigma^i\end{pmatrix}\begin{pmatrix}L\\ H_u\end{pmatrix}\right]^2 \\ &= \frac{g_1^2}{8}\left(|L|^2 - |H_u|^2\right)^2 + \frac{g_2^2}{8}\sum_{i=1}^{3}\left(L^\dagger\sigma^i L + H_u^\dagger\sigma^i H_u\right)^2. \end{aligned} \tag{C.5}$$

The second term is minimized if L and H_u have opposite weak isospin. As the inflaton potential does not otherwise depend on the $SU(2)_L$ structure of L and H_u, this condition will be satisfied during inflation, and the two terms will be identical up to $g_1 \leftrightarrow g_2$.

We can plug V_D into the inflaton potential $V(\phi_1, \phi_2)$:

$$\begin{aligned} V(\phi_1, \phi_2) &= V_0\left(1 + a_1\,\phi_1^2 + a_2\,\phi_2^2 + b_1\,\phi_1^4 + b_2\,\phi_2^4 + b_{12}\,\phi_1^2\phi_2^2\right) + \frac{g_1^2 + g_2^2}{32}\left(\phi_1^2 - \phi_2^2\right)^2 \\ &= V_0\left\{1 + a_1\,\phi_1^2 + a_2\,\phi_2^2 + (b_1 + d)\phi_1^4 + (b_2 + d)\,\phi_2^4 + (b_{12} - 2d)\,\phi_1^2\phi_2^2\right\}, \end{aligned} \tag{C.6}$$

[1] We neglect effects from canonical normalization. For tribrid inflation with a single inflaton field, it has been shown explicitly that these effects can be interpreted as higher-order corrections to the potential, which can be absorbed e.g. in the definition of b [28].

where we defined $d := \frac{g_1^2+g_2^2}{32V_0} \sim O(10^{10})$. The terms with d dominate over the small coefficients a_i, $b_{ij} \lesssim O(1)$. Therefore, we expect that the inflaton trajectory will be along a nearly D-flat direction.

Looking at trajectories near the D-flat trajectory $\phi_1^2 = \phi_2^2$, we define

$$\phi_1 = \frac{1}{\sqrt{2}}(\phi + \delta), \quad \phi_2 = \frac{1}{\sqrt{2}}(\phi - \delta). \tag{C.7}$$

If we insert this in eq. (C.6), we get

$$V(\phi, \delta) \;=\; V_\phi + V_\delta, \tag{C.8}$$

with

$$V_\phi \;=\; V_0\left\{1 + a\,\phi^2 + b\,\phi^4\right\} \tag{C.9}$$

and

$$\begin{aligned}\frac{V_\delta(\delta)}{V_0} \;&=\; -\left(2\Delta a\phi + 4\Delta b\phi^3\right)\delta + \left(a + 6b\phi^2 - 2b_{12}\phi^2 + 4d\phi^2\right)\delta^2 - \underbrace{4\Delta b\phi\,\delta^3}_{\ll 4\Delta b\phi^3\delta} + \underbrace{b\,\delta^4}_{\ll 6b\phi^2\delta^2} \\ &\simeq -2\phi\left(\Delta a + 2\Delta b\,\phi^2\right)\delta + \left[a + (6b - 2b_{12} + 4d)\,\phi^2\right]\delta^2,\end{aligned} \tag{C.10}$$

where a, b describe the averaged potential for ϕ_1 and ϕ_2, while Δa, Δb quantify the asymmetries between the potentials for ϕ_1 and ϕ_2:

$$a = \frac{a_1 + a_2}{2}, \quad b = \frac{b_1 + b_2 + b_{12}}{4}, \quad \Delta a = \frac{a_2 - a_1}{2}, \quad \Delta b = \frac{b_2 - b_1}{4}. \tag{C.11}$$

In these equations, V_ϕ contains the couplings along the perfectly D-flat direction, while V_δ contains the potential due to the inflaton's deviation from D-flatness.

The minimum of δ can be found by minimizing eq. (C.10):

$$\delta_{\min} \;\simeq\; \frac{\Delta a + 2\Delta b\,\phi^2}{a + (4d + 6b - 2b_{12})\,\phi^2}\,\phi. \tag{C.12}$$

If we assume that δ tracks its minimum perfectly, then the effective inflaton potential is given by

$$V_{\text{eff}}(\phi) \;=\; V(\phi, \delta_{\min}) \;=\; V(\phi) + V_\delta(\delta_{\min}). \tag{C.13}$$

The inflaton potential is changed by

$$V_\delta(\delta_{\min}) \;=\; \frac{-V_0\left(\Delta a + 2\Delta b\,\phi^2\right)^2\phi^2}{a + (4d + 6b - 2b_{12})\,\phi^2} + O(\delta^3) \;\simeq\; \frac{-V_0\left(\Delta a + 2\Delta b\,\phi^2\right)^2}{4d}. \tag{C.14}$$

With $d \sim O(10^{10})$ and Δa, $\Delta b \lesssim O(1)$, this correction is negligible compared to V_ϕ, so assuming D-flatness is a very good approximation.

We must still check that $m_\delta^2 \gg \mathcal{H}^2$ to justify our assumption that δ tracks its minimum:

$$\frac{m_\delta^2}{\mathcal{H}^2} \simeq \frac{3}{V_0}\frac{\partial^2 V}{\partial \delta^2} = (\underbrace{6a + 36b\,\phi^2 - 12b_{12}\,\phi^2}_{\ll 1} + 24d\,\phi^2)\underbrace{-72\Delta b\,\phi\,\delta + 36b\,\delta^2}_{\ll 1} \simeq 24d\,\phi^2. \tag{C.15}$$

For Kähler-driven tribrid inflation, the inflaton field value during inflation is bounded by $\phi^2 \gtrsim 10^{-6}$, which we can insert in eq. (C.15) to find

$$\frac{m_\delta^2}{\mathcal{H}^2} \gtrsim 10^5. \tag{C.16}$$

Therefore, $m_\delta \gg \mathcal{H}$, and our assumption that $\delta = \delta_{\min}$ is warranted.

We conclude that any deviation from D-flatness during Kähler-driven tribrid inflation is negligible, and the inflaton potential indeed reduces to the simple single-field form (C.9) studied in chapter 6.

C.2 Symmetries for the A_4 lepton flavour model

The superpotential (7.9) can be fixed by a set of suitable shaping symmetries in addition to the A_4 family symmetry. In particular, we can use an $U(1)_R$ symmetry under which the superpotential has charge 2, and one $\mathbb{Z}_n$ symmetry for each flavon field.

	A_4	$U(1)_R$	$\mathbb{Z}_{n_1}$	$\mathbb{Z}_3$	$\mathbb{Z}_{n_3}$	$\mathbb{Z}_{n_4}$	$\mathbb{Z}_6$	$\mathbb{Z}_{n_6}$	$\mathbb{Z}_{2n_7}$
S_i	**1**	2	0	0	0	0	0	0	0
A_3	**3**	2	0	0	n_3-2	0	0	0	0
A_4	**3**	2	0	0	0	n_4-2	0	0	0
P_{34}	**1**	2	0	0	n_3-1	n_4-1	0	0	0
P_{36}	**1**	2	0	0	n_3-1	0	0	n_6-1	0
P_{46}	**1**	2	0	0	0	n_4-1	0	n_6-1	0
P_{35}	**1**	2	0	0	n_3-1	0	5	0	0
P_{16}	**1**	2	n_1-1	0	0	0	0	n_6-1	0
P_{12}	**1**	2	n_1-1	2	0	0	0	0	0
D_5	**1**	2	0	0	0	0	2	0	0
D_2'	**1'**	2	0	1	0	0	0	0	0
D_2''	**1"**	2	0	1	0	0	0	0	0
Θ_1	**3**	0	1	0	0	0	0	0	0
Θ_2	**3**	0	0	1	0	0	0	0	0
Θ_3	**3**	0	0	0	1	0	0	0	0
Θ_4	**3**	0	0	0	0	1	0	0	0
Θ_5	**3**	0	0	0	0	0	1	0	0
Θ_6	**3**	0	0	0	0	0	0	1	0
Θ_S	**1**	0	0	0	0	0	0	0	2
L	**3**	1	0	0	0	0	0	0	0
H_u	**1**	0	0	0	0	0	0	0	1
H_d	**1**	0	0	0	0	0	0	0	0
N_1	**1**	1	n_1-1	0	0	0	0	0	$2n_7-1$
N_2	**1**	1	0	2	0	0	0	0	$2n_7-1$
E_1	**1**	1	0	0	0	n_4-1	0	0	0
E_2	**1**	1	0	0	0	0	5	0	0
E_3	**1**	1	0	0	n_3-1	0	0	0	0

Table C.1: One possible set of symmetries and charge assignments for the superpotential in eq. (7.9).

The $U(1)_R$ charge assignment is straightforward. The mass parameters Λ_i in the superpotential cannot be charged, so the S_i must have 2 units of $U(1)_R$ charge. Then the Θ_i cannot have any $U(1)_R$ charge. Knowing this, we also find that the other auxiliary fields A_i, P_{ij} and D_i need 2 units of $U(1)_R$ charge. The only freedom we have is in the lepton sector, where we can distribute the $U(1)_R$ charge between the Higgs doublets H_u, H_d and

the lepton fields L, N_i, E_i. We choose to keep the Higgs fields uncharged and give 1 unit of $U(1)_R$ charge to each lepton.

To construct the $\mathbb{Z}_n$ symmetries, we start with the observation that we want to keep the different flavons separate in the $S_i(\Theta_i^{n_i} - \Lambda_i^2)$ terms. For this reason, we start with one $\mathbb{Z}_{k_i n_i}$ symmetry for each flavon, with any set of positive integers k_i, under which the i-th flavon has charge k_i. To simplify the notation, we can work with $k_i = 1$ and allow fractional charges for the other fields. However, to avoid fractional charges, we choose to normalize the A_4 singlet flavon Θ_S to 2 units of charge instead.

With the flavon charges fixed, we can uniquely determine the $\mathbb{Z}_n$ charge assignments for the auxiliary fields S_i, A_i, P_{ij} and D_i by demanding that all terms in the superpotential must be allowed by the $\mathbb{Z}_n$ symmetries.

The electron Yukawa couplings $\Theta L H_d E$ can always be allowed by choosing suitable charges for the E_i, which do not appear anywhere else. This fixes the E_i charges.

Now the only remaining task is to make sure that the neutrino Yukawa coupling and mass terms are allowed by the $\mathbb{Z}_n$ symmetries. There are several possible solutions, of which we have chosen a particularly simple one for table C.1.

Comment on the couplings of the S_i to Θ_i

Since the S_i all have the same symmetry charges, each of them can couple to every $\Theta_i^{n_i}$:

$$W_{\text{flavon}} \;=\; S_i \left(C_{ij} \Theta_j^{n_j} + \Lambda_i^2 \right), \tag{C.17}$$

with implied summation over i and j. However, if the coupling constant matrix C is invertible, we can consider linear combinations

$$S'_j \;=\; C_{ij} S_i \tag{C.18}$$

such that each S'_i only couples to a single $\Theta_i^{n_i}$:

$$W_{\text{flavon}} \;=\; S'_i \left(\Theta_i^{n_i} + (C^{-1})_{ij} \Lambda_j^2 \right), \tag{C.19}$$

where C^{-1} is the matrix inverse of C.

In general, neither the S_i nor the S'_i will be canonically normalized since the Kähler potential can contain mixing terms such as $\Delta K \propto (S_1^\dagger S_2 + S_2^\dagger S_1)$. However, if we consider the canonically normalized linear combinations S''_i of the S_i, we find that these S''_i are stabilized at zero if they get large mass terms from the Kähler potential as discussed in section 5.4.3. If all S''_i are stabilized at zero during inflation, then it follows that the S_i and S'_i are stabilized at zero as well.

In chapter 7, we generally work with the S'_i so that we have no couplings between the S'_i and $\Theta_j^{n_j}$ for $i \neq j$. Since we only need the S'_i and not their linear combinations S_i, we can relabel the S'_i as S_i to simplify the notation again, which is how we arrive at the superpotential of eq. (7.10).

C.3 Supergravity corrections to the mass matrix during inflation

In this appendix, we calculate the Planck-suppressed corrections to the mass matrices of scalars and fermions for the model of chapter 8. The purpose of this appendix is to show that during inflation, the corrections take the form given by eq. (8.11) for scalars and that they are negligible for fermions. The calculations in this appendix can be easily generalized to other messenger sectors if the new messenger fields satisfy $W = W_i = 0$ (for $i \neq S$) during inflation and the Kähler potential has the form of eq. (6.4).

Though the calculation is performed for the specific model of chapter 8, it can easily be adapted to other models of tribrid inflation, and the resulting scalar mass shift $\Delta m^2_{\text{SUGRA},i} = (1 - \kappa_{Si})V_0 + d_i V_0 \phi^2$ is generic for spectator fields Y_i during tribrid inflation.

C.3.1 Supergravity potential for the scalar mass matrix

First we discuss the supergravity corrections V_{SUGRA} to the scalar mass matrix as defined in eq. (8.11).

Formally, we can find the relevant terms by a power series expansion in ξ, with A_i, B_i, H, N, $S = \mathcal{O}(\xi)$, neglecting all terms of $\mathcal{O}(\xi^3)$. We evaluate the individual building blocks defined in eq. (5.5) for the superpotential in eq. (8.6) and the Kähler potential in eq. (6.4):

$$
\begin{aligned}
|W|^2 &= \Lambda^4 |S|^2 + \mathcal{O}(\xi^3) && = \mathcal{O}(\xi^2), && \text{(C.20a)}\\
W_S &= -\Lambda^2 + g_2 A_2^2 && = \mathcal{O}(\xi^0), && \text{(C.20b)}\\
W_H &= 2 g_1 A_1 H + g_H X B_1 && = \mathcal{O}(\xi^1), && \text{(C.20c)}\\
W_N &= g_N X B_2 && = \mathcal{O}(\xi^1), && \text{(C.20d)}\\
W_{A_1} &= g_1 H^2 + m_A A_2 && = \mathcal{O}(\xi^1), && \text{(C.20e)}\\
W_{A_2} &= 2 g_2 S A_2 + m_A A_1 && = \mathcal{O}(\xi^1), && \text{(C.20f)}\\
W_{B_1} &= g_H X H + m_B B_2 && = \mathcal{O}(\xi^1), && \text{(C.20g)}\\
W_{B_2} &= g_N X N + m_B B_1 && = \mathcal{O}(\xi^1), && \text{(C.20h)}\\
W_X &= g_H H B_1 + g_N N B_2 && = \mathcal{O}(\xi^2), && \text{(C.20i)}\\
W K_X &= -\Lambda^2 S X^\dagger \left(1 + 2\kappa_{XX} |X|^2 + ...\right) && = \mathcal{O}(\xi^1), && \text{(C.20j)}\\
W K_{i \neq X} &= -\Lambda^2 S Y_i^\dagger \left(1 + \kappa_{Xi} |X|^2 + ...\right) + \mathcal{O}(\xi^3) && = \mathcal{O}(\xi^2). && \text{(C.20k)}
\end{aligned}
$$

Note that this implies that $\mathcal{D}_i = \mathcal{O}(\xi^1)$ for all $i \neq S$, and $\mathcal{D}_S = \mathcal{O}(\xi^0)$.

The inverse Kähler metric $K^{i\bar{j}}$ is always contracted with $\mathcal{D}_i \mathcal{D}_j^\dagger$ in eq. (5.4). For $i \neq S \neq j$, for which $\mathcal{D}_i \mathcal{D}_j^\dagger = \mathcal{O}(\xi^2)$, we therefore only need $K^{i\bar{j}}$ up to $\mathcal{O}(\xi^0)$, for $i \neq S = j$ up to order $\mathcal{O}(\xi^1)$, and only for the diagonal element $i = j = S$ we need $K^{S\overline{S}}$ up to $\mathcal{O}(\xi^2)$.

With this in mind, we can use eq. (6.7) to expand $K^{i\bar{j}}$ up to the required order in ξ. The diagonal element for S to order $\mathcal{O}(\xi^2)$ can be calculated as a Neumann series (defining

$\Delta K_{\bar{i}j} = K_{\bar{i}j} - \delta_{ij}$):

$$\begin{aligned} K^{S\overline{S}} &= 1 - \Delta K_{\overline{S}S} + \sum_i \Delta K_{\overline{S}i}\Delta K_{\bar{i}S} - ... \\ &= 1 - \sum_i \left(\kappa_{Si} + (\kappa_{SXi} - 2\kappa_{Si}\kappa_{SX})|X|^2\right)(1+3\delta_{Si})|Y_i|^2 + \kappa_{SX}^2|X|^2|S|^2 + ..., \end{aligned} \quad \text{(C.21)}$$

where the ... denote terms of $\mathcal{O}(\xi^3)$ and $\mathcal{O}(X^4)$ which we neglected. The diagonal element for $a \neq S$ to order $\mathcal{O}(\xi^0)$ is:

$$\begin{aligned} K^{a\overline{a}} &= 1 - \Delta K_{\overline{a}a} + \sum_i \Delta K_{\overline{a}i}\Delta K_{\bar{i}a} - ... \\ &= 1 - \kappa_{Xa}(1+3\delta_{Xa})|X|^2 + ... + \mathcal{O}(\xi^2). \end{aligned} \quad \text{(C.22)}$$

For the off-diagonal elements $a \neq b$, we have:

$$\begin{aligned} K^{a\bar{b}} &= -\Delta K_{\overline{a}b} + \sum_i \Delta K_{\overline{a}i}\Delta K_{\bar{i}b} - ... \\ &= -\left(\kappa_{ab} + \kappa_{Xab}\left(1+\delta_{Xa}+\delta_{Xb}\right)|X|^2\right)Y_aY_b^\dagger + Y_aY_b^\dagger\sum_i \kappa_{ai}\kappa_{bi}(1+\delta_{ai}+\delta_{bi})|Y_i|^2 - ... \\ &= Y_aY_b^\dagger\left(-\kappa_{ab} + (\kappa_{Xa}\kappa_{Xb} - \kappa_{Xab})(1+\delta_{Xa}+\delta_{Xb})|X|^2 + ...\right) + \mathcal{O}(\xi^3). \end{aligned} \quad \text{(C.23)}$$

This is of order $\mathcal{O}(\xi^1)$ if $a = X$ or $b = X$, and order $\mathcal{O}(\xi^2)$ otherwise. Due to $\mathcal{D}_i = \mathcal{O}(\xi^1)$ for all fields $i \neq S$, none of the off-diagonal elements contribute to the mass matrix except $\mathcal{D}_S K^{S\overline{X}}\mathcal{D}_X^\dagger$ + h.c., which generates a small inflaton-dependent mass for S:

$$\begin{aligned} \mathcal{D}_X K^{X\overline{S}}\mathcal{D}_S^\dagger &= WK_XK^{X\overline{S}}W_S + \mathcal{O}(\xi^3) \\ &= -\Lambda^2 SX^\dagger(1+...)XS^\dagger(-\kappa_{SX}+...)\left(-\Lambda^2\right) + \mathcal{O}(\xi^3) \\ &= -\kappa_{SX}\Lambda^4|X|^2|S|^2 + ... \end{aligned} \quad \text{(C.24)}$$

We evaluate the diagonal terms in turn for X, S and other fields Y_i. We start with X:

$$\begin{aligned} \mathcal{D}_X K^{X\overline{X}}\mathcal{D}_X^\dagger &= |WK_X|^2 + \mathcal{O}(\xi^3) \\ &= \Lambda^4|X|^2|S|^2 + ... + \mathcal{O}(\xi^3). \end{aligned} \quad \text{(C.25)}$$

For S, we have

$$\begin{aligned} \mathcal{D}_S K^{S\overline{S}}\mathcal{D}_S^\dagger &= |\mathcal{D}_S|^2\left[1 - \sum_i\left(\kappa_{Si} + \kappa_{SXi}|X|^2\right)(1+\delta_{Si})|Y_i|^2 + \left(\kappa_{SX}^2 + ...\right)|X|^2|S|^2\right] + \mathcal{O}(\xi^3) \\ &= \left|g_2A_2^2 - \Lambda^2(1+SX^\dagger+...)\right|^2\left(1 + \sum_i(c_i + d_i|X|^2+...)|Y_i|^2 + ...\right) + \mathcal{O}(\xi^3) \\ &= \Lambda^4 + \sum_i \Delta m_i^2|Y_i|^2 - 2g_2\Lambda^2\,\mathrm{Re}\left(A_2^2\right) + \mathcal{O}(\xi^3), \end{aligned} \quad \text{(C.26)}$$

with supergravity mass terms $\Delta m_i^2 = (c_i + d_i\,|X|^2 + ...)\Lambda^4$, where the coefficients c_i and d_i are functions of the κ_{ij} and κ_{ijk}. For the other fields Y_i ($i \neq X$), we recover the simple form

$$\mathcal{D}_i K^{i\bar{i}} \mathcal{D}_i^\dagger \;=\; |W_i|^2 \left(1 - \kappa_{Xi}|X|^2 + ...\right) \;+\; \mathcal{O}(\xi^3). \tag{C.27}$$

Another two sources of SUGRA corrections are the $|W|^2$ term in eq. (5.4), which introduces another contribution to the mass term of S that can be absorbed in the constant c_S, and the exponential e^K, which also contributes to the mass terms via

$$e^K |\mathcal{D}_S|^2 = (1 + K + ...)(\Lambda^4 + ...). \tag{C.28}$$

Correctly expanding the exponential, one finds additional contributions to the masses of all fields, which are again of order $\Delta m_i^2 \sim \mathcal{O}(\Lambda^4)$. These can also be absorbed in the definition of the c_i and d_i above.

To calculate the precise form of the d_i, one must also take into account the effect of canonical normalization, which during inflation can be achieved by a redefinition $Y_i \to Y_i/\sqrt{K_{\bar{i}i}} = (1 - \frac{\kappa_{iX}}{2}|X|^2 + ...)Y_i$ for the non-inflaton scalar fields Y_i, which generates inflaton-dependent mass terms from the non-inflaton-dependent mass terms, i.e. $d_i \to d_i - \kappa_{iX} c_i$.[2]

Collecting all the terms from above, we find that the scalar masses receive additional Hubble-scale mass terms:

$$V_{\text{SUGRA}}^{(\text{additive})} \;=\; \sum_i (c_i + d_i |X|^2 + ...)\Lambda^4 |Y_i|^2 + \mathcal{O}(\xi^3), \tag{C.29}$$

where c_i, $d_i \lesssim \mathcal{O}(1)$ are functions of the κ_{ij} and κ_{ijk}. For $X \neq i \neq S$:

$$c_S \;=\; -4\kappa_{SS}, \tag{C.30a}$$
$$c_i \;=\; 1 - \kappa_{iS}, \tag{C.30b}$$
$$d_S \;=\; 1 - 4\kappa_{SS} - 2\kappa_{XS} - 4\kappa_{XSS} + 12\kappa_{SS}\kappa_{XS} + \kappa_{XS}^2, \tag{C.30c}$$
$$d_i \;=\; 1 - \kappa_{iS} - \kappa_{XS} - \kappa_{iXS} + \kappa_{iS}\kappa_{iX} + 2\kappa_{iS}\kappa_{XS}. \tag{C.30d}$$

The exponential, the bracket in eq. (C.27), and the canonical normalization $Y_i \to Y_i/\sqrt{K_{\bar{i}i}}$ also have the effect of stretching the renormalizable masses m_{ren}^2 by a common factor:

$$\frac{m_i^2}{m_{i,\text{ren}}^2} \;=:\; \mathcal{N}_i(\phi) \;=\; \begin{cases} e^K \left(K_{\bar{i}i}\right)^{-2}, & \text{for } W \sim Y_i^2, \\ e^K \left(K_{\bar{i}i} K_{\bar{j}j}\right)^{-1}, & \text{for } W \sim Y_i Y_j, \quad j \neq i \text{ fixed.} \end{cases} \tag{C.31}$$

This multiplicative rescaling is mostly irrelevant (except for the one-loop correction due to A_2, where we keep it explicitly), so throughout most of chapter 8, we only include the additive supergravity corrections from eq. (C.29).

[2] See [28] for details on canonical normalization during tribrid inflation.

C.3.2 Supergravity corrections to fermion masses

The fermion masses in supergravity can be calculated from eq. (5.14). During inflation, we can drop all terms proportional to A_i, B_i, H, N, $S = \mathcal{O}(\xi)$. This means that $W = 0$, $K_{i\neq X} = 0$, $W_{i\neq S} = 0$, $K^{S\bar{l}} = K^{S\overline{S}}\delta_{lS}$:

$$(m_F)_{ij} \;=\; e^{K/2}\left[W_{ij} + K_X W_S\left(\delta_{iX}\delta_{jS} + \delta_{jX}\delta_{iS}\right) - K^{S\overline{S}}K_{ij\overline{S}}W_S\right]. \tag{C.32}$$

The only non-zero terms in $K_{ij\overline{S}}$ are the mixed X-S terms:

$$K_{XS\overline{S}} \;=\; K_{SX\overline{S}} \;=\; X^\dagger\left(\kappa_{SX} + 2\kappa_{SXX}\left|X\right|^2 + ...\right), \tag{C.33}$$

and therefore the fermionic mass matrix including supergravity corrections is

$$(m_F)_{ij} \;=\; e^{K/2}W_{ij} + (\Delta m_F)_{ij}\,, \tag{C.34}$$

where the supergravity correction has only one non-vanishing entry during inflation:

$$\begin{aligned}(\Delta m_F)_{SX} \;&=\; (\Delta m_F)_{XS} \;=\; -e^{K/2}W_S\left(K^{S\overline{S}}K_{XS\overline{S}} - K_X\right)\\ &=\; e^{K/2}\Lambda^2 X^\dagger\left(\kappa_{SX} - 1\right) \;+\; \mathcal{O}(X^3).\end{aligned} \tag{C.35}$$

X and S do not have other mixing terms in the fermionic mass matrix, so we can diagonalize the X-S block separately. Up to subdominant terms of $\mathcal{O}(\phi^3)$, it takes the simple form

$$m_F \;=\; \left(\kappa_{SX} - 1\right)\Lambda^2 X^\dagger\begin{pmatrix}0 & 1\\ 1 & 0\end{pmatrix}, \tag{C.36}$$

which leads to the eigenvalues

$$\left|m_{SX}^{(F)}\right| \;=\; \Lambda^2\left|(1-\kappa_{SX})X\right|. \tag{C.37}$$

With $X \ll 1$, this fermion mass is much smaller than the Hubble scale $\mathcal{H} = \Lambda^2/\sqrt{3}$, and the S-X fermions remain light during inflation. In particular, their contribution to the one-loop potential is negligible and can be safely ignored in section 8.3.

The fermion masses also receive a multiplicative stretching factor given by eq. (C.31) from the $e^{K/2}$ prefactor and canonical normalization. This rescaling is identical for the scalars and fermions,[3] and therefore does not affect the cancellation between scalar and fermionic contributions to the one-loop potential in section 8.3.

[3]For $\Lambda = 0$, there is no SUSY breaking F-term. As we know that scalar and fermion masses are identical in unbroken SUSY, the mass correction must be identical for scalars and fermions in the limit $\Lambda \to 0$. The rescaling in eq. (C.31), which does not depend on Λ, must therefore rescale fermions and scalars in the same way.

Appendix D

New inflation supplement

This appendix contains additional calculations for supersymmetric new inflation. In particular, in appendix D.1 we elaborate on the decay rates for reheating in the sneutrino preinflation model of section 10.4, appendix D.2 contains an estimate for the initial conditions from preinflation in the absence of direct mass terms from the Kähler potential, and in appendix D.3 we discuss whether S can experience resonant growth during preheating after new inflation.

D.1 Decay rates for $\ell = 4$

In this appendix, we calculate the perturbative inflaton decay rate for our example model in section 10.4, where the matter field X is identified with the right-handed sneutrino.

In the rest frame of the decaying particle, the decay rate Γ of a particle with mass m_i into two particles of mass m_f is given by [174]

$$\Gamma_{\mathrm{i}\to\mathrm{ff}} = \frac{1}{16\pi m_\mathrm{i}} |\mathcal{M}|^2 \sqrt{1-\frac{4m_\mathrm{f}^2}{m_\mathrm{i}^2}}, \tag{D.1}$$

where $\mathcal{M}$ is the matrix element for the process.

To get the total decay rate, we must sum over the decay rates for each channel. This includes summing over spin polarizations for final-state fermions and averaging over spin polarizations for initial-state fermions.

D.1.1 Inflaton decay rate Γ_ϕ

For the decay of the inflaton ϕ, there are two tree-level diagrams for the decay into scalar sneutrinos[1] and one tree-level diagram for the decay into right-handed neutrinos, see fig. D.1. The matrix elements for these decays are[2]

$$i\mathcal{M}_{\phi\to\text{fermions}} = -i\sqrt{\lambda_i m_X}\,\bar{u}(p_1,s_1)v(p_2,s_2), \tag{D.2a}$$

$$i\mathcal{M}_{\phi\to\text{scalars}} = -4i\sqrt{\lambda_i m_X^3}, \tag{D.2b}$$

[1] As a complex scalar field, the sneutrino consists of two real components, which we denote by χ and $\overline{\chi}$.

[2] The Feynman rules for Majorana fermions can be found e.g. in [175].

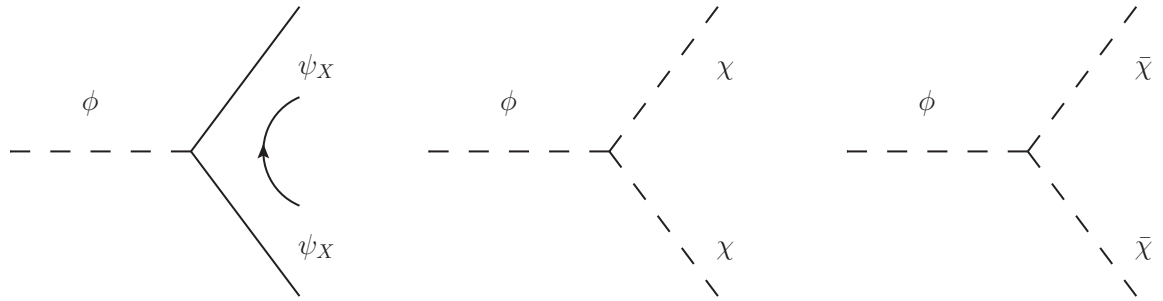

Figure D.1: Decay channels for the inflaton ϕ into right-handed neutrinos ψ_X and right-handed sneutrinos χ, $\overline{\chi}$.

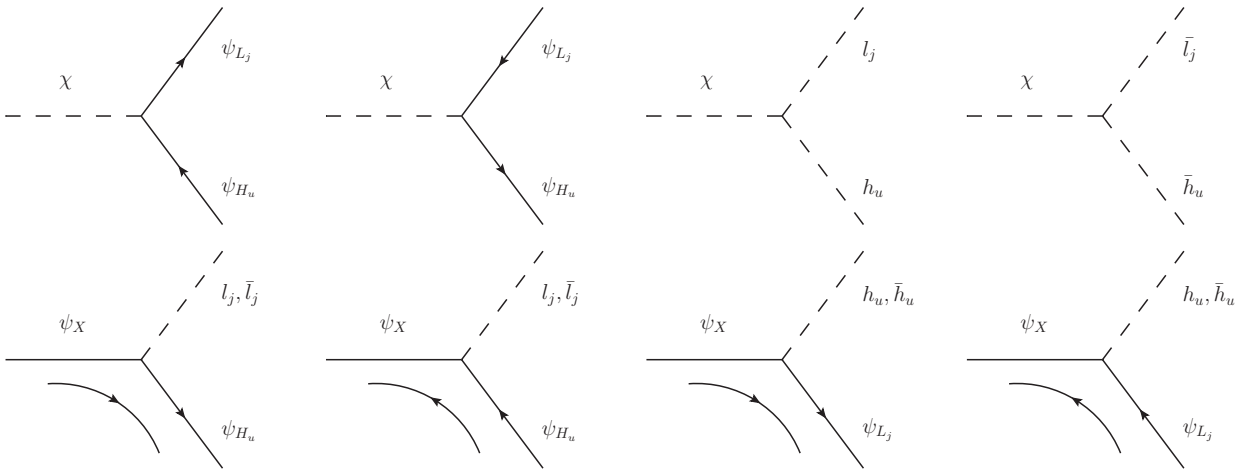

Figure D.2: Decay channels for the right-handed sneutrino χ and the right-handed neutrino ψ_X into left-handed (s)leptons and Higgs(ino) particles.

with $p_1 = (\frac{m_\phi}{2}, \vec{p_1})$ and $p_2 = (\frac{m_\phi}{2}, -\vec{p_1})$. We get the total decay rate by summing over eq. (D.1) for each of these three decay channels:

$$\Gamma_\phi = \frac{\lambda}{8\pi} m_\phi m_X \left(1 + 12\frac{m_X^2}{m_\phi^2}\right)\left(1 - 4\frac{m_X^2}{m_\phi^2}\right)^{1/2}. \tag{D.3}$$

D.1.2 Sneutrino decay rate Γ_χ

For the decay of the right-handed sneutrino χ, we have 12 decay channels into scalars and 12 decay channels into fermions, see fig. D.2. Note that each of the diagrams in fig. D.2 stands for six separate processes due to the decay into two different $SU(2)$ components (index suppressed) and three generations (index j). The matrix elements for these decays

are

$$i\mathcal{M}_{\chi\to\text{fermions}} = \frac{-i}{\sqrt{2}}\, y_{ji}\, \bar{u}(p_1, s_1)\frac{1+\gamma^5}{2}v(p_2, s_2), \tag{D.4a}$$

$$i\mathcal{M}_{\chi\to\text{scalars}} = \frac{-i}{\sqrt{2}}\, y_{ji} m_X, \tag{D.4b}$$

with $p_1 = (\frac{m_X}{2}, \vec{p_1})$ and $p_2 = (\frac{m_X}{2}, -\vec{p_1})$. We get the total decay rate by summing over eq. (D.1) for each of these eight decay channels:

$$\Gamma_\chi = \frac{\sum_j |y_{ji}|^2}{4\pi} m_X, \tag{D.5}$$

where we neglected $m_\text{f} \sim m_{H_u} \sim m_{L_j} \ll m_X$. One can easily verify that the other scalar sneutrino component $\overline{\chi}$ has the same decay rate.

D.1.3 Neutrino decay rate Γ_{ψ_X}

The right-handed neutrino ψ_X can decay into left-handed (s)leptons and Higgs(ino) particles through the diagrams in fig. D.2. The four diagrams correspond to 16 different processes for each j: one factor of two is due to the $SU(2)$ contraction and another factor of two is because the final state can contain each of the two real components of L_j or H_u. The matrix elements are

$$\left|\mathcal{M}_{\psi_X\to\text{scalar+fermion}}\right| = \frac{1}{\sqrt{8}}\left|y_{ji}\, \bar{u}(p_\text{f}, s_\text{f})\left(1+\gamma^5\right) u(p_\text{i}, s_\text{i})\right| \tag{D.6}$$

for the decay into particles, with $p_\text{f} = (\frac{m_X}{2}, \vec{p_\text{f}})$ and $p_\text{i} = (m_X, \vec{0})$. The decay into antiparticles is nearly the same, but the u-spinors are replaced by v-spinors and $(1+\gamma^5)$ is replaced by $(1-\gamma^5)$, which still leads to the same squared matrix element.

The total decay rate is the sum over the decay rates for all processes. We must also include a factor $\frac{1}{2}$ for averaging over incoming spin polarizations. The result is

$$\Gamma_{\psi_X} = \frac{\sum_j \left|y_{ji}\right|^2}{4\pi} m_X, \tag{D.7}$$

which is identical to the decay rate $\Gamma_\chi = \Gamma_{\overline{\chi}}$ of the two sneutrino components.

D.2 Initial $\langle\chi\rangle$ from preinflation with $\alpha = \beta = 0$

In single-field new inflation, the inflaton is the only field that is displaced from the vacuum during inflation, i.e. $\langle\chi\rangle = 0$ during inflation. In the context of preinflation with χ as the preinflaton, this can occur naturally in the presence of small supergravity corrections to the particle masses as discussed in section 10.2. However, if no mass terms for χ and ϕ are generated from supergravity corrections, the analysis of section 10.2 must be repeated taking into account the superpotential couplings. In this appendix, we want to discuss the initial values of $\langle\chi\rangle$ that arise from preinflation in the absence of supergravity corrections for the example of $\ell = 6$ and $v = 10^{-2}$ (chosen such that the results can be applied to chapter 11), and how these initial conditions depend on λ or equivalently the mass ratio m_χ/m_ϕ.

Since the fields are very homogeneous during preinflation and inflation, we will only deal with the homogeneous background fields $\phi = \langle\phi\rangle$ and $\chi = \langle\chi\rangle$ in this context, and throughout this appendix we drop the brackets to keep the notation simple.

D.2.1 Quantum diffusion

During preinflation in χ, we have $\chi > \phi$, with $\phi \to 0$ due to the large effective mass $m_\phi^{(\text{eff})} = \lambda\chi^2$ for ϕ induced by the vacuum expectation value of χ, whereas χ moves more slowly due to its shallower potential. Eventually, we end up close to the $\phi = 0$ axis. However, for $\phi = 0$, the gradient of the potential vanishes, and the classical slow-roll equations of motion predict static fields $\dot\phi = \dot\chi = 0$. In this region, quantum fluctuations dominate over the classical field evolution, and we must include these fluctuations in the time evolution of the fields.

Quantum fluctuations versus classical field evolution

For each light scalar field φ, we can estimate whether the classical evolution or the quantum fluctuations dominate the time evolution by comparing the classical change of the field value per Hubble time $t_\mathcal{H} = 1/\mathcal{H}$ to the growth of the quantum fluctuation amplitude as explained in section 9.3.1:

$$|\Delta\varphi_\text{cl}| \simeq \frac{|V'|}{V} \overset{?}{>} |\Delta\varphi_\text{qu}| \simeq \frac{\mathcal{H}}{2\pi}. \tag{D.8}$$

Note that eq. (D.8) assumes the quantum fluctuations for a massless scalar field in de Sitter space, i.e. $m_\varphi \ll \mathcal{H}$ and $\mathcal{H} =$ constant. This is a good approximation for flat regions of the scalar potential, including the region around $\phi = \chi = 0$ that we want to study.

When eq. (D.8) is satisfied, the evolution of φ can be calculated from its classical equation of motion. Otherwise, φ performs a random walk, moving around by $\Delta\varphi_\text{qu} \sim \mathcal{H}/2\pi$ per Hubble time.

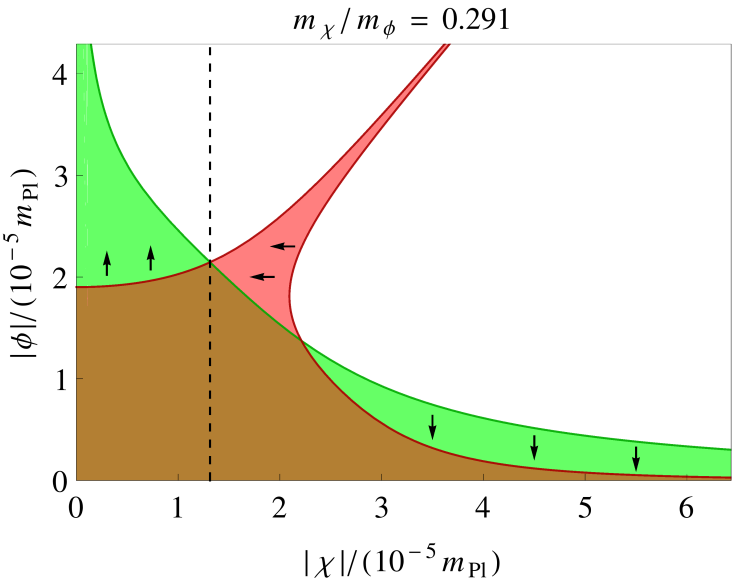

Figure D.3: Quantum diffusion region for $|\chi|$ and $|\phi|$ for $m_\chi/m_\phi = 0.291$ with $\ell = 6$ and $v = 10^{-2}$. In the brown region to the lower left, both fields' evolution is dominated by quantum fluctuations and the fields perform a random walk. In the green regions, the field ϕ evolves according to its classical equation of motion whereas χ performs a random walk, and in the red region ϕ performs a random walk and χ moves classically. The dashed black line marks a boundary between different regimes of the classical evolution: for $|\chi| > \chi_{\rm diff}^{(\rm max)} \simeq 1.3 \times 10^{-5}$, the classical equations push the fields back into the brown diffusion region when they randomly diffuse out of it, whereas for $|\chi| < \chi_{\rm diff}^{(\rm max)}$, the classical equations push $|\phi|$ towards large values away from the diffusion region. Therefore, the fields can only exit the brown diffusion region for small $|\chi| < \chi_{\rm diff}^{(\rm max)}$.

Diffusion region for ϕ and χ

We can now use the condition (D.8) to determine the "diffusion region" where ϕ and/or χ perform a random walk due to quantum fluctuations.

The diffusion region is plotted in fig. D.3 for an example value $m_\chi/m_\phi = 0.291$. In the brown region, both ϕ and χ perform a random walk. In the green regions, the field ϕ evolves according to its classical equation of motion whereas χ performs a random walk, and in the red region ϕ performs a random walk and χ is dominated by its classical equation of motion.

To understand where we can leave the brown diffusion region, it is important to understand the evolution in the red and green regions:

1. In the red region, χ moves classically and ϕ performs a random walk with $\Delta\phi \sim \mathcal{H}/2\pi$ per Hubble time. The dominant effect is the classical movement of χ, which drives χ to smaller values; in the red region, we thus move nearly horizontally to the left.[3] This

[3]We can approximate the movement as horizontal since for our choice of parameters the scales for ϕ

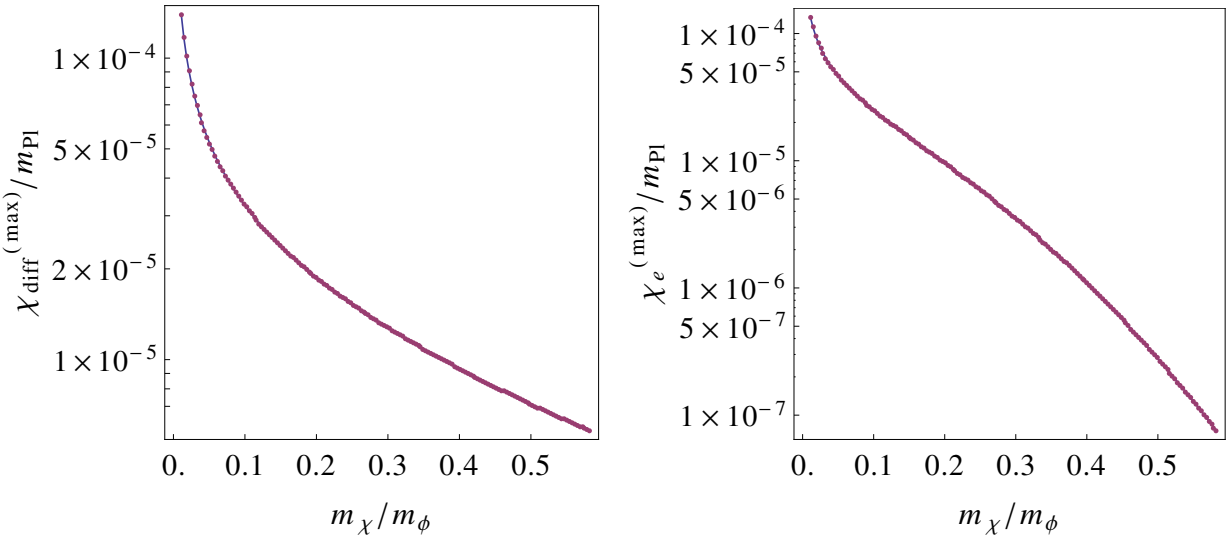

Figure D.4: Maximum values of χ at the diffusion region boundary (left) and close to the end of inflation when $\phi = 0.08v$ (right) as a function of m_χ/m_ϕ for $\ell = 6$ and $v = 10^{-2}$.

means that when we exit from the brown to the red region, the field is immediately pushed back into the brown diffusion region.

2. In the green regions, the dominant effect is the classical movement of ϕ. For $|\chi| > \chi_{\rm diff}^{(\rm max)}$ (to the right of the dashed black line), the mass of ϕ is positive, and we move vertically downwards back into the brown diffusion region. For $|\chi| < \chi_{\rm diff}^{(\rm max)}$, the mass of ϕ is tachyonic, and we move vertically upwards away from the brown diffusion region.

The combined effect is that the fields can only exit the brown diffusion region at $|\chi| < \chi_{\rm diff}^{(\rm max)}$. Where exactly they exit the diffusion region is the result of a random walk through the brown region starting at $|\chi| \gg \chi_{\rm diff}^{(\rm max)}$.

For a diffusion region with the qualitative shape of fig. D.3, $\chi_{\rm diff}^{(\rm max)}$ can be calculated as the intersection between the diffusion boundaries of ϕ and χ:

$$\text{At } (\phi_{\rm diff}^{(\rm max)}, \chi_{\rm diff}^{(\rm max)}): \qquad \frac{1}{V}\frac{\partial V}{\partial \chi} = -\frac{1}{V}\frac{\partial V}{\partial \phi} = \frac{\mathcal{H}}{2\pi}. \tag{D.9}$$

The minus sign selects the upper left boundary of the diffusion region of ϕ; this is the boundary beyond which ϕ is growing, whereas beyond the lower right boundary, the classical motion drives $\phi \to 0$.

and χ are similar. This is different from section 10.2 where we had $\chi_{\rm c} \gg \phi_{\rm b} \sim \frac{\mathcal{H}}{2\pi\beta}$: in that case, even though the field moves most quickly along the χ direction, it might hit the diffusion boundary $\phi_{\rm b}$ before χ has dropped to small values.

D.2.2 Dependence of initial $\langle\chi\rangle$ on m_χ/m_ϕ

There are two effects that make χ dependent on the mass ratio m_χ/m_ϕ:

1. The shape of the diffusion region depends on the coupling $\lambda \propto m_\chi/m_\phi$. For large λ, the potential for χ gets steeper; this makes the classical region larger and pushes the green and brown regions in fig. D.3 to the left, towards smaller χ, and thus reduces $\chi_{\rm diff}^{(\rm max)}$.

2. After the fields leave the diffusion region at some $\chi_{\rm diff}$, χ rolls along the potential gradient towards smaller χ, with $\dot\chi \propto \lambda^2 \propto (m_\chi/m_\phi)^2$. Therefore, a larger mass ratio makes χ decay faster during inflation, reducing the value $\chi_{\rm e}$ at the end of inflation.

These effects make $\chi_{\rm diff}$ and especially $\chi_{\rm e}$ monotonously decreasing with m_χ/m_ϕ, see fig. D.4. For this reason, a noticeable effect of $\chi_{\rm e}$ on preheating is only possible for small mass ratios $m_\chi/m_\phi \lesssim 0.5$. For larger m_χ/m_ϕ, $\chi_{\rm e}$ is generally subdominant compared to the vacuum quantum fluctuations $\delta\chi^{(\rm vac)}$.

D.3 Parametric resonance of S

In the discussion of preheating in chapter 11, we only considered preheating with the real scalar fields ϕ and χ. However, when the model is realized as a SUSY model with the tribrid superpotential of eq. (6.1), it features several extra fields: one additional real scalar component for X and H, and two real scalar components for S.

The additional real component of X is expected to behave exactly like χ since their scalar potentials are identical. In this appendix, we briefly discuss the preheating of S.

Around the minimum of the potential, $S = 0$ is stabilized with a positive mass. However, the mass of S around $\phi \sim v$ depends on ϕ:

$$V_S \;=\; m_\phi^2 \left(\frac{\phi}{v}\right)^{2\ell-2} |S|^2. \tag{D.10}$$

Due to this inflaton-dependent mass, the quantum fluctuations of S can be amplified during preheating. Note that around the minimum, $m_S^2 = m_\phi^2$ holds independently of the model parameters.

Some preheating already takes place during the tachyonic oscillation phase (during which ϕ is mostly homogeneous), and the amplification during this phase can be calculated using the standard techniques.

However, even after preheating has made ϕ inhomogeneous, parametric resonance for S can still occur. Assuming, as in section 11.3, that $\phi(\vec{x}, t)$ can be approximated by a single plane wave with wave vector $\vec{k}_\mathrm{p}$, we find equations for the real and imaginary parts of S analogous to eqs. (11.13)–(11.21), with the matrix $\mathcal{F}(t)$ replaced by

$$\mathcal{F}_S(t) \;=\; -m_\phi^2 \mathbb{1} - \begin{pmatrix} k_N^2 & f_S(t) & 0 & 0 & ... & 0 \\ f_S(t) & k_{N-1}^2 & f_S(t) & 0 & ... & 0 \\ 0 & f_S(t) & k_{N-2}^2 & f_S(t) & ... & 0 \\ 0 & 0 & f_S(t) & k_{N-3}^2 & ... & 0 \\ ... & ... & ... & ... & ... & f_S(t) \\ 0 & 0 & 0 & 0 & f_S(t) & k_{-N}^2 \end{pmatrix}, \tag{D.11}$$

and

$$f_S(t) \;:=\; \frac{(\ell-1) m_\phi^2 \delta\phi_0}{v} \cos(\omega_\phi t). \tag{D.12}$$

Performing the Floquet analysis for these equations with $\ell = 6$ and a cutoff $k_\mathrm{cutoff} = 5k_\mathrm{peak}$, we find the Floquet exponents shown in fig. D.5. The main result is that the perturbations δS are strongly amplified, especially for momenta $k \sim k_\mathrm{peak}$. Note that these Floquet exponents do not depend on λ, unlike those for $\delta\chi$, and δS grows exponentially even for parameters for which $\delta\chi$ remains small.

The lattice results of [150] indicate that there are some effects of δS on the preheating of χ, but the main qualitative result is unchanged: $\delta\chi$ grows strongly in the broad resonance

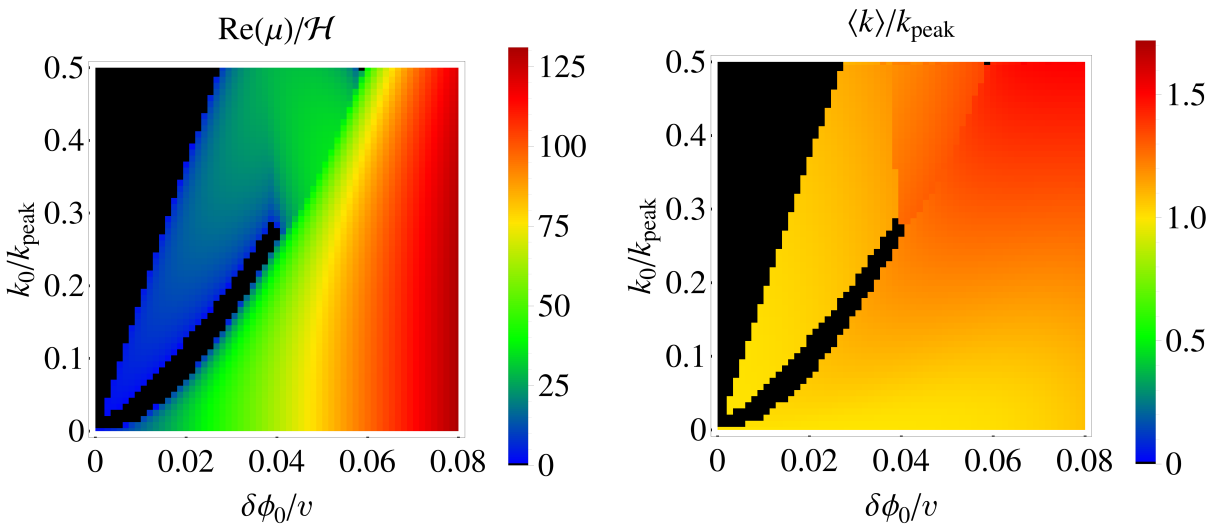

Figure D.5: Results of Floquet analysis for the perturbations of S for $v = 10^{-2}$ and $\ell = 6$, using a cutoff $k_{\rm cutoff} = 5k_{\rm peak}$. The left plot shows the largest Floquet exponent for a given k_0 and inflaton perturbation amplitude $\delta\phi_0$, indicating how strongly the fastest-growing δS perturbations are growing. Black regions indicate no growth (only oscillatory solutions), while in the coloured regions δS grows exponentially. The right plot shows the wavenumber $\langle k\rangle$ of the fastest-growing linear combination of δS_k. Strong growth occurs especially around $k \sim k_{\rm peak}$.

band at $0.25 \lesssim m_\chi/m_\phi \lesssim 0.5$, but not at larger mass ratios. In particular, even in the presence of S, the lattice simulations of [150] do not show non-perturbative growth of $\delta\chi$ at $m_\chi = m_\phi$.

Bibliography

[1] S. Antusch and D. Nolde, *Matter inflation with A_4 flavour symmetry breaking*, JCAP **1310** (2013) 028 [arXiv:1306.3501 [hep-ph]].

[2] D. Nolde, *Effects of the imaginary inflaton component in supergravity new inflation*, JCAP **1311** (2013) 028 [arXiv:1310.0820 [hep-ph]].

[3] S. Antusch, D. Nolde and S. Orani, *Hilltop inflation with preinflation from coupling to matter fields*, JCAP **1405** (2014) 034 [arXiv:1402.5328 [hep-ph]].

[4] S. Antusch and D. Nolde, *BICEP2 implications for single-field slow-roll inflation revisited*, JCAP **1405** (2014) 035 [arXiv:1404.1821 [hep-ph]].

[5] S. Antusch, F. Cefalà, D. Nolde and S. Orani, *False vacuum energy dominated inflation with large r and the importance of κ_s*, JCAP **1410** (2014) 015 [arXiv:1406.1424 [hep-ph]].

[6] S. Antusch, D. Nolde and S. Orani, *Hill crossing during preheating after hilltop inflation*, JCAP **1506** (2015) 009 [arXiv:1503.06075 [hep-ph]].

[7] S. Antusch and D. Nolde, *Realising effective theories of tribrid inflation: Are there effects from messenger fields?*, JCAP **1509** (2015) 055 [arXiv:1505.06910 [hep-ph]].

[8] N. Aghanim *et al.* [Planck Collaboration], *Planck 2015 results. XI. CMB power spectra, likelihoods, and robustness of parameters*, arXiv:1507.02704 [astro-ph.CO].

[9] P. A. R. Ade *et al.* [Planck Collaboration], *Planck 2015 results. XX. Constraints on inflation*, arXiv:1502.02114 [astro-ph.CO].

[10] M. C. Gonzalez-Garcia, M. Maltoni and T. Schwetz, *Global Analyses of Neutrino Oscillation Experiments*, arXiv:1512.06856 [hep-ph].

[11] H. Fritzsch and P. Minkowski, *Unified Interactions of Leptons and Hadrons*, Annals Phys. **93** (1975) 193.

[12] M. Lindner and M. Weiser, *Gauge coupling unification in left-right symmetric models*, Phys. Lett. B **383** (1996) 405 [hep-ph/9605353].

[13] F. Hartmann, W. Kilian and K. Schnitter, *Multiple Scales in Pati-Salam Unification Models*, JHEP **1405** (2014) 064 [arXiv:1401.7891 [hep-ph]].

[14] K. S. Babu, E. Ma and J. W. F. Valle, *Underlying A(4) symmetry for the neutrino mass matrix and the quark mixing matrix*, Phys. Lett. B **552** (2003) 207 [arXiv:hep-ph/0206292].

[15] G. Altarelli and F. Feruglio, *Tri-bimaximal neutrino mixing, A(4) and the modular symmetry*, Nucl. Phys. B **741** (2006) 215 [hep-ph/0512103].

[16] E. Ma and G. Rajasekaran, *Softly broken A(4) symmetry for nearly degenerate neutrino masses*, Phys. Rev. D **64** (2001) 113012 [hep-ph/0106291].

[17] S. Antusch, C. Gross, V. Maurer and C. Sluka, *A flavour GUT model with* $\theta_{13}^{PMNS} = \theta_C/\sqrt{2}$, Nucl. Phys. B **877** (2013) 772 [arXiv:1305.6612 [hep-ph]].

[18] J. R. Ellis, J. S. Hagelin, D. V. Nanopoulos, K. A. Olive and M. Srednicki, *Supersymmetric Relics from the Big Bang*, Nucl. Phys. B **238** (1984) 453.

[19] W. Buchmüller, V. Domcke and K. Schmitz, *WIMP Dark Matter from Gravitino Decays and Leptogenesis*, Phys. Lett. B **713** (2012) 63 [arXiv:1203.0285 [hep-ph]].

[20] L. Roszkowski, S. Trojanowski and K. Turzyński, *Neutralino and gravitino dark matter with low reheating temperature*, JHEP **1411** (2014) 146 [arXiv:1406.0012 [hep-ph]].

[21] S. Dimopoulos, S. Raby and F. Wilczek, *Supersymmetry and the Scale of Unification*, Phys. Rev. D **24** (1981) 1681.

[22] U. Amaldi, W. de Boer, P. H. Frampton, H. Furstenau and J. T. Liu, *Consistency checks of grand unified theories*, Phys. Lett. B **281** (1992) 374.

[23] S. Antusch, M. Bastero-Gil, S. F. King and Q. Shafi, *Sneutrino hybrid inflation in supergravity*, Phys. Rev. D **71** (2005) 083519 [hep-ph/0411298].

[24] S. Antusch, K. Dutta and P. M. Kostka, *SUGRA Hybrid Inflation with Shift Symmetry*, Phys. Lett. B **677** (2009) 221 [arXiv:0902.2934 [hep-ph]].

[25] S. Antusch, M. Bastero-Gil, J. P. Baumann, K. Dutta, S. F. King and P. M. Kostka, *Gauge Non-Singlet Inflation in SUSY GUTs*, JHEP **1008** (2010) 100 [arXiv:1003.3233 [hep-ph]].

[26] S. Antusch, J. P. Baumann, V. F. Domcke and P. M. Kostka, *Sneutrino Hybrid Inflation and Nonthermal Leptogenesis*, JCAP **1010** (2010) 006 [arXiv:1007.0708 [hep-ph]].

[27] S. Antusch, D. Nolde and M. U. Rehman, *Pseudosmooth Tribrid Inflation*, JCAP **1208** (2012) 004 [arXiv:1205.0809 [hep-ph]].

[28] S. Antusch and D. Nolde, *Kähler-driven Tribrid Inflation*, JCAP **1211** (2012) 005 [arXiv:1207.6111 [hep-ph]].

[29] V. N. Senoguz and Q. Shafi, *New inflation, preinflation, and leptogenesis*, Phys. Lett. B **596** (2004) 8 [hep-ph/0403294].

[30] S. Antusch, S. F. King, M. Malinsky, L. Velasco-Sevilla and I. Zavala, *Flavon Inflation*, Phys. Lett. B **666** (2008) 176 [arXiv:0805.0325 [hep-ph]].

[31] S. Antusch and F. Cefalà, *SUGRA New Inflation with Heisenberg Symmetry*, JCAP **1310** (2013) 055 [arXiv:1306.6825 [hep-ph]].

[32] K. Kumekawa, T. Moroi and T. Yanagida, *Flat potential for inflaton with a discrete R invariance in supergravity*, Prog. Theor. Phys. **92** (1994) 437 [hep-ph/9405337].

[33] K. I. Izawa, M. Kawasaki and T. Yanagida, *Dynamical tuning of the initial condition for new inflation in supergravity*, Phys. Lett. B **411** (1997) 249 [hep-ph/9707201].

[34] K. Nakayama and F. Takahashi, *Low-scale Supersymmetry from Inflation*, JCAP **1110** (2011) 033 [arXiv:1108.0070 [hep-ph]].

[35] F. Takahashi, *New inflation in supergravity after Planck and LHC*, Phys. Lett. B **727** (2013) 21 [arXiv:1308.4212 [hep-ph]].

[36] M. Kawasaki, M. Yamada, T. T. Yanagida and N. Yokozaki, *High-scale SUSY from an R-invariant New Inflation in the Landscape*, arXiv:1512.04259 [hep-ph].

[37] E. W. Kolb and M. S. Turner, *The Early Universe*, Front. Phys. **69** (1990) 1.

[38] L. Bergstrom and A. Goobar, *Cosmology and particle astrophysics*, Chichester, UK: Wiley (1999) 344 p.

[39] S. Weinberg, *Cosmology*, Oxford, UK: Oxford Univ. Pr. (2008) 593 p.

[40] D. Baumann, *TASI Lectures on Inflation*, arXiv:0907.5424 [hep-th].

[41] D. H. Lyth and A. R. Liddle, *The primordial density perturbation: Cosmology, inflation and the origin of structure*, Cambridge, UK: Cambridge Univ. Pr. (2009) 497 p.

[42] A. D. Linde, *Particle physics and inflationary cosmology*, Contemp. Concepts Phys. **5** (1990) 1 [hep-th/0503203].

[43] R. Allahverdi, R. Brandenberger, F. Y. Cyr-Racine and A. Mazumdar, *Reheating in Inflationary Cosmology: Theory and Applications*, Ann. Rev. Nucl. Part. Sci. **60** (2010) 27 [arXiv:1001.2600 [hep-th]].

[44] M. A. Amin, M. P. Hertzberg, D. I. Kaiser and J. Karouby, *Nonperturbative Dynamics Of Reheating After Inflation: A Review*, Int. J. Mod. Phys. D **24** (2014) 1530003 [arXiv:1410.3808 [hep-ph]].

[45] S. P. Martin, *A Supersymmetry primer*, Adv. Ser. Direct. High Energy Phys. **21** (2010) 1 [Adv. Ser. Direct. High Energy Phys. **18** (1998) 1] [hep-ph/9709356].

[46] D. Bailin and A. Love, *Supersymmetric gauge field theory and string theory*, Bristol, UK: IOP (1994) 322 p. (Graduate student series in physics)

[47] J. Wess and J. Bagger, *Supersymmetry and supergravity*, Princeton, USA: Univ. Pr. (1992) 259 p.

[48] M. Drees, R. Godbole and P. Roy, *Theory and phenomenology of sparticles: An account of four-dimensional N=1 supersymmetry in high energy physics*, Hackensack, USA: World Scientific (2004) 555 p.

[49] P. A. R. Ade *et al.* [Planck Collaboration], *Planck 2013 results. XVI. Cosmological parameters*, Astron. Astrophys. **571** (2014) A16 [arXiv:1303.5076 [astro-ph.CO]].

[50] P. A. R. Ade *et al.* [BICEP2 and Planck Collaborations], *Joint Analysis of BICEP2/Keck Array and Planck Data*, Phys. Rev. Lett. **114** (2015) 101301 [arXiv:1502.00612 [astro-ph.CO]].

[51] P. A. R. Ade *et al.* [BICEP2 and Keck Array Collaborations], *BICEP2/Keck Array VI: Improved Constraints On Cosmology and Foregrounds When Adding 95 GHz Data From Keck Array*, Phys. Rev. Lett. **116** (2016) 3, 031302 [arXiv:1510.09217 [astro-ph.CO]].

[52] F. Beutler *et al.*, *The 6dF Galaxy Survey: Baryon Acoustic Oscillations and the Local Hubble Constant*, Mon. Not. Roy. Astron. Soc. **416** (2011) 3017 [arXiv:1106.3366 [astro-ph.CO]].

[53] L. Anderson *et al.* [BOSS Collaboration], *The clustering of galaxies in the SDSS-III Baryon Oscillation Spectroscopic Survey: baryon acoustic oscillations in the Data Releases 10 and 11 Galaxy samples*, Mon. Not. Roy. Astron. Soc. **441** (2014) 1, 24 [arXiv:1312.4877 [astro-ph.CO]].

[54] A. J. Ross, L. Samushia, C. Howlett, W. J. Percival, A. Burden and M. Manera, *The Clustering of the SDSS DR7 Main Galaxy Sample I: A 4 per cent Distance Measure at* $z = 0.15$, Mon. Not. Roy. Astron. Soc. **449** (2015) 1, 835 [arXiv:1409.3242 [astro-ph.CO]].

[55] B. D. Fields, P. Molaro and S. Sarkar, *Big-Bang Nucleosynthesis*, Chin. Phys. C **38** (2014) [arXiv:1412.1408 [astro-ph.CO]].

[56] A. Conley *et al.* [SNLS Collaboration], *Supernova Constraints and Systematic Uncertainties from the First 3 Years of the Supernova Legacy Survey*, Astrophys. J. Suppl. **192** (2011) 1 [arXiv:1104.1443 [astro-ph.CO]].

[57] A. Rest *et al.*, *Cosmological Constraints from Measurements of Type Ia Supernovae discovered during the first 1.5 yr of the Pan-STARRS1 Survey*, Astrophys. J. **795** (2014) 1, 44 [arXiv:1310.3828 [astro-ph.CO]].

[58] S. M. Carroll and H. Tam, *Unitary Evolution and Cosmological Fine-Tuning*, arXiv:1007.1417 [hep-th].

[59] J. Preskill, *Cosmological Production of Superheavy Magnetic Monopoles*, Phys. Rev. Lett. **43** (1979) 1365.

[60] A. H. Guth, *The Inflationary Universe: A Possible Solution to the Horizon and Flatness Problems*, Phys. Rev. D **23** (1981) 347.

[61] M. Cicoli, S. Downes, B. Dutta, F. G. Pedro and A. Westphal, *Just enough inflation: power spectrum modifications at large scales*, JCAP **1412** (2014) 12, 030 [arXiv:1407.1048 [hep-th]].

[62] A. R. Liddle, P. Parsons and J. D. Barrow, *Formalizing the slow roll approximation in inflation*, Phys. Rev. D **50** (1994) 7222 [astro-ph/9408015].

[63] A. D. Linde, *Chaotic Inflation*, Phys. Lett. B **129** (1983) 177.

[64] A. D. Linde, *A New Inflationary Universe Scenario: A Possible Solution of the Horizon, Flatness, Homogeneity, Isotropy and Primordial Monopole Problems*, Phys. Lett. B **108** (1982) 389.

[65] A. D. Linde, *Hybrid inflation*, Phys. Rev. D **49** (1994) 748 [astro-ph/9307002].

[66] D. H. Lyth, K. A. Malik and M. Sasaki, *A General proof of the conservation of the curvature perturbation*, JCAP **0505** (2005) 004 [astro-ph/0411220].

[67] J. L. Cook and L. M. Krauss, *Large Slow Roll Parameters in Single Field Inflation*, arXiv:1508.03647 [astro-ph.CO].

[68] S. Renaux-Petel, *Primordial non-Gaussianities after Planck 2015: an introductory review*, Comptes Rendus Physique **16** (2015) 969 [arXiv:1508.06740 [astro-ph.CO]].

[69] S. Dodelson and E. Stewart, *Scale dependent spectral index in slow roll inflation*, Phys. Rev. D **65** (2002) 101301 [astro-ph/0109354].

[70] E. D. Stewart, *The Spectrum of density perturbations produced during inflation to leading order in a general slow roll approximation*, Phys. Rev. D **65** (2002) 103508 [astro-ph/0110322].

[71] P. F. de Salas, M. Lattanzi, G. Mangano, G. Miele, S. Pastor and O. Pisanti, *Bounds on very low reheating scenarios after Planck*, Phys. Rev. D **92** (2015) 12, 123534 [arXiv:1511.00672 [astro-ph.CO]].

[72] A. A. Starobinsky, *Multicomponent de Sitter (Inflationary) Stages and the Generation of Perturbations*, JETP Lett. **42** (1985) 152 [Pisma Zh. Eksp. Teor. Fiz. **42** (1985) 124].

[73] D. H. Lyth and Y. Rodriguez, *The Inflationary prediction for primordial non-Gaussianity*, Phys. Rev. Lett. **95** (2005) 121302 [astro-ph/0504045].

[74] M. Sasaki and E. D. Stewart, *A General analytic formula for the spectral index of the density perturbations produced during inflation*, Prog. Theor. Phys. **95** (1996) 71 [astro-ph/9507001].

[75] N. S. Sugiyama, E. Komatsu and T. Futamase, *δN formalism*, Phys. Rev. D **87** (2013) 2, 023530 [arXiv:1208.1073 [gr-qc]].

[76] E. J. Copeland, S. Pascoli and A. Rajantie, *Dynamics of tachyonic preheating after hybrid inflation*, Phys. Rev. D **65** (2002) 103517 [hep-ph/0202031].

[77] D. H. Lyth, *The hybrid inflation waterfall and the primordial curvature perturbation*, JCAP **1205** (2012) 022 [arXiv:1201.4312 [astro-ph.CO]].

[78] R. Micha and I. I. Tkachev, *Turbulent thermalization*, Phys. Rev. D **70** (2004) 043538 [hep-ph/0403101].

[79] K. Harigaya and K. Mukaida, *Thermalization after/during Reheating*, JHEP **1405** (2014) 006 [arXiv:1312.3097 [hep-ph]].

[80] A. Mazumdar and B. Zaldivar, *Quantifying the reheating temperature of the universe*, Nucl. Phys. B **886** (2014) 312 [arXiv:1310.5143 [hep-ph]].

[81] P. B. Greene and L. Kofman, *On the theory of fermionic preheating*, Phys. Rev. D **62** (2000) 123516 [hep-ph/0003018].

[82] M. Peloso and L. Sorbo, *Preheating of massive fermions after inflation: Analytical results*, JHEP **0005** (2000) 016 [hep-ph/0003045].

[83] M. Bolz, A. Brandenburg and W. Buchmüller, *Thermal production of gravitinos*, Nucl. Phys. B **606** (2001) 518 [Nucl. Phys. B **790** (2008) 336] [hep-ph/0012052].

[84] J. Pradler and F. D. Steffen, *Constraints on the Reheating Temperature in Gravitino Dark Matter Scenarios*, Phys. Lett. B **648** (2007) 224 [hep-ph/0612291].

[85] M. Kawasaki, K. Kohri, T. Moroi and A. Yotsuyanagi, *Big-Bang Nucleosynthesis and Gravitino*, Phys. Rev. D **78** (2008) 065011 [arXiv:0804.3745 [hep-ph]].

[86] A. R. Liddle and S. M. Leach, *How long before the end of inflation were observable perturbations produced?*, Phys. Rev. D **68** (2003) 103503 [astro-ph/0305263].

[87] A. V. Frolov, *DEFROST: A New Code for Simulating Preheating after Inflation*, JCAP **0811** (2008) 009 [arXiv:0809.4904 [hep-ph]].

[88] G. N. Felder and I. Tkachev, *LATTICEEASY: A Program for lattice simulations of scalar fields in an expanding universe*, Comput. Phys. Commun. **178** (2008) 929 [hep-ph/0011159].

[89] Z. Huang, *The Art of Lattice and Gravity Waves from Preheating*, Phys. Rev. D **83** (2011) 123509 [arXiv:1102.0227 [astro-ph.CO]].

[90] L. Kofman, A. D. Linde and A. A. Starobinsky, *Towards the theory of reheating after inflation*, Phys. Rev. D **56** (1997) 3258 [hep-ph/9704452].

[91] S. Davidson, E. Nardi and Y. Nir, *Leptogenesis*, Phys. Rept. **466** (2008) 105 [arXiv:0802.2962 [hep-ph]].

[92] V. A. Kuzmin, V. A. Rubakov and M. E. Shaposhnikov, *On the Anomalous Electroweak Baryon Number Nonconservation in the Early Universe*, Phys. Lett. B **155** (1985) 36.

[93] M. Fukugita and T. Yanagida, *Baryogenesis Without Grand Unification*, Phys. Lett. B **174** (1986) 45.

[94] M. A. Luty, *Baryogenesis via leptogenesis*, Phys. Rev. D **45** (1992) 455.

[95] T. Asaka, K. Hamaguchi, M. Kawasaki and T. Yanagida, *Leptogenesis in inflaton decay*, Phys. Lett. B **464** (1999) 12 [hep-ph/9906366].

[96] W. Buchmüller, V. Domcke and K. Schmitz, *Spontaneous B-L Breaking as the Origin of the Hot Early Universe*, Nucl. Phys. B **862** (2012) 587 [arXiv:1202.6679 [hep-ph]].

[97] K. A. Olive *et al.* [Particle Data Group Collaboration], *Review of Particle Physics*, Chin. Phys. C **38** (2014) 090001, `http://pdg.lbl.gov`.

[98] R. Haag, J. T. Lopuszanski and M. Sohnius, *All Possible Generators of Supersymmetries of the S-Matrix*, Nucl. Phys. B **88** (1975) 257.

[99] S. R. Coleman and J. Mandula, *All Possible Symmetries of the S Matrix*, Phys. Rev. **159** (1967) 1251.

[100] D. J. H. Chung, L. L. Everett, G. L. Kane, S. F. King, J. D. Lykken and L. T. Wang, *The Soft supersymmetry breaking Lagrangian: Theory and applications*, Phys. Rept. **407** (2005) 1 [hep-ph/0312378].

[101] E. J. Copeland, A. R. Liddle, D. H. Lyth, E. D. Stewart and D. Wands, *False vacuum inflation with Einstein gravity*, Phys. Rev. D **49** (1994) 6410 [astro-ph/9401011].

[102] G. R. Dvali, Q. Shafi and R. K. Schaefer, *Large scale structure and supersymmetric inflation without fine tuning*, Phys. Rev. Lett. **73** (1994) 1886 [hep-ph/9406319].

[103] A. D. Linde and A. Riotto, *Hybrid inflation in supergravity*, Phys. Rev. D **56** (1997) 1841 [hep-ph/9703209].

[104] E. J. Weinberg, *Radiative corrections as the origin of spontaneous symmetry breaking*, hep-th/0507214.

[105] R. Jackiw, *Functional evaluation of the effective potential*, Phys. Rev. D **9** (1974) 1686.

[106] S. Weinberg, *The quantum theory of fields. Vol. 2: Modern applications*, Cambridge, UK: Cambridge Univ. Pr. (2009), 481 p.

[107] E. J. Weinberg and A. q. Wu, *Understanding Complex Perturbative Effective Potentials*, Phys. Rev. D **36** (1987) 2474.

[108] M. Dine, L. Randall and S. D. Thomas, *Supersymmetry breaking in the early universe*, Phys. Rev. Lett. **75** (1995) 398 [hep-ph/9503303].

[109] S. Hardeman, J. M. Oberreuter, G. A. Palma, K. Schalm and T. van der Aalst, *The everpresent eta-problem: knowledge of all hidden sectors required*, JHEP **1104** (2011) 009 [arXiv:1012.5966 [hep-ph]].

[110] M. Kawasaki, M. Yamaguchi and T. Yanagida, *Natural chaotic inflation in supergravity*, Phys. Rev. Lett. **85** (2000) 3572 [hep-ph/0004243].

[111] P. Brax and J. Martin, *Shift symmetry and inflation in supergravity*, Phys. Rev. D **72** (2005) 023518 [hep-th/0504168].

[112] E. D. Stewart, *Inflation, supergravity and superstrings*, Phys. Rev. D **51** (1995) 6847 [hep-ph/9405389].

[113] M. K. Gaillard, H. Murayama and K. A. Olive, *Preserving flat directions during inflation*, Phys. Lett. B **355** (1995) 71 [hep-ph/9504307].

[114] S. Antusch, M. Bastero-Gil, K. Dutta, S. F. King and P. M. Kostka, *Solving the eta-Problem in Hybrid Inflation with Heisenberg Symmetry and Stabilized Modulus*, JCAP **0901** (2009) 040 [arXiv:0808.2425 [hep-ph]].

[115] S. Antusch, K. Dutta, J. Erdmenger and S. Halter, *Towards Matter Inflation in Heterotic String Theory*, JHEP **1104** (2011) 065 [arXiv:1102.0093 [hep-th]].

[116] V. N. Senoguz and Q. Shafi, *Testing supersymmetric grand unified models of inflation*, Phys. Lett. B **567** (2003) 79 [hep-ph/0305089].

[117] M. U. Rehman, Q. Shafi and J. R. Wickman, *Minimal Supersymmetric Hybrid Inflation, Flipped SU(5) and Proton Decay*, Phys. Lett. B **688** (2010) 75 [arXiv:0912.4737 [hep-ph]].

[118] S. Khalil, M. U. Rehman, Q. Shafi and E. A. Zaakouk, *Inflation in Supersymmetric SU(5)*, Phys. Rev. D **83** (2011) 063522 [arXiv:1010.3657 [hep-ph]].

[119] R. Armillis, G. Lazarides and C. Pallis, *Inflation, leptogenesis, and Yukawa quasiunification within a supersymmetric left-right model*, Phys. Rev. D **89** (2014) 6, 065032 [arXiv:1309.6986 [hep-ph]].

[120] W. Buchmüller, V. Domcke, K. Kamada and K. Schmitz, *The Gravitational Wave Spectrum from Cosmological $B-L$ Breaking*, JCAP **1310** (2013) 003 [arXiv:1305.3392 [hep-ph]].

[121] W. Buchmüller, V. Domcke, K. Kamada and K. Schmitz, *Hybrid Inflation in the Complex Plane*, JCAP **1407** (2014) 054 [arXiv:1404.1832 [hep-ph]].

[122] M. U. Rehman, Q. Shafi and J. R. Wickman, *Supersymmetric Hybrid Inflation Redux*, Phys. Lett. B **683** (2010) 191 [arXiv:0908.3896 [hep-ph]].

[123] G. Lazarides and C. Panagiotakopoulos, *Smooth hybrid inflation*, Phys. Rev. D **52** (1995) 559 [hep-ph/9506325].

[124] E. Di Valentino, A. Melchiorri and J. Silk, *Beyond six parameters: extending ΛCDM*, Phys. Rev. D **92** (2015) 12, 121302 [arXiv:1507.06646 [astro-ph.CO]].

[125] P. Ramond, *Group theory: A physicist's survey*, Cambridge, UK: Univ. Pr. (2010) 310 p.

[126] P. Minkowski, *$\mu \to e\gamma$ at a Rate of One Out of 10^9 Muon Decays?*, Phys. Lett. B **67** (1977) 421.

[127] S. F. King, *Neutrino Mass and Mixing in the Seesaw Playground*, arXiv:1511.03831 [hep-ph].

[128] P. F. Harrison, D. H. Perkins and W. G. Scott, *Tri-bimaximal mixing and the neutrino oscillation data*, Phys. Lett. B **530** (2002) 167 [hep-ph/0202074].

[129] S. Antusch and S. F. King, *Charged lepton corrections to neutrino mixing angles and CP phases revisited*, Phys. Lett. B **631** (2005) 42 [hep-ph/0508044].

[130] S. F. King, *Neutrino mass models*, Rept. Prog. Phys. **67** (2004) 107 [hep-ph/0310204].

[131] S. Antusch, J. Kersten, M. Lindner, M. Ratz and M. A. Schmidt, *Running neutrino mass parameters in see-saw scenarios*, JHEP **0503** (2005) 024 [hep-ph/0501272].

[132] S. F. King, *Predicting neutrino parameters from SO(3) family symmetry and quark-lepton unification*, JHEP **0508** (2005) 105 [arXiv:hep-ph/0506297].

[133] I. Masina, *A maximal atmospheric mixing from a maximal CP violating phase*, Phys. Lett. B **633** (2006) 134 [arXiv:hep-ph/0508031].

[134] J. R. C. C. C. Correia, I. S. C. R. Leite and C. J. A. P. Martins, *Effects of Biases in Domain Wall Network Evolution*, Phys. Rev. D **90** (2014) 2, 023521 [arXiv:1407.3905 [hep-ph]].

[135] M. Yamaguchi and J. Yokoyama, *Smooth hybrid inflation in supergravity with a running spectral index and early star formation*, Phys. Rev. D **70** (2004) 023513 [hep-ph/0402282].

[136] R. Dong, W. H. Kinney and D. Stojkovic, *Symmetron Inflation*, JCAP **01** (2014) 021 [arXiv:1307.4451 [astro-ph.CO]].

[137] A. Vilenkin, *The Birth of Inflationary Universes*, Phys. Rev. D **27** (1983) 2848.

[138] A. Vilenkin, *Topological inflation*, Phys. Rev. Lett. **72** (1994) 3137 [hep-th/9402085].

[139] L. Boubekeur and D. H. Lyth, *Hilltop inflation*, JCAP **0507** (2005) 010 [hep-ph/0502047].

[140] J. Elliston, D. J. Mulryne, D. Seery and R. Tavakol, *Evolution of f_{NL} to the adiabatic limit*, JCAP **1111** (2011) 005 arXiv:1106.2153 [astro-ph.CO].

[141] J. Meyers and E. R. M. Tarrant, *Perturbative Reheating After Multiple-Field Inflation: The Impact on Primordial Observables*, Phys. Rev. D **89** (2014) 6, 063535 [arXiv:1311.3972 [astro-ph.CO]].

[142] J. Elliston, S. Orani and D. J. Mulryne, *General analytic predictions of two-field inflation and perturbative reheating*, Phys. Rev. D **89** (2014) 10, 103532 [arXiv:1402.4800 [astro-ph.CO]].

[143] A. Chambers and A. Rajantie, *Lattice calculation of non-Gaussianity from preheating*, Phys. Rev. Lett. **100** (2008) 041302 [Phys. Rev. Lett. **101** (2008) 149903] [arXiv:0710.4133 [astro-ph]].

[144] H. Murayama, H. Suzuki, T. Yanagida and J. Yokoyama, *Chaotic inflation and baryogenesis in supergravity*, Phys. Rev. D **50** (1994) 2356 [hep-ph/9311326].

[145] K. Nakayama, F. Takahashi and T. T. Yanagida, *Chaotic Inflation with Right-handed Sneutrinos after Planck*, Phys. Lett. B **730** (2014) 24 [arXiv:1311.4253 [hep-ph]].

[146] R. Allahverdi and A. Mazumdar, *Reheating in supersymmetric high scale inflation*, Phys. Rev. D **76** (2007) 103526 [hep-ph/0603244].

[147] L. Covi, E. Roulet and F. Vissani, *CP violating decays in leptogenesis scenarios*, Phys. Lett. B **384** (1996) 169 [hep-ph/9605319].

[148] K. Hamaguchi, H. Murayama and T. Yanagida, *Leptogenesis from N dominated early universe*, Phys. Rev. D **65** (2002) 043512 [hep-ph/0109030].

[149] S. Davidson and A. Ibarra, *A Lower bound on the right-handed neutrino mass from leptogenesis*, Phys. Lett. B **535** (2002) 25 [hep-ph/0202239].

[150] S. Antusch, F. Cefalà, D. Nolde and S. Orani, *Parametric resonance after hilltop inflation caused by an inhomogeneous inflaton field*, arXiv:1510.04856 [hep-ph].

[151] P. Brax, J. F. Dufaux and S. Mariadassou, *Preheating after Small-Field Inflation*, Phys. Rev. D **83** (2011) 103510 [arXiv:1012.4656 [hep-th]].

[152] E. J. Copeland, M. Gleiser and H.-R. Müller, *Oscillons: Resonant configurations during bubble collapse*, Phys. Rev. D **52** (1995) 1920 [hep-ph/9503217].

[153] S. Antusch and S. Orani, *Impact of other scalar fields on oscillons after hilltop inflation*, arXiv:1511.02336 [hep-ph].

[154] L. Kofman, A. D. Linde and A. A. Starobinsky, *Reheating after inflation*, Phys. Rev. Lett. **73** (1994) 3195 [hep-th/9405187].

[155] J. Braden, J. R. Bond and L. Mersini-Houghton, *Cosmic bubble and domain wall instabilities I: parametric amplification of linear fluctuations*, JCAP **1503** (2015) 03, 007 [arXiv:1412.5591 [hep-th]].

[156] D. H. Lyth, *What would we learn by detecting a gravitational wave signal in the cosmic microwave background anisotropy?*, Phys. Rev. Lett. **78** (1997) 1861 [hep-ph/9606387].

[157] D. Baumann and D. Green, *A Field Range Bound for General Single-Field Inflation*, JCAP **1205** (2012) 017 [arXiv:1111.3040 [hep-th]].

[158] P. A. R. Ade *et al.* [BICEP2 Collaboration], *Detection of B-Mode Polarization at Degree Angular Scales by BICEP2*, Phys. Rev. Lett. **112** (2014) 24, 241101 [arXiv:1403.3985 [astro-ph.CO]].

[159] I. Ben-Dayan and R. Brustein, *Cosmic Microwave Background Observables of Small Field Models of Inflation*, JCAP **1009** (2010) 007 [arXiv:0907.2384 [astro-ph.CO]].

[160] S. Hotchkiss, A. Mazumdar and S. Nadathur, *Observable gravitational waves from inflation with small field excursions*, JCAP **1202** (2012) 008 [arXiv:1110.5389 [astro-ph.CO]].

[161] G. German, A. Herrera-Aguilar, J. C. Hidalgo and R. A. Sussman, *Canonical single field slow-roll inflation with a non-monotonic tensor*, arXiv:1512.03105 [astro-ph.CO].

[162] J. E. Lidsey, A. R. Liddle, E. W. Kolb, E. J. Copeland, T. Barreiro and M. Abney, *Reconstructing the inflation potential: An overview*, Rev. Mod. Phys. **69** (1997) 373 [astro-ph/9508078].

[163] R. Easther, W. H. Kinney and B. A. Powell, *The Lyth bound and the end of inflation*, JCAP **0608** (2006) 004 [astro-ph/0601276].

[164] J. Garcia-Bellido, D. Roest, M. Scalisi and I. Zavala, *Lyth bound of inflation with a tilt*, Phys. Rev. D **90** (2014) 12, 123539 [arXiv:1408.6839 [hep-th]].

[165] J. Bramante, S. Downes, L. Lehman and A. Martin, *Last stand of single small field inflation*, Phys. Rev. D **90** (2014) 2, 023530 [arXiv:1405.7563 [astro-ph.CO]].

[166] J. McDonald, *Sub-Planckian Two-Field Inflation Consistent with the Lyth Bound*, JCAP **1409** (2014) 09, 027 [arXiv:1404.4620 [hep-ph]].

[167] J. McDonald, *Signatures of Planck Corrections in a Spiralling Axion Inflation Model*, JCAP **1505** (2015) 05, 014 [arXiv:1412.6943 [hep-ph]].

[168] G. Barenboim and W. I. Park, *Spiral Inflation*, Phys. Lett. B **741** (2015) 252 [arXiv:1412.2724 [hep-ph]].

[169] S. Dimopoulos, S. Kachru, J. McGreevy and J. G. Wacker, *N-flation*, JCAP **0808** (2008) 003 [hep-th/0507205].

[170] P. A. R. Ade *et al.* [Planck Collaboration], *Planck 2015 results. XIII. Cosmological parameters*, arXiv:1502.01589 [astro-ph.CO].

[171] B. Audren, J. Lesgourgues, K. Benabed and S. Prunet, *Conservative Constraints on Early Cosmology: an illustration of the Monte Python cosmological parameter inference code*, JCAP **1302** (2013) 001 [arXiv:1210.7183 [astro-ph.CO]].

[172] J. Lesgourgues, *The Cosmic Linear Anisotropy Solving System (CLASS) I: Overview*, arXiv:1104.2932 [astro-ph.IM].

[173] D. Blas, J. Lesgourgues and T. Tram, *The Cosmic Linear Anisotropy Solving System (CLASS) II: Approximation schemes*, JCAP **1107** (2011) 034 [arXiv:1104.2933 [astro-ph.CO]].

[174] M. E. Peskin and D. V. Schroeder, *An Introduction to quantum field theory*, Reading, USA: Addison-Wesley (1995) 842 p.

[175] A. Denner, H. Eck, O. Hahn and J. Kublbeck, *Feynman rules for fermion number violating interactions*, Nucl. Phys. B **387** (1992) 467.